ANION SENSING IN POLAR MEDIA BY FLUORECENT SMALL MOLECULE RECEPTORS VIA HALOGEN BONDING

by

HANNAH JOSEPHINE BATES

A DISSERTATION

Presented to the Department of Chemistry and Biochemistry
and the Division of Graduate Studies of the University of Oregon
in partial fulfillment of the requirements
for the degree of
Doctor of Philosophy

September 2022

DISSERTATION APPROVAL PAGE

Student: Hannah Josephine Bates

Title: Anion Sensing in Polar Media by Fluorescent Small Molecule Receptors via Halogen Bonding

This dissertation has been accepted and approved in partial fulfillment of the requirements for the Doctor of Philosophy degree in the Department of Chemistry and Biochemistry by:

Dr. Ramesh Jasti	Chairperson
Dr. Darren Johnson	Co-Advisor
Dr. Michael Haley	Co-Advisor
Dr. Amanda Cook	Core Member
Dr. Keat Ghee Ong	Institutional Representative

and

Krista Chronister	Vice Provost for Graduate Studies

Original approval signatures are on file with the University of Oregon Division of Graduate Studies.

Degree awarded September 2022.

DISSERTATION ABSTRACT

Hannah Josephine Bates

Doctor of Philosophy

Department of Chemistry and Biochemistry

September 2022

Title: Anion Sensing in Polar Media by Fluorescent Small Molecule Receptors via Halogen Bonding

Anions are a ubiquitous class of molecule which play critical roles in many of the environments with which humans concern themselves. From our physiology to nuclear waste to our water supply, anions have been the focus of much of the host-guest chemistry to have emerged within the last five decades. Host-guest chemists have used supramolecular tools, including halogen and hydrogen bonding, along with many others, to reversibly binding these and many other analytes. The purposes of binding are as wide ranging as real-time molecular recognition, catalysis, mechanically interlocked molecules, purification, and many others. Due to the many factors that can contribute to the efficacy of host-guest systems, including solvent effects, pocket size, molecular geometry, pH and others, most systems must be fined tuned for their particular application. One frequently encountered challenge is the competitive nature of any polar solvents, especially water, in solution state binding. Halogen bonding has recently come onto the scene as a potential answer to this problem, often demonstrating higher binding affinities than comparable hydrogen bonding molecules in polar environments. Despite its promise, much remains to be learned about how to best deploy halogen bonding motifs.

This lacuna motivates the work covered in this thesis, which explores the design principles behind incorporating halogen bond donors effectively in a variety of arylethynyl; systems which were inspired by similar hydrogen bonding scaffolds published by the Johnson and Haley groups. After examining the successes and pitfalls of these halogen bond receptors in Chapter 3, Chapters 4 and 5 go on to report on the use of halogen bond and hydrogen bond systems in tandem, which are shown to bind the chloride anion notably well in appreciably polar organic solvents. These studies, suggest that the accepted definition of a halogen bond, as presented by IUPAC and discussed in Chapter 1, biases chemists to place undue importance on ensuring that the location of a polarizing group is as close as possible to the halogen-bond donor. Finally, future studies that can help flush out the ideas established in this thesis are reviewed in Chapter 6.

This dissertation includes published and unpublished co-authored material.

CURRICULUM VITAE

NAME OF AUTHOR: Hannah Josephine Bates

GRADUATE AND UNDERGRADUATE SCHOOLS ATTENDED:

University of Oregon, Eugene
Sarah Lawrence College, Bronxville

DEGREES AWARDED:

Doctor of Philosophy, Chemistry, 2022, University of Oregon
Master of Science, Chemistry, 2022, University of Oregon
Bachelor of Art, Chemistry, 2018, Sarah Lawrence College

AREAS OF SPECIAL INTEREST:

Physical Organic Chemistry
Supramolecular Chemistry
Anion Recognition
Halogen Bonding

PROFESSIONAL EXPERIENCE:

Associate Scientist, Thermo Fisher Scientific, May – December 2021
Graduate Research Fellow, University of Oregon, 2019 – 2022
Graduate Teaching Fellow, University of Oregon, 2018 – 2019

GRANTS, AWARDS, AND HONORS:

ARCS Scholar Award, ARCS Foundation Oregon, 2018-2021

PUBLICATIONS:

H. J. Bates, T. P. de Faria, A. S. Trom, F. I. D. Longnight, M. P. Miller, L. N. Zakharov, M. M. Haley & D. W. Johnson, *manuscript in prep*.

T. P. de Faria, H. J. Bates, A. S. Trom, F. I. D. Longnight, M. P. Miller, L. N. Zakharov, M. M. Haley & D. W. Johnson, *manuscript in prep*.

J. P. Bard, H. J. Bates, C.-L. Deng, L. N. Zakharov, M. M. Haley, *J. Org. Chem.* **2019**, acs.joc.9b02132.

ACKNOWLEDGMENTS

I would like to take this space to thank the countless people who offered me support through my time in grad school as well as before it. Let me begin by thanking my parents, who kept a home secure enough that my curiosity could grow uninhibited and were always a source of unconditional love. I also am so grateful to my younger siblings, Mason, Austin and Riley who, despite their youth, never fail to inspire me with their amazing strengths. Another thank you is deserved by the many STEM students at Sarah Lawrence College including: Brooke, Isabella, Ellie, Ella, Sarah, and so many others; there was such a beautiful and tight-knit, field-spanning scientific community at SLC and it wouldn't have existed without you guys. Another shout out to Emma, Ollie, and Jules for being friends I could talk to when I needed a break from science. Finally, a thank you to my many amazing professors from SLC, who taught me so much; Prof. Mike Siff and Prof. Colin Abernethy deserve a special shout out. As an advisor, Mike ensured that all of his mentees knew exactly how seriously we should take college (reminding all of us that school was not "real life", no matter how important it felt) and helping me keep a cool head until the calmer winds prevailed once again. As a lecturer, Colin transferred his enthusiasm for the field of chemistry to every student who walked through his doors; beyond being just engaging though, Colin was a safe harbor for any question, chemistry related or not, he was already ready to lend a hand or an ear as the situation required. Without the support of all of the aforementioned people I would have never made it all the way to grad school.

This brings me to the myriad of amazing people that I have met in grad school. First, let me thank my advisors, Professors Darren Johnson and Mike Haley who have

done an admirable job wrangling much of my chaotic energy into a productive four-year stint here at UO. Thanks to my other committee members, Ramesh Jasti, Amanda Cook and Keat Ghee Ong, who all gave me both the opportunity to graduate and some amazing advice my 3rd year that I still think about frequently. Another thank you to my advisors from Thermo Fisher, Adam York, Dan Cash and Eric Welch who made sure that my 6 months there were filled with lots of learning and laughs alike. Also, a huge shout out to the front office staff at UO, Janet, Christi, Kathy, Jim and Rob who keep this program running and the people in it as happy as possible.

Next let me give a hearty thank all of my labmates, past and present, in the DWJ, Haley labs and beyond – Jess, Sean, Merideth, Jordan, Hazel, Josh, Jeremy, Chun-lin, Trevor, Ngoc-Minh, Jacob, Henry, Thaís, Scout, Faith, Luca, Willow, Alex, Grace, Ben, Jack, Kiana, Efrain, Nolan, Gabby, Bella, Allison, Nick, Olivia, Mark, Russell and Haley – the amazing people that I met in grad school were easily my favorite part of the experience. Jeremy, Chun-lin, Jess, Hazel, and Thaís you guys have taught me so much and never fail to pick up the phone when I need advice or to bounce ideas off of someone. Jordan, you made every new member to the lab (myself included) feel so welcome when they joined and were always the first to person make the fun-loving and balanced culture of our lab a talked-about priority. Sean, you introduced me to motorcycles and consequently ensured every day to and from work was something to smile about. Thaís, Scout and Faith whether board games or titrations you guys saturated every moment with fun, love and support and I am unspeakably grateful for our palio-ship. Willow, Luca and Alex I am so happy my time here has overlapped with your own and that I can leave knowing that the lab is in good hands that will continue to guide it

steadily. Ben, you have been such an amazing friend, housemate and confidant for the past four years and know that Massachusetts is a great spot to consider for your post grad school aspirations.

Finally thank you to my fiancé, David. The past seven years have been filled with things that I never could have expected but together we handled them with so much more grace than I ever could have alone, and I am so grateful for the support, sage advice, good food and comfort that you never seem to run out of. No matter what the lab held for me I always look forward to coming home to you and Ezra and Kali (our two desperately snuggly kittens that never fail to put a smile on my face).

To David and Thaís –

The past several years have often been trying, but that hardship was always salved by your generous love and friendship. Both of you, in your own inimitable ways, have shown me new and beautiful meanings to the word "partner" and I could not be more grateful to have you in my life.

TABLE OF CONTENTS

Chapter Page

LIST OF FIGURES

Figure Page

LIST OF TABLES

Table Page

LIST OF SCHEMES

Scheme Page

CHAPTER ONE

INTRODUCTION

This chapter contains work in the process of being published and was written by Thaís P. de Faria and Hannah Bates, with editorial assistance from Douglas H. Banning, Dr. Trevor A. Shear, and Professors Michael M. Haley and Darren W. Johnson. This review article accounts the science and history behind anion binding, host-guest chemistry, some of the first papers on the project and foreshadows future work. However, it is by no means a comprehensive review of the field, rather a few pertinent examples have been selected for discussion to give a general sketch of the state of the field.

Anions are prevalent in the human body and vital to life. They play a variety of different roles from producing electrical signals to maintaining cell volume.[1] While there are many anions present in living systems, chloride (Cl^-) and the protic forms of phosphate (i.e. HPO_4^{2-}, $H_2PO_4^-$) play a critical role in maintaining basic metabolic pathways within the human body.

Two types of phosphorous species (organic and inorganic) are prevalent in our body's biological processes. An example of organic phosphates are the nucleotide phosphates found in adenosine monophosphate, diphosphate, and triphosphate (AMP, ADP, and ATP, respectively), molecules known for supplying energy for most biological reactions, participating in metabolism, and transferring genetic information.[2] Inorganic phosphates, on the other hand, play a part in bone formation and help maintain bone density.[3] They are normally seen in adult human serum at concentration levels of 0.8-1.45

mM;[4] however, when present in excess, inorganic phosphates can ultimately lead to cardiovascular disease due to vascular calcification and renal failure.[5] Deficient concentration of inorganic phosphate can lead to negative physical effects, like osteomalacia, central nervous system dysfunction, and muscle weakness, amongst many other disorders.[6]

Chloride anions are found within human cells in concentration levels between 5 and 15 mM[1] and are vital to cellular processes, including balancing the charges of transfer proteins and building membrane potential. The natural role and regulation of Cl^- is so critical that there are even chloride transport channels in intracellular organelles and the plasma membrane.[7,8] Mutations of these channels lead to disruption of chloride movement in and out of the cell and have been linked to many genetic diseases, such as cystic fibrosis and the degeneration of muscles.[9]

Because these anions play such important roles within the human body, there is significant interest for their detection and monitoring in physiologically-relevant media. Previous approaches to quantify the concentration of these anions has largely involved dialysis and sample dilution,[10,11] microelectrodes (for measurement within individual cells),[12,13] and imaging using yellow fluorescent proteins.[14,15] These detection methods all have major drawbacks, including difficulty in performing the measurements, pH sensitivity, and low selectivity. Because of these challenges, the use of supramolecular chemistry in this area of research has been of growing interest, as supramolecular host-guest chemistry is well studied and often allows for the ability to fine-tune the electronic and steric properties of the hosts used.[16–19] Recently, attention has shifted to the use of

these small molecule sensors that can reversibly bind and display either a colorimetric or fluorescent response upon anion binding and, finally, can be performed *in vivo*.[2,20–25]

Many research groups have been attempting to conquer the feat of designing and developing a small molecule receptor that displays a selective preference for reversibly binding one targeted anion over others, that is sensitive enough to detect minute concentrations, and that exhibits some form of optoelectronic response to binding.[19,26,27] One example of a small molecule receptor that has shown reversible binding to dihydrogenphosphate ($H_2PO_4^-$) in dimethyl sulfoxide (DMSO) involves a scaffold with a hydrogen-bond donating (bis)thiourea motif (**Figure 1.1a**); however, the receptor has a modest limit of detection, requiring at least ~1 mM concentration of analyte for detection.[28] Another example of promising binding to $H_2PO_4^-$ in acetonitrile includes a redox-based sensor that contains a ferrocene unit in addition to hydrogen-bond (HB) donors (**Figure 1.1b**).[29] The HB units provide initial binding, but after oxidation of ferrocene, the host-guest interactions get further stabilized with the electrostatic interactions of the ferrocenium moieties.[30] In addition to binding strongly with the phosphate anion, it also binds well with fluoride, and, therefore, lacks selectivity. A more recent example of phosphate anion detection comes from Sessler et al., who synthesized

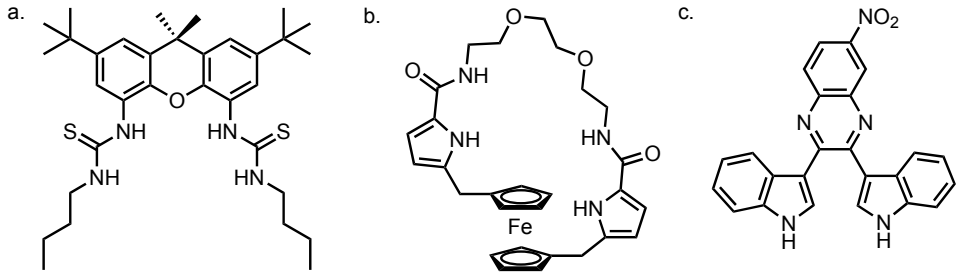

Figure 1.1. Examples from the literature of phosphate receptors containing a) bis-urea motifs, b) hydrogen-bond donors and ferrocene motifs, and c) indoles.

an indole-based receptor that showed promising colorimetric response upon binding (**Figure 1.1c**); however, this receptor lacks water solubility.[31]

Some examples of successful receptors and sensors that are able to detect chloride through non-covalent interactions include: 1) nucleic acid-based hosts that can detect anions over a wide pH range, but they either lack anion specificity because of their ion-pairing recognition mechanism or lack functionality for targeting some cellular compartments;[32–35] 2) chloride-templated rotaxanes that use redox-active interlocked systems to act as electrochemical sensors for anions, although binding only occurred in minimally polar solvents and did not show fully reversible oxidation;[36] 3) foldamers that have the ability to selectively coil around chloride and bind it tightly (albeit, the energy of organization of the helix was only optimal in certain solvents);[37–42] and numerous others.[43–46]

The original, or Gen 1, host-guest receptors to emerge from the Johnson and Haley labs have shown to bind a range of anions through non-covalent, reversible interactions.[47–52] The tunable scaffold includes urea (HB) motifs (**Figure 1.2a**) as well as three functional groups (R, R', and R") that can be synthetically modified to optimize the optoelectronics, selectivity, and binding properties of the receptors. In addition, the conjugated backbone of the arylethynyl scaffold has allowed for some receptors to show a fluorometric response upon binding.[47–49] Finally, all but one of the recent Johnson/Haley receptors have only demonstrated anion binding in organic media or wet organic solvents, which does not necessarily reflect a physiologically-relevant environment.

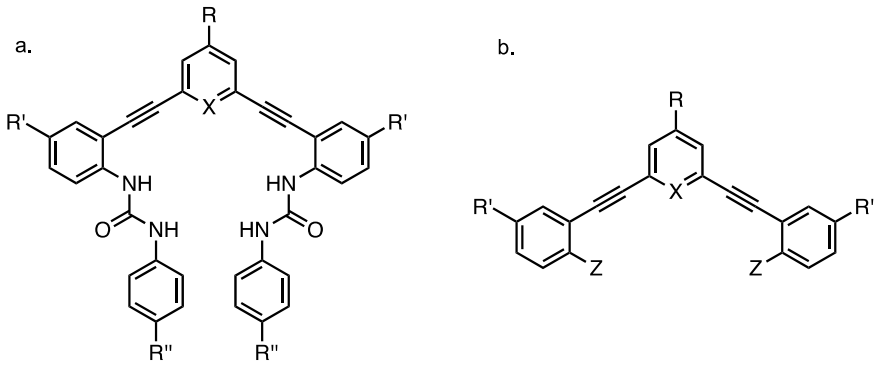

Figure 1.2. Receptor scaffolds for a) Gen 1, hydrogen-bonding where X=N, N^+–R, CH; R= H, Me, F, OMe; R'= H, ^{t}Bu, CF_3, SO_2Me, SO_2CF_3 ; R''= H, NO_2, CF_3, OMe and b) Gen 2, halogen bonding where X=N, CH; R= H, Me, R'= H, ^{t}Bu, CF_3, SO_2Me, SO_2CF_3; Z= H, I, Br. The central aromatic ring containing X is referred to as the core of the receptor, and the ligands attached to the core referred to as arm(s).

The most promising arylethynyl bis-urea scaffold to show chloride binding *in water* was synthesized and studied by Michelle Watt et al. in 2015.[21] The way that solubility was achieved in this case was by protonating the core pyridine nitrogen using 1% TFA in water. The most notable result in this paper was that a "turn-on" fluorescence was reported in water/DMSO mixtures and increased with a higher percentage of water added, peaking at about 80% water.[21] The observed fluorescence was attributed to a mechanism called "aggregation-induced emission" (AIE), that occurs through J-aggregation and is widely used in fluorophores to sense analytes.[53] Although titration studies demonstrated a strong selectivity for chloride, the receptor exhibited weak binding ($K_a \leq 100\ M^{-1}$) in DMSO/H_2O mixtures and the fluorescence was not strong enough for *in vivo* cell studies. Alas, the search for a water-soluble arylethynyl receptor that can selectivly bind to chloride in aqueous media and displays strong fluorescent properties has continued in the Johnson and Haley laboratories.

Firstly, to accomplish the goal of using our supramolecular receptors in physiological environments, we have to optimize the reversible interactions in polar,

protic solvents, like water. Sensing anions in water is a difficult mission for chemists due to the inherently low charge density which is a consequence of the large anion size. This makes the non-covalent electrostatic interactions between anions and receptors less efficient. In addition to this, anions have high free energies of solvation in water;[54] consequently, the receptors must energetically compete with the medium.[55] According to Hunter et al., a promising strategy to achieve aqueous anion detection employs halogen bonding (XB) interactions, which exhibit stronger anion binding in polar, protic solvents than their HB analogs.[56]

Halogen bonding is a type of reversible non-covalent binding interaction that has been gaining interest in the scientific community since it was first reported.[57] The nature of this interaction was defined by IUPAC in 2013[58] as: R—X···Y, where X is a polarizable halogen covalently bound to an R group and Y is an electronically-dense halogen bond acceptor (**Figure 1.3**). This attractive interaction is facilitated by the

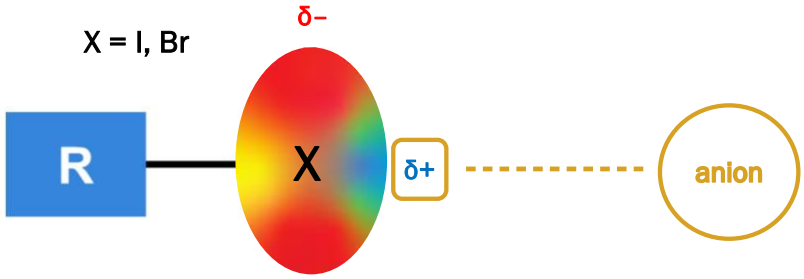

Figure 1.3. A pictogram that represents halogen bonding where blue is associated with low electron density and red is associated with high electron density.

halogen atom's ability to shift electron density with the help of the covalently bonded R group and, thus, reveal an area of positive electrostatic potential, named the σ-hole for its electron deficiency, directly opposite to the R–X σ-bond.[59] Since the σ-hole is located on the opposite side of halogen, X, to the R—X bond, the covalently attached "R" substituent influences the size of the partially positive hole with its electron-withdrawing

character. Conventinal wisdom holds that more withdrawing the substituent, R, the larger the σ-hole and, therefore, the stronger the binding to the XB acceptor. Surrounding the σ-hole is an area of high electronegativity and this feature gives the σ-hole its strong directionality, demonstrating a strong preference for non-covalent bonding at a 180˚ angle from the XB acceptor.[60,61]

New anion receptors, or Gen 2 receptors (**Figure 1.2b**), were developed in the Johnson/Haley lab to utilize halogen bonding. In place of the bis-urea hydrogen binding motif found in Gen 1 receptors, iodine was installed as a halogen bond donor in the binding pocket. To enhance the XB interactions, strong electron-withdrawing functional groups at the R' positions can be used to increase the polarization of XB donors, and consequently, the strength of binding.

Dr. Jessica Lohrman synthesized and characterized the first XB Johnson and Haley receptor (**Figure 1.4a**).[62] It was shown to bind to the halide anion family, as well as produce a "turn-on" fluorescence response; however, the receptor was not sufficiently soluble in water for biological studies. Since the desired applications of this receptor

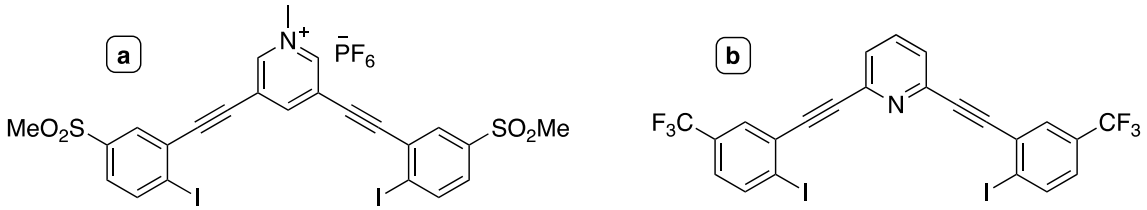

Figure 1.4. a) The first XB receptor informing modifications for b) a hydrosulfide receptor.

require water solubility, modifications to achieve solvation in aqueous media must be made. This receptor inspired another XB receptor, **Figure 1.4b**, for use with the hydrochacogenide guests, mainly hydrosulfide, HS^-, which will be discussed in more detail in Chapter 3.

We then set out to explore what is herein described as Gen 3 receptors (**Figure 1.5**). These receptors were highly influenced by the results of Dr. Lohrman's XB receptor.[62] With the target analyte, chloride, proving to be too small for the binding pocket available in the "two-arm" receptor, more simplified "one-armed" analogues were designed with: the purpose of simplifying/creating a smaller pocket for the receptors, converting their preference of binding chloride over iodide and studying their geometry of binding.

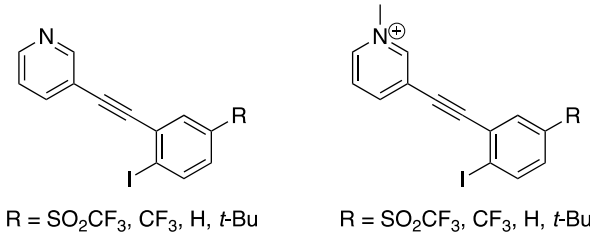

Figure 1.5. Family of One-Armed Receptors studied in Chapter Four

We investigated the *meta* isomer of the mono-dentate receptor and discovered that, in addition to halogen bonding, this receptor also utilizes hydrogen-bonding to non-covalently bind to anionic guests. The small hybrid–part XB, part HB–pocket was able to reverse the preference of binding seen in Gen. 2 receptors, now binding the smaller halides better than the larger (i.e. the target analyte, chloride, exhibited strongest binding). This study also revealed that the strongest contributor to the XB donor's σ-hole is the methyl pyridinium ion located on the core aryl ring and that the tunable functional groups on the XB donor's aryl ring play little part in increasing strength of binding through thorough theoretical, solution- and solid-state experimental structure/property relationship studies.

Finally, in Chapter Five, the fourth generation of Johnson and Haley receptors will be discussed. This chapter features two hybrid receptors (which use both HB and XB to bind anions). One receptor contains a quinoline backbone that enables the molecule to preorganize into what we anticipate being its preferred binding geometry. Its binding pocket consists of a triazole-polarized XB donor as well as multiple HB donors. We anticipate this hybrid receptor to demonstrate an optospectroscopic shift upon binding, allowing anion affinity to be measured by UV-Vis as well as ^{1}H NMR. Notably, depending upon the identity of the HB donors, this molecule could have a preoganized state in either its cationic or neutral form. This allows for the molecule to reduce the entropic energy penalty associated with maintaining a single rigid conformation, like the one associated with binding. The second receptor is a larger version of the one-arm receptors discussed in Chapter Four, bearing a urea HB donor and pyridnium polarized XB donor. This receptor was designed to have a smaller pocket that seen in the bisarylethynyl receptors discussed in Chapter Three, with the aim of flipping the prefernce of the host receptor so that it demonstrates higher bind affinities for the smaller halides over the larger ones.

Finally, yet to be mentioned is the contents of Chapter Two, which features work done on P, N containing heterocyclic fluorophores. This relatively new class of molecule is actually a spin off project, derived from the unexpected product produced when a previous graduate student used a phosphorous containing catalyst on a precursor to one of the DWJ/Haley lab HB receptors. The synthesis as well as the photophysical properties of this molecule are discussed and analyzed in detail in this chapter.

Considering the significance of anions and the important roles they play in biological and environmental systems, the need for monitoring their concentrations in aqueous media cannot be understated. Hydrogen bonding has long been used by nature and synthetic chemists alike for this purpose. And, while halogen bonding had been used in solid state crystallographic engineering for some time, it is only within the last two decades that solution-state XB has come onto the scene as an alternative molecular recognition strategy with particular promise in more competitive, polar solvents compared to that of their HB counterparts. In this short time, the field of halogen bonding has already demonstrated successful applications not just in molecular recognition but also in transmembrane transport, catalysis, template-directed synthesis, molecular motion, and many others niches as well. Despite this rapid expansion of research into halogen bonding, the number of reported receptors is still dwarfed by that of their hydrogen bonding analogues and much research remains to be done. This research is sure to be concomitant to further investigation of other sigma-hole driven interactions, like those seen in chalcogen and pnictogen bonding. There also is much to be learned about how to best use these complementary tools in tandem for even greater selectivity and strength of binding. With so much promise and still much nuance left to elucidate it is certain that the use of halogen bonding for anion binding, as well as a myriad of other applications, will continue to garner increasing attention for years to come.

CHAPTER TWO

AMPLIFICATION OF THE QUANTUM YIELDS OF 2-λ^5-PHOSPHAQUINOLIN-2-ONES THROUGH PHOSPHORUS CENTER MODIFICATION

This chapter includes previously published and co-authored material from Bard, J.P., Bates, H.J., Deng, C.-L., Zakharov, L.N., Johnson, D.W., Haley, M.M. "Amplification of the Quantum Yields of 2-λ^5-Phosphaquinolin-2-ones Through Phosphorus Center Modification." *J. Org. Chem.* **2020**, *85*, 85–91. This work highlights our work on understanding the effects of placing a phenyl group in place of the traditional phenoxy group on the P center of the phosphaquinolinone scaffold. It draws structure-property relationships with both the sumpramolecular and photophysical properties.

2.1 Introduction.

Small molecule fluorophores are used ubiquitously throughout many different fields, including chemical biology, molecular probe development, and materials for industrial and environmental sensing.[1–4] In many of these applications, a fluorophore must exhibit a few characteristics to be considered optimal: large Stokes shift, high brightness, and red-shifted emission. One such example of a molecule that meets these specifications is coumarin (Figure 2.1).[5–14] An impressive number of coumarin-containing compounds have been reported throughout the literature that are collected either from in-lab syntheses or by isolation from natural sources.[15,16] This scaffold has

been the subject of a variety of synthetic modifications, diversification by adding groups onto the backbone, or incorporation of the coumarin system into larger ring networks.[17–19] Through these modifications, a tremendous breadth of understanding upon the structure–activity relations has been developed[20–24] that have guided the design of many useful derivatives, which have emerged for applications in chemosensing and many other areas.[25–31]

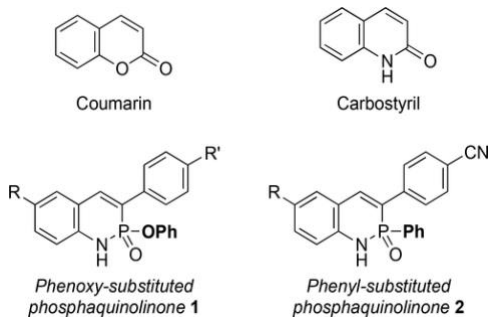

Figure 2.1 Well-studied coumarin and carbostyril scaffolds (top) compared to phosphaquinolinone analogues (bottom).

Alongside the many derivatives of the parent coumarin scaffold, there is the nitrogen-containing structural analogue known as carbostyril (Figure 2.1).[32–37] Though not as widely utilized as coumarin, carbostyril is the subject of many structure–property relationship studies, and it shows promise for use in both pharmaceutical discovery and fluorescence imaging applications.[38,39] These carbostyril analogues expand on the applications of the coumarin family through modifying the lactone core to a lactam. With further alteration of this core, new applications, functionality, and fluorescent properties are expected from this widely used fluorophore.

Recently, we reported a series of phosphorus- and nitrogen-containing (PN) phosphaquinolinone **1** derivatives (Figure 2.1).[40,41] This scaffold, which is one of only a handful of similar heterocycles,[42–52] is also an isostere to carbostyril and coumarin, with

the only difference being the replacement of the lactam carbonyl with an isolobal, chiral phosphorus center. We have performed a variety of structure–property studies that looked at the effects of both acene core modification and substitution at various points on the scaffold.[40,41,53–56] In these studies, it was found that the emission wavelength can be moderately red-shifted through careful substitution of various groups on the backbone, affording significant Stokes shifts and modest quantum yields. On the basis of these design principles, this moiety has recently been implemented in a fluorescent receptor for HSO_4^- in acidic media, showing promise for future applications of this scaffold that take advantage of both its exceptional hydrogen bonding capabilities and its inherent fluorescence.[54] As clearly shown for the coumarin and carbostyril motifs, systematic modification of various structural aspects can lead to very useful derivatives. In our continuing efforts to study the 2-λ^5-phosphaquinolin-2-one skeleton, the next facet that we wanted to explore was the variation of the group attached to the phosphorus center. Disclosed herein is the substitution of a phenyl ring in place of the standard phenoxy upon the phosphorus center, generating a racemic mixture of heterocycle **2** (Figure 2.1). We also hypothesize that this would increase the quantum yield through rigidifying the scaffold. With these modifications, the reported compounds could have greater potential for applications in phosphorus-containing chemosensors and fluorophores, expanding on this pre-existing group of molecules.[57–65]

2.2 Results and Discussion.

The synthesis of **2** starts from key arylethynylaniline intermediate **3**, prepared following previously reported methods.[40] Aniline **3** is then reacted with diphenyl

phenylphosphonite ($PhP(OPh)_2$) in pyridine at 100 °C. Subsequent hydrolysis in THF at 60 °C furnishes phenyl-appended heterocycles **2** in modest to good yields (Scheme 2.1).

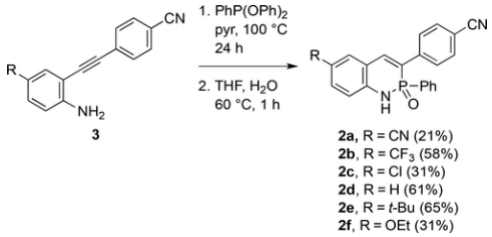

Scheme 2.1 Synthesis of Phosphaquinolinones **2**.

The photophysical properties of **2a**–**2f** in $CHCl_3$ are shown in Figure 2.2 and are compiled in Table 2.1. All derivatives share a common λ_{max} at *ca*. 300 nm, and the lowest energy absorption peaks range from 343 to 381 nm. The absorption coefficients for this scaffold stay within the range of 1.5×10^4 (for **2a**) to $2.2 \times 10^4\ M^{-1}\ cm^{-1}$ (for **2e** and **2f**). The λ_{em} values range from 447 (for **2a**) to 515 nm (for **2f**) with Stokes shifts on the order of 6350–7000 cm^{-1}. Interestingly, the emission spectra of **2** show a *ca*. 20 nm bathochromic shift from those of the analogous congeners of **1**,[40] and the quantum yields of this scaffold show a dramatic improvement, on the order of a 4–5-fold increase in most cases. Brightness values range from 6.84×10^3 (for **2b**) to $1.14 \times 10^4\ M^{-1}\ cm^{-1}$ (for **2a**), which are now on par with several optimized coumarin derivatives.[66]

Fluorescence lifetime measurements were also performed (Figure C.6), and the radiative (k_r) and nonradiative (k_{nr}) decay rate constants were determined. The k_r values range from 0.06 to 0.19 ns^{-1}, and the k_{nr} values vary from 0.06 to 0.18 ns^{-1}, showing either equal rates or a slightly larger k_{nr} in most cases.

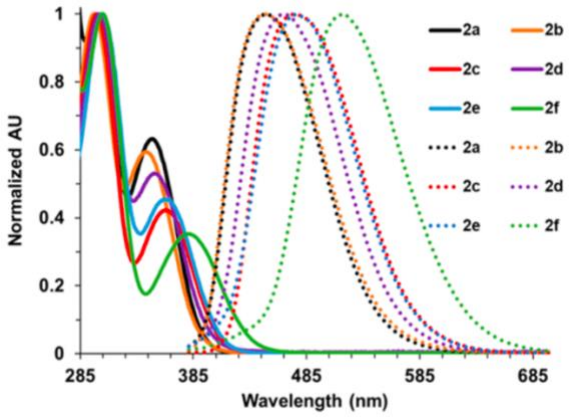

Figure 2.2 Absorption (solid lines) and fluorescne (dotted lines) specta **2** in $CHCl_3$ at 298 K.

Table 2.1 Photophysical properties and HOMO-LUMO Energy Gaps of Heterocycles **2a**

cmpd	λ_{abs} (nm)/ε (M^{-1} cm^{-1})	λ_{em} (nm)/ ϕ (%)	Stokes shift (cm^{-1})	τ^b (ns)	k_r (ns^{-1})	k_n (ns^{-1})	ΔE_{opt} (eV)	ΔE_{DFT} (eV)^c
2a	348/15000	447/76	6360	4.1	0.19	0.06	3.19	4.40
2b	343/18000	449/38	6880	3.5	0.11	0.18	3.18	4.43
2c	360/19000	474/43	6680	4.8	0.09	0.12	3.05	4.23
2d	352/18000	467/50	7000	3.9	0.13	0.13	3.15	4.30
2e	360/22000	475/51	6730	4.2	0.12	0.12	3.04	4.21
2f	381/22000	515/35	6830	6.3	0.06	0.10	2.83	3.90

[a] All values collected in $CHCl_3$. [b] Decay curves fitted using a monoexponential fitting model. [c] Calculated at the PBE0/TZVP level of theory.

These values elucidate a potential explanation for the increased quantum yields when compared to similar values of phosphaquinolinones **1**.[40] For **1**, the k_r values range from 0.10 to 0.30 ns^{-1}, which show similar values, whereas the k_{nr} values vary from 0.30 to 3.0 ns^{-1}, which are substantially faster in most cases. The diminished ratio of k_{nr} to k_r seen for **2** may suggest that the reduced degrees of freedom may indeed be the cause of the increased quantum yields.

To gain further understanding of these experimental results, the frontier orbitals for heterocycles **2** were calculated (Tables 4.1 and C.1–C.7). The narrowest HOMO–LUMO gap is seen for **2f** (3.90 eV), and the largest is for **2a** (4.40 eV). This trend arises because of a higher magnitude of HOMO destabilization than that of the stabilization of the LUMO with more donating substituents (Table C.1). These values also follow a similar trend to the optical gaps (Tables 4.1 or C.1). TD-DFT was then used to examine the S_0 to S_1 transition. It was found that the S_0 to S_1 transition is dominated by the HOMO–LUMO transition (Table C.1). Additionally, the distributions of the HOMOs and LUMOs show a slightly more pronounced separation due to a larger HOMO localization at the phosphorus center (Figure C.4). These observations suggest that π to π^* transitions are dominant, but there may be some intramolecular charge transfer (ICT) occurring in the excited state. The emission of **2** was then examined in solvents of varying polarities (Figures C.7–C.13 and Tables C.11–C.16). In these studies, bathochromatic shifting is observed in every case with more polar solvents. Compound **2f** showed the greatest shifting, ranging from emission wavelengths of 504 to 531 nm and Stokes shifts of 6070 and 7070 cm^{-1} in cyclohexane and acetonitrile, respectively.

The TD–DFT optimized S_1 state near the Franck–Condon geometry of **2f** shows that the dihedral angle between the parent core and appended 4-cyanophenyl substituent becomes smaller compared to the ground state (Figure 4.3). Additionally, the C–C bond connecting them is shortened by *ca*. 0.035 Å. The considerable geometric changes lead to a more conjugated system at the S_1 state, in which the HOMO–LUMO energy gap decreases by 0.9 eV (Figure C.5); thus, the computed emission wavelength of 541 nm is

within the observed emission maxima (Table 4.1). These computational results could further explain the large Stokes shift for this type of PN-heterocycle.

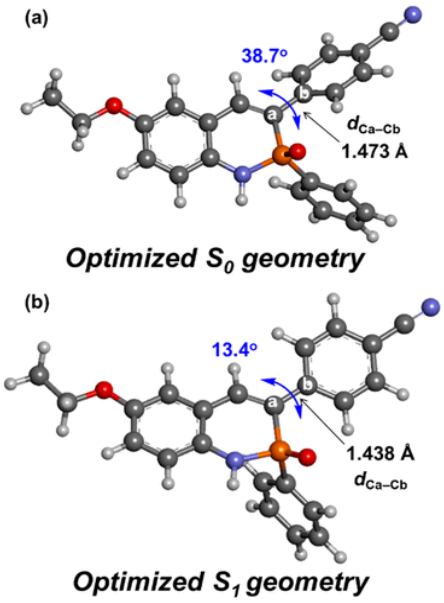

Figure 2.3 Selected bond length and dihedral angle in the optimized S_0 and S_1 structures of **2f** calculated by DFT and TD-DFT methods at the PCM($CHCl_3$)-PBE0/TZVP level of theory, respectively.

In addition to improved fluorescence properties, we were curious to see how phenyl substitution would affect the strength of hydrogen bond dimerization we typically observe for phosphaquinolinones. Variable concentration (VC) NMR experiments were performed in water-saturated $CDCl_3$ to assess the strength of dimerization (Tables 2.2 and C.17–C.21, Figures C.14–C.23w). Heterocycles **2** exhibit dimerization strengths of 22 (for **2e** and **2f**) to 82 M^{-1} (for **2b**). While these values are roughly 70–80% smaller than those measured for the analogous congeners of **1**, the strengths of dimerization for **2** again exceed those of many typical head-to-tail hydrogen bonded dimers.[67] This result suggests that this new entry into the phosphaquinolinone family can still be implemented in supramolecular systems, as found in **1**.[54]

Table 2.2 Dimerization Constants and Energies for **2**

cmpd	K_{dim} (M^{-1})	ΔG_{dim} (kcal mol^{-1})
2a[a]	-	-
2b	82	–2.6
2c	54	–2.3
2d	24	–1.8
2e	22	–1.8
2f	22	–1.8

[a] Not determined because of minimal solubility in H_2O-saturated $CDCl_3$. Values reported with errors less than 15%.

Single crystals suitable for X-ray diffraction were grown by slowly diffusing pentane into a $CHCl_3$ solution of **2f**, and the resultant data are shown in Figures 4.4 and C.1–C.3. The structure of **2f** still features the typical *meso*-dimer between racemates (Figure 2.4a); however, the N···O distance in the dimer of **2f** (2.874 Å) is longer than those of heterocycles **1** (2.768–2.821 Å),[40] which supports the observation that the molecule should form a weaker dimer in the solution-state as well. This weakened hydrogen bonding interaction can potentially be explained by examining the pseudo six-membered ring formed between the monomers. The N···O–P (115.53°), O–P–N (116.66°), and P–N···O (104.57°) angles formed between the participating atoms in the dimer formation show significant deviation from the ideal 120° orientation (Figure 4.4b), likely caused by the large O–P–N–H torsional angle of 55.35° (Figure 2.4c). With an angle so much larger than the analogous angle found in the crystal structures of several derivatives of **1** (*ca.* 30– 40°),[40] there is a less ideal orientation for the two monomers to associate, slightly weakening the interaction overall. By comparing optimized geometries of the *meso*-dimer of **2f** and its −OPh analogue, there are some additional steric clashes in **2f** among the C–

H atoms in the phenyl ring and N–H moieties, according to the noncovalent interactions (NCI) plot (Figure C.24). Moreover, the natural bond orbital (NBO) analyses predict a total contribution of the $n_O \rightarrow \sigma_{NH}^*$ interactions of 23.1 kcal mol^{-1} for **2f** and 25.0 kcal mol^{-1} for the respective −OPh analogue (Figure C.25). Therefore, the strength of dimerization may decrease to some degree due to the weaker primary hydrogen bonding and extra steric hindrance, in agreement with the observed diminished K_{dim} for **2**.

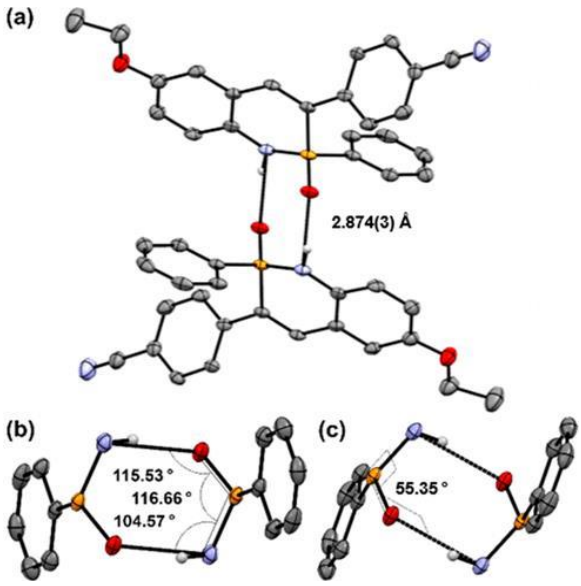

Figure 2.4 a) Characterization PN-heterocycle dimer for **2f** with the O···N distance (Å) shown as well as b) bond angles and c) torsional angles formed within monomers upon dimerization. Ellipsoids drawn at 30% probability.

2.3. Conclusion.

In summary, we have shown the effects of the attachment of a phenyl group on the phosphorus center of the phosphaquinolinone scaffold. This new class of PN-heterocycles not only has large Stokes shift values (up to 7000 cm^{-1}) but also shows a marked 4–5-fold increase in the quantum yield when compared to previously reported phenoxy-substituted compounds. Additionally, this modification retains the strong dimerization strengths of the scaffold in both the solid and solution states. This new

modification deepens the fundamental understanding of the phosphaquinolinone scaffold and allows for further possibilities in the applications of this scaffold as a biologically or industrially relevant fluorophore, like the coumarin and carbostyril scaffolds.

2.4. Experimental Section

General

All air- or water-free reactions were performed under a N_2 atmosphere using Schlenk techniques. Column chromatography was performed using silica gel (240–300 mesh), with solvent systems being referenced to the most abundant solvent. NMR spectra were acquired at room temperature on a Varian Inova 500 instrument (^{1}H: 500 MHz, ^{13}C: 126 MHz, ^{19}F: 471 MHz, ^{31}P: 202 MHz) or a Bruker Avance III HD 500 apparatus equipped with a Prodigy multinuclear cryoprobe (^{1}H: 500 MHz, ^{13}C: 126 MHz). ^{1}H and ^{13}C chemical shifts (δ) are expressed in parts per million (ppm) relative to residual $CHCl_3$ shifts (^{1}H: 7.26 ppm, ^{13}C: 77.16 ppm) or residual DMSO shifts (^{1}H: 2.50 ppm, ^{13}C: 39.52 ppm). ^{31}P and ^{19}F NMR spectra are referenced to 85% H_3PO_4 (δ 0 ppm) and to $CFCl_3$ (δ 0 ppm), respectively, as the external standards. UV–vis spectra were recorded using an Agilent Technologies Cary 60 UV–vis spectrophotometer in HPLC-grade $CHCl_3$. Fluorescence emission spectra were recorded using a Horiba Jobin Yvon FluoroMax-4 fluorimeter exciting at 365 nm. Quantum yields (φ) were determined through a comparison of the emission and absorption intensities of the analyte to that of a 0.1 M H_2SO_4/quinine sulfate solution.[68] Fluorescence lifetime measurements were recorded using a Horiba FluoroHub Single Photon Counting Controller with a TemPro Fluorescence Lifetime System attachment. High-resolution mass spectra (HRMS) were

recorded on a Waters XEVO G2-XS mass spectrometer. 2-Ethynylanilines **3a**–**3f**[40] and phenyl diphenylphosphonite ($PhP(OPh)_2$)[69] were prepared as previously described.

General Synthetic Procedure for Phosphaquinolinone 2

2-Ethynylaniline**3** (1.0 equiv.) and $PhP(OPh)_2$ (2.0 equiv.) were dissolved in pyridine (ca. 0.35 M). The vessel was sealed and heated to 100 °C for 24 h in an oil bath. The mixture was then diluted with toluene, and the solvent was removed *in vacuo*. This was repeated three times to remove all residual pyridine. The crude material was dissolved in THF, and *ca*. five drops of water were added. The solution was stirred at 60 °C for 1 h before being dried (Na_2SO_4), filtered, and concentrated *in vacuo*. The crude mixture was then purified by column chromatography on silica gel. Reported yields are given for >95% pure material (by ^{1}H NMR spectroscopy), though subsequent recrystallization from hexanes and CH_2Cl_2 was used to achieve analytically pure material.

Phosphaquinolinone 2a

Compound **2a** was synthesized from **3a** (462 mg, 1.9 mmol, 1 equiv.) and $PhP(OPh)_2$ (1.11 g, 3.8 mmol, 2 equiv.). Column chromatography (1:1 EtOAc:CH_2Cl_2, R_f = 0.20) gave **2a** (149 mg, 21%) as a pale brown solid: mp > 250 °C; ^{1}H NMR (500 MHz, DMSO-d_6) δ 10.28 (d, J = 3.8 Hz, 1H), 8.14 (d, J = 2.0 Hz, 1H), 8.05 (d, J = 30.1 Hz, 1H), 7.82 (*AB*m, J = 8.4 Hz, 4H), 7.81–7.77 (m, 1H), 7.69–7.64 (m, 2H), 7.58–7.51 (m, 1H), 7.49–7.43 (m, 2H), 7.21 (d, J = 8.5 Hz, 1H); ^{13}C{^{1}H} NMR (126 MHz, DMSO-d_6) δ 143.1 (d, J = 3.8 Hz), 140.9 (d, J = 11.7 Hz), 139.3, 135.8, 133.8, 132.6, 132.5 (d, J = 2.7 Hz), 132.4 (d, J = 137.0 Hz), 132.2 (d, J = 10.8 Hz), 128.6 (d, J = 13.2 Hz), 128.1 (d, J = 6.1 Hz), 126.9 (d, J = 115.9 Hz), 119.2, 119.0 (d, J = 9.9 Hz), 118.5, 117.7 (d, J = 8.1

Hz), 110.6, 102.1; $^{31}P\{^{1}H\}$ NMR (202 MHz, DMSO-d_6) δ 7.77; HRMS (ASAP) [M + H]$^+$ calcd for $C_{22}H_{15}N_3OP$ 368.0953, found 368.0977.

Phosphaquinolinone 2b

Compound **2b** was synthesized from **3b** (700 mg, 2.4 mmol, 1 equiv.) and $PhP(OPh)_2$ (1.40 g, 4.8 mmol, 2 equiv.). Recrystallization from CH_2Cl_2 and hexanes gave **2b** (580 mg, 58%) as a yellow solid: mp > 250 °C; ^1H NMR (500 MHz, DMSO-d_6) δ 10.14 (d, J = 4.1 Hz, 1H), 8.16 (d, J = 30.1 Hz, 1H), 8.06 (d, J = 2.2 Hz, 1H), 7.85 (d, J = 8.3 Hz, 2H), 7.80 (d, J = 8.4 Hz, 2H), 7.73–7.63 (m, 3H), 7.53 (td, J = 7.4, 1.5 Hz, 1H), 7.49–7.43 (m, 2H), 7.25 (d, J = 8.5 Hz, 1H); $^{13}C\{^{1}H\}$ NMR (126 MHz, DMSO-d_6) δ 142.5 (d, J = 3.7 Hz), 141.1 (d, J = 12.0 Hz), 139.9, 132.7 (d, J = 136.9 Hz), 132.6, 132.4 (d, J = 2.7 Hz), 132.2 (d, J = 10.7 Hz), 130.5, 128.5 (d, J = 13.2 Hz), 128.1 (d, J = 6.1 Hz), 127.4 (d, J = 3.7 Hz), 126.5 (d, J = 116.3 Hz), 124.5 (q, J = 271.2 Hz), 120.6 (q, J = 32.3 Hz), 118.6 (d, J = 13.0 Hz), 118.5, 117.4 (d, J = 7.9 Hz), 110.5; $^{31}P\{^{1}H\}$ NMR (202 MHz, DMSO-d_6) δ 7.86; ^{19}F NMR (471 MHz, DMSO-d_6) δ −59.92; HRMS (ASAP) [M + H]$^+$ calcd for $C_{22}H_{15}N_2OF_3P$ 411.0874, found 411.0909.

Phosphaquinolinone 2c

Compound **2c** was synthesized from **3c** (645 mg, 2.6 mmol, 1 equiv.) and $PhP(OPh)_2$ (1.5 g, 5.1 mmol, 2 equiv.). Column chromatography (1:1:1 hexanes:EtOAc:CH_2Cl_2, R_f = 0.10) followed by two rounds of recrystallization from CH_2Cl_2 and hexanes gave **2c** (300 mg, 31%) as a yellow solid: mp > 250 °C; ^1H NMR (500 MHz, DMSO-d_6) δ 9.80 (d, J = 4.2 Hz, 1H), 7.99 (d, J = 29.8 Hz, 1H), 7.83 (d, J = 8.4 Hz, 2H), 7.78 (d, J = 8.5 Hz, 2H), 7.73 (d, J = 2.5 Hz, 1H), 7.69–7.57 (m, 2H), 7.56–7.49 (m, 1H), 7.48–7.38 (m, 3H), 7.11

(d, J = 8.7 Hz, 1H); $^{13}C\{^{1}H\}$ NMR (126 MHz, DMSO-d_6) δ 141.3 (d, J = 12.0 Hz), 139.4, 138.3 (d, J = 3.7 Hz), 132.8 (d, J = 136.6 Hz), 132.5, 132.3, 132.2, 130.7, 129.9, 128.5 (d, J = 13.1 Hz), 128.1 (d, J = 6.2 Hz), 126.5 (d, J = 116.8 Hz), 123.6, 120.2 (d, J = 12.6 Hz), 118.6, 118.4 (d, J = 8.1 Hz), 110.3; $^{31}P\{^{1}H\}$ NMR (202 MHz, DMSO-d_6) δ 7.69; HRMS (ASAP) $[M + H]^+$ calcd for $C_{21}H_{15}N_2OPCl$ 377.0611, found 377.0641.

Phosphaquinolinone 2d

Compound **2d** was synthesized from **3d** (151 mg, 0.69 mmol, 1 equiv.) and $PhP(OPh)_2$ (463 mg, 1.4 mmol, 2 equiv.). Column chromatography (1:1:1 hexanes:EtOAc:CH_2Cl_2, R_f = 0.20) gave **2d** (144 mg 61%) as a yellow solid: mp > 250 °C; ^{1}H NMR (500 MHz, $CDCl_3$) δ 7.73 (d, J = 8.1 Hz, 2H), 7.66 (d, J = 30.4 Hz, 1H), 7.71–7.66 (m, 2H), 7.54 (d, J = 8.2 Hz, 2H), 7.47–7.42 (m, 2H), 7.38–7.32 (m, 3H), 7.06 (t, J = 7.5 Hz, 1H), 6.97 (d, J = 8.0 Hz, 1H), 6.83 (br s, 1H); $^{13}C\{^{1}H\}$ NMR (126 MHz, $CDCl_3$) δ 141.5 (d, J = 11.8 Hz), 141.0 (d, J = 3.0 Hz), 138.8 (d, J = 4.3 Hz), 132.7 (d, J = 10.8 Hz), 132.6 (d, J = 2.8 Hz), 132.5, 132.2 (d, J = 139.3 Hz), 131.5, 131.2, 128.6 (d, J = 13.8 Hz), 128.4 (d, J = 6.2 Hz), 126.0 (d, J = 119.5 Hz), 121.4, 119.4 (d, J = 12.1 Hz), 118.8, 117.3 (d, J = 7.7 Hz), 111.6; $^{31}P\{^{1}H\}$ NMR (202 MHz, $CDCl_3$) δ 10.52; HRMS (ASAP) $[M + H]^+$ calcd for $C_{21}H_{16}N_2OP$ 343.1000, found 343.1030.

Phosphaquinolinone 2e

Compound **2e** was synthesized from **3e** (549 mg, 2.0 mmol, 1 equiv.) and $PhP(OPh)_2$ (1.3 g, 4.0 mmol, 2 equiv.). Column chromatography (1:1:1 EtOAc:CH_2Cl_2, R_f = 0.25) gave **2e** (520 mg, 65%) as a yellow solid: mp > 250 °C; ^{1}H NMR (500 MHz, $CDCl_3$) δ 7.73 (d, J = 8.0 Hz, 2H), 7.72–7.67 (m, 2H), 7.68 (d, J = 30.3 Hz, 1H), 7.53 (d, J = 8.1 Hz, 2H),

7.48– 7.39 (m, 3H), 7.37–7.32 (m, 2H), 6.90 (d, J = 8.4 Hz, 1H), 6.48 (br s, 1H), 1.35 (s, 9H); $^{13}C\{^{1}H\}$ NMR (126 MHz, $CDCl_3$) δ 144.4, 141.7 (d, J = 12.1 Hz), 141.5, 136.4, 132.7 (d, J = 10.8 Hz), 132.5, 132.5, 132.4 (d, J = 139.2 Hz), 129.1, 128.5 (d, J = 13.6 Hz), 128.4 (d, J = 6.4 Hz), 127.6, 125.8 (d, J = 119.9 Hz), 119.0, 118.9 (d, J = 8.4 Hz), 116.9 (d, J = 7.3 Hz), 111.4, 34.4, 31.5; $^{31}P\{^{1}H\}$ NMR (202 MHz, $CDCl_3$) δ 10.44; HRMS (ASAP) $[M + H]^+$ calcd for $C_{25}H_{24}N_2OP$ 399.1628, found 399.1629.

Phosphaquinolinone 2f

Compound **2f** was synthesized from **3f** (430 mg, 1.7 mmol, 1 equiv.) and $PhP(OPh)_2$ (969 g, 3.3 mmol, 2 equiv.). Column chromatography (1:1:1 hexanes:EtOAc:CH_2Cl_2, R_f = 0.25) gave **2f** (200 mg, 31%) as a pale yellow solid: mp > 250 °C; ^{1}H NMR (500 MHz, $CDCl_3$) δ 7.73–7.65 (m, 2H), 7.71 (d, J = 8.6 Hz, 2H), 7.59 (d, J = 30.4 Hz, 1H), 7.53 (d, J = 8.2 Hz, 2H), 7.47–7.42 (m, 1H), 7.37–7.31 (m, 2H), 6.98–6.93 (m, 2H), 6.88 (d, J = 8.5 Hz, 1H), 6.60 (br s, 1H), 4.04 (q, J = 7.0 Hz, 2H), 1.43 (t, J = 7.0 Hz, 3H); $^{13}C\{^{1}H\}$ NMR (126 MHz, $CDCl_3$) δ 153.5, 141.6 (d, J = 12.0 Hz), 140.7, 132.8 (d, J = 10.7 Hz), 132.7, 132.6 (d, J = 3.0 Hz), 132.5, 132.1 (d, J = 140.4 Hz), 128.5 (d, J = 13.8 Hz), 128.4 (d, J = 6.4 Hz), 126.7 (d, J = 119.9 Hz), 119.9, 119.8 (d, J = 11.8 Hz), 118.8, 118.2 (d, J = 7.7 Hz), 114.8, 111.5, 64.3, 15.0; $^{31}P\{^{1}H\}$ NMR (202 MHz, $CDCl_3$) δ 10.51; HRMS (ASAP) $[M + H]^+$ calcd for $C_{23}H_{20}N_2O_2P$ 387.1261, found 387.1283.

CHAPTER THREE
TOWARDS THE MOLECULAR RECOGNITION OF THE HYDROSULFIDE AND CHLROIDE ANIONS WITH AN ARYL ETHYNYL RECEPTOR

3.1. Introduction to DWJ-Haley Lab Receptors and Halogen Binding.

Research groups at the University of Oregon have been collaborating to synthesize supramolecular receptors for ion recognition for over a decade now.[1–7] Like many in the supramolecular field of host guest chemistry much of our efforts have been focused on anions, which are conventionally thought of as more difficult to bind that their cationic counterparts, due to their relatively high pH sensitivity, powerful solvation energies and lower charge density.[8–10] Most of the receptors out of the DWJ and Haley laboratories were rigid and highly conjugated diethynyl system that not only can bind anions but also have an inherent fluorescence that allows for spectroscopic recognition upon binding. Originally the receptors featured HB donors, with amine and urea functional groups, and were used to bind the halide anions: chloride, bromide and iodide. Eventually, through careful design and several structure-property relationship studies, the binding capabilities of these hosts were expanded to include oxoanions - nitrate, phosphate and perchlorate - as well as hydrochalcogenides - hydrosulfide and hydroselenide.[2,4,11]

While these guests were bound by HB donors with appreciable affinities, competition from similar guest molecules became apparent when attempting to bind them in highly competitive polar solvents like DMSO and water.[6,11,12] As stated earlier in this dissertation (see Chapter I), XB donors have typically demonstrated stronger binding in

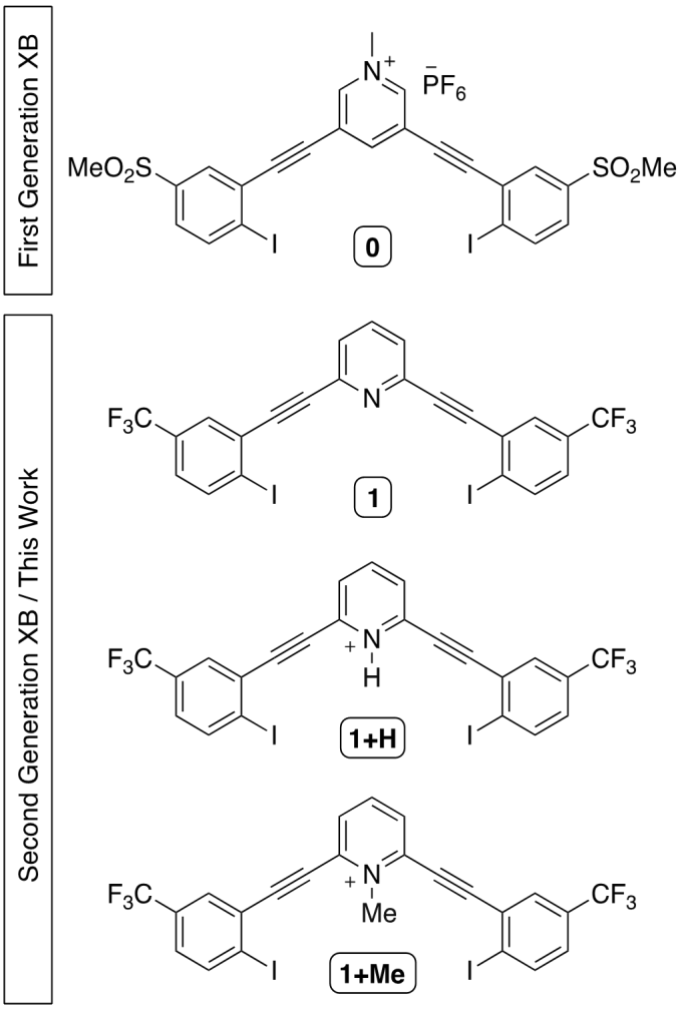

Figure 3.1 – Comparison between (top) the previously published "first generation" DWJ-Haley XB receptor **0** & (bottom) the current generation XB receptor **1** that is the focus of this chapter

more competitive environments when compared to analogous HB donors.[13] With this in mind, Dr. Jess Lohrman synthesized and characterized a XB receptor from the traditional arylethynyl core seen in DWJ-Haley lab receptors (see structure **0** in **Figure 3.1**).[3] This scaffold maintained the highly extended conjugation that gave previous hydrogen bonding analogues of these scaffolds their inherent fluorescence but, in place of the traditional HB donors, two iodine atoms were installed to act as the XB donors. These XB donors were polarized by sulfonyl functional groups, bridging acetylene units and a methylated pyridinium core to yield a sigma hole. When titrated with the halides in DMSO, the receptor **0** demonstrated K_as ranging from 690 to 3600 M^{-1} with the strongest binding affinity being demonstrated for the largest halide, iodide.

Having proven the utility of anion binding with this class of XB receptors, the next step was to investigate whether XB interactions would also be an effective strategy for binding the hydrochalcogenides, initially hydrosulfide (HS^-), in highly polar media,

like those encounters in cells. With this purpose in mind, XB receptor **1** was designed, building upon the design principles mentioned above. The new structure maintained the highly conjugated arylethynyl scaffold, enabling spectroscopic measurement of binding interactions by UV-Vis. Additionally, the central pyridine ring was inverted, giving a 1,2,6- orientation between the two ethynyl arms and the central pyridine nitrogen, as opposed to the original 1,3,5 geometry. This orients the pyridine's lone pair towards the intended internal binding pocket of **1.** Previous work with similar urea-based systems has shown that an internally-directed pyridine core has weakened overall binding to Cl^- and HS^- while concomitantly demonstrating a higher selectivity for HS^- over Cl^-, compared to its benzene ring analog.[2] This is possibly explained as a destabilizing electron-electron repulsion between the pyridine's lone pair and the anionic guest, Cl^-. However, if the guest anion has a polarized hydrogen atom, then this internal lone pair could also serve as a HB acceptor to the anion's HB donor.[14] In a system like the one seen in receptor **1** it is postulated that, with a protic guest, the host could coordinate the guest with bidentate halogen bond donation and a single point of hydrogen bond acceptance at the pyridine core. However, further studies will have to be done to confirm this as the rigid 180 ° directionality of XB donors might hold the guest molecule too far away to experience either attractive or repulsive forces from the lone pair of the pyridine core.

To mitigate this electron repulsion between the pyridine lone pair and to add a hydrogen bond donation site, a charged pyridinium core created by either protonation or methylation (**1+H** and **1+Me** in **Figure 3.1**) would serve as a very strong receptor for the halides. Additionally, the charge of the pyridinium moiety would both serve to further polarize the XB donating iodine atoms through induction, thus creating stronger XB

donors, as well as add a site of HB donor to the central pocket! It should be noted, however, that this would not be an effective strategy for making an HS^- host, as that hydrochalcogenide is a particularly nucleophilic guest. A previous group member, Dr. Hazel Fargher, had documented similar problems with a neutral HB host and hydroselenide (HSe^-) in which the nucleophile attacked one of the acetylene carbons, causing decomposition to begin within minutes of guest addition.[12] The assumption while designing the next generation of XB receptors was that any positively charged host (like **1+H** or **1+Me**) would open itself up to decomposition by the reactive hydrochalcogenides, which would likely result in breaking the aromaticity of the molecule in order to accommodate the addition of HS^-. This vulnerability drove many of the changes seen between receptor **0** and the iterations of receptor **1.** The methane sulfonyl group was exchanged for a trifluoro methyl group, which is less challenging synthetically and won't promote inviting unwanted reactions with the guest (but is otherwise a relatively similar EWG, having a σ_p of 0.54, compared to the 0.72 of SO_2Me – although the lion's share of the polarization in receptor **0** came from the methylate pyridinium).[15] The pyridine ring was inverted, as discussed above, and the protonated or methylated pyridinium functionalities (**1+H** and **1+Me**) were set to be exclusively used with the less reactive halide guests.

3.2 Methods.

The modular nature of the synthesis of receptor **1** makes it easily tunable and synthetically accessible. In the initial attempt to synthesize receptor **1** (Appendix A for Chapter 3 – **Scheme A.2**), a triazene functional group was incorporated on the

trifluoromethyl sidearms via a Sandmeyer reaction;[16] however, an alternative synthetic path was required because the triazene moiety produced an impurity which made isolation of the final product impractical. To avoid this impurity, **Scheme 3.1** was developed, wherein the aniline side arms were left unprotected, completely side stepping the reaction required to append the triazene species, and still furnishing the final product. To start, 4-trifluormethylaniline is iodinated under acidic conditions to create 2-iodo-1-methyl-4-(trifluoromethyl) benzene, **2**, in very good yield. Afterwards, a Sonogashira cross-coupling with trimethylsilyl acetylene (TMSA) provides the trimethylsilyl-protected ethynyl aniline **3**.[3,17,18] This was subsequently deprotected with a basic workup to afford the respective terminal acetylene that is immediately subjected to a second Sonogashira cross coupling with 2, 6-dibromopyridine, at a 2.5:1 molar ratio, to obtain the dianiline **4**.[19] After being purified *via* silica gel flash column chromatography followed by recrystallization, the final step is a variant on the Sandmeyer reaction which

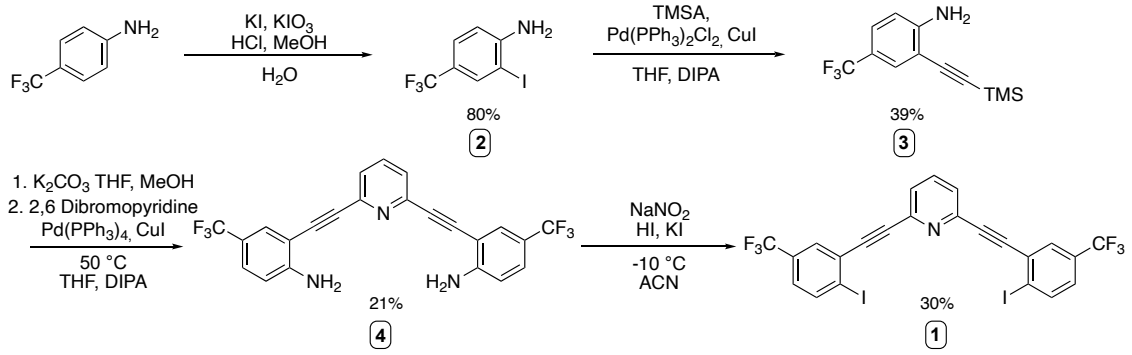

Scheme 3.1 – Synthetic route to access second generation DWJ-Haley XB anion receptor **1**

cleaves the amine and installs two iodines inside the binding pocket. The final receptor is purified through recrystallizations and a series of plugs to give **1** in 30% yields.[3] This reaction pathway not only avoids the aforementioned impurities, but it also removes the low-yielding protection step altogether.

3.3 Results and Discussion.

To corroborate the identity of the scaffold and give valuable information about solid-state host-guest interactions, crystals of **1** suitable for x-ray crystallography were obtained *via* slow evaporation of a concentrated solution of **1** and TBACl in dichloromethane (DCM) (**Figure 3.2**). The C(I) bond lengths fell around a normal range of 2.100 or 2.0092 Å and all aryl protons demonstrated a C(H) bond length ranging from 0.949 to 0.951 Å. The receptor can be seen in its W-conformation, with the XB donors directed outside of the intended binding pocket. Interestingly, in place of the desired Cl^- guest, a molecule of DCM was bound in a 2:1 host:DCM ratio. The W-conformation adopted by the host is likely due to the size of the DCM molecule. This geometry allows for C-H groups meta to the XB donor to coordinate with the Cl atoms of the DCM (at C(H)-Cl distances of 3.779 Å and 3.769 Å). Notably, one of the C-H groups of the DCM can be seen interacting with the internal pyridine nitrogen (C(H) ⋯ N distance = 3.248 Å) of the host molecule, perhaps supporting some of the earlier speculation on the benefits of having a lone pair in the pocket of the host. Finally, a third C-H HB, from a second host receptor, also coordinates to one of the guest's Cls (C(H)-Cl = 3.678 Å) to complete multidentate binding of DCM in a 2:1 host-guest complex. Contrary to what

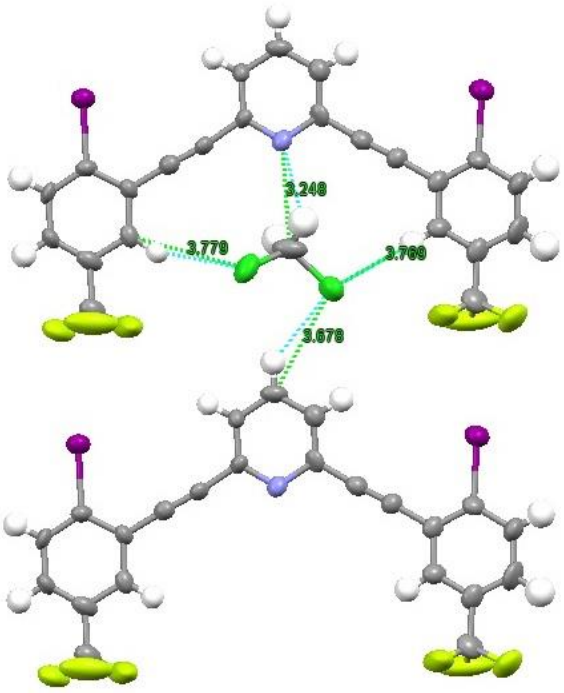

Figure 3.2: Crystallographic data of receptor **1** binding DCM

was expected or intended, the coordination of the guest with **1** occurs *via* HBing rather than XBing. This result served to emphasize the challenge of predicting binding geometry and although it is hard to say for certain whether a smaller guest, capable of more energetically favorable interactions, would persuade the receptor to adopt the intended U-shaped conformation, it is abundantly clear that the DCM molecule is too large for such a geometry.

To build upon the initial host-guest interactions seen with receptor **1** in the solid-state as well as previous success demonstrated by previous DWJ-Haley HB receptors, initial investigations into the binding nature of this host in solution were undertaken. Cl^- was chosen as the first guest to be tested because these anions are relatively similar in size (Cl^- having an ionic radius of 1.81 Å relatively the 1.84 Å of S^{-2}) but Cl^- is far less volatile, dangerous, and difficult to work with than HS^-. These were carried out with tetrabutylammonium chloride (TBACl) as a Cl^- source in chloroform, a non-competitive solvent (λ cutoff < 245 nm). $CHCl_3$ has a relatively low dielectric constant, ε =4.8, in comparison to water, where ε = 80.4, which solvates charges, but not large organic host receptors, especially well.[20] As mentioned before, this is one of the greatest challenges associated with anion binding in aqueous environments. Consequently, the non-

competitive nature of $CHCl_3$ mitigated the likelihood that weak binding interactions will be out competed by solvent interactions and therefore can be observed. There are a number of ways in which binding data can be obtained so that binding strength can be calculated; these include isothermal titration calorimetry (ITC), UV-Vis, Fluorescence, potentiometric or NMR spectroscopy titration data. ^{1}H, and ^{19}F NMR titrations were tested as possible routes for determining the association constant of this receptor (**1**); however, none of these NMR active atoms played a direct enough role in coordination of the guest during the solution state binding event to track anion binding. As a result, titrations were performed using UV-Vis spectroscopy instead (**Figure 3.3a)**. These allowed for the generation of an isotherm which plots the relative absorbance units at the λ max (275 nm & 325 nm)of the host as a function of the concentration of guest relative to the concentration of host (**Figure 3.3b**).[21] With nonlinear regression analysis, utilizing a 1:1 host-guest complexation fitting model, titration isotherms can be used to quantify the binding affinity of the H-G system. Here, BindFit is used to process the raw UV-Vis data collected.[22] In a typical isotherm, the absorbance of the host is expected to increase for a period before binding saturation is seen, indicating saturation of the host receptor. In the isotherm of receptor **1**, no leveling off is seen, indicating weak to negligible binding. This was supported by a highly variable association constant measuring anywhere in the range of $0.3 - 6.7 \times 10^3\ M^{-1}$.

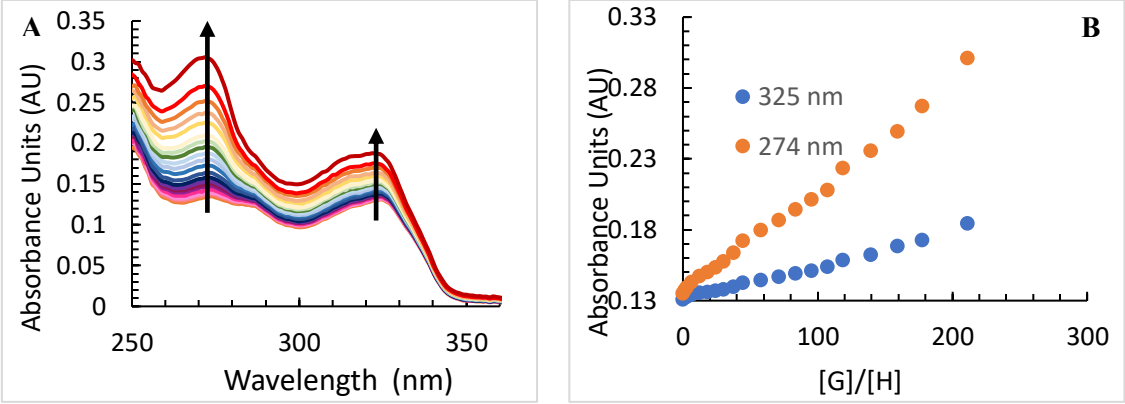

Figure 3.3 – (a) Absorbance data & (b) binding isotherm for host **1** with TBACl in $CHCl_3$.

From both the work of Dr. Jess Lohrman with receptor **0** and similar receptors from Dr. Orion Berryman, it has been demonstrated that the bisarylethynyl receptor's pocket size is preferential to the iodide anion due to its larger size, which is likely a contributing factor to the limited interaction between chloride and the neutral host, and might explain the weak binding discussed above.[3,23] Restrictive 180° XB angles do not allow binding in the internal pocket close. For chloride to be coordinated to both XB donors, it would have to fit further inside the pocket which would pull it off course of the sigma hole and hit the electron belt instead. Another possible explanation for the apparent weak binding of receptor **1** is the neutral charge of the molecule. The neutral analog of receptor **1** was a relatively ineffective host compared to that of the hypothetical cationic versions of the receptor, **1+H and 1+Me**.[3] A final consideration for this point is the internal facing pyridine core – which, when neutral, selects for HS^- over Cl^-, but has been shown to decrease binding strength for both.[2]

When designing the receptor at the center of this chapter, **1**, the main guest of interest was HS^-. But the other guest of interest hadn't been forgotten; it was hypothesized that the pyridinium core (seen in **1+H** and **1+Me**) would enhance Cl^-

binding. The cationic core holds much promise in the form of an additional HB donor as well as in the generation of a charged species, with attractive electrostatics for the anionic guests. To this end, several protonation experiments were carried out in DCM. Initial protonation attempts were carried out by introducing the host to a variety of acids. It wasn't until using triflic acid (CF_3SO_3H) that precipitate of the supposed pyridinium was able to be collected. Many of the initial acids likely failed because they are less effective in organic solvents, having higher pKas than those reported in water because of their relatively unstable conjugate bases. Triflic acid, having a sufficiently charge disperse conjugate base, was finally able to protonate the core pyridine (that might look misleadingly basic in organic conditions, considering it also has a decent ability to delocalize charge). When an ^1H NMR spectrum was taken of the protonated compound in acetone-*d6* it did demonstrate an expected shift in all of the resonance environments. However, it was notable that there was not an easily identifiable peak associated with the proton assumed to be on the pyridine. This is likely due to exchange with the solvent under the highly acidic conditions in which the NMR spectrum was taken. This could potentially be resolved by taking the NMR spectrum in another solvent, at a lower temperature, in an acidic solvent system (like 1% TFA acetone-*d6* or similar) or with a shorter time delay between collection. But regardless of how we choose to trouble shoot characterizing that receptor, it quickly became clear that the protonated **1+H** was too labile to be applied in practical settings for anion recognition (**1+Me** presents a more promising target, with regards to stability of the host as it would not be directly influenced as easily by changing pH).

Due to its high acidity, the receptor **1+H** proved unstable in water, deprotonating upon any aqueous treatment. This means that, while this receptor would likely show stronger binding when protonated, the pyridinium is too acidic to be used successfully in the more competitive polar environments it was designed to compete in. Though it should be noted that despite its water instability, it is still likely possible to do titrations with the protonated receptor in organic solvents. Thus, knowing that this wouldn't be a newly developed small molecule fluorescent probe able to compete with water for anions, as we had wanted, we decided to forgo further characterization (like fluorescent studies) and instead move on to a new hybrid host design.

If the next generation of receptors are to be successful in the aim of getting into water and cells, then they should abide (as closely as possible) to Lipinski's rule of five, which is a set of parameters intended to assess how likely a small molecule is to be cell permeable.[24] These parameters include having a molecular mass of less than 500 amu, as well as limiting the amount of HB donors and acceptors to less than 5 and 10, respectively. Future chapters in this thesis feature receptors which do a much better job following these general rules of thumb, with the hope of find more success not only in aqueous environment, but *in vivo* applications specifically. This was accomplished by abandoning the two-arm structure for a more compact, lighter "one arm" motif and leverage the best parts of both HB and XB systems by using both in tandem! While initial experiments with receptors **1** and **1+H** seemed less successful than we might have hoped there is still much promise to be found in the **1+Me** scaffold. The methylated pyridinium could serve to further polarize the XB donors, add an electrostatic attraction to all anion guests, as well as append 3 additional C-H HB donors to the inside of the pocket. This

final change might also serve to shrink the effective size of pocket, potentially switching the preference for larger halides seen in receptor **0**.

3.4. Conclusion.

In conclusion, a new fluorescent aryl ethynyl receptor with XB capabilities was synthesized and characterized. Characterizations were carried out via ^{1}H NMR, ^{19}F NMR, UV-vis spectroscopy, and X-Ray crystallography. Preliminary data suggests that the neutral host does not strongly bind chloride, even in a non-competitive solvent, which bodes ill for its ability to bind the more reactive HS^- guest. This supports data previously seen by XB hosts out of the DWJ and Haley lab, which showed a preference for larger halides.[3] While there have been many efficient and clever Cl^- receptors published since Park and Simmons' first host in 1968, few of them are both fluorescent and sufficiently strong enough to bind chloride in water.[19,25] Continued efforts shall be made in optimizing this receptor to close the gap between anion and cation binding in aqueous media. This remains incredibly important for applications *in vivo*, where the high solvation energy of anions make them significantly more difficult to track and quantify than their positively charged counterparts.

Bridge to Chapter IV.

The next generation of XB receptors, alluded to in the above paragraphs, are the focus of the next two Chapters, IV and V, which explore a derivatized family of one-armed arylethynyl hybrid, or XB and HB, receptors and then another new tridentate hybrid receptor, respectively. The family of one-armed receptors were intended to

elucidate some of the more fundamental preferences for mixed HB and XB systems with a simpler host and, hopefully, so more promise for *in vivo* studies. This is in part motivated by the difficulty our colleague Dr. Jess Lohrman experienced trying to solubilize the receptor into polar environments, making it nonviable for work in cells, as well as the weak bind that the large flexible bis-arylethynyl XB host scaffold, **0**, displayed towards Cl^-, given its huge pocket.[3] Additionally, in her receptor, chloride was bound out of pocket, something thought to be due to the scaffold's large pocket size. Thus, new receptors (in Chapters 4 and 5) were tailor-made with smaller pockets, to increase the receptors' affinity towards Cl^- anion recognition.

CHAPTER FOUR

SUBSTITUENT EFFECTS IN A SERIES OF COMPACT ARYLETHNYL "MONODENTATE" HALOGEN BONDING HOSTS FOR ANION

This chapter includes previously published and co-authored material from T. P. de Faria, H. J. Bates, A. S. Trom, F. I. D. Longnight, M. P. Miller, L. N. Zakharov, M. M. Haley & D. W. Johnson, *manuscript in prep*. This work investigates the structural changes, made by modification of tunable groups with various EWGs and EDGs, to assess the influence of substituent effects in neutral versus charged receptors in this series. The results of the comparison of experimental binding trends and theoretical calculations will heavily influence future designs of small-molecule, halogen-bonding receptors from this scaffold family to bind to smaller anions more successfully and selectively in polar solvents.

4.1. Introduction.

Anions are ubiquitous in nature—they play especially critical roles within our cells as well as in our external environment. Some of the most fundamental anions, the halides (I^-, Br^-, Cl^-, F^-), are crucial to human health and well-being. Examples include the misregulation of chloride in cells associated with disease states like cystic fibrosis[1] and iodine deficiency causing thyroid disease and goiter formation.[2] Despite their significance, non-covalent binding of these anions still proves to be difficult for several reasons, but most notably because the entire halide family shares the same spherical shape, similar basicities for the three heaviest halides, and only slightly increasing sizes, leaving little margin for error when designing a suitable selective binding pocket.

Additionally, anions are well-solvated, particularly by the polar, protic media that make up many of the more interesting applications of these systems, *in vivo* sensing, for example.[3-5] In fact, the Hofmeister series illustrates how, especially as halides get smaller, the energy required to free a halide anion from water becomes increasingly costly in energetic terms.[6,7] In spite of these challenges, there have been many supramolecular systems that successfully bind anions, like chloride, in competitive polar protic solvents.[8-12] Many of these hydrogen bonding hosts feature multi-dentate coordination that seems necessary for these hosts to compete in aqueous media. Further preorganization through macrocyclization often further enhances binding, although can be synthetically challenging and may make cellular uptake and compatibility less likely, per Lipinski's Rules, for *in vivo* cell studies.[13,14]

Recent work in the field of host-guest chemistry has expanded the supramolecular toolset beyond that of traditional hydrogen-bonding (HB) to now also include sigma-hole interactions, like those seen in halogen-[15], chalcogen-[16] and pnictogen-[17] bonding.[18] Previous studies by other groups have shown that halogen-bonding (XB), while often comparable in strength to hydrogen-bonding, tends to be favored in polar protic solvents.[9,19,20] For this reason, our group, among many others, has recently begun investigating halogen bonding as a tool for binding halides and other anions.[21–24] The work we present here was largely influenced by our previously studied bis-aryl-ethynyl or "two-armed" receptors (**Figure 4.1a**), whose pocket size seemed to be too large to accommodate our target anion, chloride.[22]

A crystallographic study showed the "two-arm" receptor changing configurations and binding chloride out of the intended pocket, unlike larger anions like iodide which fit

well. The new studies reported herein focus in on a compact "one-armed" structure (**Figure 4.1b and 4.1c**) that (1) eliminates the pre-determined pocket in hopes to shift binding preference to chloride over iodide and (2) enables the study of small, discreet changes on binding geometry.[25,26]

This paper will also describe the modification of the R substituents and how various electron-withdrawing and -donating groups affect the binding affinity in neutral *vs* charged receptors in this family. These results will allow for a number of observations to be made about the fundamental nature of the halogen bond—something often

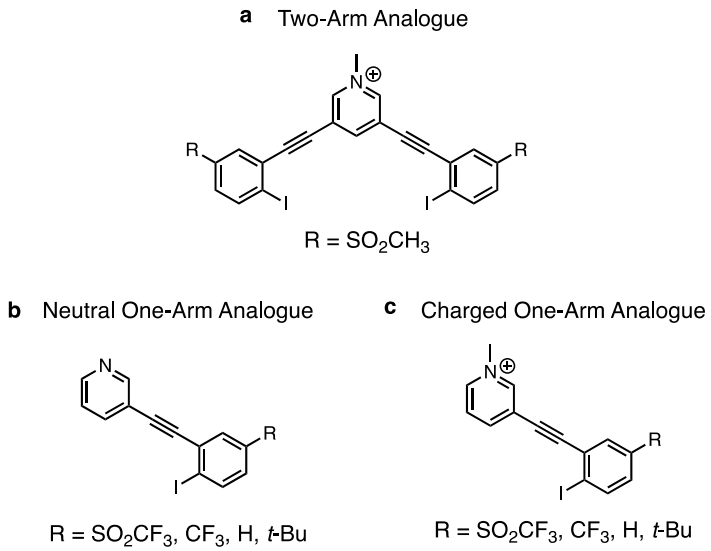

Figure 4.1. Previously studied bis-arylethynyl XB receptor, **a**. Novel "one-armed" neutral, **b**, and charged, **c**, arylethynyl receptors.

reductively characterized as an attractive R–X -- :A interaction (where R is a sufficiently electron withdrawing atom, X is a halide and A is an anion or other Lewis base)—through a structure-property relationship study.[27]

4.2. Results and Discussion.

Electrostatic potential surface (ESP) maps were generated for all potential neutral, **4a-d**, and charged, **5a-d**, host receptors (**Figure 4.2**) to see which synthetic alteration would have the greatest effect on the XB donor's ability to noncovalently bind guests: the

positively charged *N*-methylpyridinium core, or the tunable R groups attached to the "arm" of the receptors. The results of the maps corroborate trends our group has seen in previous computational studies.[22] When looking at the area of partial positivity—quantified and described as $V_{s,max}$—created from the σ-hole of the XB donor, it shows a

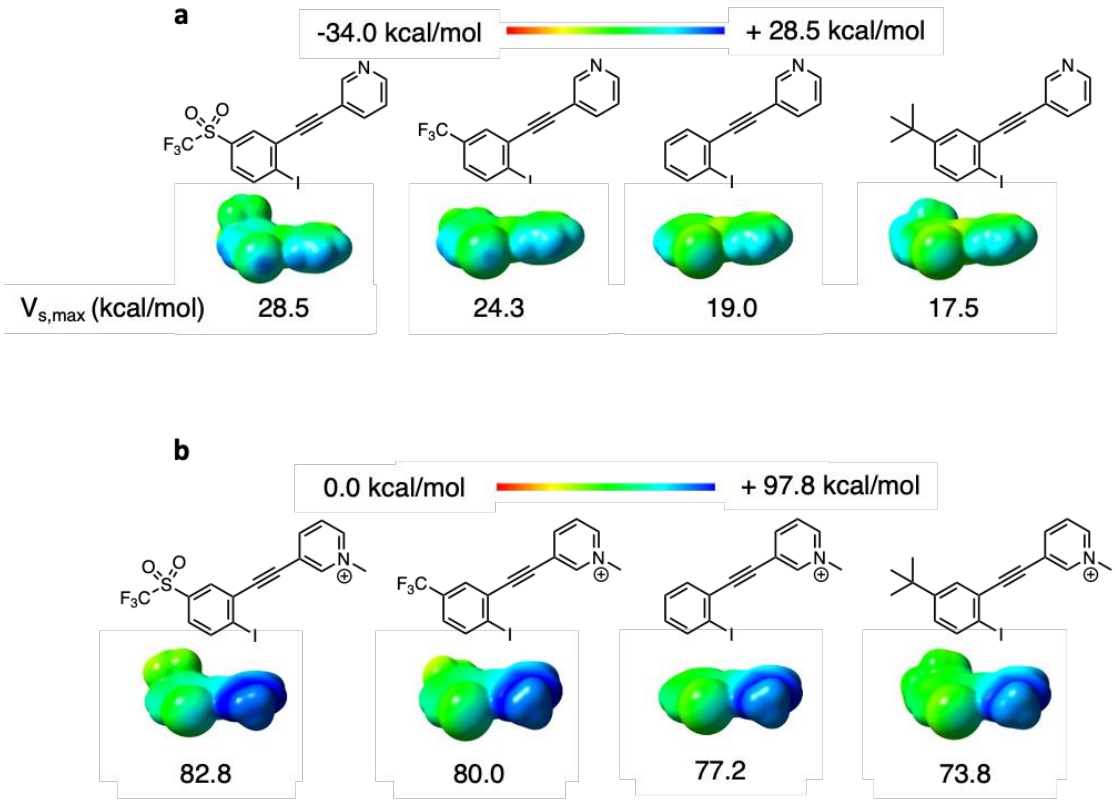

Figure 4.2. ESP maps of the entire family of receptors with the σ-hole values underneath each structure. Neutral structures are in panel **a**, and methylated structures in panel **b**. This figure clearly illustrates the outsized effect the methylated pyridinium unit plays in polarizing our halogen bond donor (compared to the changing ID of the FG para to it).

decrease in magnitude of about 11 kcal/mol as the R-groups *para* to the iodo XB donor become more electron-donating in the neutral pyridyl receptors **4a-d**. In the pyridine-N-Me cationic receptors **5a-d**, the change is similar with a 9 kcal/mol decrease across the series of electron withdrawing/donating R-groups. However, when comparing the neutral receptors with similar σ_p values as their charged

analogues, the $V_{s,max}$ values significantly increase with a ~54-58 kcal/mol difference providing evidence that what contributes more in the XB σ-hole enhancement of these arylethynyl scaffolds is the presence of the cationic *N*-methylpyridinium core, despite its distance from the XB donor.

To further verify this theoretical trend, all the scaffolds were synthesized for later solution-state binding studies, according to the modular synthetic path shown in **Scheme 4.1**. The starting aniline with the desired R-group was iodinated using KI

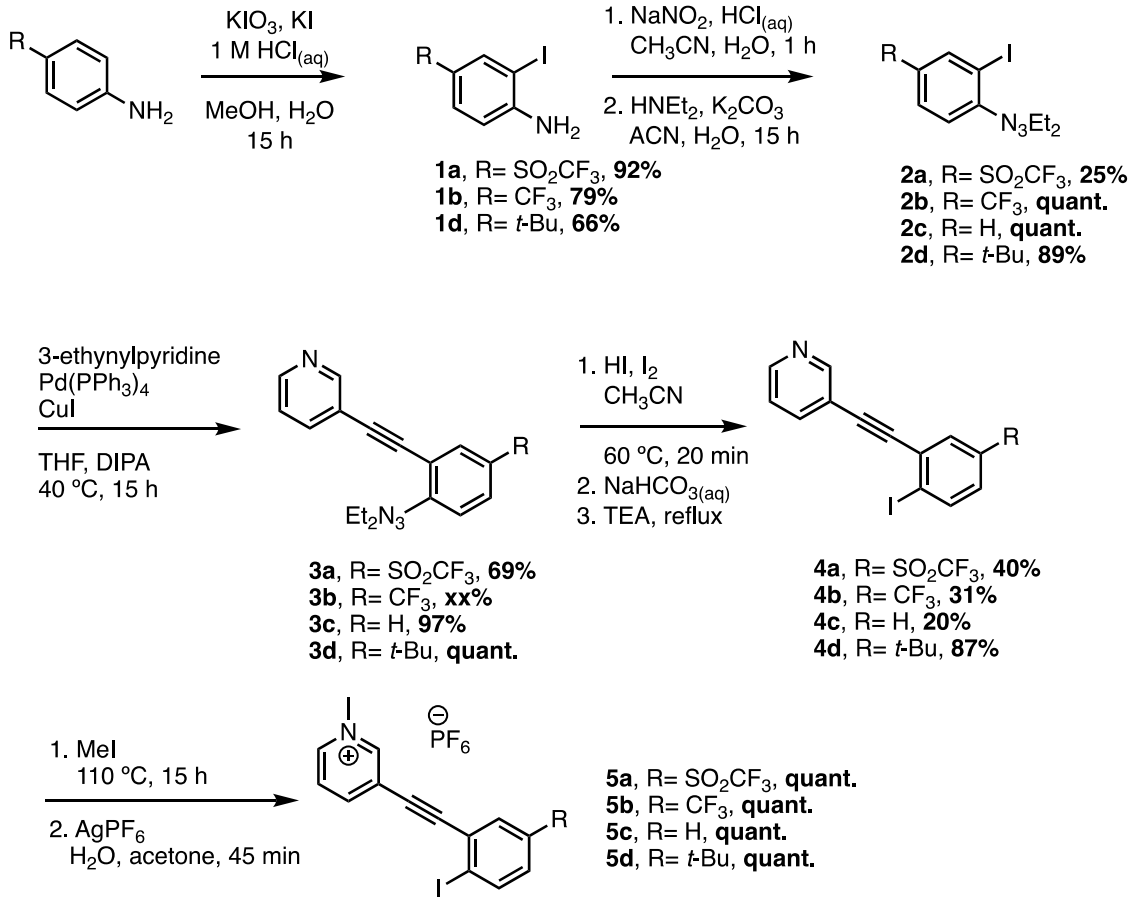

Scheme 4.1. Synthetic pathway and yields for the formation of the neutral, **4a-d**, and charged, **5a-d**, receptors.

and KIO_3 to furnish **1a-d**. Diazotization of the aniline group followed by trapping with Et_2NH afforded triazenes **2a-d**. Next, Sonogashira cross-coupling with 3-ethynylpyridine gave compounds **3a-d**. The triazene group was then transformed

into an iodine, the XB donor chosen for each of our scaffolds, by heating with HI/I_2 to produce neutral hosts **4a-d**. The neutral receptors were transformed into the charged receptors through alkylation using MeI with I^- as the counter ion, **5a-d • I⁻**. To enhance the apparent association constants for these charged receptors, the iodide counterion was then exchanged for the less competitive PF_6^- (**5a-d • PF_6^-**).

The solution-state binding trend seen between our group's previously studied two-arm analogue and the series of halides showed that the preferred binding pocket fit best with the largest anion, iodide;[22] bromide demonstrated the second-strongest affinity and chloride last. To test the hypothesis that the two-arm pocket was too large to preferentially bind chloride over larger anions, ^{1}H NMR titrations were performed with 1 mM solutions of single arm host receptor, **5a • PF_6^-**, and 20-30 mM guest solutions of the tetrabutylammonium salts of chloride, bromide, and iodide in CD_3CN. Association constants (K_a) were determined by tracking proton peaks and fitting the change in chemical shift to a 1:1 binding model using the Bindfit software.[28,29] Receptor **5a • PF_6^-** bound to Cl^-, Br^-, and I^- with K_a values of 137, 104, and 103 M^{-1}, respectively, demonstrating a modest yet inverse trend seen from our previous two-arm host analogue. This provides evidence that by changing the size of the pocket and reducing the entropic penalty associated with the previous host's pre-organization, it is possible to shift the preference of anionic guest to slightly favor chloride despite the fact that iodide typically features stronger halogen bonding interactions in polar solvents, presumably due to lower solvation energies.[30] The proton peaks that exhibited the largest change in chemical environment helped to elucidate the solution-state binding geometry of the receptors, which matched that of the calculated lowest energy state of the charged receptor (**Figure**

4.2) with the iodine XB donor facing the methylated pyridinium core. In all cases, the two hydrogens active in binding the halide guests are the pyridyl C–H in between the alkyne and the N atom, and one of the C–Hs of the pyridinium methyl group (**Figure C1**). A similar geometry was observed in the solid-state crystal data of our analogous bidentate XB host receptor that showed binding with the XB donor twisted out of the too-large pocket and HB participation by the polarized C–Hs on the core and the methyl of the pyridinium. Neutral receptors **4a-d** did not show measurable binding to chloride in acetonitrile, demonstrating that XB donors with σ-holes with $V_{s,max}$ of ~17-29 kcal/mol may not be significantly electron-withdrawn to participate in halogen binding. Charged receptors **5a-d•PF$_6^-$**, and most notably those with lower σ_p values, were still able to bind to chloride in a trend that follows well with their calculated $V_{s,max}$ values (**Table 4.1**).

Table 4.1. Binding constants, in M–1, of charged receptors 5a-d with guest chloride and their calculated sigma-hole values in kJ/mol.

	5a • PF$_6^-$	**5b • PF$_6^-$**	**5c • PF$_6^-$**	**5d • PF$_6^-$**
K_a with Cl^- (M^{-1})	137 ± 5	120 ± 6	98 ± 4	85 ± 2
$V_{s,max}$ (kJ/mol)	82.8	80.0	77.2	73.8

With the binding constants determined, we sought out to better comprehend the receptors' binding sensitivity to chloride through the use of the Hammett relationship ($\log(K_a^R/K_a^H)$ vs σ_p) by fitting the K_as to eq 1.

$$\log\frac{K_a^R}{K_a^H} = \rho\sigma_p + \varepsilon \qquad (1)$$

Plotting these values against the σ_p of the R substituents revealed that there is a weak linear response between the K_a and the electron-donating/-withdrawing nature of the substituent (**Figure 4.3**). The equation inset in **Figure 4.3** describes the parameters of

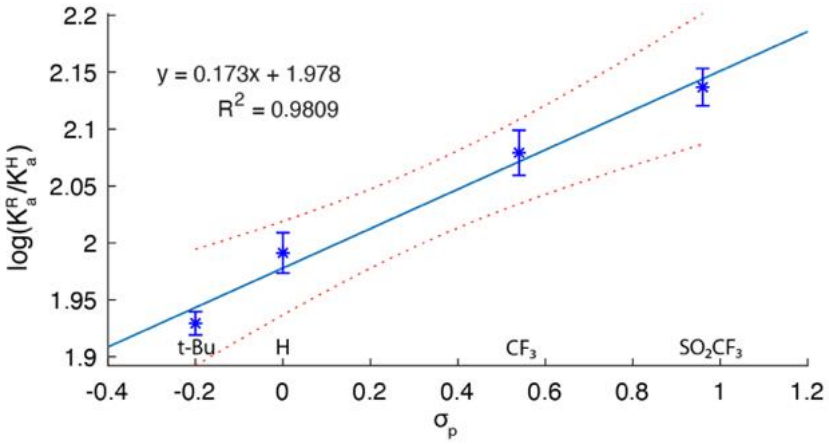

Figure 4.3. Hammett plot between **5a-d** and I^-. The slope of the line indicated that substituents in this receptor has little role in affecting the sensitivity of the halogen-bond donor. The dotted lines represent the 95% confidence interval.

the linear fit, resolved through linear regression. The slope of the line's positive magnitude tells us that chloride binding is favored with more electron-withdrawing *para* R substituents. The value of ρ, 0.173, reveals that the halogen bond in this system is less sensitive to substituent effects compared to the standard, benzoic acid; therefore, the σ_p of the tunable R group is a statistically insignificant predictor of binding sensitivity in the one-armed arylethynyl receptor, further corroborating the hypothesis that the methylpyridinium dominates this family of receptors' binding affinity compared to the *para* R–X's σ_p values. This result is contrary to what we found for CH H-bond donors in related neutral bis-arylethynyl urea scaffolds. The CH hydrogen-bonding motifs in those systems were more susceptible to *para* substituent effects than that of our novel XB receptor with a ρ value of 0.71.[31] It remains to be determined if substituent effects in charged CH receptors would be mitigated by the overall charge of the host, a topic we will address in the future.

After getting a handle on the one-armed XB receptors' binding geometries and properties in solution-state, we set out to study solid-state binding geometries. Crystals suitable for x-ray diffraction were grown of 5a,d•I^- (**Figures 4.4b** and **4.4d**)

from a 2:1 mixture of CH_2Cl_2:acetone via slow evaporation. These structures revealed that the solid-state geometry of binding is similar to what we see in solution-state. Atomic distances calculated in the crystal structures were less than the sum of the van der Waals radii of the guest and the iodine XB donor, the aryl H, and the methyl H. These results indicate supramolecular binding occurs with not only our intentional XB donor, but also with the polarized CHs as H-bond donors.

Table 4.2. XB or HB distances, in Å, of receptors 5a, 5b, and 5d binding to chloride or iodide as calculated from their crystal structures in **Figure 4.4.**

	5a • Cl^-	**5a • I^-**	**5b • I^-**	**5d • I^-**
$C–H_{aryl}$ -- X^- distance (Å)	2.904	3.173	2.928	3.187
$C–H_{me}$ -- X^- distance (Å)	2.833	3.522	3.626	3.558
C–I -- X^- distance (Å)	3.403	3.705	N/A	3.824

When comparing the binding distances in 5a and 5d, both binding I^-, in the solid-state (**Table 4.2**), there is little difference in either of the C–H--I^- distances of the HB donors – about 0.01-0.03 Å. The distance between the XB donor and

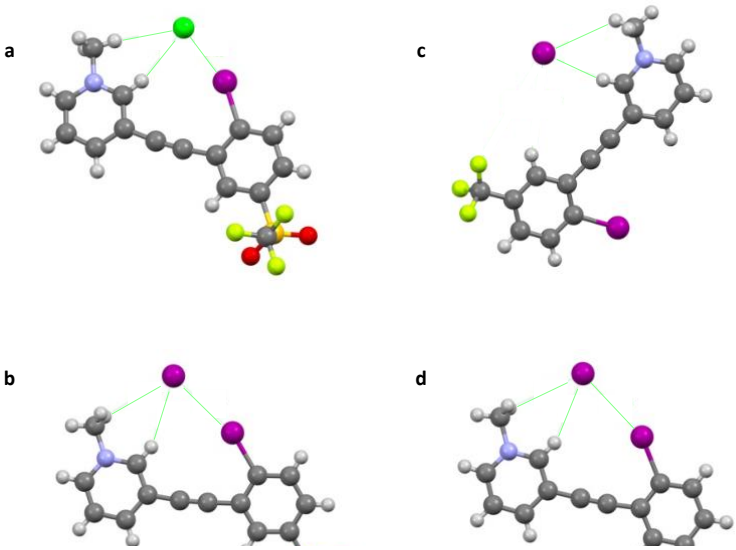

Figure 4.4. Crystals structures of: **a**, **5a** binding to chloride; **b**, **5a** binding to iodide; **c**, **5b** binding to iodide; and **d**, **5d** binding to iodide.

iodide, C–I--X^-, however, shows an order of magnitude greater difference with 0.12 Å. Receptor 5a, with the most electron-withdrawing substituent, showed a closer distance of guest to XB donor than 5d, the receptor with the most electron-donating substituent, suggesting that even in solid-state binding, there is a slight preference for substituents with electron-withdrawing characteristics.

Crystals of 5a•Cl^- were grown from a 1:2 acetone:CH_3CN mixture via evaporation. When comparing the SO_2CF_3 receptor, 5a, binding to the largest guest, I^-, and smallest guest, Cl^-, an even larger shift is observed. The aryl C–H--I^- distance changes by 0.27 Å, the methyl C–H--I^- by 0.69 Å, and the C–H--X^- by 0.30 Å with the guest halide becoming more tightly bound to the receptor with decreasing size of the anion. This trend is also shown subtly in the solution-state binding studies with a stronger K_a observed for chloride over iodide by 27 M^{-1}.

Finally, crystals of 5b•I^- (**Figure 4.4c**) were grown from a mixture of 1:1:1 CH_2Cl_2:acetone:CH_3CN. The crystals in this sample showed solid state binding of iodide with only the HB donors, C–H(aryl and methyl)--I^-, which appeared to hold no trend with the previous bonding distances. The aryl C–H to iodide distance is 2.93 Å, the second shortest aryl C–H to iodide distance of the four crystal structures; however, the methyl C–H to iodide distance is 3.63 Å, the largest methyl C–H to iodide distance. Notably, this structure is showing a binding geometry with the XB donor facing away from the iodide guest and not participating in binding at all. This result begs further investigation to help understand the significance of solvent effects in supramolecular binding through crystal packing of host-guest molecules.

Conclusion

In conclusion, the data reported for this compact series of receptors suggest that when designing XB receptors with an arylethynyl foundation, a charged pyridinium core will provide a greater enhancement to the size and strength of the σ-hole than any adjacent functional groups. This knowledge allows for the purpose of the R group to shift away from that of only a XB enhancer to, instead, a number of other purposes including being a modular handle for other desired applications, such as polymerization, increased water-solubility, various cell compartment targeting functional groups, fluorophores, etc. without disrupting the most important portion of the anion recognition (the charge-polarized XB donor). Additionally, recognizing that the R-group does not contribute significantly to the polarization of the XB donor in these charged hosts allows for future host-guest chemists to dodge the synthetic pitfalls that come with appending extremely electron withdrawing functional groups, like SO_2CF_3. These design principles, in addition to the binding demonstrated by the halogen/hydrogen bonding receptor in a polar solvent, will inform future host receptors for the halide anions.

CHAPTER FIVE

FUTURE RECEPTORS AND FUTURE DIRECTIONS: AN UPDATE ON CURRENT WORK AND WHERE IT IS GOING

5.1. Introduction.

Throughout the previous chapters of this thesis, several host receptors were discussed in detail. Their strengths and weaknesses have been scrutinized to further the understanding of effective host-guest design principles, motivated by the prospect of more selective future hosts. In this chapter, two final hybrid XB-HB scaffolds will be explored for their potential as hosts for the halide anions (**Figure 5.1**). Specifically, both hybrid receptors were designed to have a smaller binding pocket than the receptors discussed in Chapter 3, and thus should show a preference for the smaller Cl^- anion. The deliberate use of XB and HB donors in tandem is also expected to show some of the HB enhanced XB that Berryman and coworkers have discussed in past publications (see red dashed line in **Figure 5.1**).[1] These interactions have been shown to both further strengthen and stabilize the XB donor as well as preorganize the binding pocket into the geometry hypothesized to be best for binding. These hosts (**1** and **2**) also feature functional moieties and strategies developed in previous studies: this includes i) reliable anion

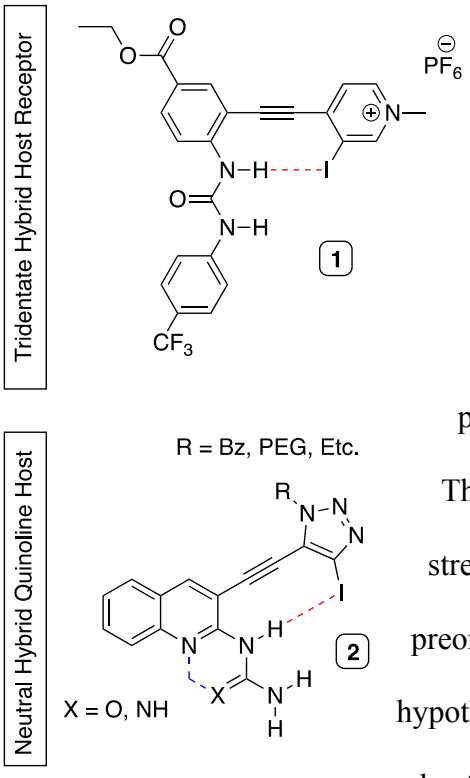

Figure 5.1. The two receptors that will be the focus of this chapter.

recognition motifs used in the early generation of XB and HB hosts developed in the DWJ/Haley laboratories; ii) urea (or related guanidine) HB donors, iii) acetylene bridging units, and iv) XB polarization *via* a pyridinium group (discussed in Chapters 3 and 4) or the well-known iodotriazoles popularized by Beer et al..[2–11] In addition to these motifs, there are design strategies derived from the success of the family of one arm receptors, discussed in Chapter 4. Both receptors **1** and **2** feature XB and HB donors working in tandem to bind anion guests, which produced appreciable affinity for the halide anions in the more polar organic solvent, ACN. Additionally, much like the family of one-armed receptors, the size of the binding pocket of receptors **1** and **2** is smaller compared to the large cavity seen in the earliest generations of the DWJ-Haley XB receptors (reviewed in Chapter 3). Our hypothesis is that the smaller binding pocket of **1** and **2** will invert the preference of the host to preferentially bind Cl^- over the iodine anion, I^-.[6]

The beginning of this chapter will focus on the synthesis and results from receptor **1**. The latter half will focus on the synthesis of receptor **2**, further design principles that inspired the scaffold, and some computational work which compares **2** to the receptors discussed in Chapter 4.

5.2. Synthesis of Tridentate Hybrid Receptor 1.

Tridentate hybrid receptor **1** was synthesized in seven steps (Scheme 5.1). The first five synthetic steps were performed by Thaís de Faria. First, benzocaine is iodinated under acidic conditions to yield intermediate **1.1**. A TMS protected alkyne is then deprotected and installed through Sonogashira cross-coupling of **1.1** with the acetylene. The ethynylaniline precursor **1.2** is then subjected to a second Sonogashira cross-

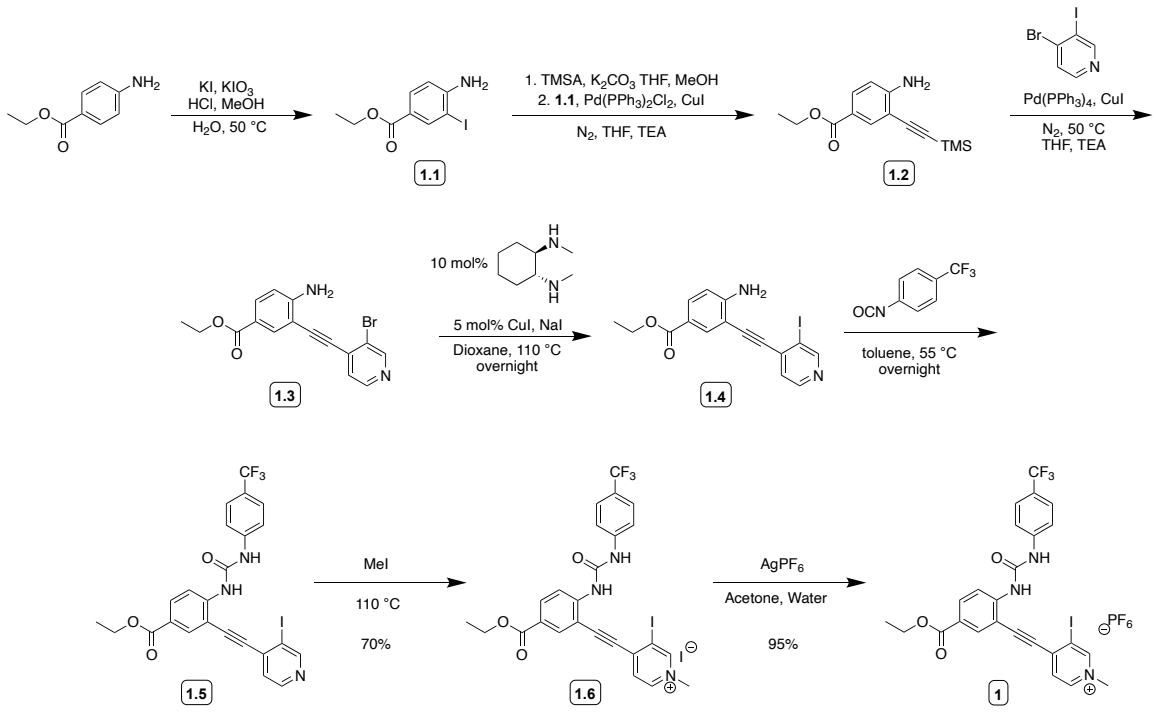

Scheme 5.1. The synthetic route to host receptor **1.**

coupling reaction with 4-bromo-3-iodopyridine to yield **1.3**. The bromine on the pyridine moiety is exchanged for iodine because iodine is known to be a stronger XB donor.[12] Next, a urea HB donor is installed *via* addition of trifluoromethylphenyl isocyanate to the aniline moiety on **1.4**. Neutral receptor **1.5** was refluxed with MeI to yield a pyridinium moiety, which was expected to polarize the XB donor. Finally, **1.6** undergoes a counter ion exchange with $AgPF_6$, to give the final host receptor in good yield (95%).

5.3. Results and Discussion of Tridentate Hybrid Receptor 1.

To test the anion binding ability of **1**, titrations with the halides Cl^-, Br^-, and I^- were performed in 10% DMSO in ACN. Unlike previous generations of XB hosts (like those discussed in Chapter 3) the incorporation of HB donors enabled the binding constant to be measured by ^1H NMR spectroscopy, which concomitantly gives

information about binding geometry and stoichiometry (example shown in **Figure 5.1a**). The downfield chemical shift of the urea protons (starred in **Figure 5.2**) indicates their participation in binding and can be plotted against the concentration of guest (16-42 mM) present, relative to that of host (0.73-1.90 mM), and fitted to 1:1 binding isotherms through non-linear regression to give the association constants reported in **Table 5.1**.[13,14]

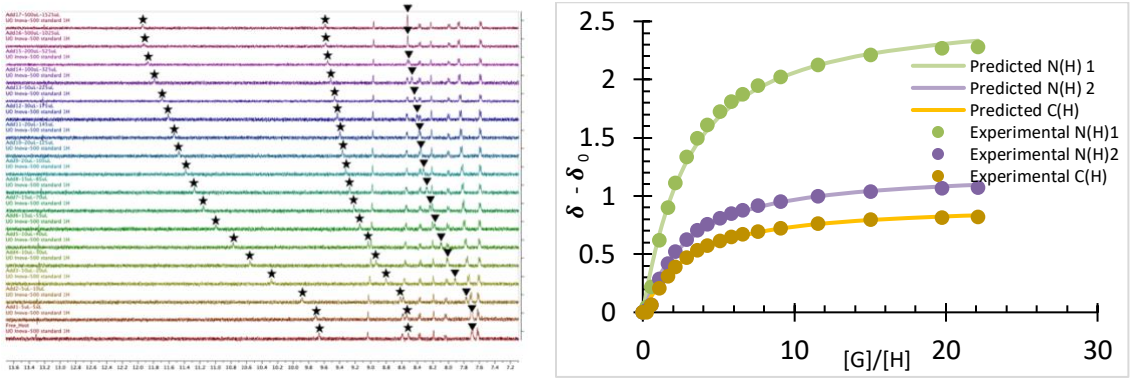

A **B**

Figure 5.2. (a) Representative ^{1}H NMR spectroscopy titrations of the tridentate receptor **1** with TBACl, where the urea protons are starred and CH HB donor is marked with a triangle, and (b) the binding isotherm associated with that titration.

Interestingly a third peak can also be seen shifting over the course of the titration (marked with a triangle in **Figure 5.2**) this is suspected to correspond to the hydrogen in the meta position, relative to our XB donor, acting as a C(H) HB donor. This suggests that, with the smaller anions, the iodine XB donor flips out of pocket and the anionic guest experiences tridentate coordination from exclusively HB donors, rather than the intended hybrid binding.

These binding affinities indicates that the new receptor design successfully inverted the preference of the XB hosts to the smaller halide, Cl^- (the reverse trend demonstrated by the first DWJ-Haley XB receptor reviewed in Chapter 3) as Cl^- shows the strongest affinity for the receptor **1**. This is an important finding because it highlights

that it is possible to tailor binding pocket size in future generations of these hosts to improve guest selectivity. Interestingly, Receptor **1** shows a stronger affinity for Cl^- than for Br^-, indicating that the size of the binding pocket is an important factor in anion binding and this small pocket favored smaller anions.

If the size trend was to continue, it would be expected that then the affinity for I^- would be even weaker. Instead, I^- binding demonstrated a complexity not seen in the titrations with either Cl^- or Br^-. This is likely due to I^- binding with this host differently from the other two halides, as indicated by the appearance of new peaks which growing in up field of the original receptor, suggesting a second species forming in solution. Additionally, when titrated with TBAI, the host peaks shifting only weakly downfield and decreasing in the intensity of the host peaks as more guest is added. Further experiments will be done to discern whether this is due to slow exchange, aggregation, some other complex binding pattern, or decomposition. These include performing diffusion-ordered spectroscopy (DOSY) NMR experiments (to assess whether aggregation is occurring), increasing the delay between scans (to better resolve any slow exchange), and performing VT NMR if both methods fail to elucidate clearer results. Additionally, post titration samples could be condensed and analyzed to verify whether decomposition has occurred. Solid state data from x-ray quality crystals could also help elucidate whether the larger anion is potentially binding out of pocket and/or interacting with more than one host molecule at a time. Finally, it should be noted that this titration of receptor **1** is conducted a fairly polar solvent system, which is relatively competitive, and demonstrates a marked improvement in anion recognition over that observed from data obtained in $CHCl_3$, in the titrations discussed in Chapter 3.

Table 5.1. Titrations done with receptor **1** & the halides at r.t. in ACN 10% DMSO via ^{1}H NMR - *the titration sets obtained for the I^- anion cannot be fitted to a 1:1 binding model with **1** (consistent with the other anions) because there is a complex binding event occurring (See appendix D for more details) it is possible that slow exchange or higher order aggregation is occurring with the I^- anion that was not seen with the Cl^- and Br^- anions.

Halide Anion Guest	K_a (M^{-1})	Ionic Radii (pm)[15]
Cl^-	440	181
Br^-	90	196
I^-	*	220

Synthesis of Quinoline-Based Receptor 2.

The quinoline-based receptor **2** highlights all the design features discussed over the course of this thesis. Its extended π system gives the host (and many of its intermediates) an inherent bright fluorescence opening the door to equal parts beautiful and useful applications, like bio-imaging.[16–18] It is also likely that the binding of this receptor could be tracked by ^{1}H NMR, fluorimetry or UV-Vis spectroscopy. A new motif is seen in the triazole ring, bearing the pendant XB donor. Triazoles are seen throughout host-guest chemistry literature as an effective means of polarizing XB donors while maintaining a charge neutral molecule.[10,19–21] Finally, the nitrogen atom in the quinoline backbone enables the preorganization of the molecule into a hydrogen bonded 6-membered ring (shown in blue in **Figure 5.1**) with the guanidino HB donor group, which would reduce the entropic penalty associated with maintaining the conformation predicted to be most favorable for binding.[22]

The synthesis for receptor **2** (**Scheme 5.2**) began with the protection of the amine functional group on the 2-aminoquinoline by acetyl chloride under basic conditions to afford **2.1**. After this, the lone pair on the nitrogen atom in the amino group coordinated *n*-BuLi for a regioselective iodination in the 3-position of the quinoline intermediate,[23] before then undergoing deprotection by refluxing in acid overnight. 2-Amino 3-

iodoquinoline (intermediate **2.3**) then is subjected to a Sonogashira cross coupling with the selectively deprotected 1,4-bis(trimethylsilyl)butadiyne (**2.3a**). The outermost diyne relative to the quinoline is then iodinated with *n*-iodosuccinimide, which undergoes a click reaction with benzyl azide to furnish the XB triazole ring in **2.6**. Finally, the HB donor is added *via* either a cyanamide or isocyanate addition. Precursors **2.1-2.4** were synthesized and characterized completely and, while the latter intermediates and receptor **2.5-2** were synthesized, they were not fully isolated and characterized due to time constraints. Synthesis of **2** was confirmed by high resolution MS; more details on all of these molecules' properties can be found in Appendix D.

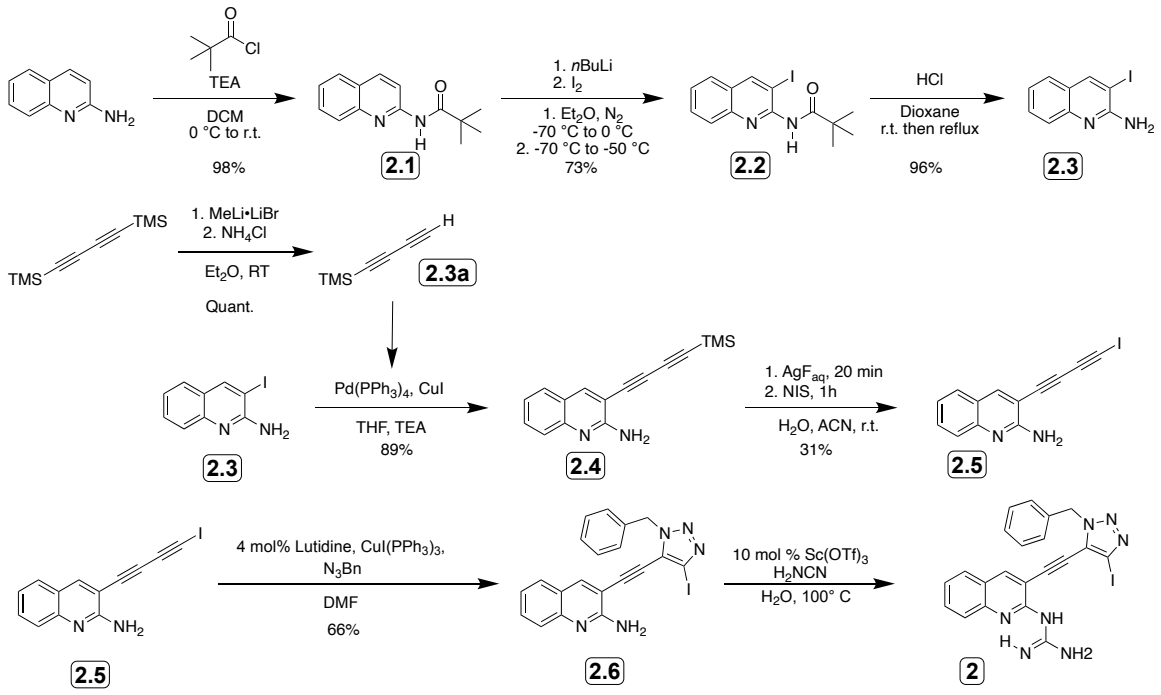

Scheme 5. 2 Synthetic scheme for derivatives of receptor **2** (R = benzyl).

5.5. Computation Work with Library of Receptors.

Although empirical tests were not performed with receptor **2**, computational work by Michael Miller was used to determine the energy levels associated with σ-hole formation in nearly all the receptors

Figure 5.3 Family of one arm receptors discussed in chapter 4 and **Table 5.3**

discussed in this thesis for direct comparisons between the systems. All calculations are done with Gaussian 09, using B97D3 as the level of theory and def2tzvp as the basis set.

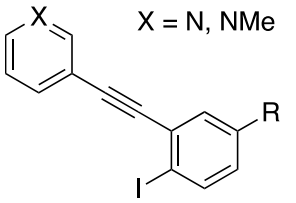

These are listed in **Table 5.3** and a variety of observations can be made from them. First, as established in Chapter 4, it is clear the primary driver behind XB donor polarization in the family of one-armed receptors (easily referenced in **Figure 5.3**) is the methylation of the pyridine moiety; the cationic hosts are always more than 50 kcal/mol stronger than their neutral analogs. This is particularly notable because it suggests that the IUPAC definition of the XB interaction (discussed in detail in Chapter 1) might be biasing host guest chemists to ascribe an undue significance to place EWG groups as near as possible to the XB donor. In the family of one arm hosts the nearest EWG (the pendant R-groups listed in **Table 5.3**) are much less effective at forming the σ-hole needed for XB donation when compared to the methylation of the nitrogen atom on the other side of the molecule.

The complexity of effectively polarizing the XB donors is further emphasized by the results of the calculations done on receptor **1**, in which after methylation of the much closer nitrogen atom, the σ-hole value actually decreases by 4 kcal/mol. This result is surprising to us given the previously noted influence of the positive charge on the σ-hole. To verify and study this result, we would perform ^{1}H NMR spectroscopy titrations to be done with the neutral version of receptor **1** (labelled **1.5** in **Scheme 5.1**) to determine binding constants and compare with the methylated receptor. Finally, the calculated σ-hole value for the quinoline receptor shows that the triazole moiety will elicit similar energy levels comparable to an aryl ring with an appended EWG. Although further

empirical and computation data must be collected to reinforce this idea, the suggestion that electron-deficient aryl rings can be used as comparable drivers of XB donors, relative to the much more regularly used triazole units, could open the door to novel XB host designs in future receptors.

Table 5.3. Summary of the calculated energy value of sigma holes for XB donors in all of the receptors discussed in Chapters 4 and 5 (first 8 entries refer to the one arm family in Chapter 4)

Chapter	Number	Receptor Name	Sigma Hole Energy (kcal/mol)
4	4a	Neutral SO_2CF_3	28.5
4	4b	Neutral CF_3	24.3
4	4c	Neutral H	19.0
4	4d	Neutral *t*-Bu	17.5
4	5a	Methylated SO_2CF_3	82.8
4	5b	Methylated CF_3	80.0
4	5c	Methylated H	77.2
4	5d	Methylated *t*-Bu	73.8
5	2	Quinoline Receptor	26.8
5	1	Neutral	11.8
5	1.5	Methylated	7.1

5.6. Conclusion.

The receptors presented in this chapter highlight the complexity of designing an effective XB donor. Despite the nuance involved with XB host design, the latest generation of DWJ-Haley XB-HB hybrid receptors, like **1** (and those discussed in Chapter 4), have demonstrated a noteworthy ability to bind Cl^- in polar solvents. These will undoubtedly pave the way towards future DWJ-Haley receptors and their use in aqueous media, fulfilling a long sought-after goal of binding these important anion species in critical environments, such as *in vivo* and in aqueous ecological environments.

CHAPTER SIX

CONCLUSIONS AND OUTLOOKS

The research in this thesis discussed many of the most recent XB and HB receptors to come out of the DWJ and Haley laboratories for anion recognition. Chapter Two begins by exploring modifications made to improve the quantum yield, and other photophysical properties of a relatively newly discovered P-N containing heterocyclic fluorophore. This family of molecules beautifully highlights the nuanced understanding that can be derived from thorough structure-property relationships. It also sets the groundwork for thinking about many of the other fluorescent molecules discussed throughout this thesis.

In Chapter Three the second XB receptor to come out of the DWJ and Haley group is discussed. This receptor was designed with two goals in mind: first, binding the hydrochacogenide, HS^- and second, competing in a significant way with polar media. While falling short of these goals the failed hypothesis did reinforce fundamental design principles suggested by the first DWJ and Haley XB receptor (also discussed in Chapter Three). These design principles were then used to conceptualize and synthesize the much more successful receptors that are the subject of Chapters Four and Five.

In Chapter Four a family of one-armed receptors capable of binding the halide anions in the polar solvent acetonitrile are discussed. In this family the size of the pocket is sufficiently shrunk to flip the preference of the XB guest to bind the smaller halide (Cl^-) over that of the larger halides (Br^- or I^-). This family demonstrated some HB

coordination of these anions, making it the first hybrid receptor to be published by the DWJ and Haley labs.

Finally, In Chapter Five, two more hybrid receptors are explored. The first is a slightly larger one-arm receptor that demonstrate a similar preference for the smaller halide (Cl^-) with an even larger association constant in more competitive solvent conditions (10% DMSO in ACN). It also was the subject of relatively surprising computation work, which suggested that methylating the pyridine ring (on which the XB donor is appended) had a minimal effect on the size of the σ-hole, bucking the outsized effect that methylation had with the earlier XB receptors. This result begs much further investigation. The small pocket of this receptor could also be an interesting case study in the effect of changing the identity of the XB donor (namely, from I to Br) and how that effects the halide guest preference, given a slightly less crowded pocket. Also mentioned in Chapter Five is the synthesis of a quinoline based scaffold that combines many of the design principles explored through the rest of the thesis. It has fluorescent properties, can preorganize into the state hypothesized to be best for binding and could be synthesized in either a neutral or cationic motif, depending upon the pH the receptor is intended to be utilized at. Further synthesis and characterization remain to be done with the quinoline receptor and should be finished shortly.

The receptors discussed in Chapters Four and Five, in particular, present a library of receptors which seem to buck the IUPAC definition of a halogen bond as a simple interaction between R—X···Y, where X is a polarizable halogen covalently bound to an R group and Y is an electronically-dense halogen bond acceptor. This definition biases supramolecular chemists to give undue important to the electron withdrawing nature of

groups closest to the XB donor. In Chapter 4 it is shown that the much closer functional groups (which ranged from highly electron withdrawing to slightly electron donating) had a meager effect on XB polarization, relative to the methylation of the pyridine ring on the otherside of the molecule. But, as evidence by the receptors explored in Chapter 5, the answer is not as simple as adding a cation charge anywhere on the XB donor molecule. On the contrary, despite its signifigantly closer position to the XB donor in this receptor the methylation of the pyridine ring served to only marginally increase the size of the σ-hole.

In conclusion, anions are an incredibly important class of molecule that are ubiquitious in human physiology and ecological niches around the world. Unfortunately, given their signifigance, the environments in which they are most pertinent (polar, aqueous ones) are also the mediums in which anions are the hardest to pin down. Their low charge density, high solvation energy and pH sensitivy makes them more difficult to bind than their cationic counterparts in water. Water's ability to act as both an HB donor and acceptor makes it a highly competitive solvent for any synthetic host looking to bind anions. This makes XB an incredibly attractive tool, as study after study has shown that these σ-hole interactions outcompete the HB counterparts in competitive polar media in otherwise analogous host receptors. Despite this promise, and the growing interest of the past two decades, much still remains to be discovered about the best way to polarize and utilize XB donors for anion coordination. This, along with puzzling out how to best use this tool in tandem with other recognition techniques, including the other σ-hole interactions (chalcogen and pnictogen bonding) or anion$\cdots\pi$ interactions, is sure to drive research interests for decades to come.

APPENDIX A
SUPPLEMENTARY CONTENT FOR CHAPTER TWO

Experimental Details

1. Crystallographic Data for **2f**

General. Diffraction intensities for **2f** were collected at 173 K on a Bruker Apex2 CCD diffractometer using CuKα radiation, λ= 1.54178 Å. Space group was determined based on systematic absences. Absorption correction was applied by SADABS.[1] Structure was solved by direct methods and Fourier techniques and refined on F^2 using full matrix least-squares procedures. All non-H atoms were refined with anisotropic thermal parameters. H atoms were refined in calculated positions in a rigid group model except the H atom at the N atom involved in H-bond which was found on the residual density map and refined with isotropic thermal parameter. In the crystal structure the main molecules form a dimer unit via N-H•••O H-bonds which are packed in columns. Solvent molecules $CHCl_3$ fill out empty space between such the columns and are highly disordered. These disordered solvent molecules were treated by SQUEEZE.[2] The corrections of the X-ray data by SQUEEZE are 220 electron/cell; the required values are 232 electron/cell for four $CHCl_3$ molecules in the full unit cell. All calculations were performed by the Bruker SHELXL-2014 package.[3]

Crystallographic Data for **2f**: $C_{24}H_{20}Cl_3O_2P$, M = 505.74, 0.15 x 0.08 x 0.06 mm, T = 173(2) K, Monoclinic, space group $P2_1/c$, a = 17.7865(8) Å, b = 8.1543(4) Å, c = 18.4012(8) Å, β = 117.199(3)°, V = 2373.7(2) Å^3, Z = 4, D_c = 1.415 Mg/m^3, μ(Cu) = 4.335 mm^{-1}, F(000) = 1040, $2\theta_{max}$ = 133.15°, 13893 reflections, 4116 independent reflections [R_{int} = 0.0465], R1 = 0.0570, wR2 = 0.1562 and GOF = 1.021 for 4116 reflections (257 parameters) with I>2σ(I), R1 = 0.0699, wR2 = 0.1630 and GOF = 1.021 for all reflections, max/min residual electron density +0.588/–0.275 eÅ^{-3}. CCDC 1944053.

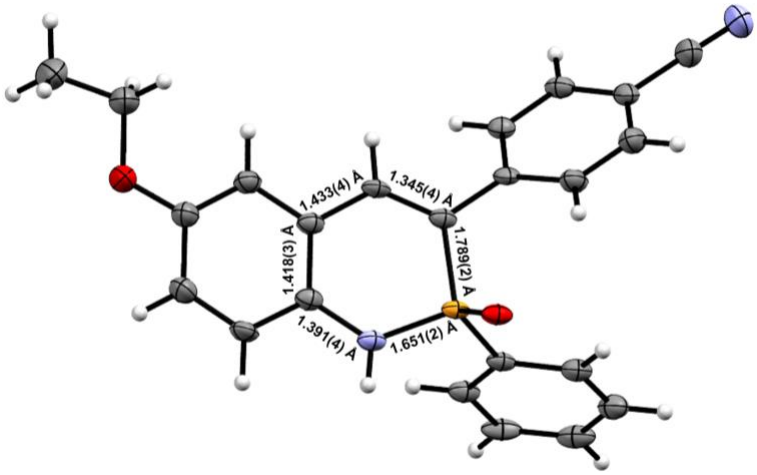

Figure A.1. ORTEP drawing of **2f** with selected bond lengths listed; thermal ellipsoids drawn at 30% probability. Crystals grown with slow diffusion of pentane into a solution of **2** in $CHCl_3$.

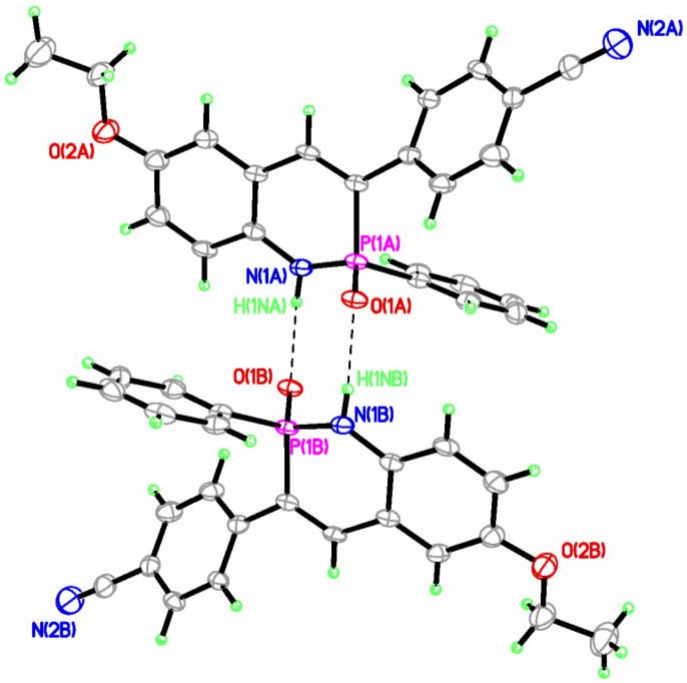

Figure A.2. ORTEP drawing of the racemic dimer of **2f**; thermal ellipsoids drawn at 30% probability.

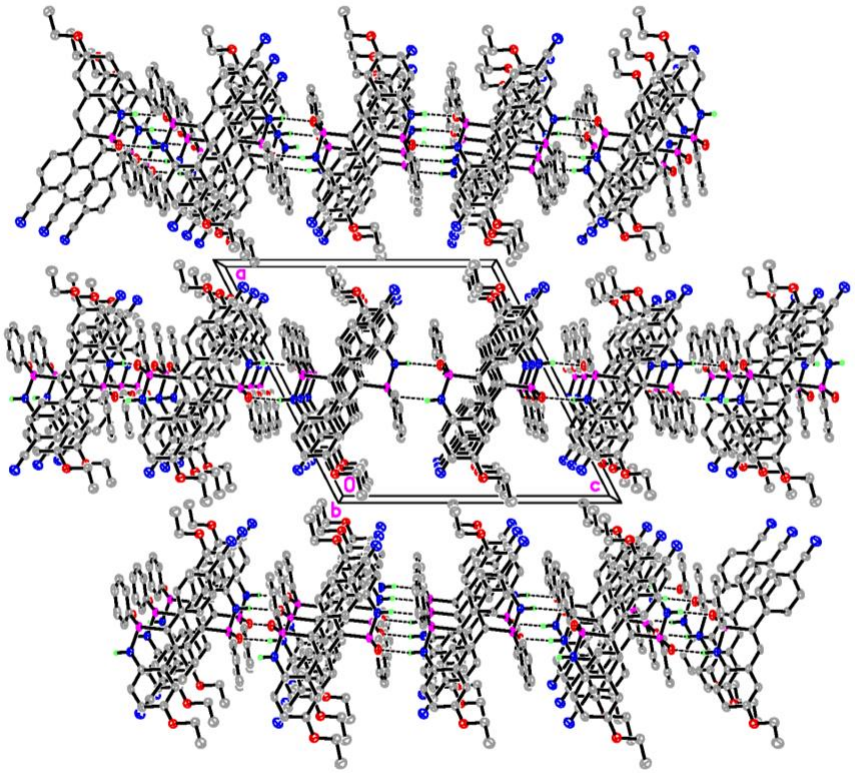

Figure A.3. ORTEP drawing of the crystal packing of **2f** looking down the b-axis.

2. Frontier Orbital Values and TD-DFT Excitations

Ground state calculations

Table A.1. Calculated Frontier Orbitals and First Excitation Values for **2**[a]

cmpd	E_{HOMO}	E_{LUMO}	ΔE_{DFT}	$S_0 \rightarrow S_1$ computed (nm), osc. Strength
2a	–6.800	–2.405	4.395	341, 0.505
2b	–6.750	–2.319	4.431	337, 0.535
2c	–6.531	–2.296	4.235	354, 0.392
2d	–6.510	–2.294	4.303	348, 0.486
2e	–6.481	–2.178	4.207	358, 0.361
2f	–6.353	–2.146	3.896	389, 0.195

[a]Calculated at the PBE0/TZVP level of theory; values reported in eV.

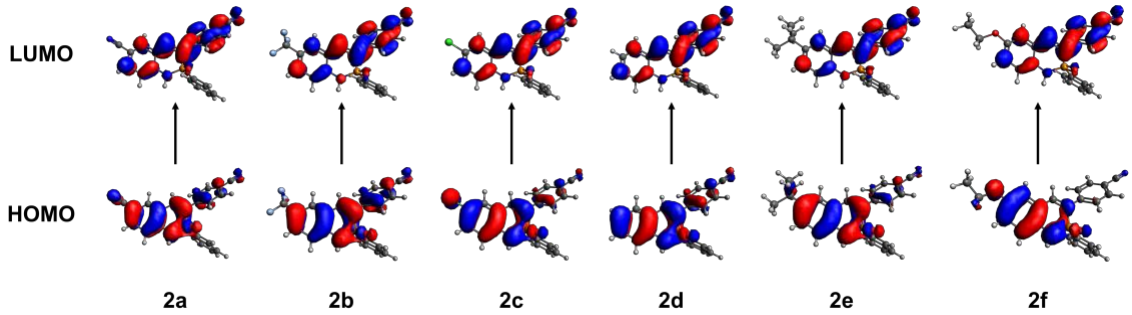

Figure A.4. Frontier orbital shapes (isovalue = 0.3) of heterocycles **2**; calculated at the PBE0/TZVP level of theory.

Excited state calculations

These initial structures were optimized using the functional PBE0[4,5] (25% full-range HF exchange) and TZVP basis set[6] as implemented in Gaussian 09.[7] In addition, all the optimized structures were confirmed by frequency analysis and the number of imaginary frequencies was zero. TD-DFT vertical excitation calculations and geometry optimization of the first excited state (S_1) were performed at the same level of theory. The PCM solvation model[8,9] was used to account for the solvent effects of the chloroform.

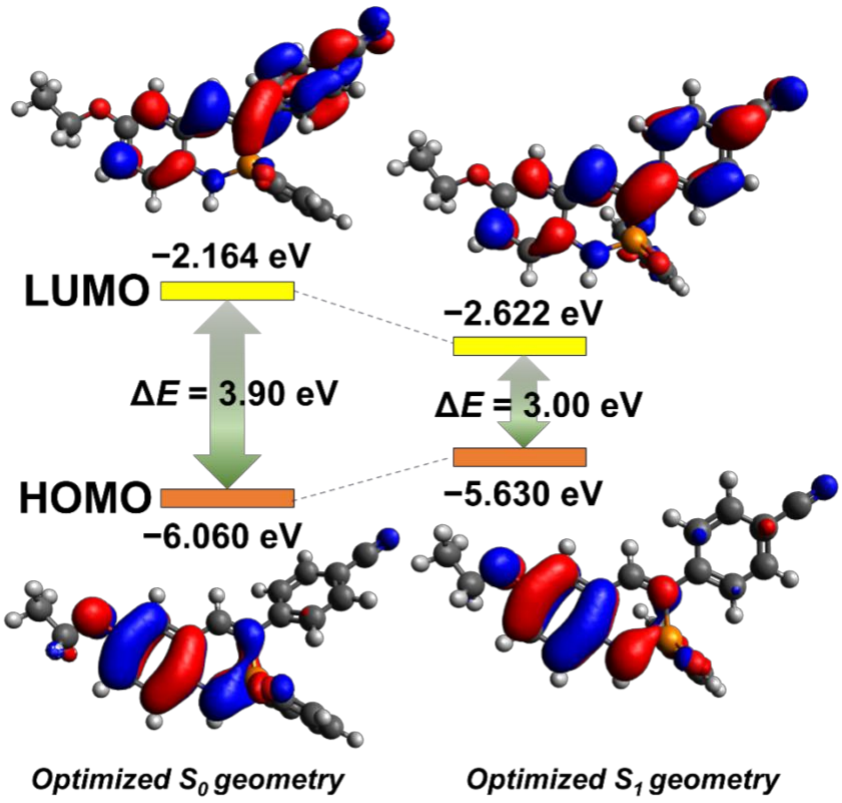

Figure A.5. HOMO-LUMO pictorial representations (isovalue = 0.3), energies and their differences (ΔE) in the optimized S_0 and S_1 structures of **2f** calculated by the DFT and TD-DFT methods at the PCM($CHCl_3$)-PBE0/TZVP level of theory, respectively.

3. Geometry Optimizations and Coordinates

Ground state geometries

Table A.2. Cartesian coordinates of the optimized geometry of **2a** determined at the PBE0/TZVP level of theory

Atom	x	y	z
C	-4.85224	-0.99453	0.24314
C	-5.06467	0.36876	-0.01362
C	-3.99796	1.19772	-0.26557
C	-2.68944	0.69768	-0.26948
C	-2.46321	-0.67090	-0.00881
C	-3.55816	-1.49676	0.24538
N	-1.62915	1.54068	-0.48129
P	-0.05268	1.09981	-0.96544
C	0.01373	-0.57214	-0.28708
C	-1.13106	-1.21587	0.02816
C	1.32888	-1.22391	-0.17733
C	2.32937	-1.00360	-1.13093
C	3.55719	-1.62907	-1.02594
C	3.81064	-2.48996	0.04330
C	2.82419	-2.71342	1.00652
C	1.60209	-2.08011	0.89538
O	0.24116	1.20873	-2.43673
H	-6.07224	0.76605	-0.01630
H	-4.16680	2.24964	-0.46799
H	-3.38832	-2.54835	0.44662
H	-1.86453	2.51486	-0.62006
H	-1.06114	-2.25919	0.32868
H	2.13135	-0.35505	-1.97675
H	4.32091	-1.45850	-1.77493
H	3.02505	-3.37115	1.84342
H	0.85418	-2.23445	1.66438
C	5.07615	-3.13557	0.15614
N	6.10029	-3.65817	0.24771
C	1.00594	2.19506	0.01314
C	1.97814	2.94304	-0.64517

C	0.86604	2.29013	1.39720
C	2.80595	3.78889	0.08033
H	2.07444	2.85806	-1.72158
C	1.69724	3.13388	2.11728
H	0.10786	1.70840	1.91080
C	2.66562	3.88319	1.45833
H	3.56138	4.37440	-0.43113
H	1.59006	3.20904	3.19339
H	3.31411	4.54305	2.02388
C	-5.95519	-1.85468	0.50419
N	-6.85123	-2.54976	0.71725

Zero-point correction = 0.306046 (Hartree/Particle); Thermal correction to energy = 0.328311; Thermal correction to enthalpy = 0.329256; Thermal correction to Gibbs free energy = 0.252414; Sum of electronic and zero-point energies = -1426.281789; Sum of electronic and thermal energies = -1426.259523; Sum of electronic and thermal enthalpies = -1426.258579; Sum of electronic and thermal free energies = -1426.335421.

Table A.3. Cartesian coordinates of the optimized geometry of **2b** determined at the PBE0/TZVP level of theory

Atom	**x**	**y**	**z**
C	4.33256	0.25239	0.07266
C	4.36740	-1.12574	-0.14433
C	3.19680	-1.82533	-0.36097
C	1.96424	-1.16425	-0.36534
C	1.91814	0.22872	-0.13593
C	3.11747	0.91433	0.07864
N	0.79435	-1.87023	-0.54497
P	-0.71412	-1.24659	-1.00223
C	-0.55995	0.42532	-0.35685
C	0.66485	0.93655	-0.08900
C	-1.78476	1.23382	-0.22255
C	-2.83620	1.11740	-1.14210
C	-3.97972	1.88534	-1.01112
C	-4.09599	2.78768	0.05013

C	-3.05815	2.90828	0.97984
C	-1.92102	2.13323	0.84339
O	-1.06879	-1.33987	-2.44972
H	5.31560	-1.64935	-0.14765
H	3.22816	-2.89645	-0.53066
H	3.08031	1.98498	0.25349
H	0.90195	-2.87056	-0.65853
H	0.72898	1.98857	0.18318
H	-2.74143	0.43697	-1.98120
H	-4.78302	1.79523	-1.73288
H	-3.15443	3.59763	1.81044
H	-1.13530	2.20738	1.58703
C	-5.27351	3.57973	0.18954
N	-6.22685	4.22181	0.30316
C	-1.87332	-2.16682	0.02964
C	-2.99233	-2.74612	-0.56830
C	-1.67521	-2.28375	1.40740
C	-3.90785	-3.44425	0.21021
H	-3.13095	-2.64787	-1.63956
C	-2.59376	-2.97976	2.18044
H	-0.80363	-1.83295	1.87151
C	-3.70888	-3.55955	1.58133
H	-4.77702	-3.89756	-0.25393
H	-2.44117	-3.07162	3.25034
H	-4.42561	-4.10321	2.18781
C	5.58540	1.02927	0.31687
F	5.71872	2.05264	-0.54614
F	6.68573	0.27257	0.20460
F	5.60776	1.57440	1.54852

Zero-point correction = 0.312616 (Hartree/Particle); Thermal correction to energy = 0.335712; Thermal correction to enthalpy = 0.336656; Thermal correction to Gibbs free energy = 0.257793; Sum of electronic and zero-point energies = -1670.857410; Sum of electronic and thermal energies = -1670.834315; Sum of electronic and thermal enthalpies = -1670.833370; Sum of electronic and thermal free energies = -1670.912234.

Table A.4. Cartesian coordinates of the optimized geometry of **2c** determined at the PBE0/TZVP level of theory

Atom	x	y	z
C	4.76530	-0.84753	-0.21352
C	4.95235	0.51406	0.01777
C	3.85707	1.32309	0.25213
C	2.56393	0.79136	0.25768
C	2.37737	-0.58478	0.01677
C	3.49994	-1.39313	-0.21621
N	1.46788	1.61180	0.44837
P	-0.06873	1.13040	0.96633
C	-0.10263	-0.53610	0.28870
C	1.05876	-1.16265	-0.01869
C	-1.40505	-1.21599	0.17783
C	-2.41834	-1.00066	1.12223
C	-3.63596	-1.64912	1.01591
C	-3.86748	-2.52873	-0.04558
C	-2.86886	-2.74659	-1.00019
C	-1.65681	-2.09032	-0.88811
O	-0.35888	1.22487	2.42868
H	5.95108	0.93373	0.01736
H	4.00140	2.38257	0.43708
H	3.36185	-2.45261	-0.39989
H	1.67299	2.59782	0.54848
H	1.01106	-2.21043	-0.31023
H	-2.23659	-0.33867	1.96189
H	-4.40883	-1.48285	1.75717
H	-3.05318	-3.41765	-1.83095
H	-0.90062	-2.23953	-1.65088
C	-5.12144	-3.19771	-0.15958
N	-6.13694	-3.74019	-0.25236
C	-1.17198	2.18283	0.00032
C	-2.19830	2.86079	0.65770
C	-1.02047	2.31216	-1.38225
C	-3.06654	3.67011	-0.06545
H	-2.30167	2.75103	1.73180

C	-1.89224	3.11874	-2.10022
H	-0.22075	1.78506	-1.89284
C	-2.91380	3.79763	-1.44141
H	-3.86269	4.20063	0.44554
H	-1.77547	3.22002	-3.17380
H	-3.59348	4.42828	-2.00484
Cl	6.14889	-1.86580	-0.50514

Zero-point correction = 0.298482 (Hartree/Particle); Thermal correction to energy = 0.320018; Thermal correction to enthalpy = 0.320963; Thermal correction to Gibbs free energy = 0.245463; Sum of electronic and zero-point energies = -1793.507492; Sum of electronic and thermal energies = -1793.485956; Sum of electronic and thermal enthalpies = -1793.485012; Sum of electronic and thermal free energies = -1793.560511.

Table A.5. Cartesian coordinates of the optimized geometry of **2d** determined at the PBE0/TZVP level of theory

Atom	**x**	**y**	**z**
C	4.87957	-2.33820	-0.55510
C	5.40340	-1.07460	-0.27234
C	4.56839	-0.01982	0.04974
C	3.18339	-0.20570	0.09586
C	2.63866	-1.47362	-0.19415
C	3.51235	-2.52485	-0.51570
N	2.34180	0.85710	0.37539
P	0.75066	0.75975	0.93800
C	0.26395	-0.80418	0.19669
C	1.21640	-1.68909	-0.18898
C	-1.17160	-1.12470	0.11863
C	-2.06875	-0.69107	1.10523
C	-3.41442	-1.00319	1.02777
C	-3.89511	-1.75842	-0.04594
C	-3.01376	-2.19077	-1.04236
C	-1.67175	-1.86848	-0.95930
O	0.53974	0.85819	2.41437
H	6.47569	-0.91258	-0.30076
H	4.98133	0.95935	0.27178

H	3.08676	-3.49915	-0.73586
H	2.80016	1.74837	0.51685
H	0.89018	-2.67426	-0.51917
H	-1.69940	-0.12656	1.95449
H	-4.09666	-0.67053	1.80128
H	-3.38796	-2.76407	-1.88250
H	-1.00217	-2.17782	-1.75409
C	-5.28099	-2.08196	-0.12992
N	-6.40367	-2.34505	-0.19896
C	-0.07738	2.10620	0.06374
C	-0.88916	2.97892	0.78798
C	0.06664	2.26802	-1.31618
C	-1.55170	4.01136	0.13447
H	-0.98883	2.84211	1.85939
C	-0.59871	3.29914	-1.96466
H	0.70009	1.58949	-1.87873
C	-1.40739	4.16985	-1.23917
H	-2.18113	4.69171	0.69792
H	-0.48711	3.42552	-3.03617
H	-1.92673	4.97494	-1.74843
H	5.53887	-3.16167	-0.80375

Zero-point correction = 0.308146 (Hartree/Particle); Thermal correction to energy = 0.328403; Thermal correction to enthalpy = 0.329347; Thermal correction to Gibbs free energy = 0.257198; Sum of electronic and zero-point energies = -1334.037270; Sum of electronic and thermal energies = -1334.017013; Sum of electronic and thermal enthalpies = -1334.016068; Sum of electronic and thermal free energies = -1334.088218.

Table A.6. Cartesian coordinates of the optimized geometry of **2e** determined at the PBE0/TZVP level of theory

Atom	**x**	**y**	**z**
C	4.35248	0.21049	0.07235
C	4.33995	-1.17064	-0.16139
C	3.16166	-1.86961	-0.36931
C	1.93366	-1.21055	-0.35366
C	1.90847	0.17770	-0.11411

C	3.12016	0.85067	0.09372
N	0.74735	-1.90753	-0.51892
P	-0.74060	-1.26142	-0.99010
C	-0.56897	0.40515	-0.33619
C	0.66375	0.89745	-0.06005
C	-1.78056	1.23340	-0.20894
C	-2.83472	1.12515	-1.12718
C	-3.96518	1.91354	-1.00623
C	-4.06710	2.83118	0.04353
C	-3.02744	2.94420	0.97248
C	-1.90413	2.14776	0.84649
O	-1.09672	-1.34365	-2.43972
H	5.27024	-1.72536	-0.18728
H	3.19132	-2.94032	-0.54750
H	3.06805	1.91990	0.27852
H	0.84423	-2.90826	-0.63491
H	0.73924	1.94775	0.21772
H	-2.75058	0.43374	-1.95842
H	-4.76930	1.82839	-1.72779
H	-3.11227	3.64495	1.79488
H	-1.11817	2.21716	1.59035
C	-5.22999	3.64586	0.17141
N	-6.17152	4.30702	0.27540
C	-1.92693	-2.16603	0.02901
C	-3.05613	-2.71550	-0.57772
C	-1.73891	-2.29931	1.40660
C	-3.99141	-3.39891	0.19059
H	-3.18671	-2.60599	-1.64895
C	-2.67669	-2.98045	2.17009
H	-0.85902	-1.87219	1.87731
C	-3.80214	-3.52974	1.56168
H	-4.86839	-3.82863	-0.28143
H	-2.53109	-3.08441	3.23994
H	-4.53410	-4.06162	2.16049
C	5.63766	1.00664	0.30357
C	5.74841	2.11833	-0.75049
H	5.77949	1.69730	-1.75979

H	4.90443	2.81180	-0.70109
H	6.66472	2.69643	-0.59303
C	6.88485	0.12698	0.20409
H	6.88632	-0.66501	0.95924
H	6.97790	-0.33603	-0.78307
H	7.77572	0.74011	0.36767
C	5.60079	1.63565	1.70446
H	5.53400	0.86334	2.47670
H	6.51095	2.21793	1.88161
H	4.74564	2.30666	1.82388

Zero-point correction = 0.420029 (Hartree/Particle); Thermal correction to energy = 0.445957; Thermal correction to enthalpy = 0.446901; Thermal correction to Gibbs free energy = 0.362564; Sum of electronic and zero-point energies = -1491.024374; Sum of electronic and thermal energies = -1490.998446; Sum of electronic and thermal enthalpies = -1490.997502; Sum of electronic and thermal free energies = -1491.081839.

Table A.7. Cartesian coordinates of the optimized geometry of **2f** determined at the PBE0/TZVP level of theory

Atom	**x**	**y**	**z**
C	4.47588	-0.49543	-0.11516
C	4.55087	0.88383	0.10641
C	3.39489	1.62204	0.31345
C	2.14145	1.01628	0.30167
C	2.05466	-0.37183	0.06988
C	3.22937	-1.10406	-0.13277
N	0.98169	1.76709	0.45969
P	-0.51584	1.18392	0.96994
C	-0.42817	-0.48686	0.30598
C	0.77737	-1.03553	0.01956
C	-1.67841	-1.25610	0.18321
C	-2.71804	-1.10476	1.11169
C	-3.88606	-1.83701	0.99485
C	-4.04100	-2.73965	-0.06140
C	-3.01604	-2.89482	-1.00048
C	-1.85444	-2.15464	-0.87810

O	-0.83990	1.26621	2.42738
H	5.50541	1.39434	0.12376
H	3.46976	2.69084	0.48664
H	3.17401	-2.17336	-0.30815
H	1.11904	2.76509	0.55595
H	0.80395	-2.08652	-0.26323
H	-2.59360	-0.42479	1.94740
H	-4.67904	-1.71914	1.72410
H	-3.14145	-3.58368	-1.82771
H	-1.07896	-2.25603	-1.62926
C	-5.24310	-3.49585	-0.18623
N	-6.21661	-4.10928	-0.28810
C	-1.68565	2.14206	-0.01896
C	-2.78685	2.71979	0.61264
C	-1.51424	2.28933	-1.39736
C	-3.71017	3.44529	-0.13109
H	-2.90542	2.59902	1.68402
C	-2.44008	3.01266	-2.13633
H	-0.65624	1.84030	-1.88745
C	-3.53719	3.59020	-1.50293
H	-4.56501	3.89692	0.36070
H	-2.30706	3.12759	-3.20671
H	-4.25970	4.15509	-2.08268
O	5.54569	-1.30193	-0.32098
C	6.84268	-0.72057	-0.29182
C	7.84268	-1.82535	-0.52364
H	7.01082	-0.23888	0.68006
H	6.92205	0.04825	-1.07137
H	8.85712	-1.41944	-0.50995
H	7.76385	-2.58608	0.25638
H	7.67376	-2.30144	-1.49231

Zero-point correction = 0.368617 (Hartree/Particle); Thermal correction to energy = 0.393025; Thermal correction to enthalpy = 0.393970; Thermal correction to Gibbs free energy = 0.312175; Sum of electronic and zero-point energies = -1487.682390; Sum of electronic and thermal energies = -1487.657981; Sum of electronic and thermal enthalpies = -1487.657037; Sum of electronic and thermal free energies = -1487.738831.

Representative excited state geometry

Table A.8. Cartesian coordinates for compound **2f** (S_1)

Atom	x	y	z
C	4.19754	0.83011	0.04258
C	4.43859	-0.30536	-0.75296
C	3.34960	-0.99099	-1.24675
C	2.02893	-0.57501	-0.98158
C	1.76910	0.59205	-0.18219
C	2.87518	1.25433	0.31293
N	0.98402	-1.27177	-1.48236
P	-0.70551	-1.07234	-1.17069
C	-0.75456	0.54008	-0.40889
C	0.43970	1.06313	0.08325
C	-2.03546	1.16742	-0.22284
C	-3.26152	0.49519	-0.47023
C	-4.47749	1.09997	-0.26071
C	-4.54758	2.42475	0.21555
C	-3.34562	3.11750	0.45118
C	-2.13156	2.50968	0.23727
O	-1.47016	-1.33310	-2.42262
H	5.44102	-0.64467	-0.97311
H	3.50091	-1.87627	-1.85654
H	2.75354	2.14216	0.92323
H	1.20261	-2.08660	-2.04452
H	0.38969	1.94048	0.71954
H	-3.25594	-0.52378	-0.83955
H	-5.39269	0.55342	-0.45885
H	-3.38120	4.14509	0.79654
H	-1.23161	3.09014	0.40068
C	-5.79638	3.04886	0.44241
N	-6.82004	3.56105	0.62818
C	-1.02320	-2.31567	0.10097
C	-1.88954	-3.36767	-0.20702
C	-0.43713	-2.24196	1.36922
C	-2.16463	-4.33891	0.74848
H	-2.34218	-3.41212	-1.19192

C	-0.71523	-3.21626	2.31544
H	0.22229	-1.41627	1.61968
C	-1.57745	-4.26674	2.00635
H	-2.84004	-5.15319	0.50835
H	-0.26328	-3.15571	3.29972
H	-1.79397	-5.02592	2.75041
O	5.14428	1.57982	0.58991
C	6.52855	1.25640	0.38195
C	7.34720	2.28195	1.12018
H	6.73510	1.27453	-0.69282
H	6.71378	0.24638	0.76081
H	8.40933	2.06646	0.98366
H	7.14692	3.28556	0.73949
H	7.12518	2.25966	2.18909

Geometries of 2 *meso*-dimer and analogous 1 *meso*-dimer

Table A.9. Cartesian coordinates for compound **2f·2f** (*meso*-dimer)

Atom	**x**	**y**	**z**
P	-1.95724	0.60235	-0.15810
O	-1.13426	0.91794	1.07453
O	-4.86819	-5.45211	-0.32378
N	-1.72792	-0.90711	-0.85743
N	-6.92721	6.54145	1.19270
C	-3.73766	0.57706	0.11224
C	-4.39950	-0.59867	0.11116
H	-5.45545	-0.58653	0.37173
C	-3.84837	-1.89655	-0.20763
C	-2.54204	-2.01925	-0.69556
C	-2.07237	-3.28570	-1.07125
H	-1.07359	-3.37896	-1.48229
C	-2.86947	-4.39809	-0.93597
H	-2.50799	-5.37646	-1.22553

C	-4.17029	-4.28817	-0.42388
C	-4.65455	-3.04354	-0.07520
H	-5.65812	-2.91755	0.30781
C	-4.41821	1.86371	0.36187
C	-5.70140	2.08442	-0.14977
H	-6.17936	1.31735	-0.74569
C	-6.35626	3.28249	0.06722
H	-7.34684	3.44695	-0.33573
C	-5.72281	4.29106	0.79408
C	-4.43772	4.09287	1.29858
H	-3.95194	4.87940	1.86064
C	-3.79259	2.88822	1.08154
H	-2.80197	2.72981	1.49055
C	-6.39194	5.54025	1.01540
C	-1.60300	1.78258	-1.48582
C	-0.61820	2.74784	-1.31084
H	-0.06610	2.78759	-0.38140
C	-0.34559	3.65095	-2.33102
H	0.42602	4.39841	-2.19596
C	-1.06490	3.59304	-3.51740
H	-0.85633	4.29959	-4.31093
C	-2.05424	2.62939	-3.69172
H	-2.61274	2.58634	-4.61790
C	-2.32146	1.72118	-2.67885
H	-3.08473	0.96234	-2.81326
C	-6.18694	-5.38880	0.20600
H	-6.80431	-4.74129	-0.42516
H	-6.15489	-4.95833	1.21243

C	-6.73651	-6.79556	0.23574
H	-7.74918	-6.78877	0.63901
H	-6.76584	-7.21498	-0.76966
H	-6.11603	-7.43412	0.86410
H	-0.75384	-1.07946	-1.13391
P	1.95156	-0.64866	0.19274
O	1.08688	-0.96110	-1.01172
O	4.69506	5.48289	0.53051
N	1.68726	0.83535	0.93440
N	7.06869	-6.35013	-1.57736
C	3.71838	-0.55160	-0.13926
C	4.34473	0.64290	-0.10761
H	5.39135	0.67402	-0.40224
C	3.76786	1.90828	0.28504
C	2.47046	1.97330	0.80554
C	1.97625	3.20980	1.24574
H	0.98434	3.25755	1.68084
C	2.74001	4.34850	1.13996
H	2.35923	5.30349	1.47902
C	4.03159	4.29657	0.59628
C	4.54060	3.08158	0.18481
H	5.53862	2.99783	-0.22352
C	4.43069	-1.80350	-0.46702
C	5.73087	-2.00838	0.00685
H	6.19822	-1.25657	0.63004
C	6.41634	-3.17373	-0.28147
H	7.41988	-3.32672	0.09277
C	5.79805	-4.16492	-1.04428

C	4.49709	-3.98263	-1.51265
H	4.02348	-4.75542	-2.10340
C	3.82065	-2.81055	-1.22348
H	2.81680	-2.66345	-1.60302
C	6.50213	-5.37893	-1.34047
C	1.69613	-1.88524	1.49285
C	0.64469	-2.78840	1.38896
H	-0.01285	-2.74941	0.53080
C	0.44143	-3.73291	2.38765
H	-0.38232	-4.43095	2.30814
C	1.29730	-3.78013	3.48005
H	1.14343	-4.52010	4.25539
C	2.35300	-2.87906	3.58311
H	3.01798	-2.91732	4.43630
C	2.55094	-1.92835	2.59314
H	3.36803	-1.21946	2.67405
C	6.00897	5.47632	-0.01461
H	6.65036	4.82286	0.58592
H	5.97823	5.08342	-1.03618
C	6.51872	6.89823	0.00350
H	7.52896	6.93518	-0.40423
H	6.54128	7.28223	1.02310
H	5.87721	7.54089	-0.59909
H	0.70937	0.98002	1.21499

Table A.10. Cartesian coordinates for compound **2f‘·2f‘** (*meso*-dimer for -OPh analogue)

Atom	**x**	**y**	**z**
P	1.92141	0.79131	-0.26147
O	0.78543	1.51236	-0.92423

O	6.53956	-3.99151	-1.19988
N	2.02262	-0.82536	-0.62475
N	4.97709	8.03803	0.16496
C	3.59102	1.36451	-0.52551
C	4.57382	0.46252	-0.73510
H	5.58336	0.84492	-0.86408
C	4.43734	-0.97249	-0.81836
C	3.18131	-1.58317	-0.74275
C	3.09026	-2.97766	-0.82535
H	2.11643	-3.44875	-0.76712
C	4.22370	-3.74153	-0.97276
H	4.15972	-4.82045	-1.03252
C	5.48901	-3.14105	-1.05234
C	5.58959	-1.76691	-0.97746
H	6.54735	-1.26819	-1.03595
C	3.87197	2.80945	-0.37778
C	5.03179	3.22763	0.28458
H	5.69956	2.49146	0.71451
C	5.32555	4.57143	0.42127
H	6.22247	4.88754	0.93716
C	4.44618	5.52323	-0.09631
C	3.27888	5.12301	-0.74537
H	2.60112	5.86640	-1.14344
C	2.99450	3.77540	-0.88166
H	2.09196	3.46511	-1.39128
C	4.74073	6.91971	0.04861
C	7.83932	-3.42380	-1.31227
H	8.06387	-2.84264	-0.41180
H	7.86840	-2.74857	-2.17381
C	8.82206	-4.55834	-1.48203
H	9.83191	-4.16050	-1.58264

H	8.79387	-5.22113	-0.61745
H	8.58521	-5.13637	-2.37497
H	1.13240	-1.32490	-0.52414
P	-1.83870	-0.83501	-0.24159
O	-0.58006	-1.54000	0.16537
O	-6.03526	4.24836	0.94534
N	-1.79480	0.81008	-0.03092
N	-4.96926	-7.90305	1.34215
C	-3.39028	-1.28890	0.51650
C	-4.28646	-0.31809	0.79650
H	-5.24232	-0.62508	1.21435
C	-4.11342	1.10510	0.61877
C	-2.88448	1.63685	0.21450
C	-2.74464	3.02402	0.08792
H	-1.78912	3.43301	-0.21776
C	-3.81060	3.85580	0.33656
H	-3.71118	4.92879	0.23273
C	-5.05144	3.33451	0.73214
C	-5.19474	1.96973	0.87834
H	-6.13228	1.53222	1.19349
C	-3.71128	-2.72292	0.68277
C	-4.99895	-3.18586	0.38912
H	-5.74136	-2.49828	0.00330
C	-5.33121	-4.51660	0.56144
H	-6.32798	-4.86844	0.33091
C	-4.36480	-5.41187	1.02114
C	-3.07251	-4.96965	1.30158
H	-2.32861	-5.67016	1.65720
C	-2.74907	-3.63508	1.12870
H	-1.74774	-3.29074	1.35074
C	-4.70057	-6.79521	1.19888

C	-7.30470	3.76745	1.37118
H	-7.69766	3.06517	0.62875
H	-7.19240	3.23607	2.32210
C	-8.21923	4.96014	1.52189
H	-9.20286	4.63183	1.85789
H	-8.33183	5.47687	0.56903
H	-7.81697	5.65942	2.25452
H	-0.90390	1.25228	-0.29356
O	1.65012	0.93158	1.34869
O	-2.03326	-1.14197	-1.84182
C	2.42198	0.19621	2.24001
C	3.51657	0.80032	2.83895
C	2.06499	-1.11320	2.52760
C	4.27398	0.07137	3.74738
H	3.75515	1.82865	2.59475
C	2.83279	-1.83172	3.43459
H	1.19713	-1.54270	2.04046
C	3.93610	-1.24381	4.04341
H	5.12751	0.53465	4.22565
H	2.56580	-2.85461	3.66811
H	4.52892	-1.80929	4.75059
C	-3.06789	-0.51671	-2.52823
C	-4.25761	-1.20300	-2.71875
C	-2.88728	0.76802	-3.01906
C	-5.29228	-0.58260	-3.40703
H	-4.35624	-2.20940	-2.33039
C	-3.93080	1.38009	-3.70142
H	-1.94065	1.27030	-2.86233
C	-5.13323	0.70995	-3.89317
H	-6.22390	-1.11125	-3.56359
H	-3.80062	2.38351	-4.08590

H	-5.94271	1.19250	-4.42543

4. Photophysical Properties in Different Solvents

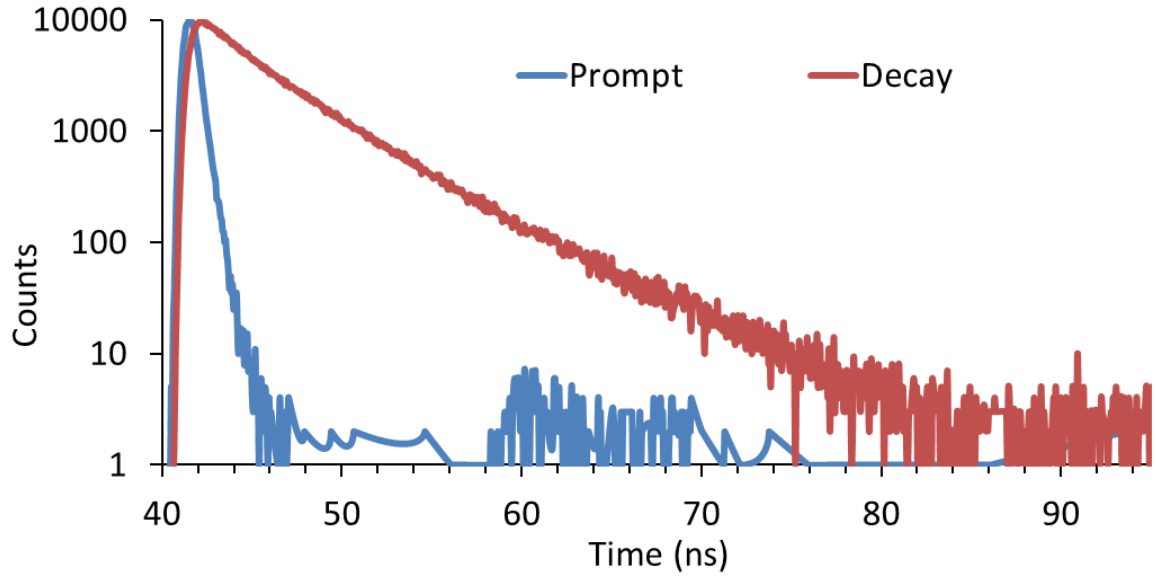

Figure A.6. Fluorescence decay curve of **2d** vs Ludox Prompt sample.

Solvent effects on fluorescence

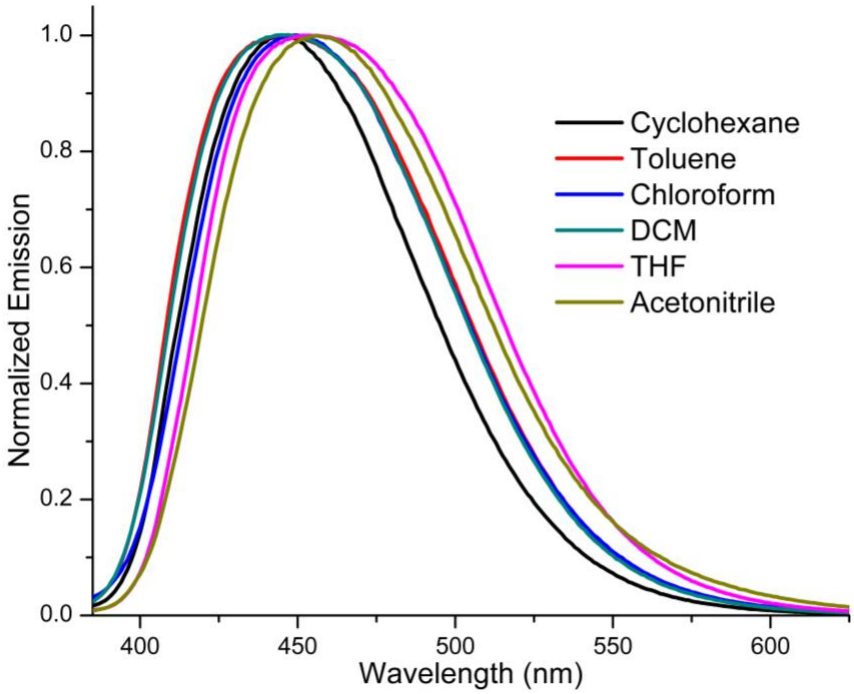

Figure A.7. Emission spectra of **2a** in various solvents.

Table A.11. Photophysical properties of **2a** in various solvents

	Cyclohexane	Toluene	Chloroform	DCM	THF	Acetonitrile
λ_{abs}	353	351	348	349	358	350
λ_{em}	445	446	452	448	456	456
Stokes Shift (nm)	92	95	104	99	98	106

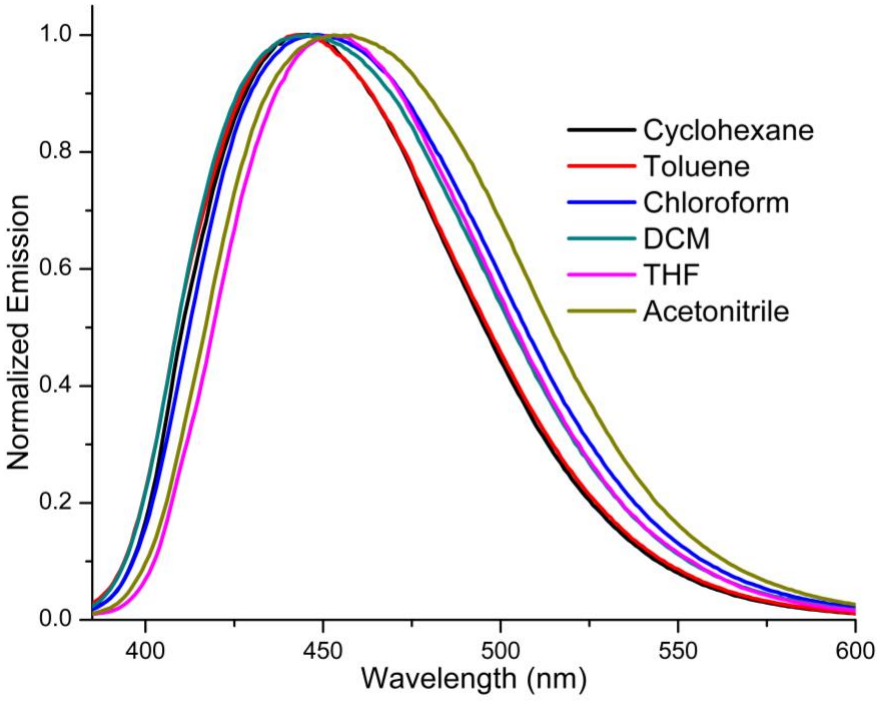

Figure A.8. Emission spectra of **2b** in various solvents.

Table A.12. Photophysical properties of **2b** in various solvents

	Cyclohexane	Toluene	Chloroform	DCM	THF	Acetonitrile
λ_{abs}	346	346	343	344	358	345
λ_{em}	442	442	447	445	453	458
Stokes Shift (nm)	96	96	104	101	95	113

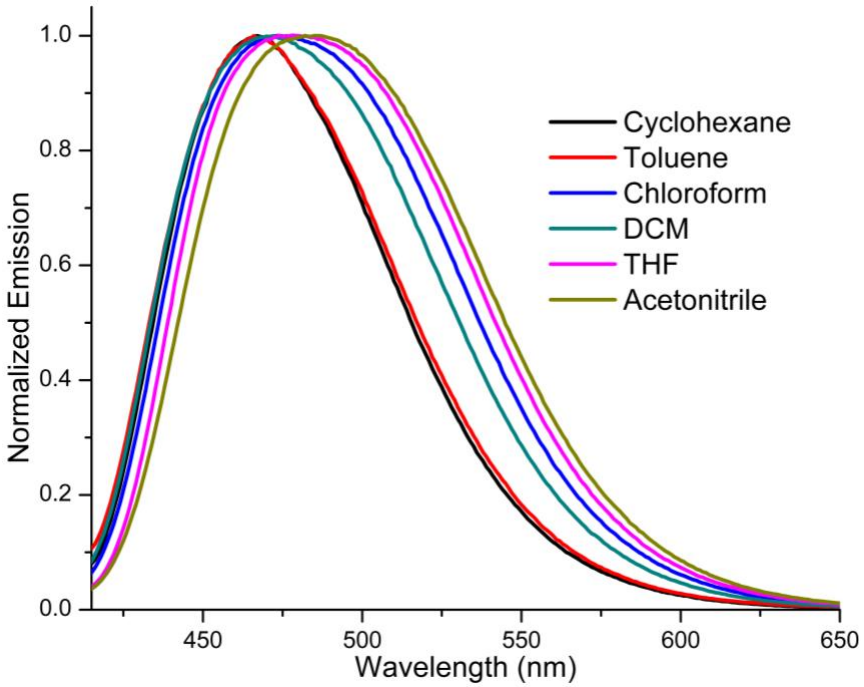

Figure A.9. Emission spectra of **2c** in various solvents.

Table A.13. Photophysical properties of **2c** in various solvents

	Cyclohexane	Toluene	Chloroform	DCM	THF	Acetonitrile
λ_{abs}	366	365	360	365	367	363
λ_{em}	467	466	474	472	480	486
Stokes Shift (nm)	101	101	114	107	113	123

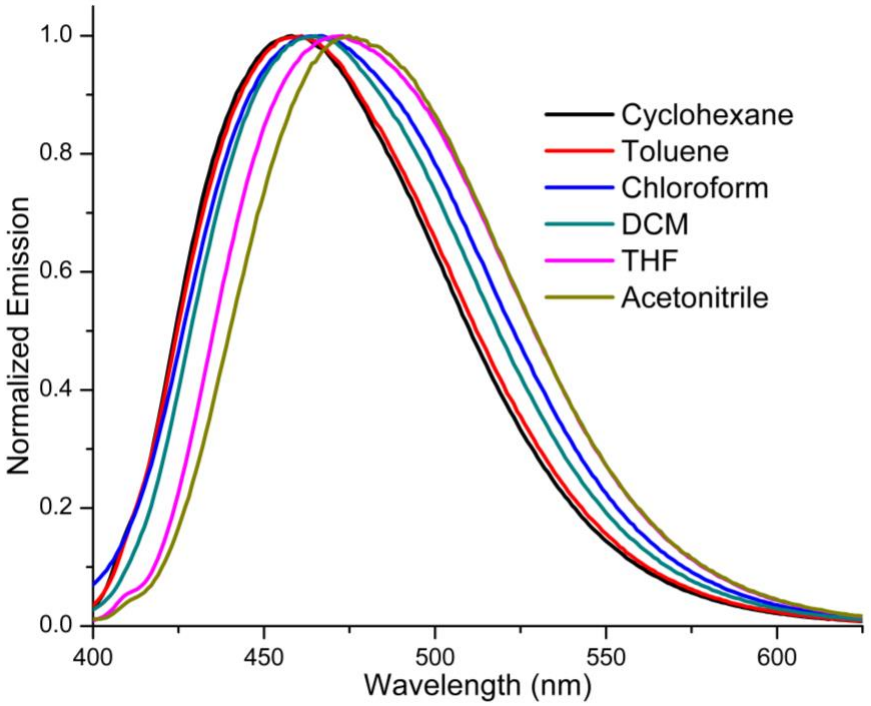

Figure A.10. Emission spectra of **2d** in various solvents.

Table A.14. Photophysical properties of **2d** in various solvents

	Cyclohexane	Toluene	Chloroform	DCM	THF	Acetonitrile
λ_{abs}	355	353	352	365	361	357
λ_{em}	458	461	467	465	473	475
Stokes Shift (nm)	103	108	115	100	112	118

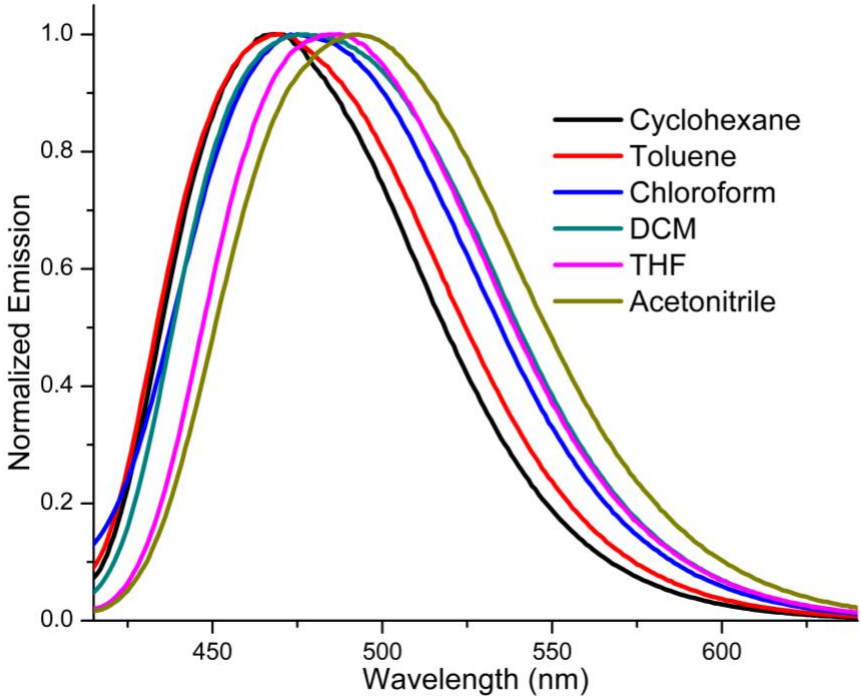

Figure A.11. Emission spectra of **2e** in various solvents.

Table A.15. Photophysical properties of **2e** in various solvents

	Cyclohexane	Toluene	Chloroform	DCM	THF	Acetonitrile
λ_{abs}	365	361	360	362	368	365
λ_{em}	467	469	473	478	488	493
Stokes Shift (nm)	102	108	113	116	120	128

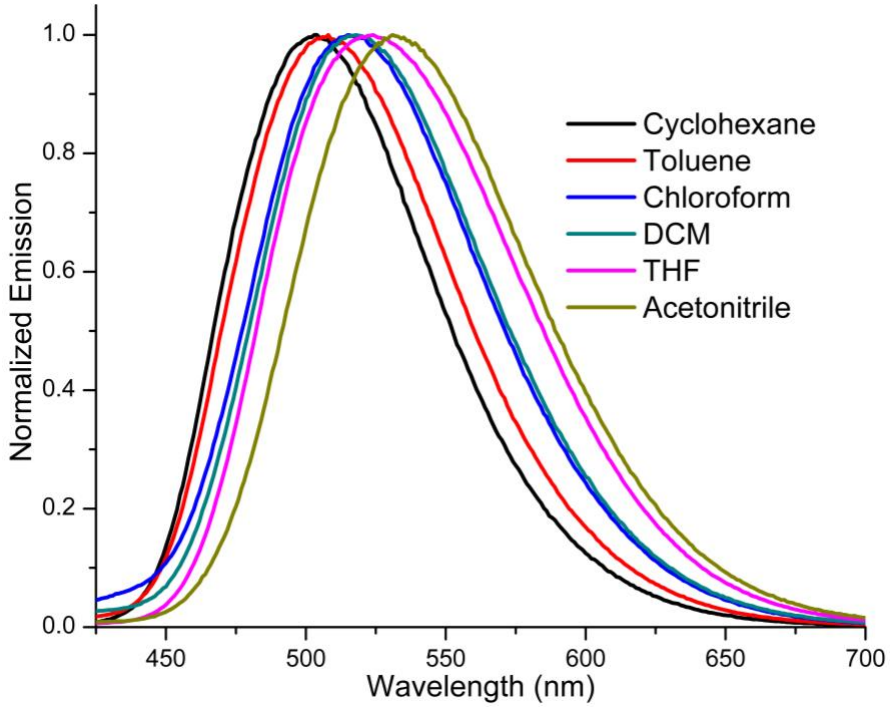

Figure A.12. Emission spectra of **2f** in various solvents.

Table A.16. Photophysical properties of **2f** in various solvents

	Cyclohexane	Toluene	Chloroform	DCM	THF	Acetonitrile
λ_{abs}	386	384	381	386	387	386
λ_{em}	504	508	515	518	524	531
Stokes Shift (nm)	118	124	134	132	137	145

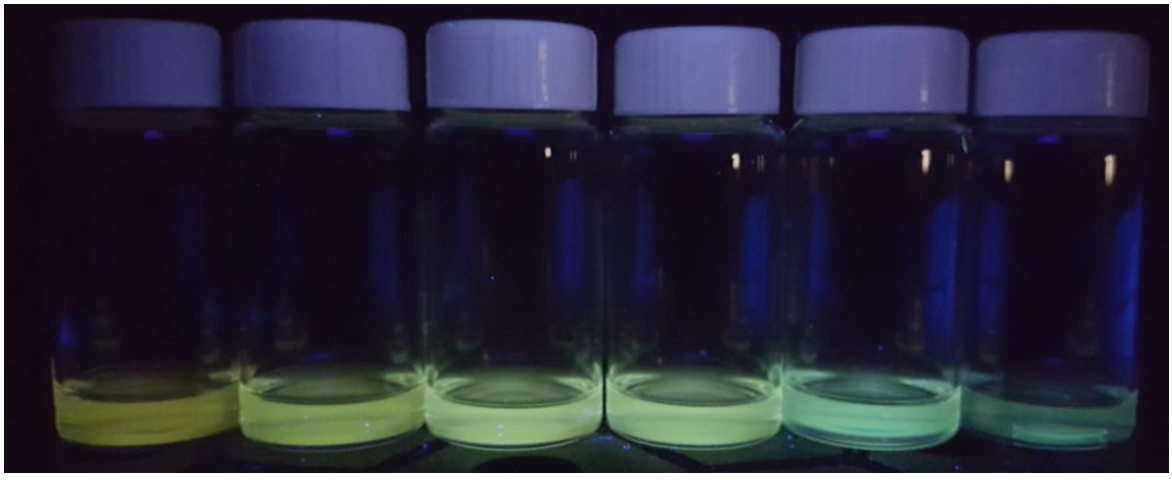

Figure A.13. Fluorescent image of **2f** in Acetonitrile, THF, DCM, Chloroform, Toluene, Cyclohexane (left to right)

5. Experimental and Computational Examination of the Dimer

Solution-state studies of dimer strength

General procedure for variable concentration (VC) NMR experiments. $CDCl_3$ was added in a 1:1 ratio to H_2O, shaken vigorously, then allowed to separate. The organic phase was then separated and used to prepare *ca.* 10 mM solutions of heterocycle **2**. These solutions were then diluted through addition of known amounts of the H_2O-saturated $CDCl_3$ solvent, with ^{31}P NMR spectra being collected after each addition. The ^{31}P NMR spectra were chosen over those of ^{1}H NMR for these experiments since they give comparable results to ^{1}H NMR signals and the ^{1}H NMR signals become impossible to track at lower concentrations due to complex splitting of multiple signals by the phosphorus center. The chemical shift of the phosphorus signal was tracked and fitted to generate the dimerization values.[10]

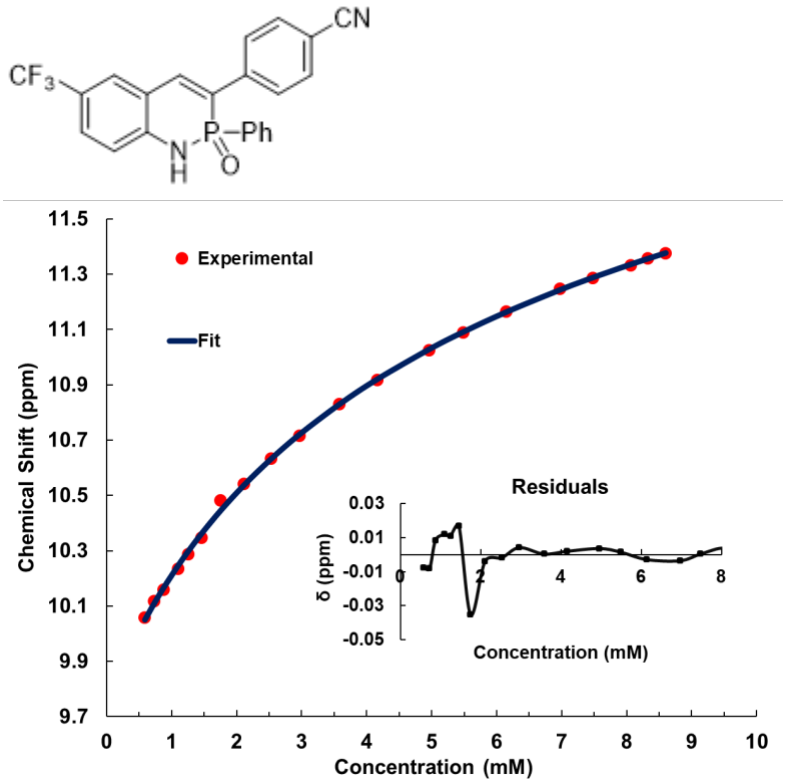

Figure A.14. Binding isotherm (red), fit (blue), and residuals (inset) of VC NMR of **2b**.

Table A.17. Experimental and fitting data for VC NMR experiment of **2b**

Concentration (mM)	Experimental δ (ppm)	Fit δ (ppm)
8.60	11.3755	11.37636588
8.32	11.3583	11.35553759
8.06	11.3315	11.33535491
7.48	11.2871	11.28750165
6.97	11.2465	11.24300097
6.14	11.1654	11.16255996
5.49	11.09	11.09160143
4.96	11.0247	11.02836421
4.16	10.918	10.92008376
3.58	10.8299	10.83033275
2.96	10.7164	10.72063772
2.53	10.6342	10.6324564
2.11	10.5421	10.53825939
1.76	10.4816	10.44649514
1.46	10.3465	10.36343269
1.25	10.2875	10.29857999
1.10	10.2345	10.24644727
0.877	10.1592	10.16767483
0.731	10.1191	10.11087501
0.585	10.0577	10.05013847

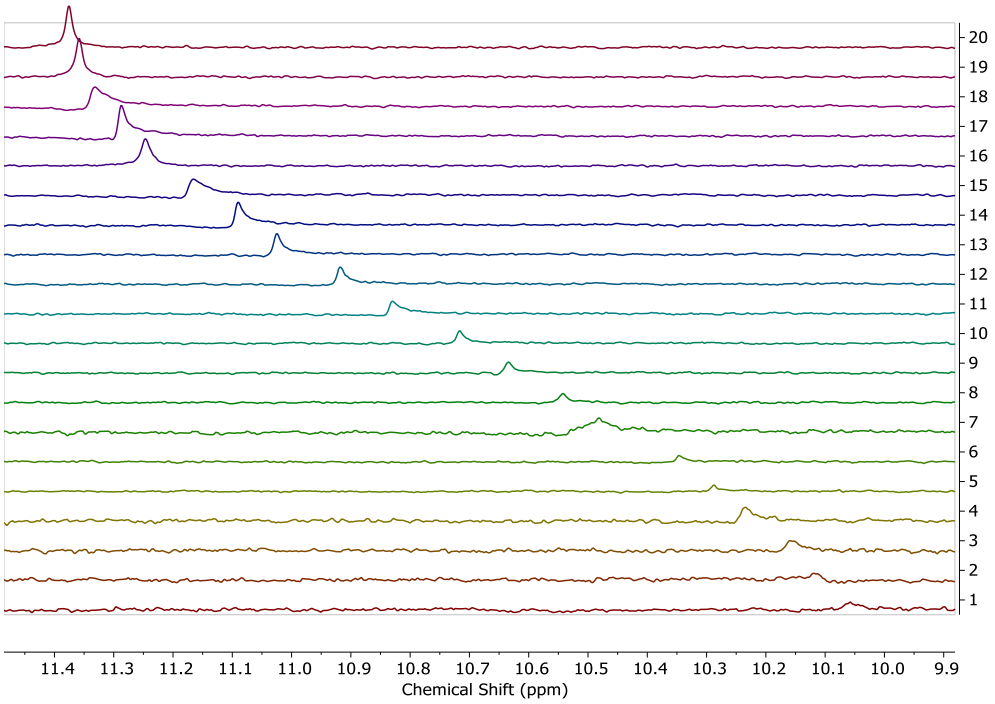

Figure A.15. Representative ^{31}P NMR spectra for VC NMR of **2b**.

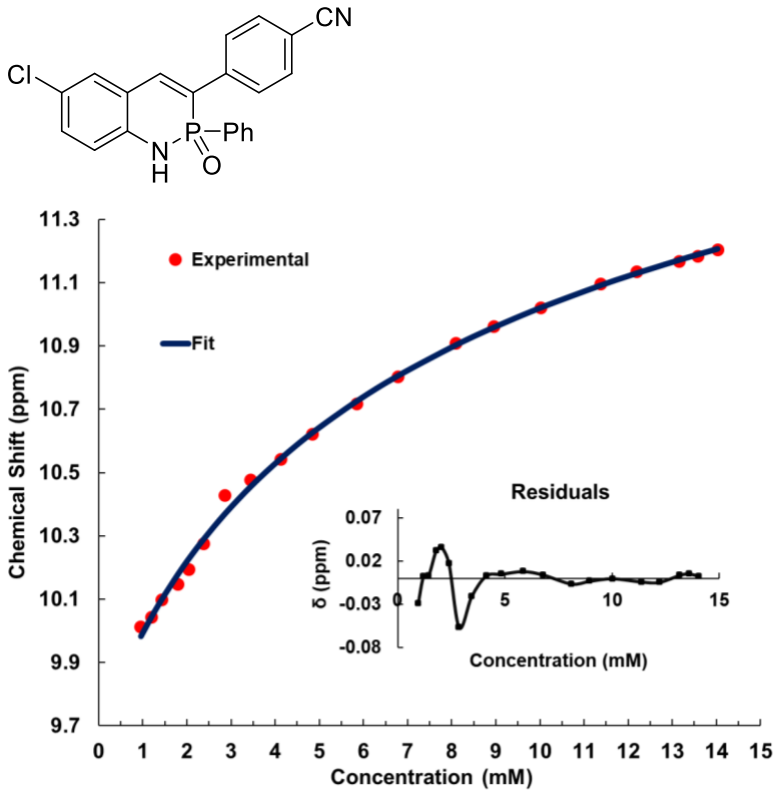

Figure A.16. Binding isotherm (red), fit (blue), and residuals (inset) of VC NMR of **2c**.

Table A.18. Experimental and fitting data for VC NMR experiment of **2c**

Concentration (mM)	Experimental δ (ppm)	Fit δ (ppm)
14.0	11.2039	11.2064793
13.6	11.1831	11.1885475
13.2	11.1672	11.1711442
12.2	11.1341	11.1297717
11.4	11.0951	11.0911563
10.0	11.0212	11.0209934
8.96	10.9617	10.9586984
8.09	10.9091	10.9028468
6.79	10.8023	10.8064342
5.84	10.7176	10.7257245
4.84	10.6209	10.6260187
4.12	10.5419	10.5449533
3.45	10.4777	10.4573812
2.86	10.4277	10.3710209
2.39	10.2748	10.2918817
2.04	10.1932	10.2294034
1.79	10.1464	10.1787126
1.43	10.0982	10.1012771
1.19	10.0425	10.0447712
0.954	10.0123	9.98368372

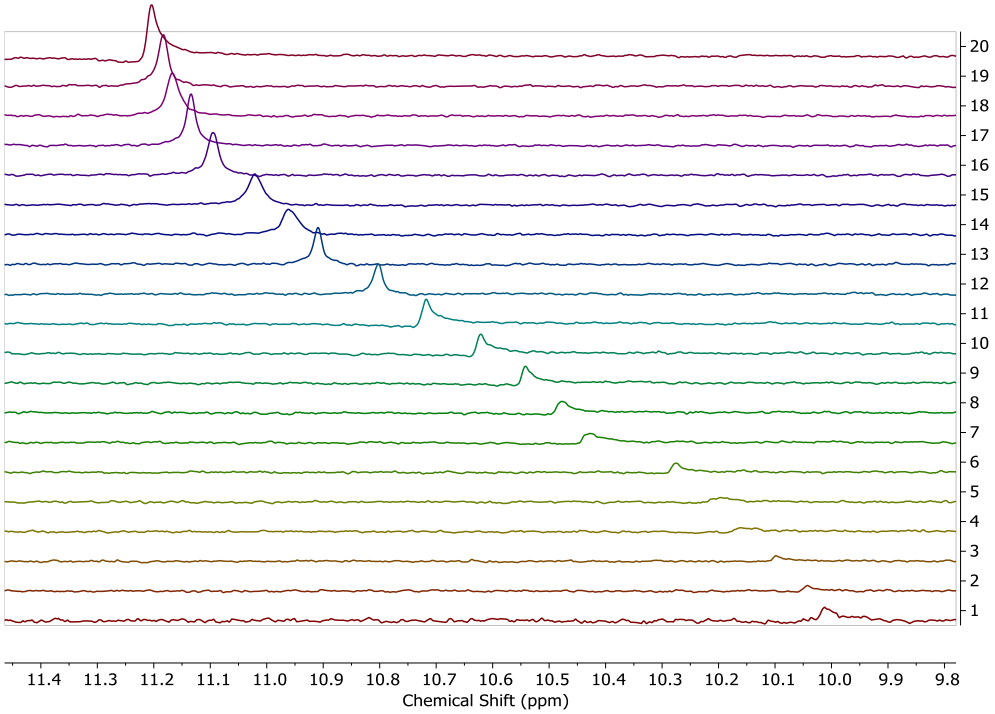

Figure A.17. Representative ^{31}P NMR spectra for VC NMR of **2c**.

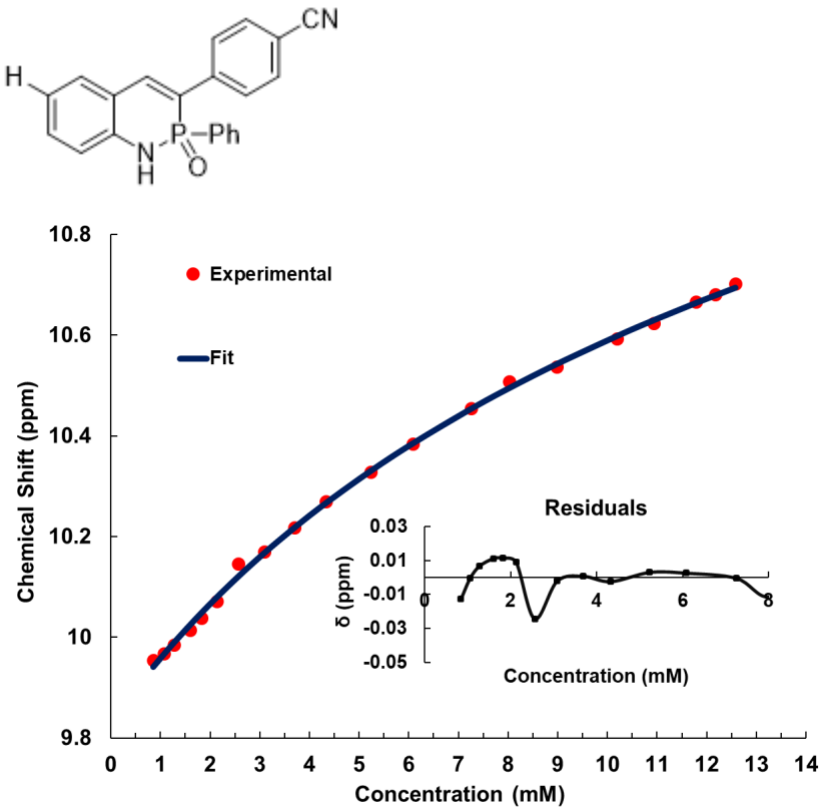

Figure A.18. Binding isotherm (red), fit (blue), and residuals (inset) of VC NMR of **2d**.

Table A.19. Experimental and fitting data for VC NMR of **2d**

Concentration (mM)	Experimental δ (ppm)	Fit δ (ppm)
12.6	10.7014	10.694546
12.2	10.6799	10.679281
11.8	10.6658	10.664594
10.9	10.6234	10.630185
10.2	10.5926	10.598709
9.00	10.5362	10.543093
8.03	10.5069	10.495405
7.25	10.4546	10.453992
6.09	10.3830	10.385454
5.24	10.3280	10.330913
4.34	10.2696	10.267033
3.70	10.2173	10.217883
3.09	10.1697	10.167531
2.57	10.1452	10.120592
2.14	10.0711	10.079881
1.83	10.0379	10.049254
1.60	10.0143	10.025362
1.28	9.9839	9.9904767
1.07	9.9667	9.9662182
0.856	9.9540	9.9410965

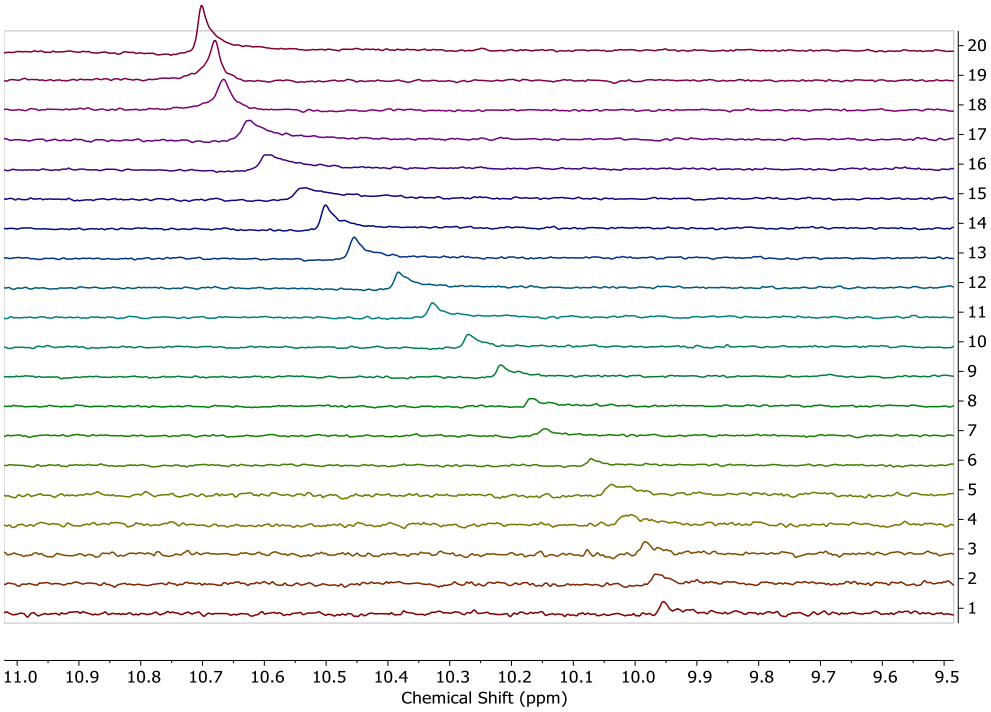

Figure A.19. Representative ^{31}P NMR spectra for VC NMR of **2d**.

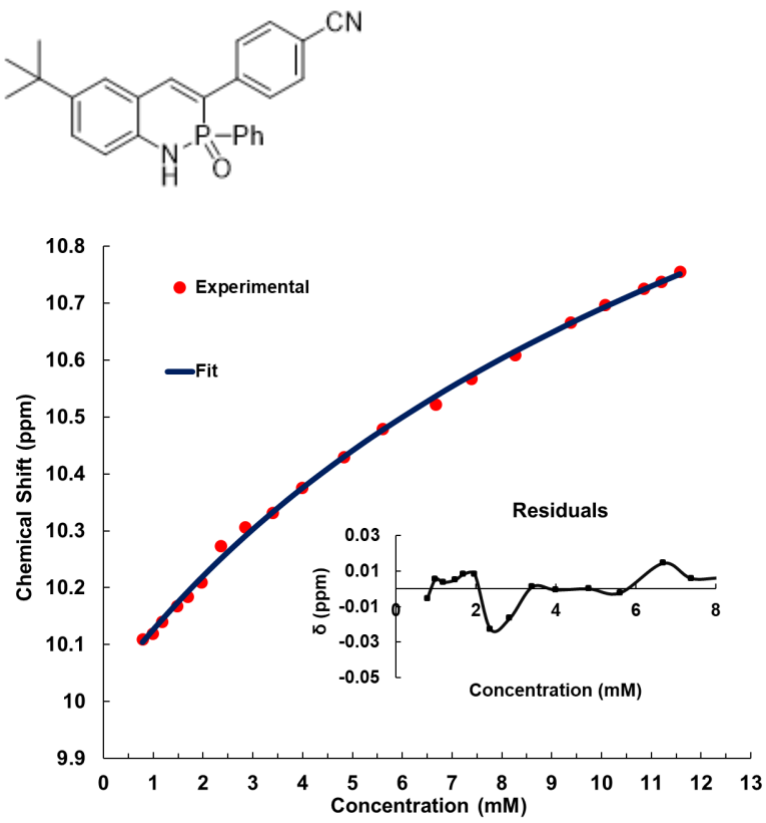

Figure A.20. Binding isotherm (red), fit (blue), and residuals (inset) of VC NMR of **2e**.

Table A.20. Experimental and fitting data for VC NMR of **2e**

Concentration (mM)	Experimental δ (ppm)	Fit δ (ppm)
11.6	10.7552	10.75070613
11.2	10.7379	10.73691784
10.9	10.7255	10.72367435
10.1	10.6966	10.69273486
9.39	10.6656	10.66454316
8.27	10.609	10.61499453
7.39	10.5668	10.57278564
6.68	10.5217	10.53634355
5.60	10.4786	10.47648406
4.83	10.4291	10.42926445
3.99	10.3749	10.37444554
3.41	10.3314	10.33263873
2.85	10.3066	10.29015441
2.36	10.2735	10.25087549
1.97	10.2087	10.21706939
1.69	10.1835	10.19180097
1.48	10.1671	10.17218912
1.18	10.1399	10.14371351
0.985	10.1185	10.12402601
0.788	10.109	10.1037383

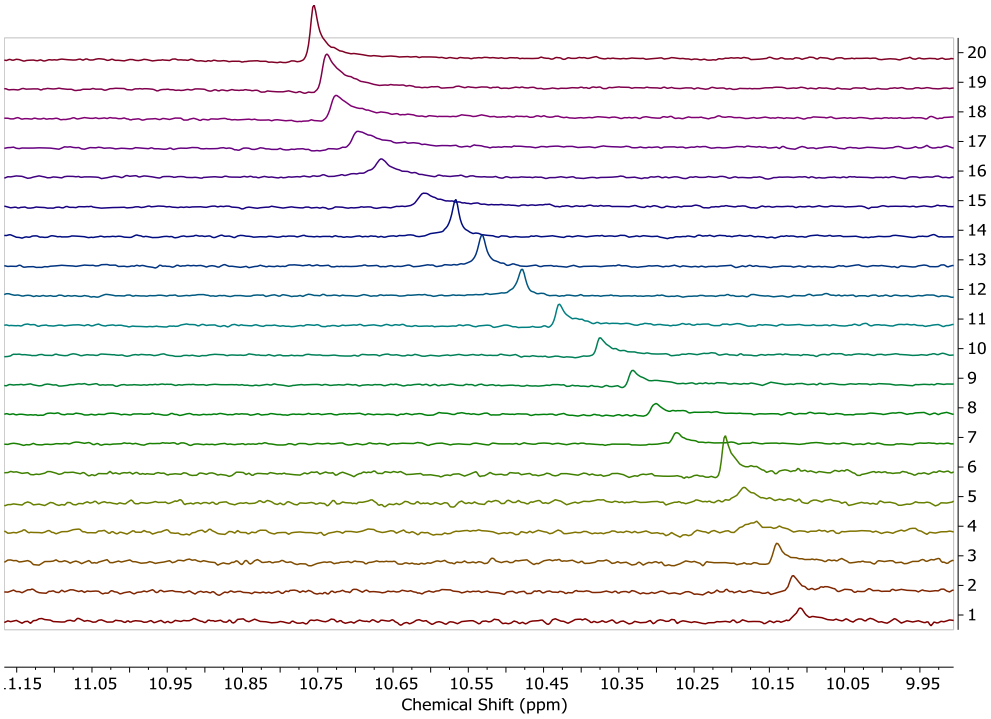

Figure A.21. Representative ^{31}P NMR spectra for VC NMR of **2e**.

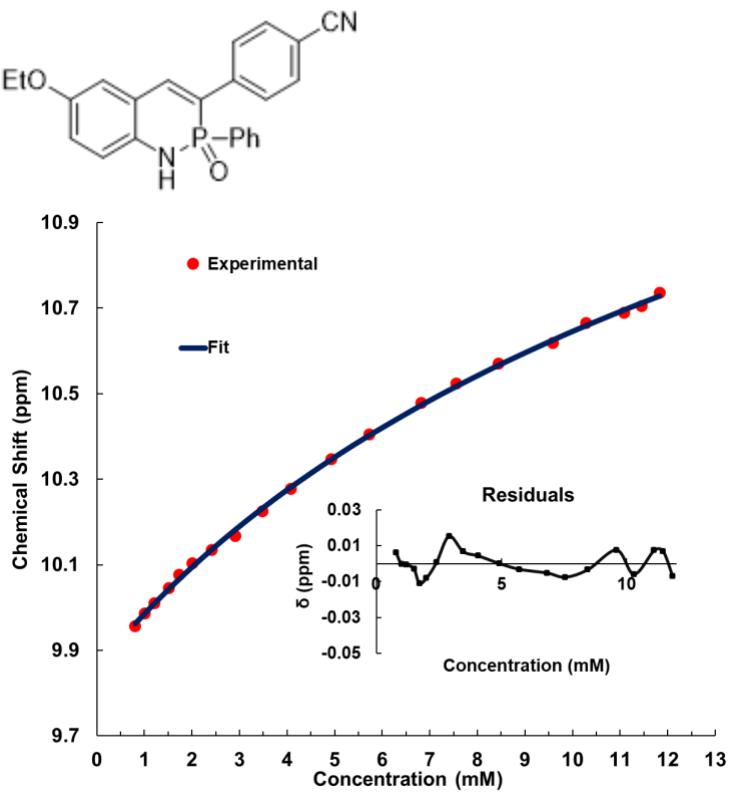

Figure A.22. Binding isotherm (red), fit (blue), and residuals (inset) of VC NMR of **2f**.

Table A.21. Experimental and fitting data for VC NMR of **2f**

Concentration (mM)	Experimental δ (ppm)	Fit δ (ppm)
11.8	10.7356	10.7285531
11.4	10.7052	10.712116
11.0	10.689	10.6963319
10.3	10.6654	10.6594712
9.59	10.6183	10.6259015
8.45	10.5703	10.5669423
7.55	10.5243	10.51676
6.83	10.4787	10.4734671
5.72	10.4056	10.4024241
4.93	10.3464	10.3464462
4.08	10.2772	10.2815335
3.48	10.2254	10.2320847
2.91	10.1666	10.1818864
2.41	10.1348	10.1355237
2.01	10.1038	10.0956594
1.72	10.0768	10.0658868
1.51	10.0456	10.0427937
1.21	10.01	10.0092865
1.01	9.9864	9.98613666
0.805	9.9561	9.96229545

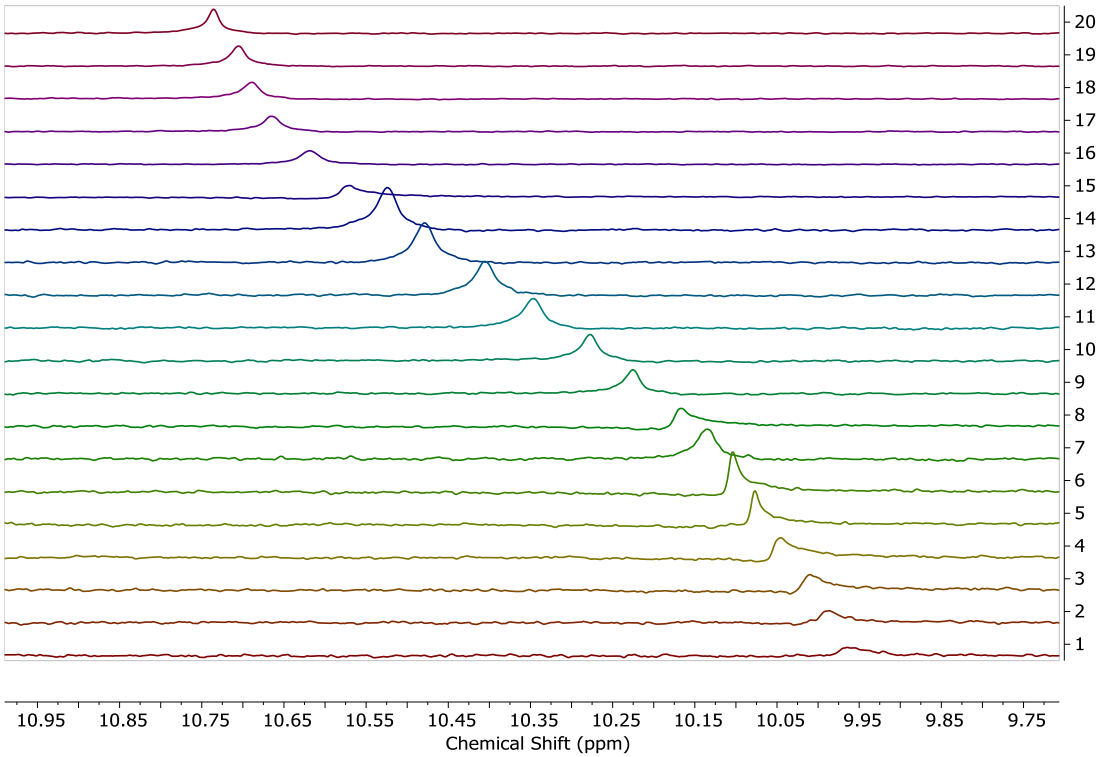

Figure A.23. Representative ^{31}P NMR spectra for VC NMR experiment of **2f**.

Computational studies on dimer interactions

The geometries for dimeric complexes of **2f** and its -OPh counterpart were fully optimized without symmetry constraint by using the functional M06-2X[11] (accounting for the contributions of H-bond/dispersion forces) and TZVP basis set as implemented in Gaussian 09. The PCM solvation model was used to account for the effects of the chloroform environment. All of the optimized structures were confirmed by frequency calculations to be minima using the same level of theory. The solution-phase optimized geometries were used in the following calculations. The natural bond order (NBO) analyses were carried out using NBO 3.1 embedded in Gaussian 09 package. The NCI plot were performed by using the Multiwfn program.[12]

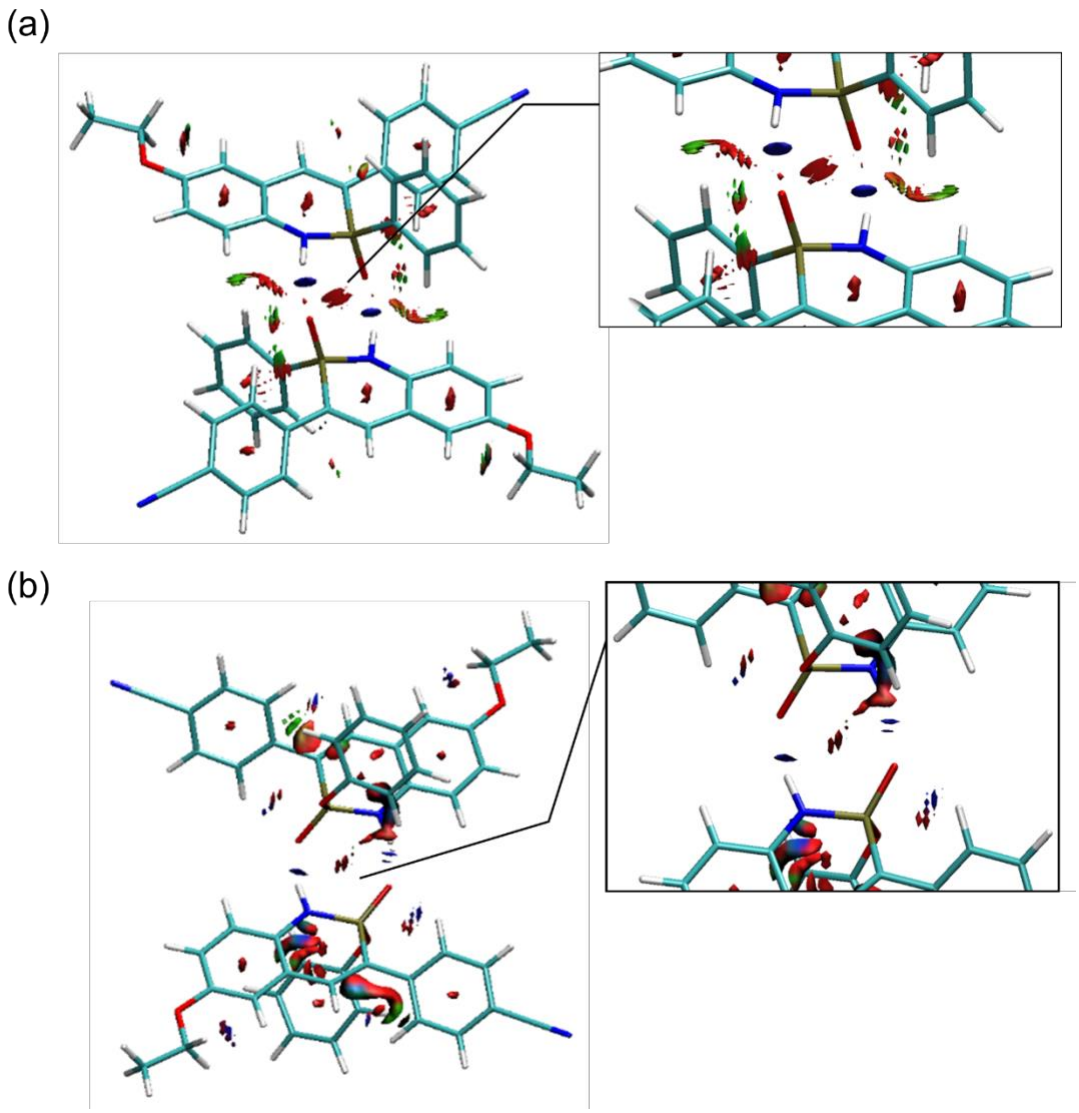

Figure A.24. The NCI plots for (a) **2f** and (b) its -OPh analogue *meso*-dimeric motifs at the PCM($CHCl_3$)-M06-2X/TZVP equilibrium geometries. NCI regions are represented as solid surfaces and blue−green−red scaling from $-0.02 < \text{sign}(\lambda_2)\rho(r) < 0$ (in a.u.), where red surface indicates strong repulsion, blue surface strong attraction and green surface relatively weak interactions. Isosurface cutoff for NCI = 0.5.

(a)

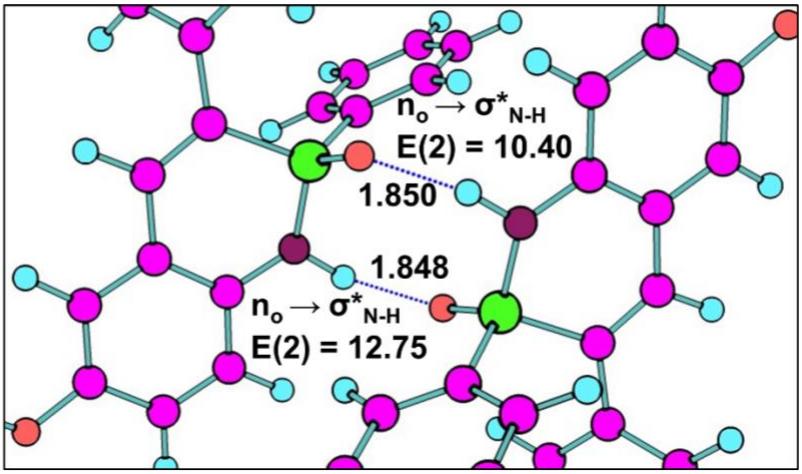

(b)

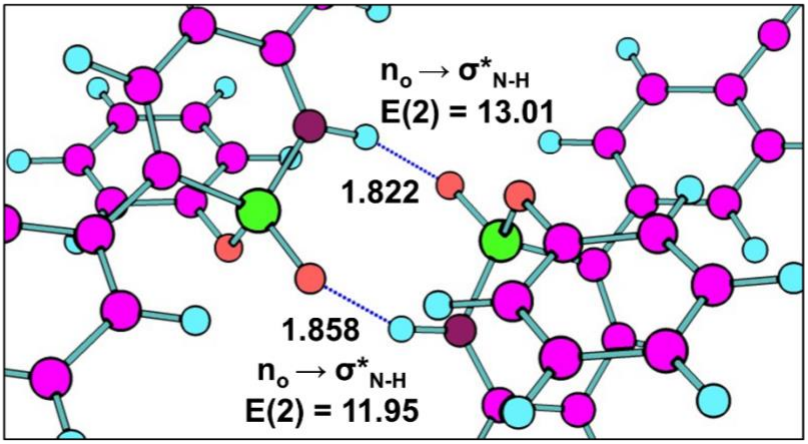

Figure A.25. The NBO charge transfer stabilization energy [second-order perturbation energies E(2), in kcal/mol] for the indicated H-bond interactions in (a) **2f** and (b) its -OPh analogue at PCM($CHCl_3$)-M06-2X/TZVP equilibrium geometries of the *meso*-dimeric motifs. The indicated H-bond interactions shown by the broken line, and H-bond distances in Å.

6. References:

(1) Sheldrick, G. M. Bruker/Siemens Area Detector Absorption Correction Program, Bruker AXS, Madison, WI, 1998.

(2) Van der Sluis, P.; Spek, A. L. BYPASS: an effective method for the refinement of crystal structures containing disordered solvent regions. *Acta Cryst., Sect. A* **1990**, *A46*, 194−201.

(3) Sheldrick, G. M. Crystal structure refinement with SHELXL. *Acta Cryst.* **2015**, *C71*, 3−8.

(4) Adamo, C.; Barone, V. Toward reliable density functional methods without adjustable parameters: The PBE0 model *J. Chem. Phys.* **1999**, *110*, 6158-6169.

(5) Bremond, E.; Savarese, M.; Su, N. Q.; Perez-Jimenez, A. J.; Xu, X.; Sancho-Garcia, J. C.; Adamo, C. Benchmarking density functionals on structural parameters of small-/medium-sized organic molecules *J. Chem. Theory Comput.* **2016**, *12*, 459–465.

(6) Schuafer, A.; Huber, C.; Ahlrichs, R. Fully optimized contracted Gaussian basis sets of triple zeta valence quality for atoms Li to Kr *J. Chem. Phys.* **1994**, *100*, 5829–5835.

(7) Gaussian 09, Revision E.01, Frisch, M. J.; Trucks, G. W.; Schlegel, H. B.; Scuseria, G. E.; Robb, M. A.; Cheeseman, J. R.; Scalmani, G.; Barone, V.; Mennucci, B.; Petersson, G. A.; Nakatsuji, H.; Caricato, M.; Li, X.; Hratchian, H. P.; Izmaylov, A. F.; Bloino, J.; Zheng, G.; Sonnenberg, J. L.; Hada, M.; Ehara, M.; Toyota, K.; Fukuda, R.; Hasegawa, J.; Ishida, M.; Nakajima, T.; Honda, Y.; Kitao, O.; Nakai, H.; Vreven, T.; Montgomery, J. A., Jr.; Peralta, J. E.; Ogliaro, F.; Bearpark, M.; Heyd, J. J.; Brothers, E.; Kudin, K. N.; Staroverov, V. N.; Kobayashi, R.; Normand, J.; Raghavachari, K.; Rendell, A.; Burant, J. C.; Iyengar, S. S.; Tomasi, J.; Cossi, M.; Rega, N.; Millam, J. M.; Klene, M.; Knox, J. E.; Cross, J. B.; Bakken, V.; Adamo, C.; Jaramillo, J.; Gomperts, R.; Stratmann, R. E.; Yazyev, O.; Austin, A. J.; Cammi, R.; Pomelli, C.; Ochterski, J. W.; Martin, R. L.; Morokuma, K.; Zakrzewski, V. G.; Voth, G. A.; Salvador, P.; Dannenberg, J. J.; Dapprich, S.; Daniels, A. D.; Farkas, Ö.; Foresman, J. B.; Ortiz, J. V.; Cioslowski, J.; Fox, D. J. Gaussian, Inc., Wallingford CT, **2013**.

(8) Miertus, S.; Scrocco, E.; Tomasi, Electrostatic interaction of a solute with a continuum. A direct utilizaion of AB initio molecular potentials for the prevision of solvent effects J. *Chem. Phys.* **1981**, *55*, 117–129.

(9) Barone, V.; Cossi, M.; Tomasi, J. Geometry optimization of molecular structures in solution by the polarizable continuum model *J. Comput. Chem.* **1998**, *19*, 404–417.

(10) Thordarson, P. Determining association constants from titration experiments in supramolecular chemistry. *Chem. Soc. Rev.* **2011**, *40*, 1305−1323.

(11) Zhao, Y.; Truhlar, D. G. The M06 suite of density functionals for main group thermochemistry, thermochemical kinetics, noncovalent interactions, excited states, and transition elements: two new functionals and systematic testing of four M06-class functionals and 12 other functionals *Theor. Chem. Acc.* **2008**, *120*, 215–241.

(12) Lu, T.; Chen, F. Multiwfn: A multifunctional wavefunction analyzer *J. Comput. Chem.* **2012**, *33*, 580–592.

7. Copies of NMR Spectra

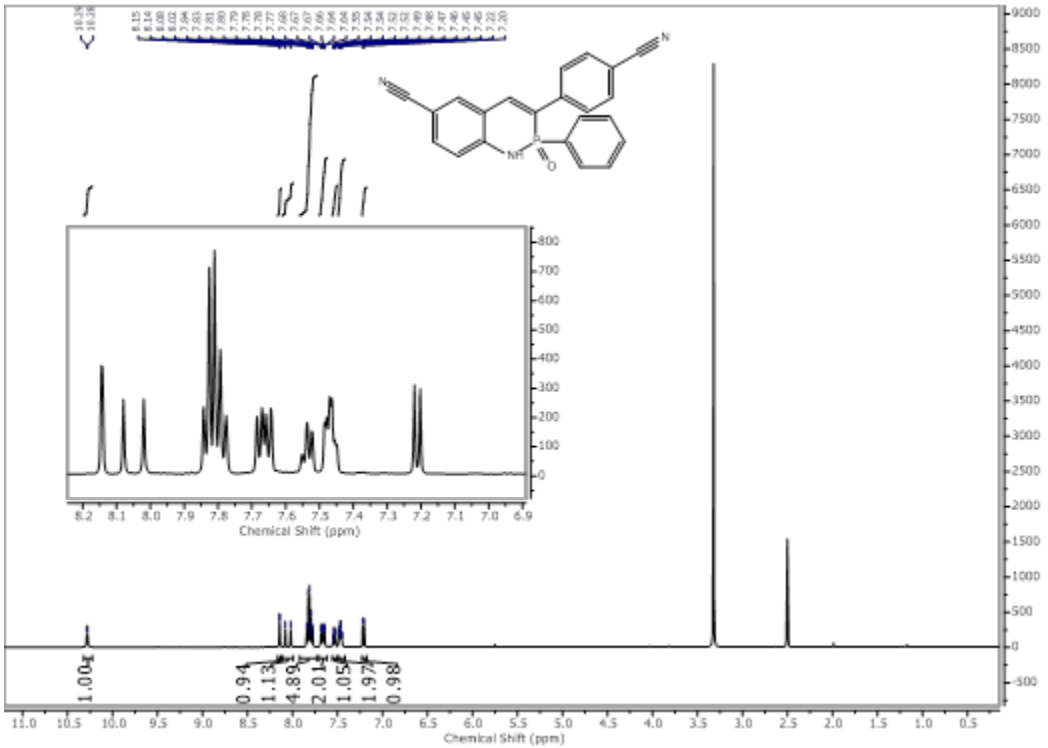

Figure A.26. ^{1}H NMR spectrum of **2a** in DMSO-d$_6$.

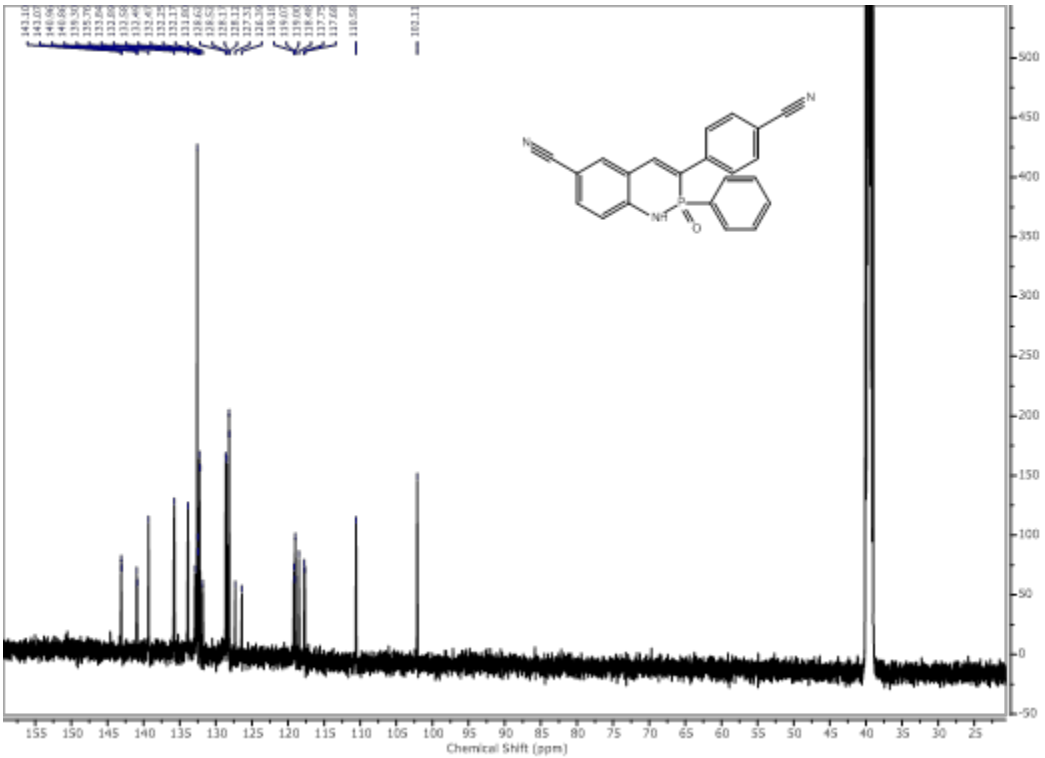

Figure A.27. ^{13}C NMR spectrum of **2a** in DMSO-d$_6$.

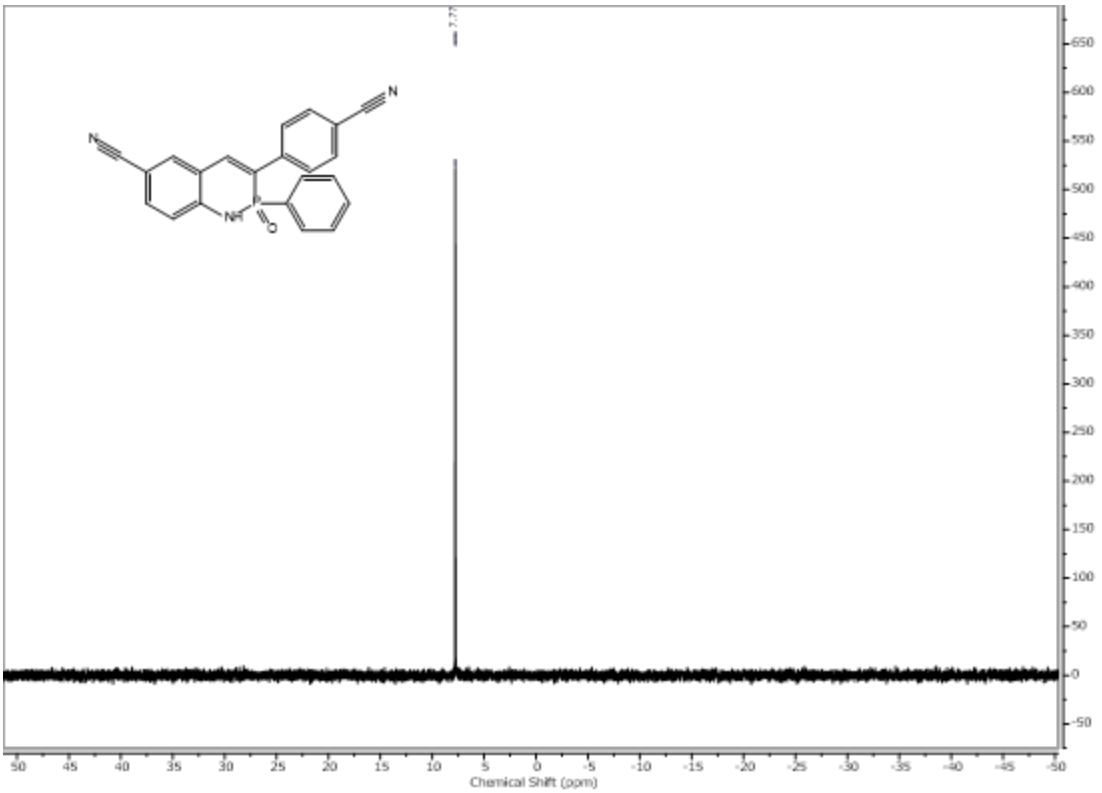

Figure A.28. ^{31}P NMR spectrum of **2a** in DMSO-d$_6$.

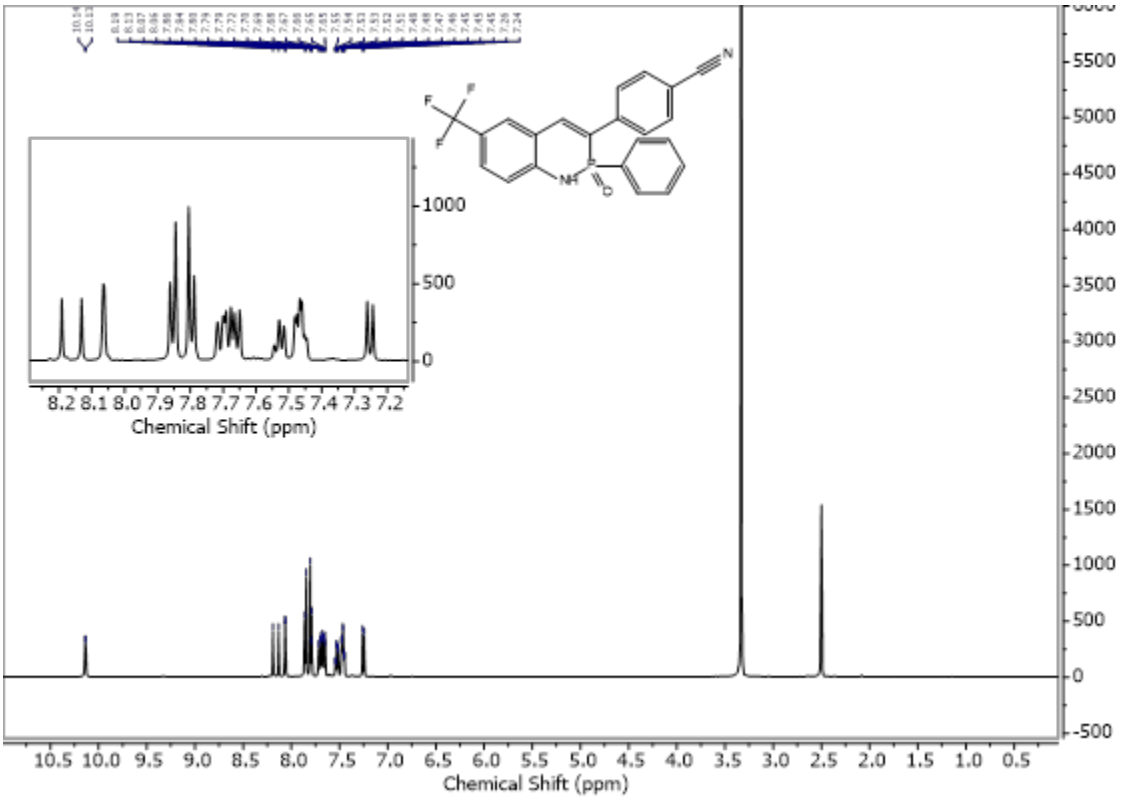

Figure A.29. ^{1}H NMR spectrum of **2b** in DMSO-d$_6$.

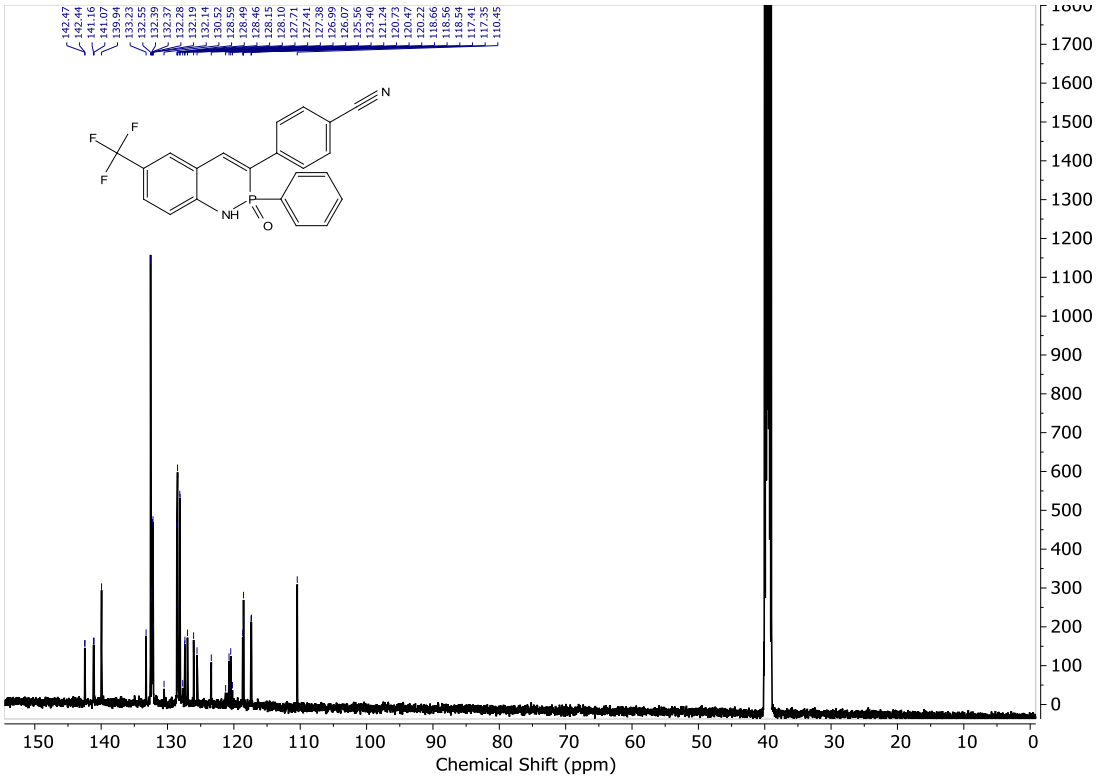

Figure A.30. ^{13}C NMR spectrum of **2b** in DMSO-d_6.

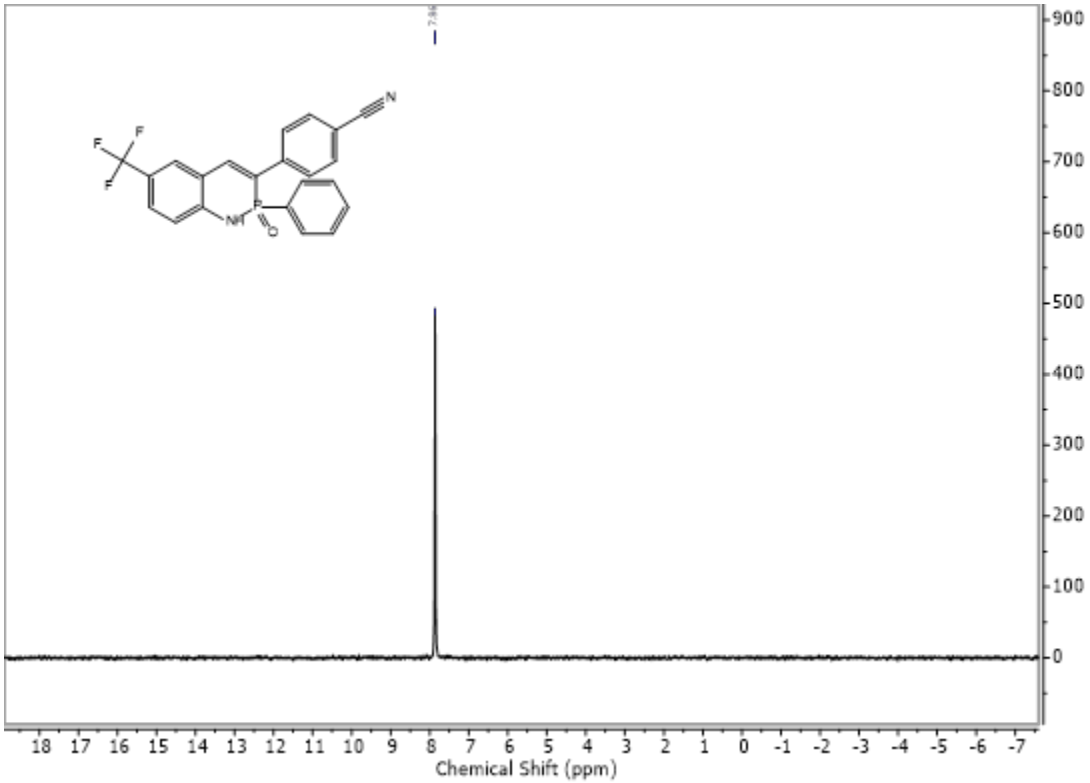

Figure A.31. ^{31}P NMR spectrum of **2b** in DMSO-d_6.

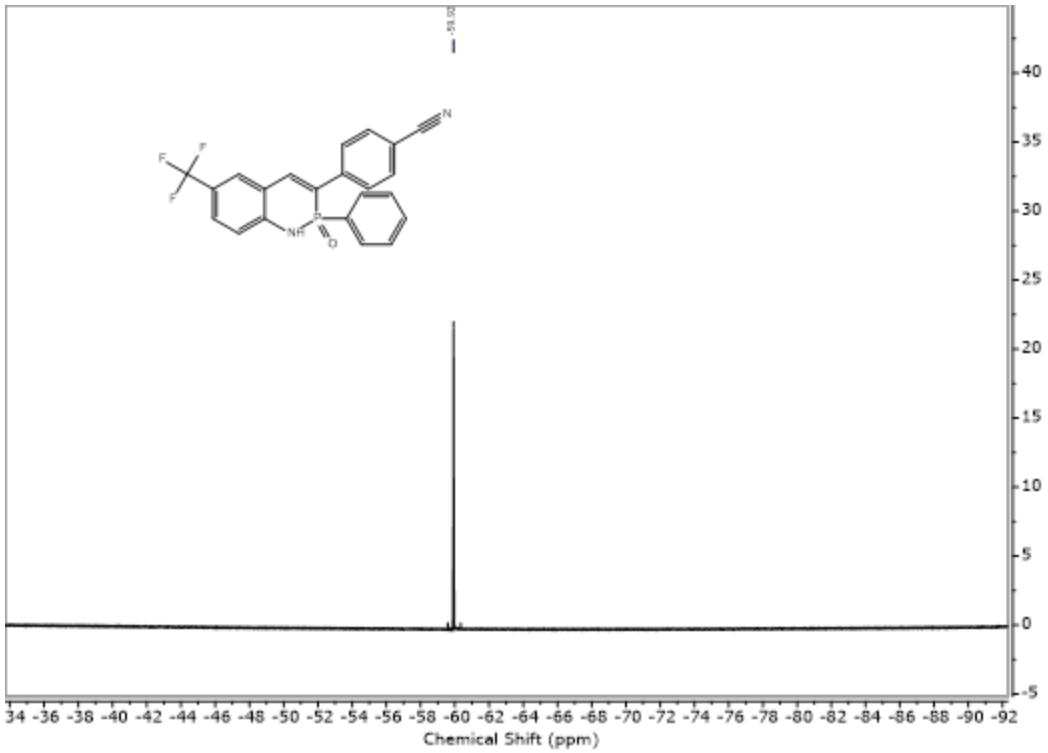

Figure A.32. ^{19}F NMR spectrum of **2b** in DMSO-d$_6$.

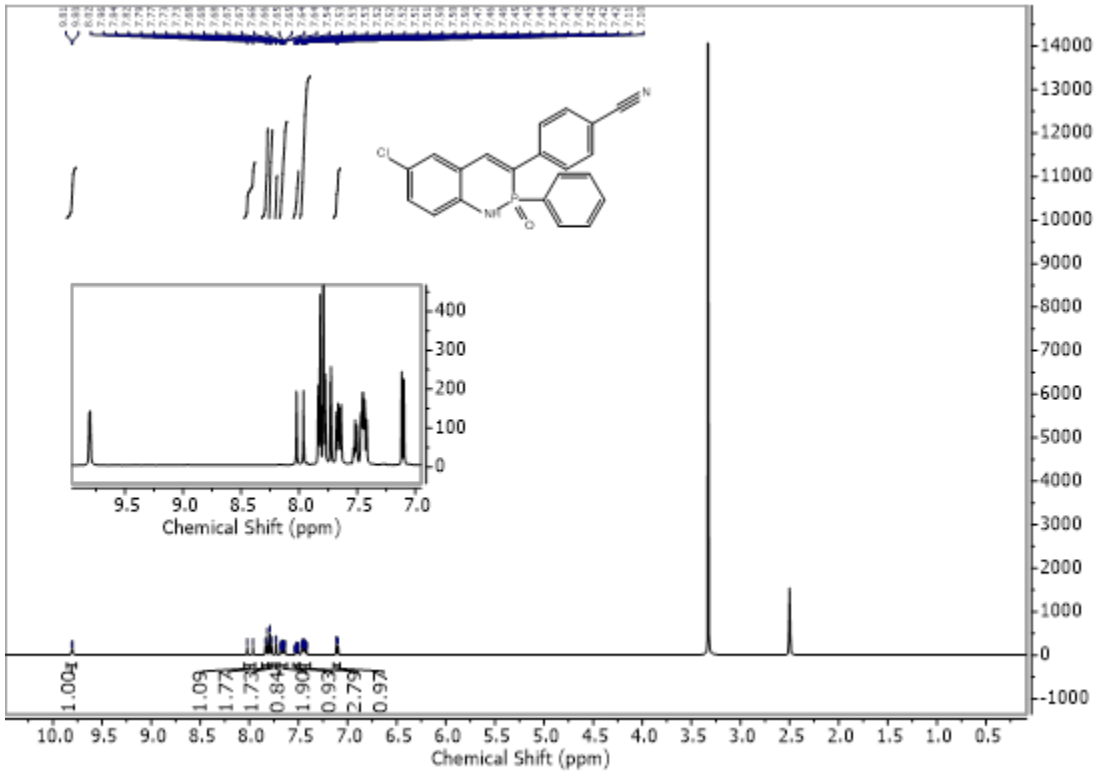

Figure A.33. ^{1}H NMR spectrum of **2c** in DMSO-d$_6$.

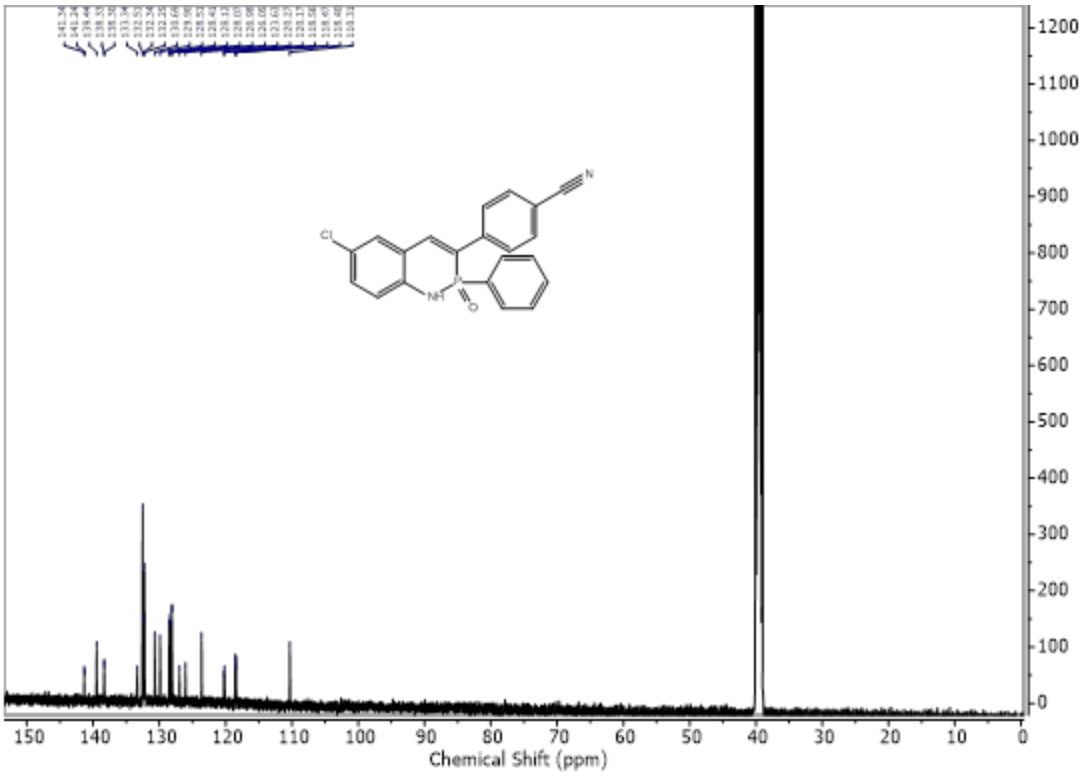

Figure A.34. ^{13}C NMR spectrum of **2c** in DMSO-d$_6$.

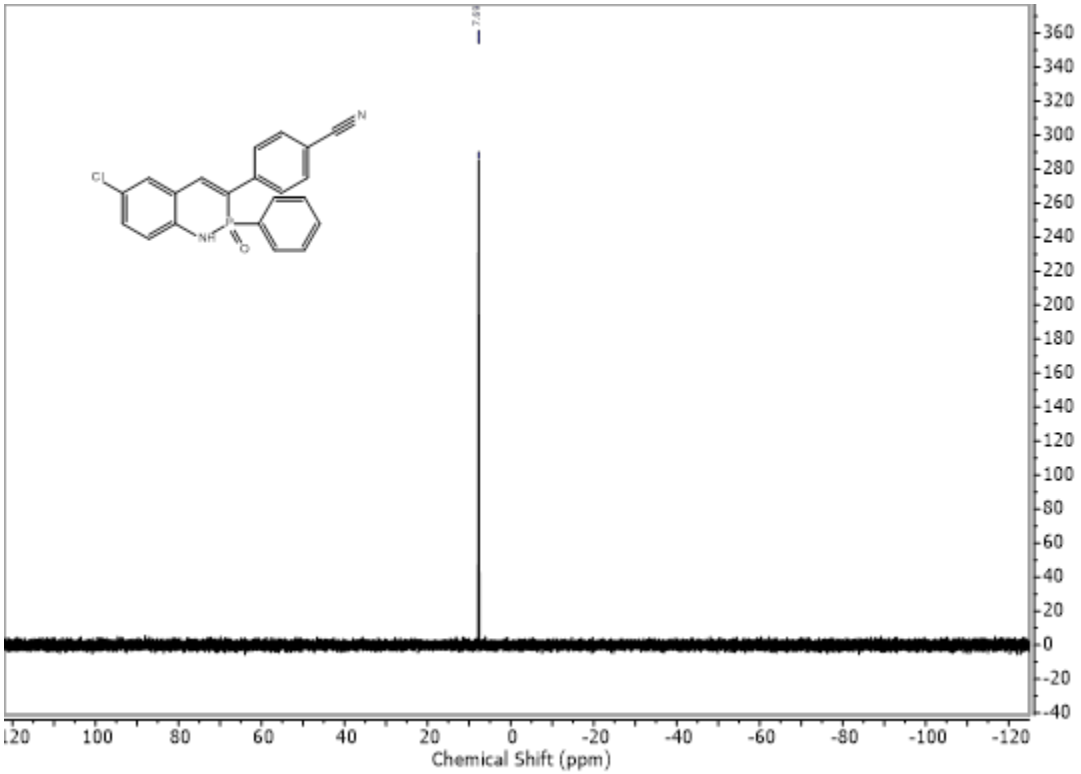

Figure A.35. ^{31}P NMR spectrum of **2c** in DMSO-d$_6$.

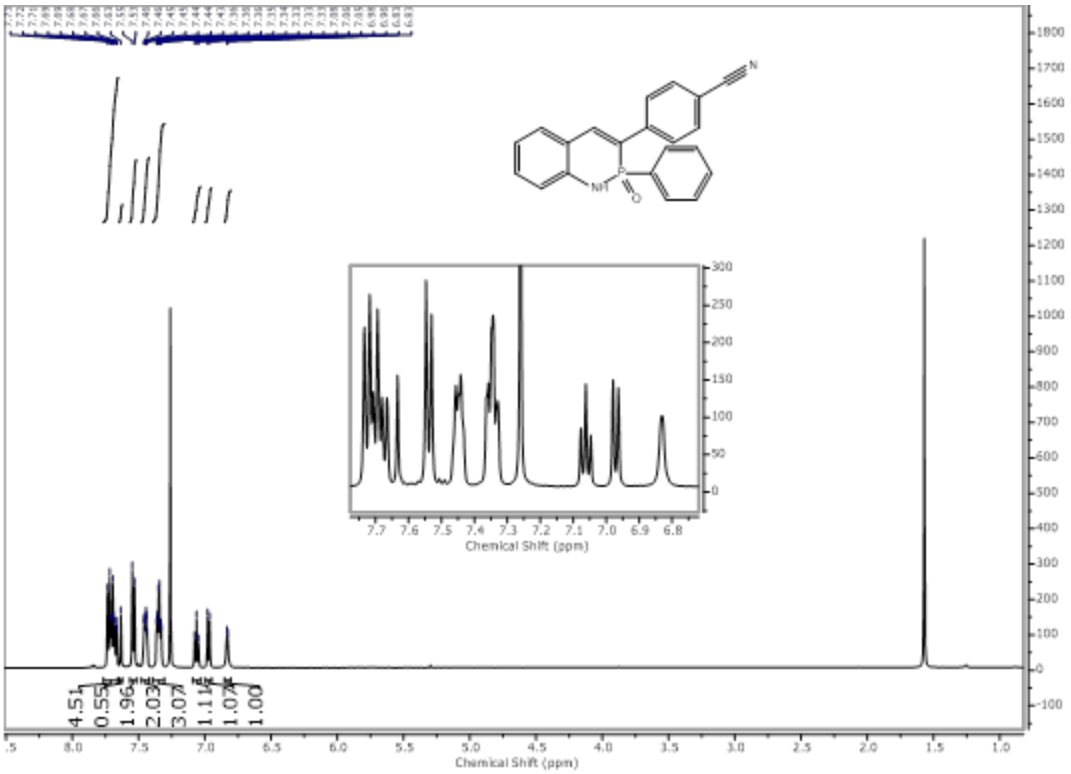

Figure A.36. ^{1}H NMR spectrum of **2d** in $CDCl_3$.

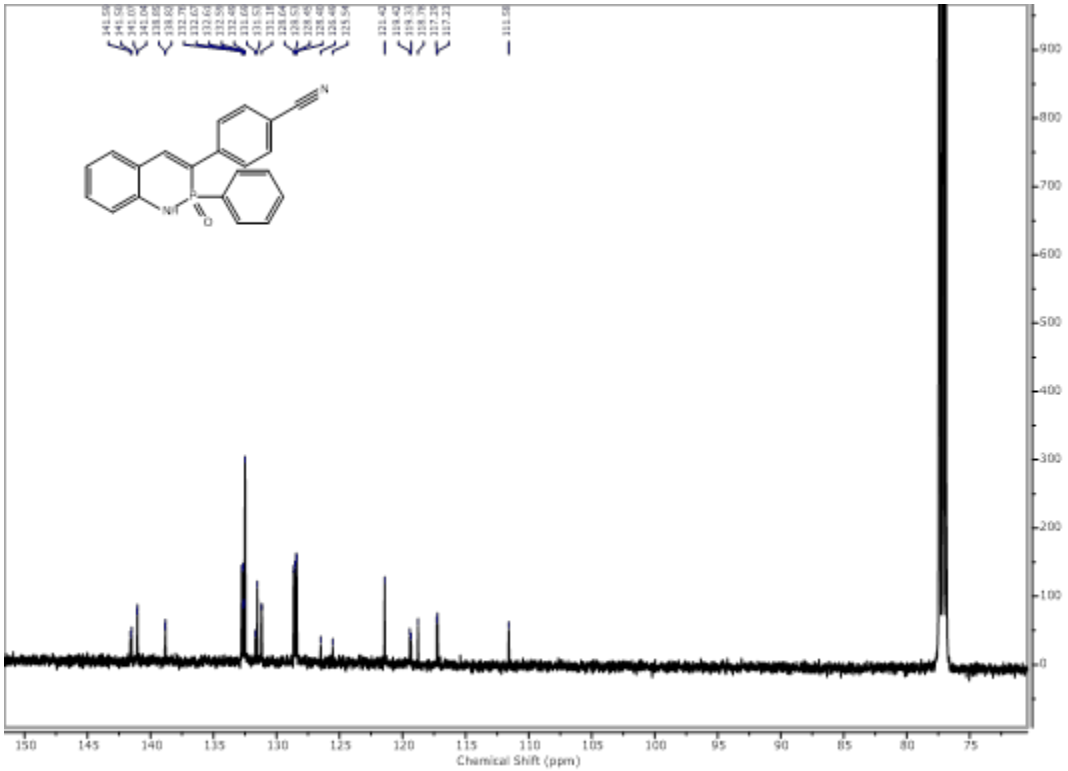

Figure A.37. ^{13}C NMR spectrum of **2d** in $CDCl_3$.

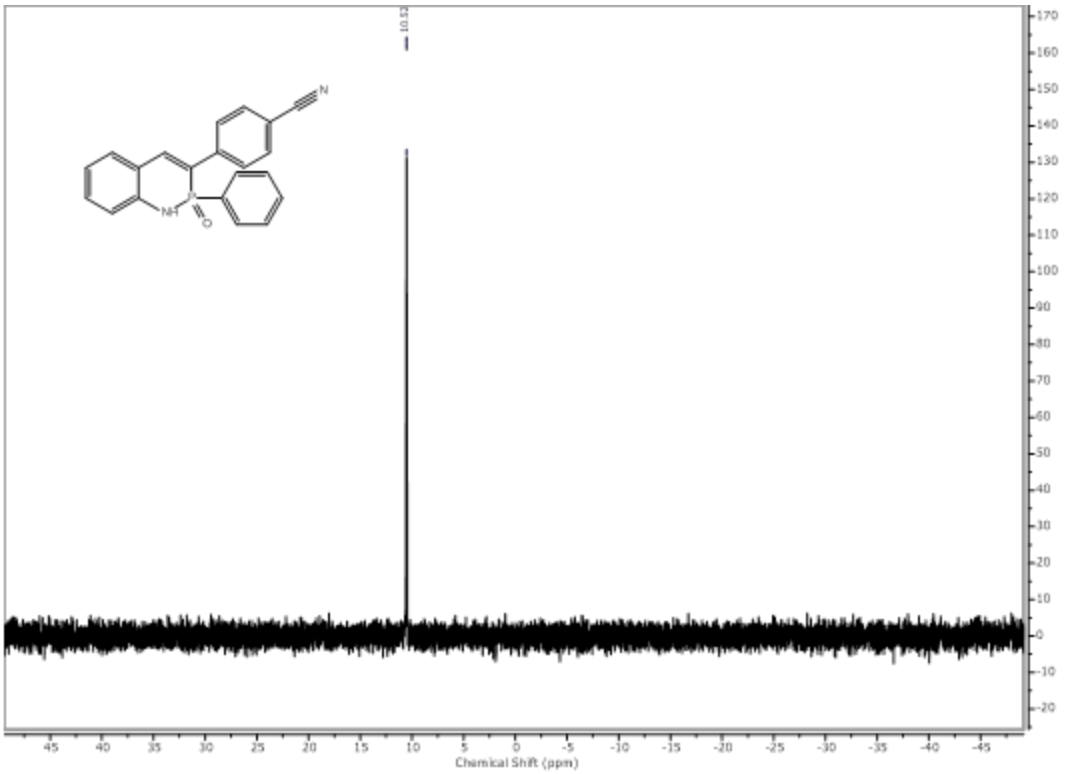

Figure A.38. ^{31}P NMR spectrum of **2d** in $CDCl_3$.

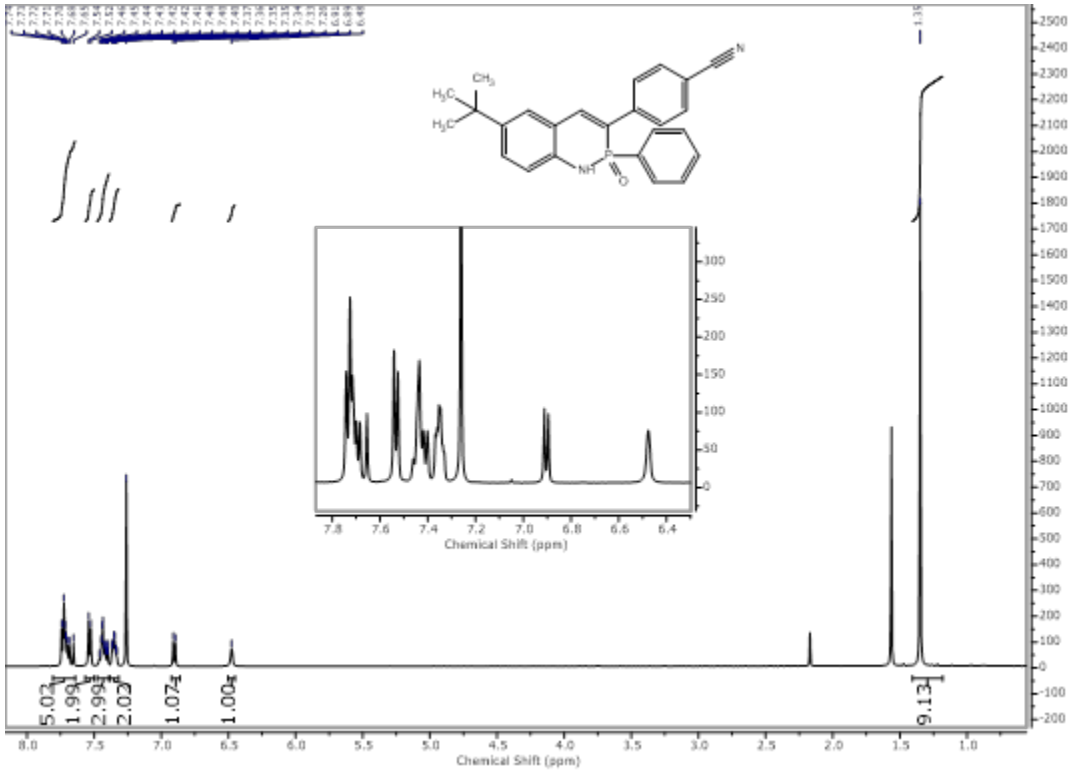

Figure A.39. ^{1}H NMR spectrum of **2e** in $CDCl_3$.

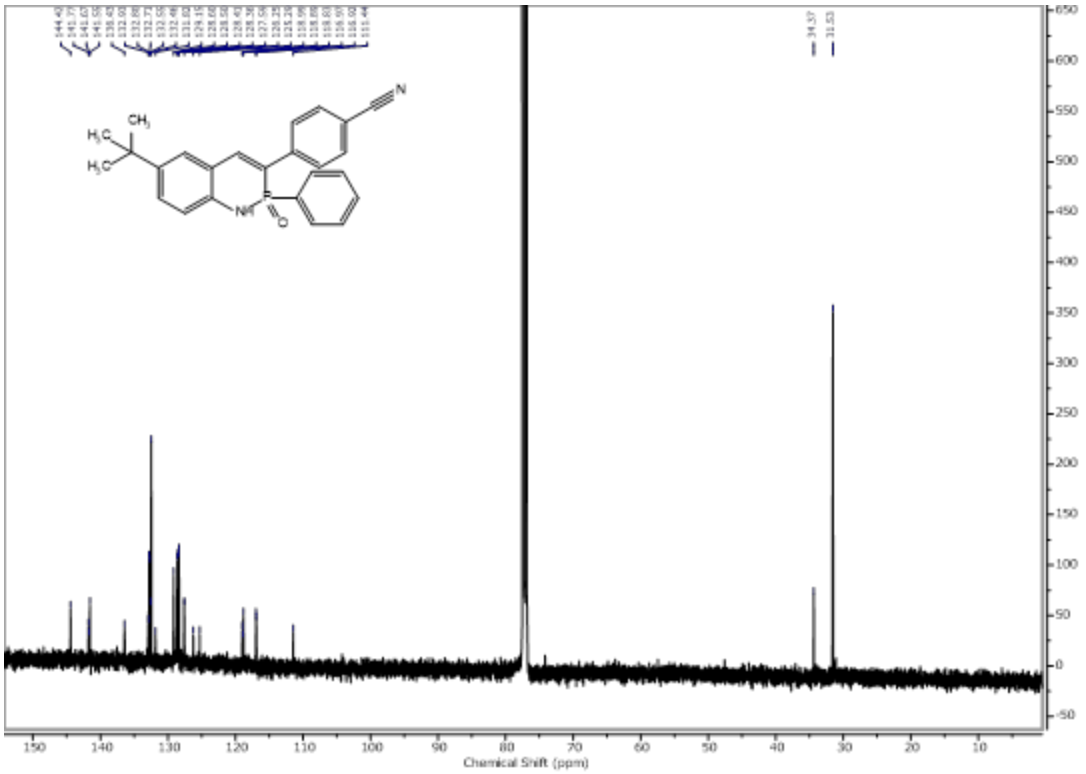

Figure A.40. ^{13}C NMR spectrum of **2e** in $CDCl_3$.

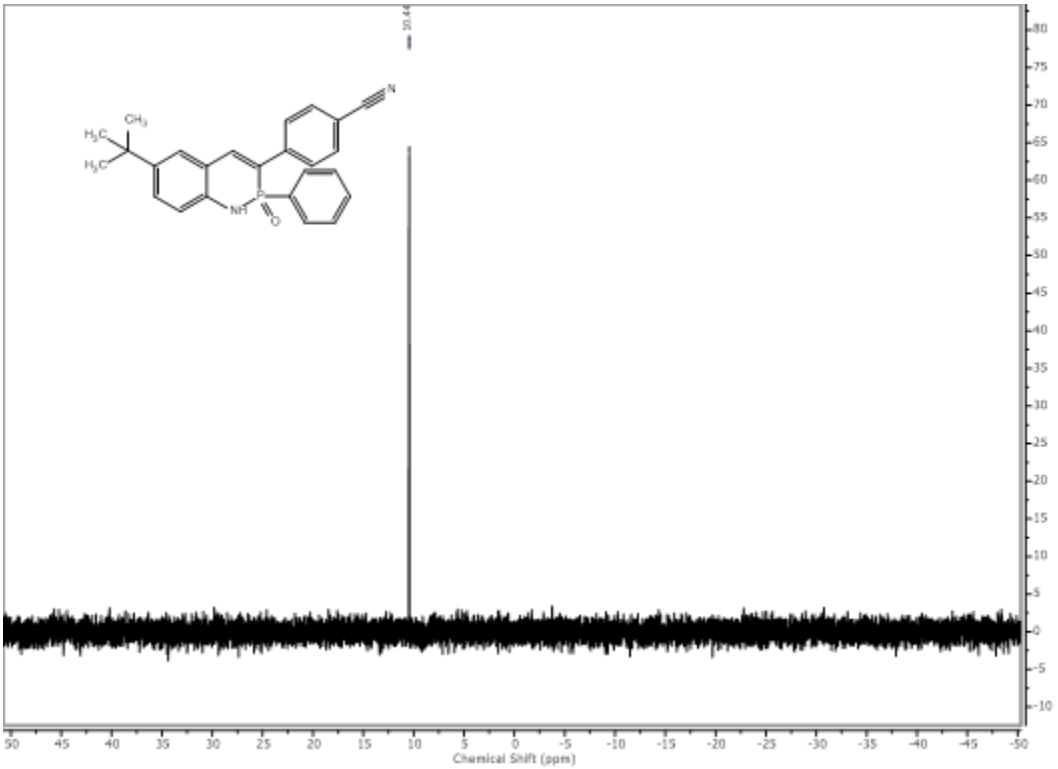

Figure A.41. ^{31}P NMR spectrum of **2e** in $CDCl_3$.

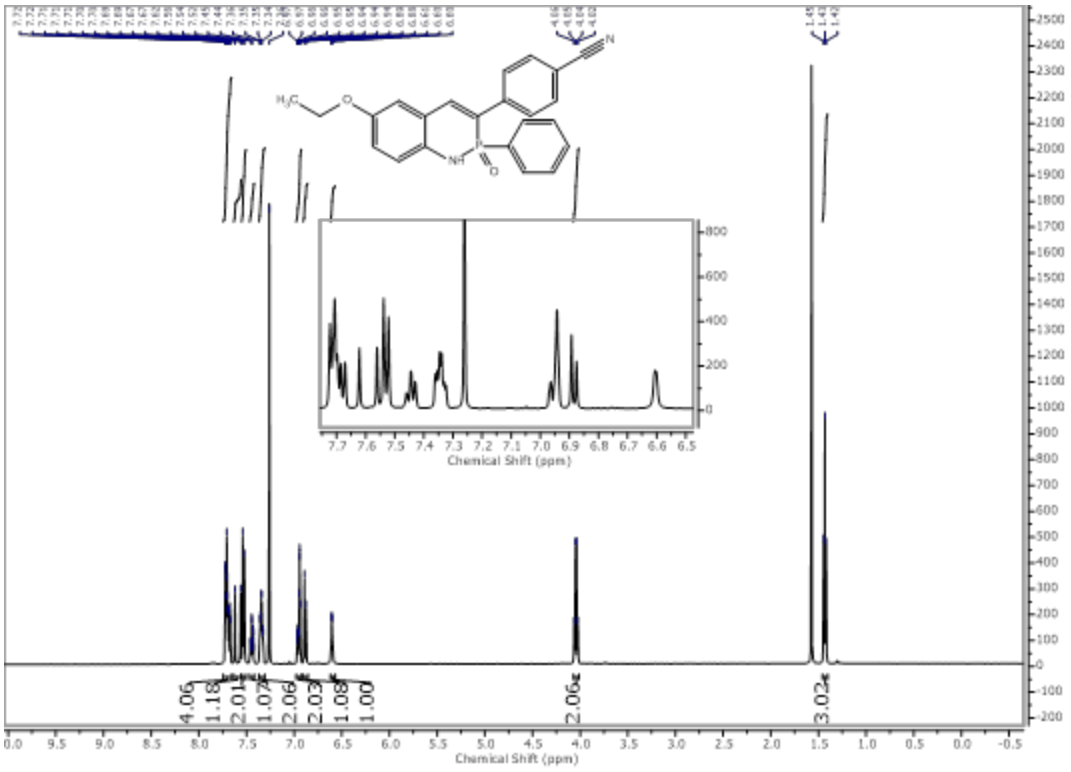

Figure A.42. ^{1}H NMR spectrum of **2f** in $CDCl_3$.

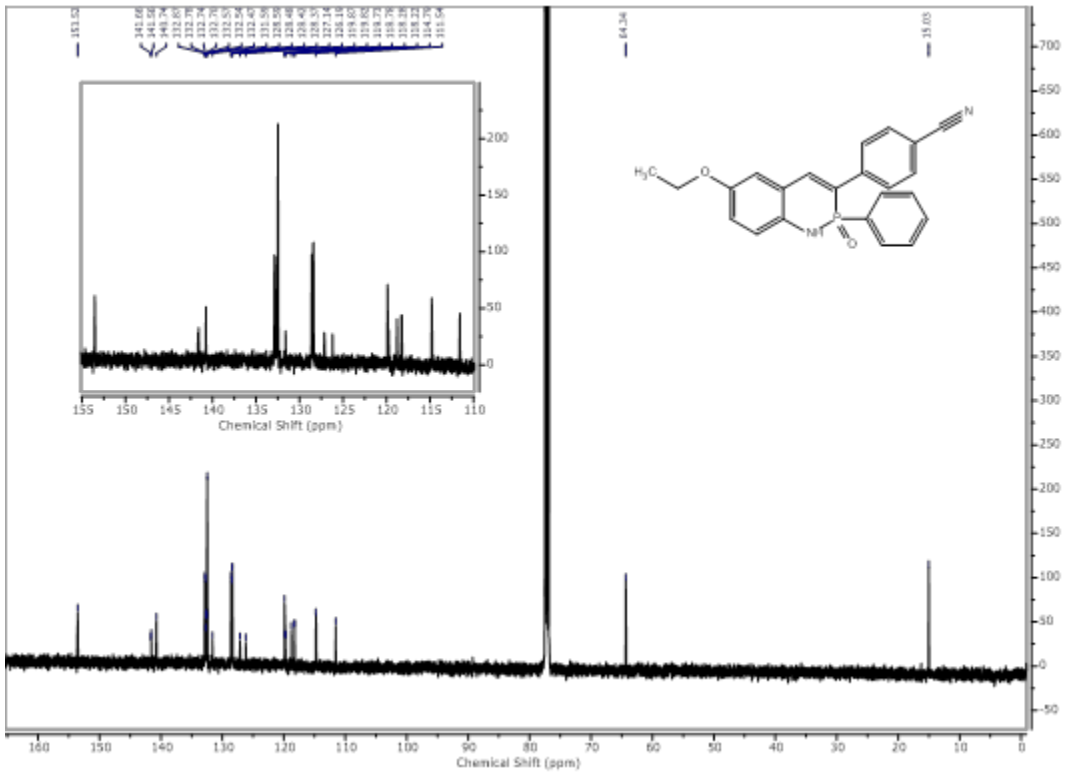

Figure A.43. ^{13}C NMR spectrum of **2f** in $CDCl_3$.

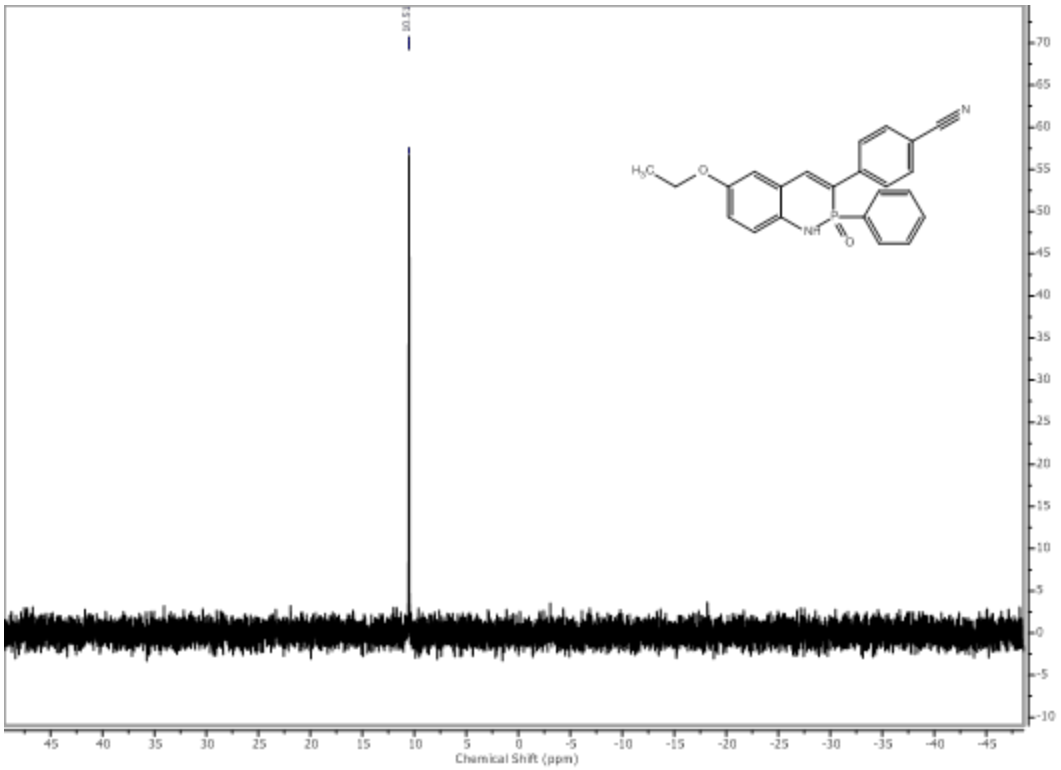

Figure A.44. ^{31}P NMR spectrum of **2f** in $CDCl_3$.

APPENDIX B

SUPPLEMENTARY CONTENT FOR CHAPTER THREE

Synthesis

General Methods: All reagents were purchased from conventional commercial sources and used as received, unless otherwise noted. All NMR spectra were acquired at room temperature on a ^{1}H NMR, ^{13}C NMR, and ^{19}F spectra were obtained using a Bruker 500 MHz spectrometer (^{1}H 500 MHz, ^{13}C 126 MHz, ^{19}F 471 MHz). All ^{1}H and ^{13}C chemical shifts (δ) are reported in ppm relative to the residual $CHCl_3$ (^{1}H: 7.26 ppm, ^{13}C: 77.16 ppm) or $(CH_3)_2CO$ (^{1}H: 2.05, ^{13}C: 206.26, 29.84).

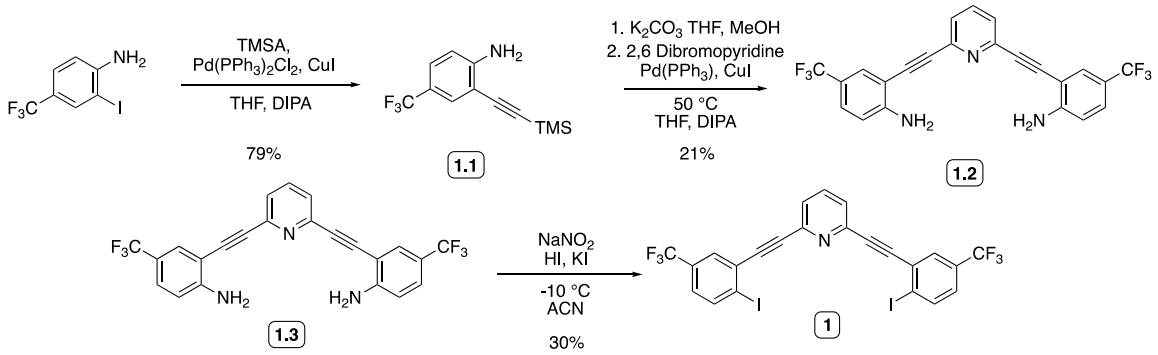

Scheme B1: The second, more successful, synthetic path for reaching host receptor **1**

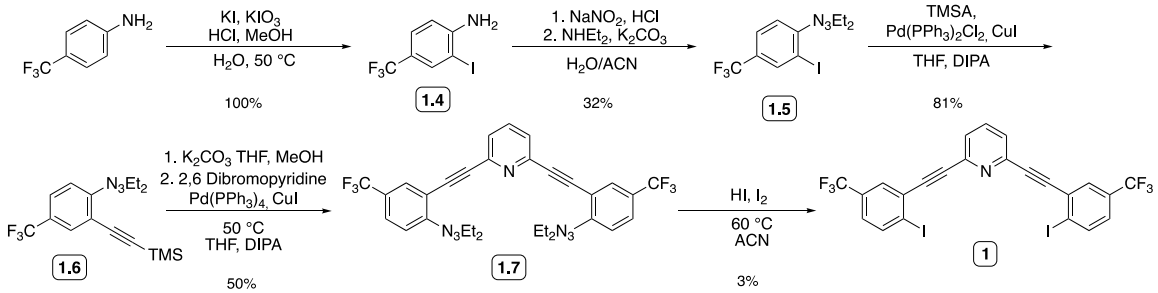

Scheme B2: The original, low yielding, synthetic path for accessing receptor **1**

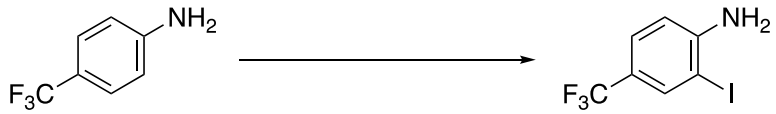

2-Iodo-4-Trifluoromethyl Aniline (1.4)

KI (2.1638g, 13 mmol) and KIO_3 (1.5762, 7.4 mmol) were added to a RBF containing DI water (60mL) and set stirring. 2-iodo-4-trifluoromethyl aniline (3.0216g, 18.8 mmol) was then dissolved in MeOH (10 mL) and added to the aqueous solution dropwise. Once everything was dissolved in solution 1M HCl was added dropwise (20.5 mL, 20.5 mmol). The reaction was then left to stir overnight. The next day the reaction was worked up *via* extraction with DCM. The organic phase was washed twice with saturated solution of $NaHCO_3$, then water and finally brine. The organic phase was then dried with $NaSO_4$, filtered and the solvent removed *in vacuo* to yield **1.4** in quantitative yields (3.73 g). ^1H NMR (500 MHz, Acetone-d_6) δ = 7.87 (s, 1H), 7.42 (d, *J*=9.8, 1H), 6.94 (d, *J*=8.5, 1H), 5.53 (s, 2H).

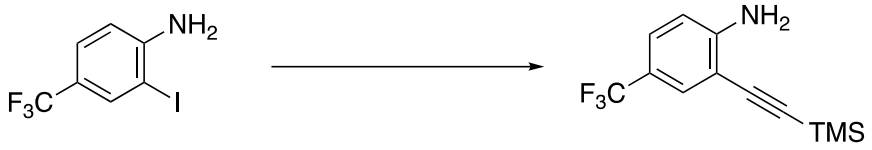

4-(Trifluoromethyl)-2-((trimethylsilyl)ethynyl)aniline (1.1)

The iodo-aniline (8.899g, 31.0 mmol) was dissolved in 200 mL of a 50/50 mixture of THF and DIPA then set outgassing under N_2 for ~3.3 hours. After this time $Pd(PPh_3)_2Cl_2$. (1.088g, 1.55 mmol) and CuI (0.118g, 0.62 mmol) was weighed out and added to the air free flask. Finally, TMSA (12.95 mL, 186 mmol) was added to the solution dropwise via an addition funnel. The solution was run overnight and worked up the next day, assuming TLC control showed all of the starting material gone. The crude product was purified by

column chromatography on silica with EtOAc/Hexanes. The product was produced in 79% yield (6.30 g).

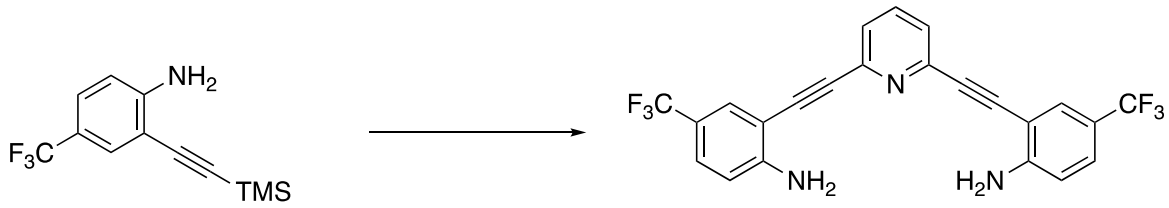

2,2′-(2,6-pyridinediyldi-2,1-ethynediyl)bis[4-(trifluoromethyl)-benzeneamine (1.2)

The TMS protected aniline was (10.3084g, 40 mmol) was dissolved in a minimal amount of a 50/50 mixture of MeOH and THF. K2CO3 (31.295g, 240 mmol) was then added (not all of it will dissolve). The reaction was monitored by TLC control and, after completion, the reaction was filtered and solvent removed by rotary evaporation. The crude product was then redissolved in EtOAc and washed thrice with a saturated aqueous solution of ammonium chloride, then water and finally brine. The organic phase was then dried with $NaSO_4$ and filtered before the EtOAc was removed by rotary evaporator to give the deprotected product in quantitative yields. This was then dissolved in 200 mL of 50/50 THF and DIPA and set outgassing under N_2. In a second flask 2,6-dibromopyridine (5.26 g, 17.2 mmol) was set sparging in 50 mL of THF and DIPA. After sparging was complete $Pd(PPh_3)_4$ (1.37g, 1.72 mmol) and CuI (0.09047g, 0.65 mmol) was added to the first RBF. Then the solution of "elbow" was then cannulated into the first RBF dropwise. The solution was set stirring overnight, and the next day solvent was removed in vacuo and then purified over silica by column chromatography to furnish the bis-aniline in 21% yield (3.74 g).

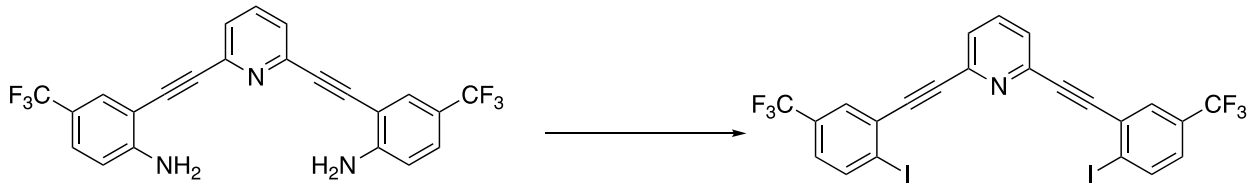

Host Receptor (1)

The bis-aniline (5.53 g, 12.3 mmol) was dissolved in 300 mL of ACN and set stirring in a brine and ice bath until it reaches -10 °C. In a separate RBF concentrated HI was diluted with 100 mL ACN and then cannulated in dropwise, the solution went from a light yellow to a bright orange. Then a 10 mL solution of $NaNO_2$ was added by syringe, dropwise, after which the solution was a dark red. The solution was monitored by TLC and after ~90 minutes the reaction had run to completion. At this point the reaction was cannulated over to a quench solution of KI (5.615g, 30.9 mmol) in water. This solution was washed twice with sodium bicarbonate, water and brine before the organic phase was then dried with $NaSO_4$. The ACN was then removed by rotary evaporation and the product was redissolved in DCM and run through a silica plug. The filtrate was reduced, *in vacuo* to furnish the final receptor in a 30% yield (2.46 g).

NMR Spectra

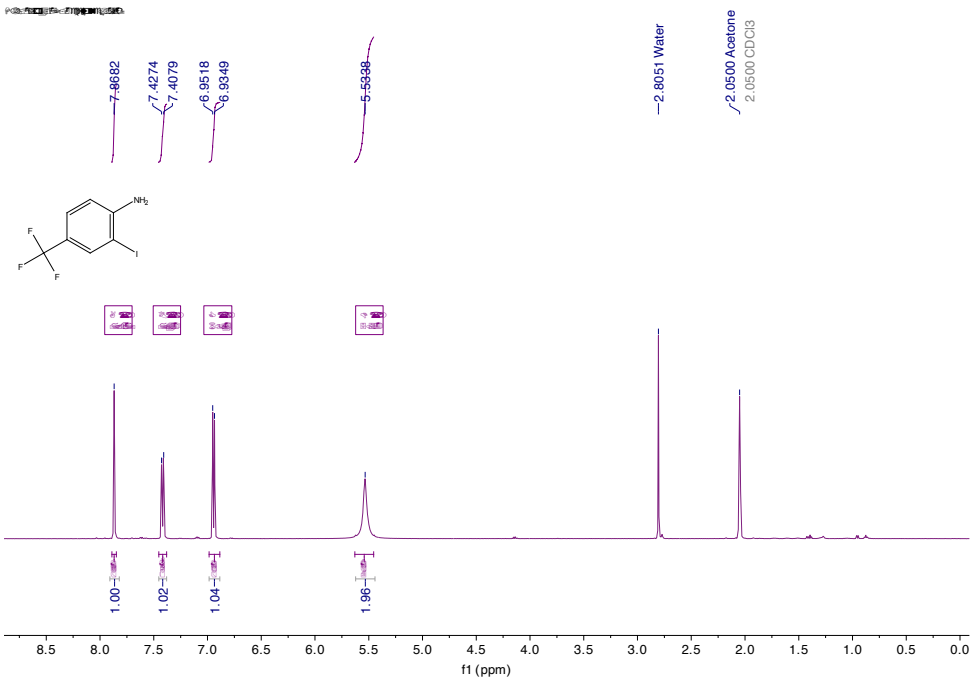

Figure C.1. [1]H NMR spectrum of 2-Iodo-4-Trifluoromethyl Aniline (**1.4**) in acetone-*d6*.

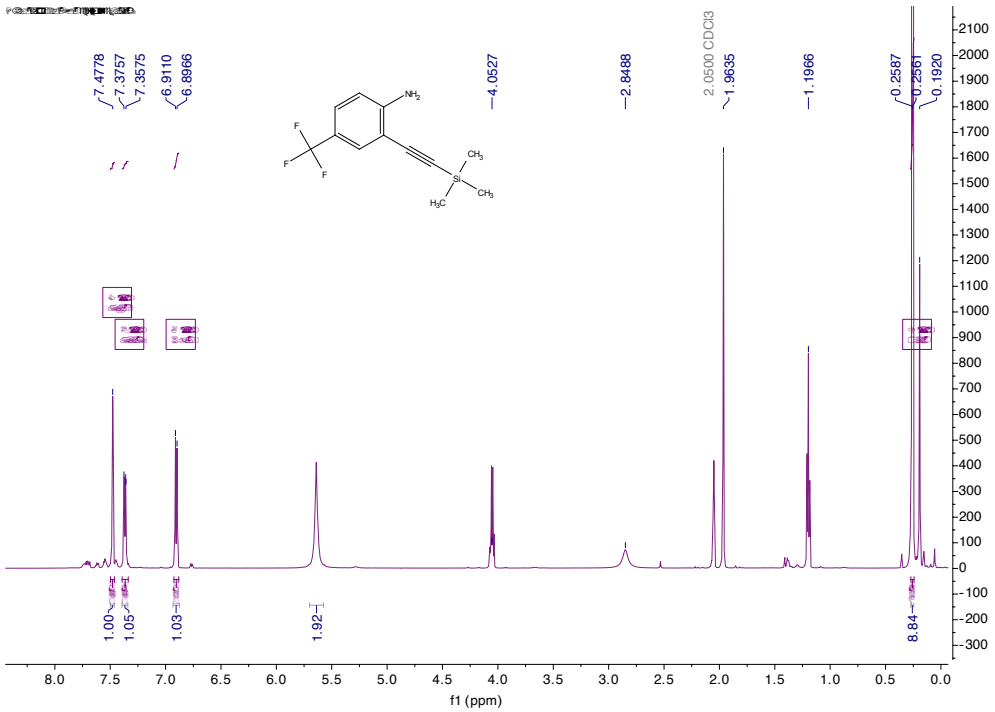

Figure C.2. [1]H NMR spectrum of 4-(Trifluoromethyl)-2-((trimethylsilyl)ethynyl)aniline (**1.1**) in acetone-*d6*.

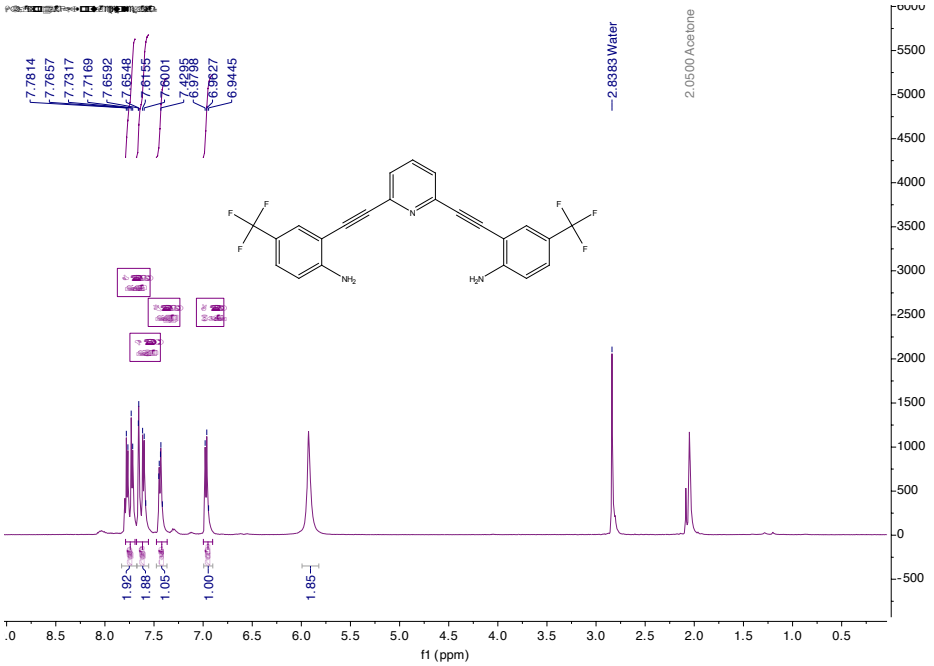

Figure C.3. [1]H NMR spectrum of 2,2′-(2,6-pyridinediyldi-2,1-ethynediyl)bis[4-(trifluoromethyl)-benzeneamine (**1.2**) in acetone-*d6*.

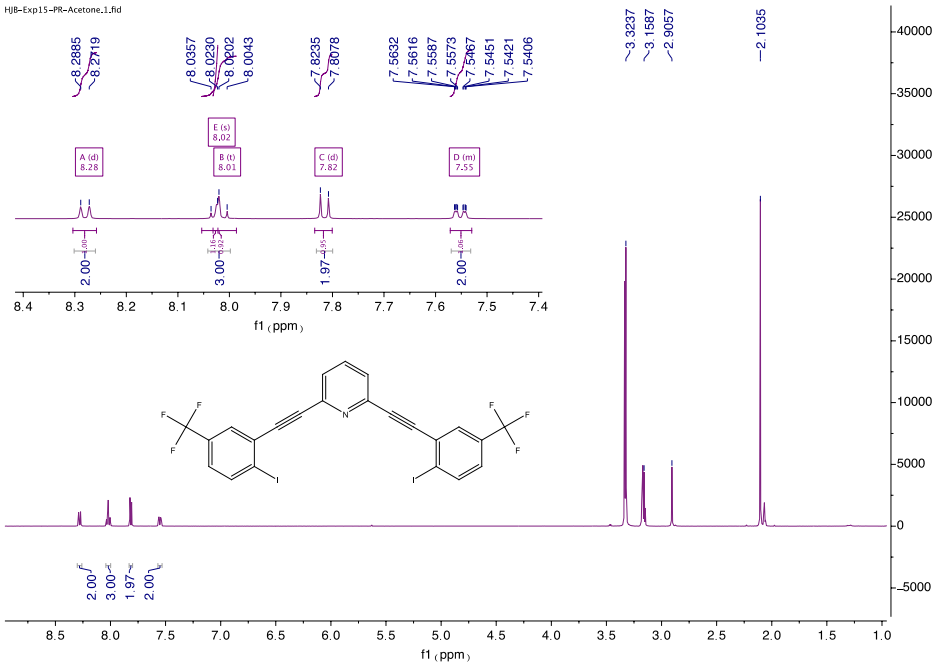

Figure C.4. [1]H NMR spectrum of host receptor (**1.3**) in acetone-*d6*.

UV-Vis titrations:

General Titration Procedure: A stock solution of host receptor **1** (0.1 mM) was prepared in $CHCl_3$ and sonicated until dissolved. The stock solution was then used to prep experimental host solutions at a concentration of XXX +/- uM of which 1.75 mL was transferred to a septum sealed quartz cuvette. To maintain a constant host concentration, the remaining experimental host solution was then used to dissolve NBu_4Cl salt which was prepared in vol. flasks and transferred to a septum sealed vial. Aliquots of NBu_4Cl were added to the host cuvette with a gas-tight Hamilton syringe, and a spectrum was recorded after each addition. Binding constants were determined by non-linear regression fit to a 1:1 model using the Bindfit software.

Figure C.5. Representative UV-Vis spectroscopic titration of **1** with TBACl in $CHCl_3$ out to 32 equivalents.

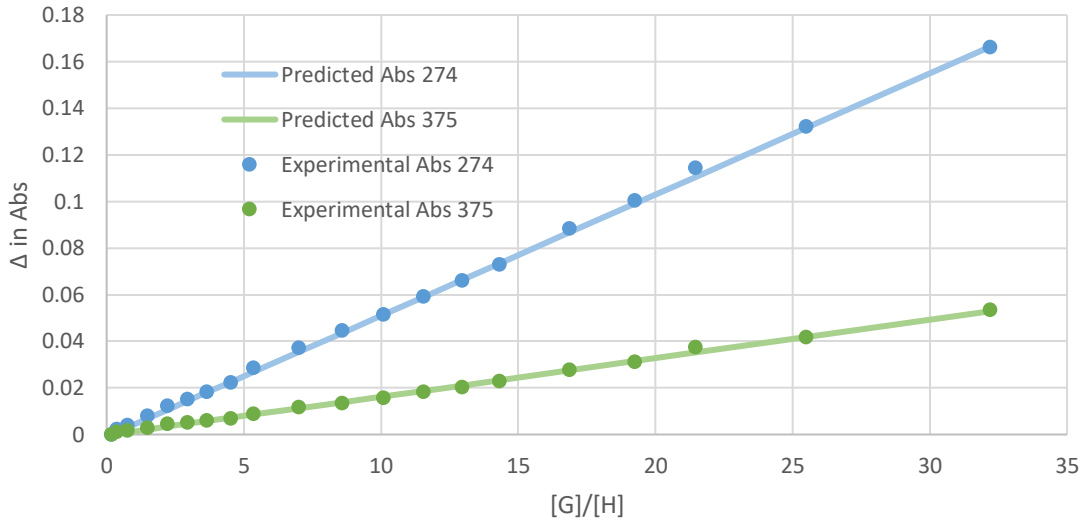

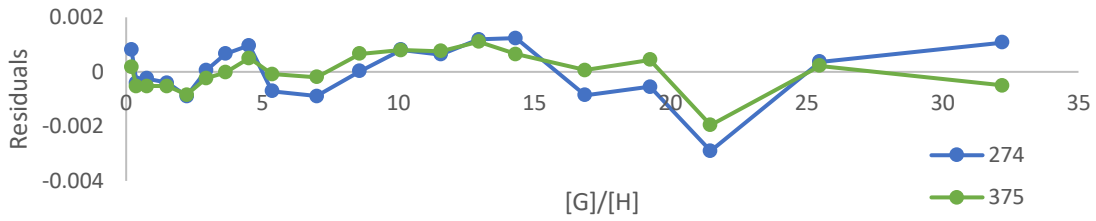

Figure C.6. The absorption binding isotherm and residuals of TBACl and host **1** at 274 and 325 nm.

Table C.1. Calculated association constants (Ka) for **1** in $CHCl_3$ obtained by fitting to a 1:1 host-guest model in Bindfit.

Addition #	VGuest (μL)	Guest M	Host M	Equiv. Anion	λ1: 274.0	λ2: 325.0
1	5	4.8023E-06	2.5216E-05	0.190449	0.13496858	0.13089709
2	5	9.5834E-06	2.5216E-05	0.38005531	0.13717921	0.13191755
3	10	1.9082E-05	2.5216E-05	0.75676211	0.13897592	0.13253617
4	20	3.7831E-05	2.5216E-05	1.50030567	0.14299439	0.13376707
5	20	5.6256E-05	2.5216E-05	2.23097401	0.1472857	0.1352873
6	20	7.4364E-05	2.5216E-05	2.94909869	0.15005948	0.13586836
7	20	9.2164E-05	2.5216E-05	3.65499997	0.1531345	0.13683006
8	25	0.00011399	2.5216E-05	4.52065786	0.15732685	0.13772386
9	25	0.00013537	2.5216E-05	5.36828121	0.16341333	0.1397128
10	50	0.0001768	2.5216E-05	7.0116326	0.17213741	0.14254235
11	50	0.00021658	2.5216E-05	8.58924994	0.1794094	0.14429528
12	50	0.00025481	2.5216E-05	10.1049999	0.18651174	0.14666025
13	50	0.00029156	2.5216E-05	11.5624518	0.19426057	0.14910294
14	50	0.00032692	2.5216E-05	12.9649056	0.20099705	0.15107825
15	50	0.00036097	2.5216E-05	14.3154166	0.20796648	0.15375777

16	100	0.00042543	2.5216E-05	16.871741	0.22334722	0.15857396
17	100	0.00048545	2.5216E-05	19.2517671	0.23541191	0.16212441
18	100	0.00054146	2.5216E-05	21.4731248	0.24931185	0.168189
19	200	0.00064299	2.5216E-05	25.4993358	0.26696813	0.1726637
20	400	0.00081219	2.5216E-05	32.2096873	0.30114302	0.18446825

Table C.2. Titration of **1** with TBACl

APPENDIX C
SUPPLEMENTARY CONTENT FOR CHAPTER FOUR

Experimental Details

General Methods.

Unless otherwise noted all reactions were run open to the atmosphere and consequently were exposed to air and water. All reagents were used as purchased from commercial sources. The ^{1}H NMR, ^{13}C NMR, and ^{19}F spectra were obtained using a Bruker 500 MHz spectrometer (^{1}H 500 MHz, ^{13}C 126 MHz, ^{19}F 471 MHz), and the ^{1}H NMR titrations were performed on a Varian 500 MHz spectrometer (^{1}H 500.10 MHz) using *d3*-ACN. All ^{1}H NMR and ^{13}C NMR chemical shifts (δ) are reported in parts per million and referenced to residual solvent peaks ($CHCl_3$: ^{1}H 7.26 ppm, ^{13}C 77.16 ppm; $(CH_3)_2CO$: ^{1}H 2.05ppm, ^{13}C 29.84 and 206.26 ppm; CH_3CN ^{1}H 1.94 ppm, ^{13}C 118.26 and 1.32 ppm). Masses for novel compounds were determined with a Waters Xevo G2-XS ToF spectrometer.

Full Receptor Synthesis.

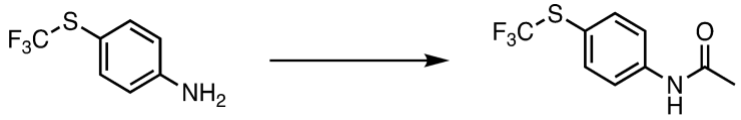

4-(trifluoromethylthio)acetamide.

4-(trifluoromethylthio)aniline (7.4 mL, 71.8 mmol) was added under N_2 to an oven-dried, vacuum-cooled round bottom flask. Acetic anhydride (10.2 mL, 108 mmol) was added to the flask dropwise and a white precipitate crashed out upon addition. The mixture was stirred at room temperature for one hour. Afterwards, the solid was dissolved using ethyl acetate and washed with water and brine. The organic layer was dried (Na_2SO_4), filtered, and concentrated to give the crude protected aniline. The white powdered product was purified by running the crude product through a plug with dichloromethane. (12 g, 71% yield). ^{1}H NMR (500 MHz, Acetone-d_6) δ 9.44 (s, 1H), 7.80 (d, J = 8.7 Hz, 2H), 7.63 (d, J = 8.7 Hz, 2H), 2.11 (s, 3H).

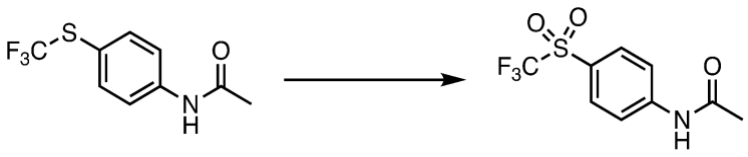

N-[4-[(trifluoromethyl)sulfonyl]phenyl]acetamide.

In an oven-dried, vacuum-cooled round bottom flask, the 4-(trifluoromethyl)thio phenyl acetamide (12 g, 51.0 mmol) was dissolved in 200 mL of dry dichloromethane and cooled to 0 ºC. mCPBA (26 g, 153 mmol) was added in 4 portions under a heavy $N_{2\,(g)}$ flow. The reaction was allowed to warm up to room temperature while stirring overnight. The

reaction mixture was diluted with more dichloromethane and $Na_2S_2O_3$ was used to quench any excess mCPBA. The mixture was extracted with dichloromethane and the combined organic layers were washed with $Na_2S_2O_3$, $NaHCO_3$, water and brine, then dried (Na_2SO_4) and concentrated to afford a white precipitate (11.4 g, 84% yield). ^{1}H NMR (500 MHz, Acetone-*d*$_6$) δ 9.84 (s, 1H), 8.08 – 8.00 (m, 4H), 2.18 (s, 3H).

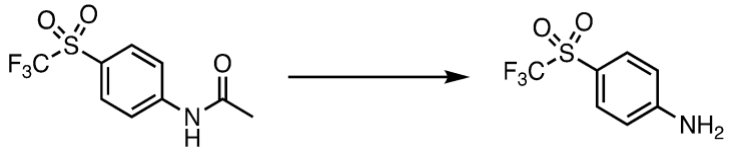

N-[4-[(trifluoromethyl)sulfonyl]phenyl]aniline.

N-[4-[(trifluoromethyl)sulfonyl]phenyl]acetamide (6.2 g, 23.15 mmol) was dissolved in 200 mL of EtOH; KOH (1.43 g, 25.46 mmol) was added, and the reaction mixture was set to 60 ºC and allowed to stir. After 3 hours, the mixture was concentrated to afford a crude solid which was then dissolved in water. White precipitate formed and collected via vacuum filtration to afford pure product (4.7 g, 90% yield). ^{1}H NMR (500 MHz, Chloroform-*d*) δ 7.75 (d, *J* = 8.8 Hz, 2H), 6.75 (d, *J* = 8.8 Hz, 2H), 4.54 (s, 2H).

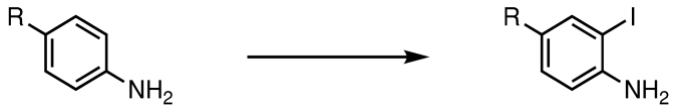

Iodoaniline derivatives, 1a-d.

The aniline derivative (20.76 mmol, 1.0 equiv.) was dissolved in 40 mL methanol. In another flask, KIO_3 (7.27 mmol, 0.35 equiv.) and KI (13.7 mmol, 0.66 equiv.) were dissolved in 100 mL water. The aqueous solution was added to the solution containing the aniline derivative then 1 M HCl (23 mL, 1.1 equiv.) was added dropwise. After the

reaction stirred at room temperature overnight, the mixture was extracted with ethyl acetate. The combined organic layers were then washed with $Na_2S_2O_3$, $NaHCO_3$, water, and brine, then dried (Na_2SO_4) and concentrated to afford crude product.

R= SO_2CF_3 (red/brown solid, 92% yield). ^{1}H NMR (500 MHz, Chloroform-*d*) δ 8.22 (d, *J* = 2.1 Hz, 1H), 7.74 (dd, *J* = 8.6, 2.1 Hz, 1H), 6.81 (d, *J* = 8.6 Hz, 1H), 4.99 (s, 2H). ^{13}C NMR (126 MHz, $CDCl_3$) δ 153.83, 142.11, 132.45, 123.86, 121.27, 118.88, 118.68, 116.09, 113.44, 81.85, 77.16. ^{19}F NMR (471 MHz, $CDCl_3$) δ -78.79. MASS SPEC NEEDED.

R= CF_3 (brown solid, 79% yield). ^{1}H NMR (500 MHz, Chloroform-*d*) δ 7.87 (s, 1H), 7.38 (dd, *J* = 8.5, 2.2 Hz, 1H), 6.74 (d, *J* = 8.4 Hz, 1H), 4.41 (s, 2H).

R= H commercially available

R= *t*Bu (brown solid, 66% yield). ^{1}H NMR (500 MHz, Chloroform-*d*) δ 7.65 (d, *J* = 1.7 Hz, 1H), 7.19 (d, *J* = 2.0 Hz, 1H), 6.70 (d, *J* = 8.4 Hz, 1H), 3.99 (s, 2H), 1.28 (d, *J* = 1.7 Hz, 9H).

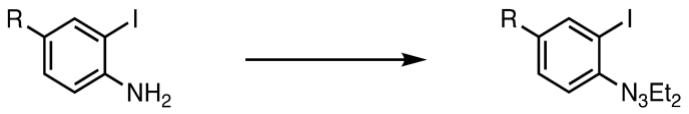

Iodotriazene derivatives, 2a-d.

The iodoaniline derivative (8.55 mmol, 1.0 equiv.) was dissolved in 30 mL acetonitrile and set to cool at -10 ºC. Concentrated HCl (5.7 mL, 8.0 equiv.) was added to the flask. In another flask, a solution of $NaNO_2$ (20.51 mmol, 2.4 equiv.) in 30 mL water was prepared. The aqueous $NaNO_2$ solution was added dropwise to the solution of the iodoaniline derivative and left to stir at -10 ºC. This reaction mixture was monitored by TLC for consumption of starting material. Once consumed, the reaction mixture was

added to a quench solution of: $HNEt_2$ (85.45 mmol, 10 equiv.) and K_2CO_3 (49.56 mmol, 5.8 equiv.) in 50 mL of acetonitrile and 100 mL of water at -10 ºC. This quenched reaction mixture was allowed to warm up to room temperature while continuously stirring overnight. The reaction was extracted with ether and the combined organic layers were washed with $Na_2S_2O_3$, $NaHCO_3$, water, and brine. The organic layer was collected and dried (Na_2SO_4) and concentrated to afford the crude iodotriazene that was purified by column chromatography (gradient from pure hexanes to 1:9, dichloromethane:hexanes) to afford pure iodotriazene.

R= SO_2CF_3 (orange solid, 25% yield). ^{1}H NMR (500 MHz, Chloroform-*d*) δ 8.11 (d, *J* = 2.2 Hz, 1H), 7.56 (dd, *J* = 8.6, 1.9 Hz, 1H), 7.27 (d, *J* = 8.7 Hz, 1H), 3.60 (qd, *J* = 7.2, 5.1 Hz, 4H), 1.07 (dt, *J* = 30.0, 7.2 Hz, 6H). ^{13}C NMR (126 MHz, $CDCl_3$) δ 157.06, 141.51, 131.04, 126.15, 123.75, 121.16, 118.56, 117.34, 115.97, 96.24, 50.42, 43.64, 14.29, 10.69. ^{19}F NMR (471 MHz, $CDCl_3$) δ -77.75. MASS SPEC NEEDED.

R= CF_3 (orange solid, quant. yield). ^{1}H NMR (500 MHz, Chloroform-*d*) δ 8.07 (s, 1H), 7.51 (dd, *J* = 8.6, 2.0 Hz, 1H), 7.42 (d, 1H), 3.84 (q, *J* = 7.2 Hz, 4H), 1.34 (dt, *J* = 24.0, 7.3 Hz, 6H).

R= H (orange solid, quant. yield). ^{1}H NMR (500 MHz, Chloroform-*d*) δ 7.86 (dd, *J* = 7.9, 1.4 Hz, 1H), 7.38 (dd, *J* = 8.1, 1.6 Hz, 1H), 7.29 (ddd, *J* = 8.3, 7.2, 1.4 Hz, 1H), 6.85 (td, *J* = 7.5, 1.6 Hz, 1H), 3.81 (q, *J* = 7.2 Hz, 4H), 1.34 (t, *J* = 7.2 Hz, 6H).

R= *t*Bu (orange solid, 89% yield). ^{1}H NMR (500 MHz, Chloroform-*d*) δ 7.88 (d, *J* = 2.0 Hz, 1H), 7.60 – 7.01 (m, 2H), 3.80 (q, *J* = 7.2 Hz, 4H), 1.74 – 0.92 (m, 15H).

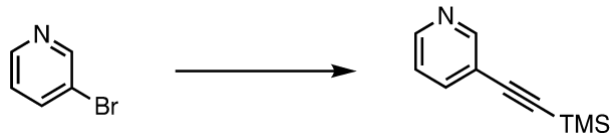

TMS-protected 3-ethynylpyridine.

After a mixture of 10 mL tetrahydrofuran and 10 mL acetonitrile, 3-bromopyridine (0.31 mL, 3.16 mmol), $Pd(PhCN)_2Cl_2$ (0.16 mmol, 5 mol%) and CuI (0.16 mmol, 5 mol%) was outgassed with $N_{2\,(g)}$ for at least 20 minutes, the ligand P(*t*Bu)$_3$ (0.316 mmol, 10 mol%) was added. The alkyne, TMSA (4.74 mmol, 1.5 equiv.) was then added dropwise. The reaction was allowed to stir at room temperature under a steady flow of $N_{2\,(g)}$ overnight. The reaction mixture was run through a silica/celite plug and washed with DCM to afford the crude product that was then purified by column chromatography (gradient from pure hexanes to 2:8, ethylacetate:hexanes) to afford a pure brown oil. (0.549 g, quant. yield). ^{1}H NMR (500 MHz, Chloroform-*d*) δ 8.59 (s, 1H), 8.41 (dd, *J* = 4.9, 1.9 Hz, 1H), 7.62 (dt, *J* = 7.8, 1.8 Hz, 1H), 7.10 (dd, *J* = 7.9, 4.8 Hz, 1H), 0.16 (s, 6H).

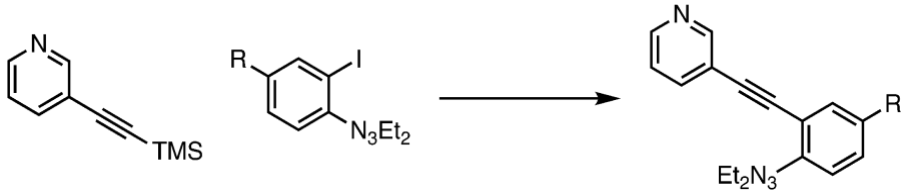

Triazene receptor intermediate, 3a-d.

The 3-ethynylpyridine (1.71 mmols, 1.0 equiv.) was dissolved in Et_2O and set to stir in a flask. Tetrabutylammonium fluoride (TBAF, 2.40 mmols) was then added to the solution and left to stir until the starting material had disappeared by TLC (~ 20 min.). The reaction mixture was quenched with NH_4Cl and extracted with water and brine x2. The organic layer was dried ($NaSO_4$), and the solvent was removed *in vacuo* to furnish 3-ethynylpyridine in quantitative yields. While this was going on a new flask of 50% THF

and 50% DIPA (20 mL total) was outgassed with $N_{2(g)}$ for at least twenty minutes. Once isolated 3-ethynylpyridine (2.28 mmol, 1.3 equiv.) was dissolved in a minimal amount of THF and outgassed for at least 1 min/mL of solvent. After outgassing, the iodotriazene compound (1.76 mmol, 1.0 equiv.), $Pd(PPh_3)_4$ (0.18 mmol, 0.10 equiv.), and CuI (0.11 mmol, 0.06 equiv.) were added to the RBF with the THF/DIPA mixture and set to stir. The separate solution of 3-ethynylpyridine in THF was then cannulated dropwise to the iodotriazene/catalyst mixture and the reaction was left stirring at 45 °C overnight. The next day, the reaction was passed through a silica/celite plug, washed with DCM, and concentrated to afford the crude product that was purified by column chromatography (gradient from 1:9, DCM:hexanes to 100% DCM)

R= SO_2CF_3 (yellow solid, 69% yield). ^{1}H NMR (500 MHz, Chloroform-*d*) δ 8.77 (s, 1H), 8.58 (s, 1H), 8.17 (d, *J* = 2.2 Hz, 1H), 7.85 (dd, *J* = 8.8, 2.2 Hz, 1H), 7.81 (d, *J* = 7.9 Hz, 1H), 7.71 (d, *J* = 8.8 Hz, 1H), 7.31 (dd, *J* = 7.9, 4.8 Hz, 1H), 3.91 (dq, *J* = 11.1, 7.2 Hz, 4H), 1.38 (dt, *J* = 30.4, 7.2 Hz, 6H). CHECKING WITH MIKE IN SUBGROUP ^{13}C NMR (126 MHz, $CDCl_3$) δ 159.95, 153.74, 150.39, 139.86, 137.42, 132.52, 126.79, 125.30, 124.71, 122.71, 120.43, 120.12, 119.17, 117.53, 93.63, 90.41, 51.86, 44.69, 15.84, 12.24. ^{19}F NMR (471 MHz, $CDCl_3$) δ -78.49. HRMS (TOF-MS-ES+) for $C_{18}H_{17}N_4SO_2F_3$ [M+H] +: calcd 410.10, found 410.1024.

R= CF_3 (76% yield). NEED NMRS. HRMS (TOF-MS-ES+) for $C_{18}H_{17}N_4F_3$ [M+H] +: calcd 346.14 , found 346.1405.

R= H (yellow solid, 97% yield). ^{1}H NMR (500 MHz, Chloroform-*d*) δ 8.77 (s, 1H), 8.53 (s, 1H), 7.79 (dd, *J* = 7.8, 1.8 Hz, 1H), 7.54 (dd, *J* = 7.6, 1.5 Hz, 1H), 7.45 (d, *J* = 8.4 Hz, 1H), 7.34 – 7.27 (m, 2H), 7.10 (t, *J* = 7.5 Hz, 1H), 3.82 (q, *J* = 7.2 Hz, 4H), 1.33 (t, *J* =

7.2 Hz, 6H). NEED DRY HNMR. NEED CARBON. HRMS (TOF-MS-ES+) for $C_{17}H_{18}N_4$ [M+H] +: calcd 278.15, found 278.1531.

R= *t*Bu (light brown oil, quant. yield). ^{1}H NMR (500 MHz, Chloroform-*d*) δ 7.88 (d, *J* = 2.0 Hz, 1H), 7.60 – 7.01 (m, 2H), 3.80 (q, *J* = 7.2 Hz, 4H), 1.74 – 0.92 (m, 15H). ^{13}C NMR (126 MHz, $CDCl_3$) δ 207.02, 152.31, 150.42, 148.14, 147.85, 147.66, 138.25, 129.58, 127.08, 123.10, 116.83, 116.79, 92.40, 89.24, 34.52, 31.41, 31.04. HRMS (TOF-MS-ES+) for $C_{21}H_{26}N_4$ [M+H] +: calcd 334.22, found 334.2157.

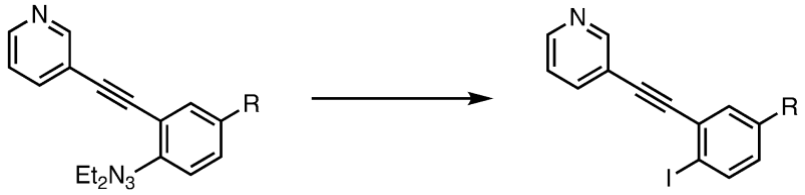

Neutral ethynyl pyridine receptor, 4a-d.

HI (0.54 mmol, 3.0 equiv.) and I_2 (0.54 mmol, 3.0 equiv.) were dissolved in ACN (5 mL) then set to stir at 60 °C. While the first solution was coming up to temperature the triazene (0.18 mmol, 1.0 equiv.) was dissolved in ACN (5 mL), which was then added dropwise into the first flask and stirred at 60 °C while monitoring via TLC. After the starting material was consumed (~40 min), the mixture was extracted with EtOAc and washed with $NaHCO_3$, $Na_2S_2O_3$, and water x2 each. The organic layer was then dried with Na_2SO_4 and concentrated to form an oil which was purified on silica via column chromatography (gradient from 100% hexanes to 3:7 ethylacetate:hexanes).

R= SO_2CF_3 (tan solid, 40% yield). ^{1}H NMR (500 MHz, Acetone-d_6) δ 8.88 (s, 1H), 8.66 (d, *J* = 3.9 Hz, 1H), 8.50 (d, *J* = 8.4 Hz, 1H), 8.23 (d, *J* = 2.3 Hz, 1H), 8.06 (dt, *J* = 7.8, 1.9 Hz, 1H), 7.83 (dd, *J* = 8.4, 2.3 Hz, 1H), 7.50 (dd, *J* = 8.0, 4.8 Hz, 1H). NEED TO

CHECK CARBON WITH MIKE IN SUBGROUP.^{13}C NMR (126 MHz, Acetone) δ 152.99, 150.93, 142.45, 139.48, 134.12, 132.75, 132.13, 131.48, 124.46, 121.88, 119.78, 119.29, 116.70, 113.65, 93.60, 92.97. ^{19}F NMR (471 MHz, $CDCl_3$) δ -79.33. HRMS (TOF-MS-ES+) for $C_{14}H_7INSO_2F_3$ [M+H]+: calcd 436.92, found 436.9194.

R= CF_3 (yellow solid, 31% yield). ^{1}H NMR (500 MHz, Chloroform-*d*) δ 8.62 (d, *J* = 2.5 Hz, 1H), 8.42 (dd, *J* = 4.9, 1.7 Hz, 1H), 8.01 (d, *J* = 8.3 Hz, 1H), 7.89 – 7.75 (m, 1H), 7.70 (d, *J* = 2.2 Hz, 1H), 7.35 – 7.13 (m, 2H). NEED TO CHECK CARBON WITH MIKE IN SUBGROUP. ^{19}F NMR (471 MHz, $CDCl_3$) δ -58.44. HRMS (TOF-MS-ES+) for $C_{14}H_7INF_3$ [M+H] +: calcd 372.96, found 372.9575. HRMS (TOF-MS-ES+) for $C_{13}H_8IN$ [M+H] +: calcd 304.97, found 304.970.

R= H (tan solid, 20% yield). ^{1}H NMR (500 MHz, Chloroform-*d*) δ 8.83 (d, *J* = 2.1 Hz, 1H), 8.58 (dd, *J* = 5.0, 1.7 Hz, 1H), 7.92 – 7.85 (m, 2H), 7.54 (dd, *J* = 7.7, 1.7 Hz, 1H), 7.35 (td, *J* = 7.6, 1.2 Hz, 1H), 7.31 (ddd, *J* = 7.8, 4.9, 0.8 Hz, 1H), 7.05 (td, *J* = 7.8, 1.7 Hz, 1H).

R= *t*Bu (yellow solid, 87% yield). ^{1}H NMR (500 MHz, Chloroform-*d*) δ 8.84 (s, 1H), 8.57 (d, *J* = 3.3 Hz, 1H), 7.89 (dt, *J* = 7.9, 2.0 Hz, 1H), 7.79 (d, *J* = 8.4 Hz, 1H), 7.57 (d, *J* = 2.4 Hz, 1H), 7.31 (dd, *J* = 7.9, 4.9 Hz, 1H), 7.09 (dd, *J* = 8.4, 2.4 Hz, 1H), 1.32 (s, 9H). ^{13}C NMR (126 MHz, $CDCl_3$) δ 152.49, 151.68, 149.09, 138.75, 138.72, 130.16, 128.84, 127.96, 123.36, 120.54, 97.64, 95.49, 89.14, 34.89, 31.34. HRMS (TOF-MS-ES+) for $C_{17}H_{16}IN$ [M+H] +: calcd 361.03, found 361.0327.

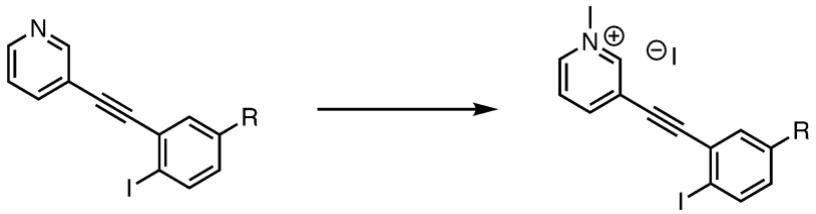

Methylated ethynyl pyridine.

The neutral receptor (0.067 mmol) was added to a bomb flask followed by an excess of MeI (5 mL). The reaction vessel was then sealed and set to stir at 110 °C overnight. Over the next 24 hours, the product would precipitate out of solution. The yellow precipitate was collected and washed with minimal DCM to afford pure product.

R= SO_2CF_3 (yellow solid, quant. yield). ^{1}H NMR (500 MHz, Acetone-d_6) δ 9.65 (s, 1H), 9.30 (d, J = 6.1 Hz, 1H), 8.94 (d, J = 8.1 Hz, 1H), 8.53 (d, J = 8.4 Hz, 1H), 8.42 – 8.32 (m, 1H), 8.26 (d, J = 2.4 Hz, 1H), 7.91 (dd, J = 8.4, 2.3 Hz, 1H). NEED CARBON. ^{19}F NMR (471 MHz, Acetone) δ -79.27. HRMS (TOF-MS-ES+) for $C_{14}H_7I_2NSO_2F_3$ [M+H] +: calcd 451.94, found 451.9429.

R= CF_3 (yellow solid, quant. yield). ^{1}H NMR (500 MHz, Acetone-d_6) δ 9.62 (s, 1H), 9.30 (d, J = 6.2 Hz, 1H), 8.89 (d, J = 8.1 Hz, 1H), 8.38 (t, J = 7.2 Hz, 1H), 8.29 (d, J = 8.3 Hz, 1H), 8.00 (d, J = 2.2 Hz, 1H), 7.60 (d, J = 8.2 Hz, 1H), 4.76 (s, 3H). NEED CARBON. ^{19}F NMR (471 MHz, Acetone-d_6) δ -63.70. HRMS (TOF-MS-ES+) for $C_{14}H_7I_2NF_3$ [M+H] +: calcd 387.98, found 387.9810.

R= H (yellow solid, quant. yield). ^{1}H NMR (500 MHz, Acetone-d_6) δ 9.40 (s, 1H), 9.16 (d, J = 6.1 Hz, 1H), 8.84 (d, J = 8.1 Hz, 1H), 8.38 – 8.31 (m, 1H), 8.05 (d, J = 8.0 Hz, 1H), 7.71 (dd, J = 7.9, 1.7 Hz, 1H), 7.59 – 7.52 (m, 1H), 7.30 (td, J = 7.7, 1.5 Hz, 1H), 4.71 (s, 3H). NEED CARBON. NEED FLUORINE. HRMS (TOF-MS-ES+) for $C_{13}H_8I_2N$ [M+H] +: calcd 319.99, found 319.9936.

R= *t*Bu (yellow solid, quant. yield). ^{1}H NMR (500 MHz, Acetone-d_6) δ 9.48 (s, 1H), 9.23 (d, J = 6.1 Hz, 1H), 8.84 (d, J = 8.0 Hz, 1H), 8.39 – 8.32 (m, 1H), 7.94 (d, J = 8.5 Hz, 1H), 7.73 (d, J = 2.4 Hz, 1H), 7.37 (dd, J = 8.5, 2.5 Hz, 1H), 4.74 (s, 3H), 1.34 (s, 9H).

NEED CARBON. No peaks shown on ^{19}F NMR. HRMS (TOF-MS-ES+) for $C_{17}H_{16}I_2N$ [M+H] +: calcd 376.06, found 376.0562**.**

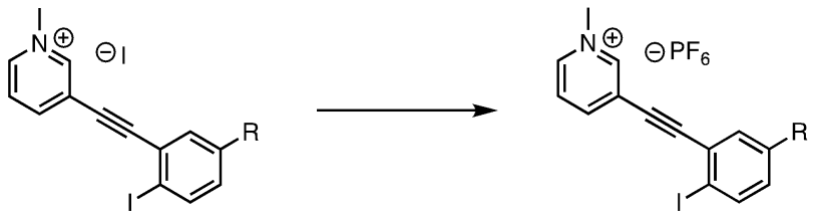

Methylated PF_6 pyridine receptor, 5a-d.

The methylated receptor (0.423 mmol, 1.0 equiv.) was dissolved in 10 mL of acetone and 40 mL of water and set to stir. To this flask, $AgPF_6$ (1.068 mmol, 2.5 equiv.) was added and stirred for about 40 minutes during which time gray precipitate (AgI) formed. This precipitate was filtered off and the filtrate solvent mixture was removed *in vacuo* until only water remained. At this point white precipitate (final product) began to crash out of the water and was collected via filtration and washed with minimal water to give the final pure product.

R= SO_2CF_3 (white solid, quant. yield). ^1H NMR (500 MHz, Acetone-d_6) δ 9.52 (s, 1H), 9.24 (d, J = 6.2 Hz, 1H), 8.95 (d, J = 8.2 Hz, 1H), 8.57 (d, J = 8.4 Hz, 1H), 8.41 (t, 1H), 8.27 (d, J = 2.3 Hz, 1H), 7.94 (dd, J = 8.4, 2.3 Hz, 1H), 4.74 (s, 3H). NEED CARBON. ^{19}F NMR (471 MHz, Acetone) δ -71.74, -73.24, -79.32.

R= CF_3 (white solid, quant. yield). NEED PROTON AND CARBON IN ACETONE. ^{19}F NMR (471 MHz, Acetone-d_6) δ -63.79, -71.90, -73.41.

R= H (white solid, quant. yield). ^1H NMR (500 MHz, Acetone-d_6) δ 9.32 (s, 1H), 9.07 (d, J = 6.1 Hz, 1H), 8.80 (d, J = 8.1 Hz, 1H), 8.29 (dd, J = 8.2, 6.2 Hz, 1H), 8.02 (d, J = 8.0 Hz, 1H), 7.71 (dd, J = 7.8, 1.6 Hz, 1H), 7.54 (t, J = 7.6 Hz, 1H), 7.28 (td, J = 7.7, 1.6

Hz, 1H), 4.65 (s, 3H). ^{13}C NMR (126 MHz, Acetone) δ 148.34, 147.55, 145.97, 140.09, 134.29, 132.54, 129.45, 129.12, 128.23, 124.80, 101.12, 99.26, 85.80, 49.52. ^{19}F NMR (471 MHz, Acetone) δ -71.64, -73.14.

R= *t*Bu (white solid, quant. yield). ^{1}H NMR (500 MHz, Acetone-d_6) δ 9.34 (s, 1H), 9.09 (d, J = 6.1 Hz, 1H), 8.81 (d, J = 8.1 Hz, 1H), 8.33 – 8.25 (m, 1H), 7.93 (d, J = 8.4 Hz, 1H), 7.73 (d, J = 2.5 Hz, 1H), 7.36 (dd, J = 8.5, 2.5 Hz, 1H), 4.67 (s, 3H), 1.33 (s, 9H)). CHECKING CARBON WITH MIKE IN SUBGROUP. ^{13}C NMR (126 MHz, Chloroform-*d*) δ 152.88, 148.35, 147.55 (d, J = 14.2 Hz), 145.94 (d, J = 18.2 Hz), 139.80 (d, J = 22.4 Hz), 131.42 (d, J = 24.9 Hz), 130.25 (d, J = 8.7 Hz), 129.15 (d, J = 21.9 Hz), 127.90, 124.96, 99.75, 97.42, 85.31, 49.54, 35.28, 31.13. ^{19}F NMR (471 MHz, Acetone) δ -71.91, -73.41.

Titrations

General Methods. ^{1}H NMR spectra were acquired at room temperature on a Varian Inova 500 MHz spectrometer (500.11 MHz). ^{1}H chemical shifts (δ) are expressed in ppm relative to residual CH_3CN (calibrated to 1.94 ppm) shifts.

General Procedure. A 4.0 mL host solution (0.9-1.5 mM in CD_3CN) was prepared. Of this, 500 μL was added to a septum-sealed NMR tube. A 19-30 mM host/guest (TBAX, where X = I, Br, or Cl) stock solution was prepared using the remaining 3.5 mL of host solution. Aliquots of the host/guest solution were added to the NMR tube using Hamilton gas-tight syringes, and ^{1}H NMR spectra were recorded at 25 °C after each addition of

guest. The Δδ of the CH_{aryl} and CH_{methyl} protons were used to follow the progress of the titration, and association constants were determined using the Thordarson method.

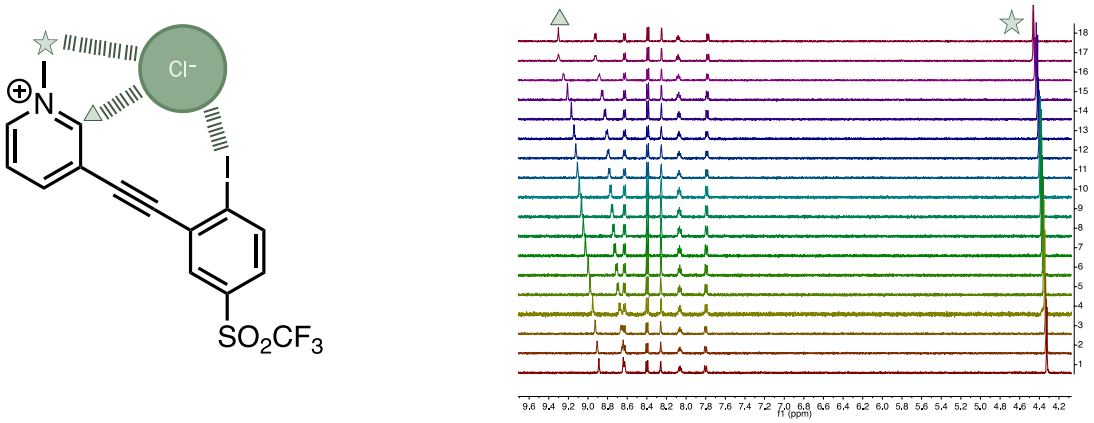

Figure C.1. Representative ^{1}H NMR titration done in CD_3CN with **5a** where participating protons can be seen shifting with increasing chloride concentration.

Table C.1. Representative ^{1}H NMR Titration of **5a • PF6**$^-$ with I^- in CD_3CN at 25 ºC.

Entry	V_{Guest} (μL)	[Host] (M)	[I^-] (M)	Equiv.	δ CH_{aryl}	δ CH_{methyl}
0	0	1.32E-03	0.00E+00	0.00	8.888	4.322
1	5	1.32E-03	2.08E-04	0.16	8.892	4.324
2	5	1.32E-03	4.11E-04	0.31	8.897	4.326
3	10	1.32E-03	8.06E-04	0.61	8.905	4.329
4	10	1.32E-03	1.19E-03	0.90	8.912	4.332
5	10	1.32E-03	1.55E-03	1.18	8.918	4.334
6	15	1.32E-03	2.08E-03	1.58	8.928	4.339
7	15	1.32E-03	2.57E-03	1.95	8.934	4.340
8	15	1.32E-03	3.05E-03	2.31	8.940	4.343
9	20	1.32E-03	3.64E-03	2.76	8.947	4.346
10	20	1.32E-03	4.19E-03	3.18	8.954	4.349

11	20	1.32E-03	4.71E-03	3.57	8.960	4.351
12	30	1.32E-03	5.44E-03	4.12	8.967	4.354
13	50	1.32E-03	6.51E-03	4.93	8.978	4.359
14	100	1.32E-03	8.26E-03	6.26	8.992	4.364
15	200	1.32E-03	1.07E-02	8.14	9.008	4.371
16	500	1.32E-03	1.41E-02	10.68	9.016	4.375
17	500	1.32E-03	1.58E-02	11.97	9.028	4.379
18	500	1.32E-03	1.68E-02	12.75	9.035	4.381

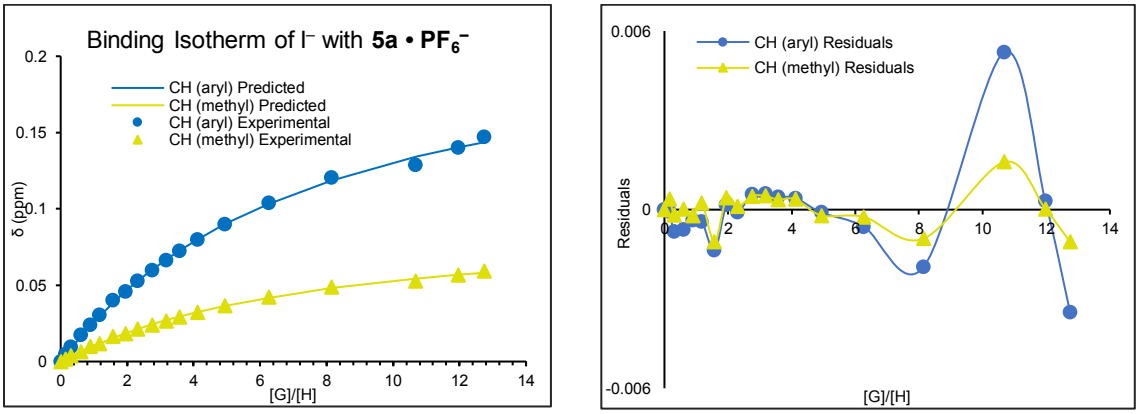

Figure C.2. Representative binding isotherm and residuals for I^- titration of receptor **5a • PF_6^-** in CD_3CN at 25 °C determined by ^1H NMR spectroscopy.

Table C.2. Representative ^1H NMR Titration of **5a • PF6**$^-$ with Br^- in CD_3CN at 25 ºC.

Entry	V_{Guest} (µL)	[Host] (M)	[Br^-] (M)	Equiv.	δ CH_{aryl}	δ CH_{methyl}
0	0	1.25E-03	0.00E+00	0.00	8.888	4.323
1	5	1.25E-03	2.34E-04	0.19	8.896	4.326
2	5	1.25E-03	4.64E-04	0.37	8.905	4.329
3	10	1.25E-03	9.10E-04	0.73	8.922	4.335
4	10	1.25E-03	1.34E-03	1.07	8.938	4.341
5	10	1.25E-03	1.75E-03	1.40	8.951	4.345
6	15	1.25E-03	2.35E-03	1.87	8.967	4.351
7	15	1.25E-03	2.91E-03	2.32	8.982	4.357

8	15	1.25E-03	3.44E-03	2.75	8.994	4.361
9	20	1.25E-03	4.11E-03	3.28	9.008	4.366
10	20	1.25E-03	4.73E-03	3.78	9.022	4.371
11	20	1.25E-03	5.32E-03	4.25	9.033	4.375
12	30	1.25E-03	6.14E-03	4.90	9.047	4.381
13	50	1.25E-03	7.35E-03	5.87	9.065	4.387
14	100	1.25E-03	9.32E-03	7.45	9.093	4.398
15	200	1.25E-03	1.21E-02	9.68	9.124	4.408
16	500	1.25E-03	1.59E-02	12.71	9.157	4.420
17	500	1.25E-03	1.78E-02	14.24	9.160	4.422

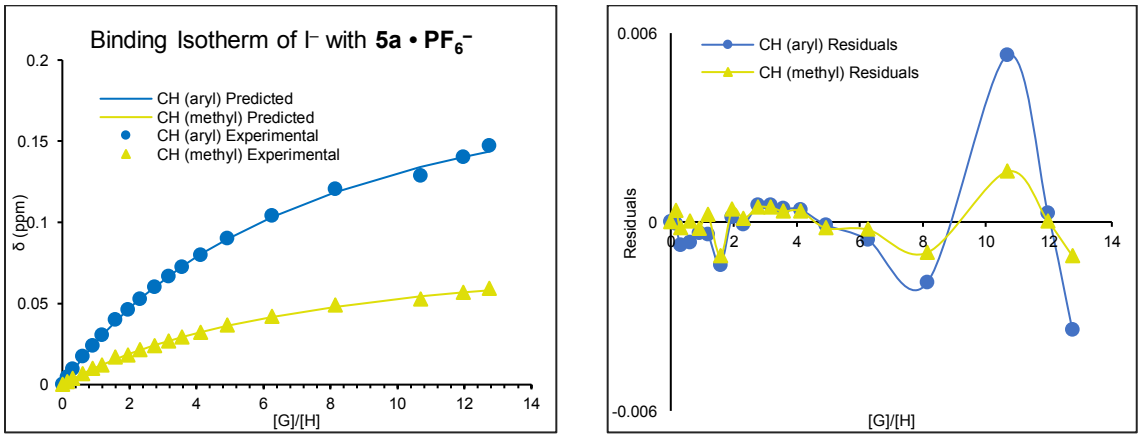

Figure C.3. Representative binding isotherm and residuals for Br^- titration of receptor **5a • PF_6^-** in CD_3CN at 25 °C determined by ^1H NMR spectroscopy.

Table C.3. Representative ^1H NMR Titration of **5a • PF6**$^-$ with Cl^- in CD_3CN at 25 ºC.

Entry	V_{Guest} (µL)	[Host] (M)	[Cl^-] (M)	Equiv.	δ CH_{aryl}	δ CH_{methyl}
0	0	9.58E-04	0.00E+00	0.00	8.887	4.322
1	5	9.58E-04	1.99E-04	0.21	8.905	4.328
2	5	9.58E-04	3.93E-04	0.41	8.911	4.330
3	10	9.58E-04	7.72E-04	0.81	8.941	4.340

4	10	9.58E-04	1.14E-03	1.19	8.957	4.346
5	10	9.58E-04	1.49E-03	1.55	8.972	4.351
6	15	9.58E-04	1.99E-03	2.08	9.006	4.362
7	15	9.58E-04	2.46E-03	2.57	9.019	4.367
8	15	9.58E-04	2.91E-03	3.04	9.037	4.372
9	20	9.58E-04	3.48E-03	3.63	9.057	4.380
10	20	9.58E-04	4.01E-03	4.19	9.079	4.386
11	20	9.58E-04	4.51E-03	4.71	9.090	4.390
12	30	9.58E-04	5.20E-03	5.43	9.108	4.396
13	50	9.58E-04	6.23E-03	6.50	9.134	4.405
14	100	9.58E-04	7.90E-03	8.25	9.170	4.417
15	200	9.58E-04	1.03E-02	10.73	9.205	4.429
16	500	9.58E-04	1.35E-02	14.08	9.262	4.449
17	500	9.58E-04	1.51E-02	15.77	9.263	4.448

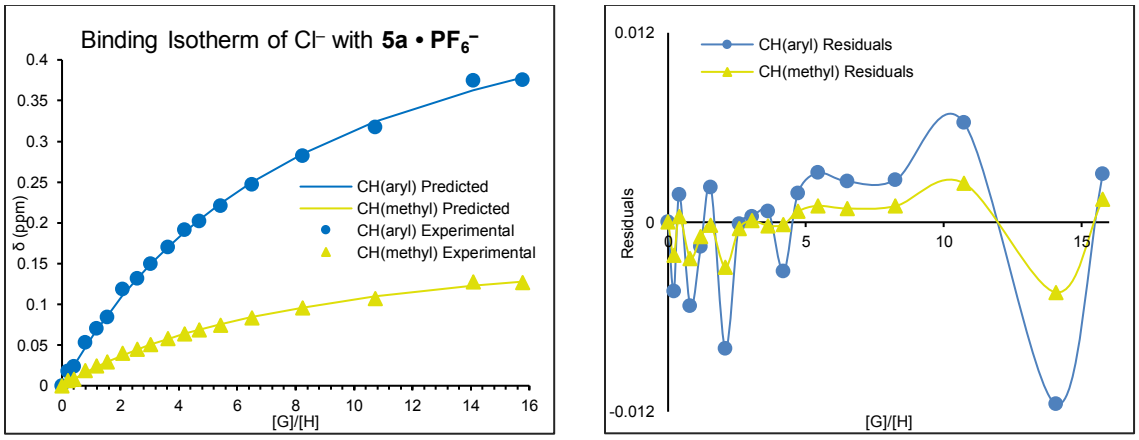

Figure C.4. Representative binding isotherm and residuals for Cl^- titration of receptor **5a • PF_6^-** in CD_3CN at 25 °C determined by ^1H NMR spectroscopy.

Table C.4. Representative ^1H NMR Titration of **5b • PF6**$^-$ with Cl^- in CD_3CN at 25 ºC.

Entry	V_{Guest} (µL)	[Host] (M)	[Cl^-] (M)	Equiv.	δ CH_{aryl}	δ CH_{methyl}

0	0	1.35E-03	0.00E+00	0.00	8.864	4.318
1	5	1.35E-03	2.46E-04	0.18	8.874	4.322
2	5	1.35E-03	4.88E-04	0.36	8.888	4.327
3	10	1.35E-03	9.57E-04	0.71	8.911	4.335
4	10	1.35E-03	1.41E-03	1.04	8.932	4.342
5	10	1.35E-03	1.84E-03	1.37	8.951	4.349
6	15	1.35E-03	2.47E-03	1.83	8.974	4.357
7	15	1.35E-03	3.06E-03	2.26	8.993	4.364
8	15	1.35E-03	3.62E-03	2.68	9.010	4.370
9	20	1.35E-03	4.32E-03	3.20	9.029	4.376
10	20	1.35E-03	4.98E-03	3.69	9.045	4.382
11	20	1.35E-03	5.59E-03	4.14	9.060	4.387
12	30	1.35E-03	6.45E-03	4.78	9.079	4.394
13	50	1.35E-03	7.72E-03	5.72	9.106	4.403
14	100	1.35E-03	9.80E-03	7.26	9.140	4.415
15	200	1.35E-03	1.27E-02	9.44	9.176	4.428
16	500	1.35E-03	1.67E-02	12.39	9.192	4.434
17	500	1.35E-03	1.87E-02	13.88	9.217	4.442

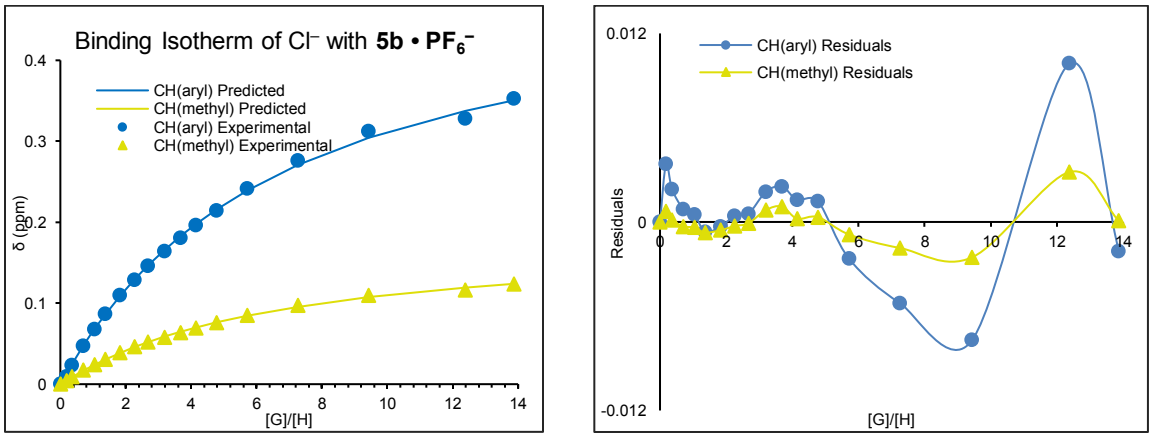

Figure C.5. Representative binding isotherm and residuals for Cl^- titration of receptor **5b** • **PF_6^-** in CD_3CN at 25 °C determined by ^1H NMR spectroscopy.

Table C.5. Representative ^{1}H NMR Titration of **5c • PF6**$^-$ with Cl^- in CD_3CN at 25 ºC.

Entry	V_{Guest} (μL)	[Host] (M)	[Cl^-] (M)	Equiv.	δ CH_{aryl}	δ CH_{methyl}
0	0	1.36E-03	0.00E+00	0.00	8.838	4.309
1	5	1.36E-03	2.45E-04	0.18	8.847	4.312
2	5	1.36E-03	4.85E-04	0.36	8.857	4.316
3	10	1.36E-03	9.52E-04	0.70	8.877	4.324
4	10	1.36E-03	1.40E-03	1.03	8.891	4.330
5	10	1.36E-03	1.83E-03	1.35	8.907	4.336
6	15	1.36E-03	2.45E-03	1.80	8.918	4.340
7	15	1.36E-03	3.04E-03	2.23	8.941	4.348
8	15	1.36E-03	3.60E-03	2.64	8.954	4.354
9	20	1.36E-03	4.29E-03	3.16	8.969	4.359
10	20	1.36E-03	4.95E-03	3.64	8.982	4.363
11	20	1.36E-03	5.56E-03	4.09	8.997	4.371
12	30	1.36E-03	6.41E-03	4.72	9.013	4.377
13	50	1.36E-03	7.68E-03	5.65	9.034	4.384
14	100	1.36E-03	9.75E-03	7.17	9.064	4.397
15	200	1.36E-03	1.27E-02	9.32	9.094	4.405
16	500	1.36E-03	1.66E-02	12.23	9.138	4.424
17	500	1.36E-03	1.86E-02	13.70	9.142	4.425

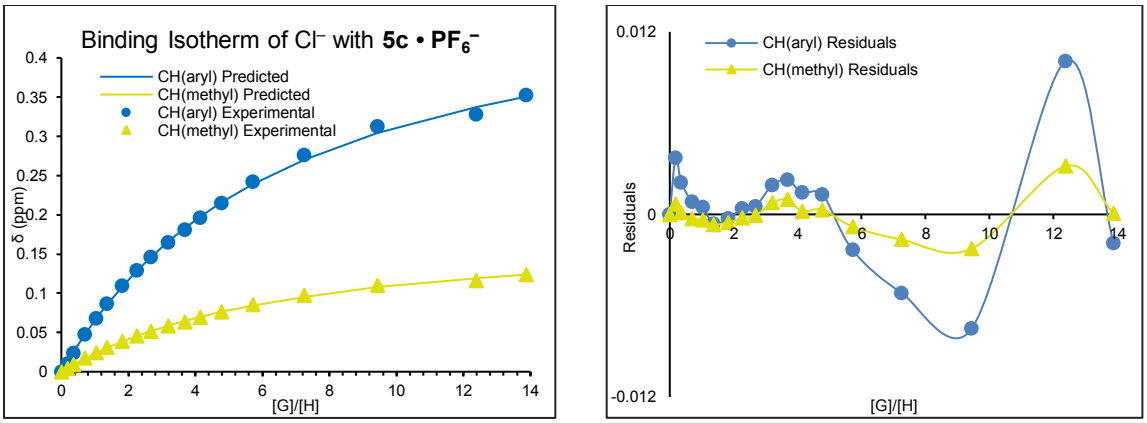

Figure C.6. Representative binding isotherm and residuals for Cl^- titration of receptor **5c • PF_6^-** in CD_3CN at 25 °C determined by ^1H NMR spectroscopy.

Table C.6. Representative ^1H NMR Titration of **5d • PF6⁻** with Cl^- in CD_3CN at 25 ºC.

Entry	V_{Guest} (µL)	[Host] (M)	[Cl^-] (M)	Equiv.	δ CH_{aryl}	δ CH_{methyl}
0	0	1.73E-03	0.00E+00	0.00	8.828	4.310
1	5	1.73E-03	2.33E-04	0.14	8.834	4.312
2	5	1.73E-03	4.62E-04	0.27	8.843	4.316
3	10	1.73E-03	9.07E-04	0.53	8.859	4.322
4	10	1.73E-03	1.33E-03	0.77	8.873	4.328
5	10	1.73E-03	1.75E-03	1.01	8.885	4.333
6	15	1.73E-03	2.34E-03	1.35	8.903	4.340
7	15	1.73E-03	2.90E-03	1.68	8.917	4.345
8	15	1.73E-03	3.43E-03	1.98	8.929	4.350
9	20	1.73E-03	4.09E-03	2.37	8.944	4.356
10	20	1.73E-03	4.72E-03	2.73	8.958	4.361
11	20	1.73E-03	5.30E-03	3.07	8.970	4.366
12	30	1.73E-03	6.11E-03	3.54	8.985	4.372
13	50	1.73E-03	7.32E-03	4.24	9.006	4.380
14	100	1.73E-03	9.29E-03	5.38	9.037	4.392
15	200	1.73E-03	1.21E-02	6.99	9.078	4.407
16	500	1.73E-03	1.58E-02	9.18	9.106	4.418

17	500	1.73E-03	1.78E-02	10.28	9.110	4.419

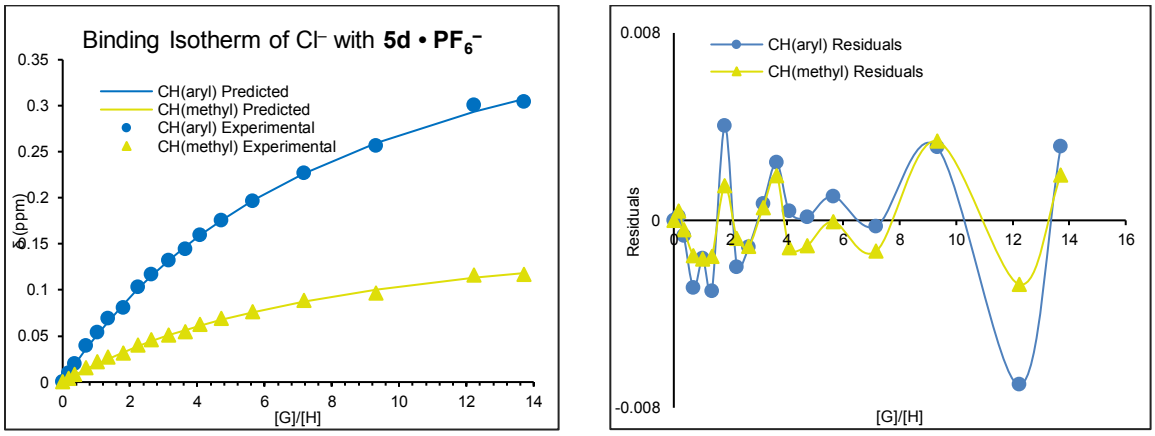

Figure C.7. Representative binding isotherm and residuals for Cl^- titration of receptor **5d** • $\mathbf{PF_6^-}$ in CD_3CN at 25 °C determined by ^1H NMR spectroscopy.

Linear Regression Fitting and Statistics of log(KaR/KaH) and σ_p

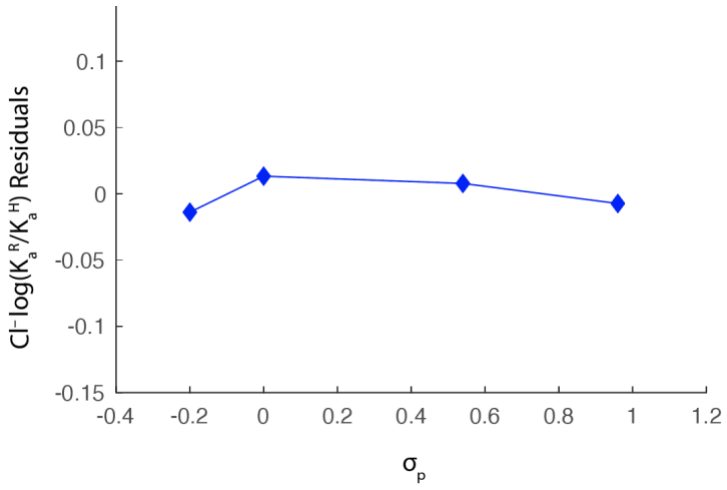

Figure C.8. Linear regression residuals of $\log(K_a^R/K_a^H)$ of Cl^- and σ_p.

X-Ray Crystallography

Waiting on Lev for crystal data

Computational Details

General. Gas phase optimization and frequency analyses were performed for structures **4a-d** and **5a-d** via Gaussian 09.[1] All computations were ran using B97-D3 density functional theory[2] with a Def2-TZVP basis set.[3] This work utilized the resources of the University of Oregon's high-performance computer, Talapas. Electrostatic potential surface (ESP) maps and figures were generated using Gaussian 09. The σ–hole values ($V_{S,max}$) were assessed using Multiwfn, an open-source software.[4]

Table C.7. Cartesian coordinates for **5a**.

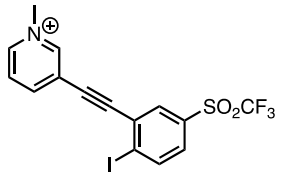

	X	Y	Z
H	0.56677	3.82829	-1.70301
C	0.47593	2.87918	-1.18175
C	0.35303	0.46906	0.15123
C	-0.729	2.18606	-1.13094
C	-0.7917	0.97061	-0.45739
C	1.5382	1.19649	0.07591

H	-1.61602	2.58904	-1.61598
H	-1.73203	0.42135	-0.415
C	0.3235	-0.77869	0.84392
C	0.32554	-1.82742	1.43
C	0.34676	-3.08209	2.12455
C	0.31521	-5.58703	3.40306
C	-0.70468	-3.97748	1.89278
C	1.37881	-3.44364	3.00595
C	1.36104	-4.69326	3.64051
C	-0.71983	-5.21743	2.54135
H	-1.50099	-3.71063	1.19888
H	2.16216	-4.9904	4.31555
H	0.32672	-6.56422	3.88476
I	3.00298	-2.17607	3.42256
S	-2.03813	-6.37912	2.20256
O	-2.68494	-5.90191	0.98831
O	-1.41507	-7.69345	2.21649
C	-3.12485	-6.14675	3.64653
F	-4.24422	-6.91894	3.59412
F	-2.49414	-6.44563	4.81836
F	-3.54626	-4.85335	3.76174
N	1.57981	2.38196	-0.57785
C	2.85121	3.122	-0.65002
H	3.38779	2.99487	0.29388
H	2.64531	4.18346	-0.80889
H	3.42333	2.70879	-1.4843
H	2.46056	0.84427	0.53021

Table C.8. Cartesian coordinates for **5b**.

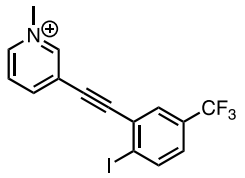

	X	Y	Z
H	-1.53275	3.76493	-1.78037
C	-1.38771	2.79981	-1.30259
C	-1.01487	0.40151	0.00457
C	-1.15997	1.64474	-2.04358
C	-0.97322	0.43414	-1.38441
C	-1.24573	1.58185	0.70669
H	-1.12618	1.68659	-3.13058
H	-0.79381	-0.47476	-1.9582
C	-0.82222	-0.8228	0.71243
C	-0.66365	-1.83578	1.33849
C	-0.47692	-3.03151	2.10796
C	-0.10428	-5.43182	3.51025
C	-0.25728	-4.23164	1.41783
C	-0.50752	-3.04179	3.50985
C	-0.32245	-4.24067	4.2072
C	-0.06163	-5.43967	2.10936
H	-0.23499	-4.23489	0.32754
H	-0.34636	-4.26692	5.29513
H	0.03456	-6.35798	4.06876
I	-0.82882	-1.30413	4.64765
N	-1.43308	2.75067	0.04866
C	-1.66487	3.9834	0.82046
H	-2.27816	3.74318	1.69296
H	-2.19203	4.70953	0.19661

H	-0.688	4.36885	1.12262
C	0.15158	-6.72706	1.34718
F	0.87956	-6.54656	0.21043
F	-1.02302	-7.28983	0.95554
F	0.80825	-7.67594	2.06716
H	-1.2821	1.60883	1.7926

Table C.9. Cartesian coordinates for **5c**.

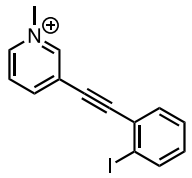

	X	Y	Z
H	-0.50817	4.43527	-1.02704
C	-0.48071	3.41393	-0.65688
C	-0.29988	0.84185	0.31428
C	-1.55026	2.54177	-0.82891
C	-1.45968	1.24356	-0.33803
C	0.74749	1.74798	0.46379
H	-2.45066	2.87027	-1.3443
H	-2.29234	0.553	-0.46944
C	-0.17051	-0.48405	0.82552
C	-0.01911	-1.59256	1.26293
C	0.19677	-2.90886	1.78928
C	0.50705	-5.50189	2.8093
C	-0.91261	-3.75041	1.94049
C	1.46802	-3.37775	2.155
C	1.62015	-4.67304	2.66367
C	-0.75745	-5.0417	2.44871
H	-1.90818	-3.40942	1.66417

H	2.59794	-5.05314	2.9514
H	0.62686	-6.50848	3.20466
I	3.20272	-2.2032	1.9755
N	0.64043	3.00945	-0.01598
C	1.75685	3.95646	0.14343
H	2.49346	3.55124	0.84114
H	1.35543	4.89386	0.53772
H	2.20639	4.10522	-0.84168
H	-1.62362	-5.68993	2.56328
H	1.67384	1.47574	0.96261

Table C.10. Cartesian coordinates for **5d**.

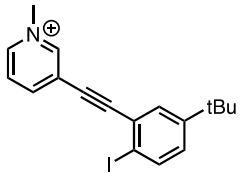

	X	**Y**	**Z**
H	-0.54887	4.16441	-0.7044
C	-0.51057	3.13011	-0.3736
C	-0.31151	0.52189	0.49514
C	-1.654	2.34004	-0.31213
C	-1.55373	1.02329	0.12489
C	0.80703	1.34771	0.41795
H	-2.62042	2.74803	-0.6018
H	-2.44459	0.39789	0.17638
C	-0.17184	-0.8223	0.9528
C	-0.01105	-1.94687	1.34322
C	0.21552	-3.28282	1.81312
C	0.52861	-5.91198	2.71504

C	-0.88599	-4.14825	1.90275
C	1.48227	-3.74708	2.18082
C	1.63549	-5.05929	2.63044
C	-0.75653	-5.47874	2.35418
H	-1.86683	-3.77401	1.61326
H	2.61127	-5.44248	2.92192
H	0.7066	-6.9238	3.07203
I	3.20389	-2.5473	2.09002
N	0.69275	2.6251	-0.01688
C	1.89375	3.47511	-0.07706
H	2.06597	3.87004	0.9272
H	1.73022	4.28734	-0.78969
H	2.73915	2.86676	-0.40925
C	-1.9942	-6.39185	2.43575
C	-2.62474	-6.53738	1.03391
H	-1.90222	-6.94502	0.31692
H	-2.97777	-5.57963	0.63624
H	-3.48855	-7.21207	1.05718
C	-3.03161	-5.77468	3.39845
H	-2.6044	-5.62872	4.39768
H	-3.90929	-6.42335	3.50238
H	-3.39314	-4.801	3.05015
C	-1.6871	-7.81715	2.94834
H	-1.26652	-7.80011	3.96056
H	-0.97955	-8.33808	2.29277
H	-2.59754	-8.42723	2.98847
H	1.79828	1.0032	0.70098

Table C.11. Cartesian coordinates for **4a**.

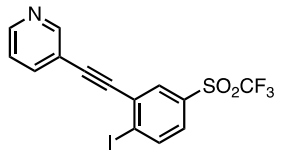

	X	Y	Z
H	0.12833	4.06952	-1.50739
C	0.09491	3.1812	-0.8827
C	0.03654	0.8788	0.59272
C	-0.17191	3.27212	0.47482
C	-0.20114	2.0976	1.22376
C	0.29564	0.89081	-0.77145
H	-0.3525	4.23526	0.93901
H	-0.40727	2.13987	2.28997
N	0.32942	2.01632	-1.52557
C	0.01373	-0.34359	1.33028
C	-0.00662	-1.36417	1.96397
C	-0.03199	-2.58061	2.72196
C	-0.07289	-5.02761	4.1081
C	-0.0645	-3.79005	2.01574
C	-0.0238	-2.60209	4.12583
C	-0.04077	-3.82364	4.81352
C	-0.09988	-5.0029	2.71216
H	-0.05583	-3.77896	0.92616
H	-0.02193	-3.8516	5.90152
H	-0.06927	-5.96817	4.65676
I	0.02064	-0.85142	5.2863
S	-0.11451	-6.54016	1.8013
O	0.52307	-6.25747	0.52367
O	0.46727	-7.53929	2.68596
C	-1.8991	-6.82928	1.58524

F	-2.16671	-7.97659	0.90112
F	-2.55334	-6.92652	2.7788
F	-2.50587	-5.81711	0.90043
H	0.48998	-0.02813	-1.31777

Table C.12. Cartesian coordinates for **4b**.

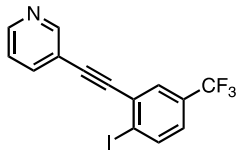

	X	Y	Z
H	-0.61441	3.63972	-1.96172
C	-0.53895	2.79105	-1.28756
C	-0.36464	0.58185	0.31563
C	-0.33555	2.97446	0.07163
C	-0.24718	1.84722	0.88575
C	-0.56718	0.50125	-1.05576
H	-0.24789	3.97198	0.48754
H	-0.08809	1.96166	1.95474
N	-0.65718	1.57898	-1.87258
C	-0.27887	-0.59429	1.12059
C	-0.20507	-1.57517	1.81055
C	-0.11666	-2.74377	2.63628
C	0.05041	-5.10381	4.14315
C	-0.18469	-3.99616	2.00876
C	0.03487	-2.68174	4.02822
C	0.11909	-3.86099	4.7776
C	-0.11009	-5.18559	2.7531
H	-0.29901	-4.04976	0.92543
H	0.24008	-3.82845	5.85847
H	0.12133	-6.01176	4.74169

I	0.14907	-0.86677	5.07889
C	-0.16172	-6.5257	2.05983
F	-0.94596	-6.51885	0.94655
F	1.06761	-6.94205	1.65112
F	-0.65058	-7.51908	2.853
H	-0.66647	-0.45794	-1.55648

Table C.13. Cartesian coordinates for **4c**.

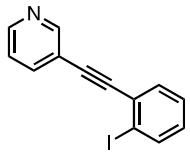

	X	**Y**	**Z**
H	-0.25865	3.86017	-1.8606
C	-0.23302	2.99815	-1.19981
C	-0.15813	0.75799	0.3676
C	-0.31725	3.15014	0.17583
C	-0.27884	2.00716	0.97164
C	-0.08068	0.70888	-1.01796
H	-0.41053	4.1356	0.61829
H	-0.34277	2.0964	2.05291
N	-0.11545	1.80251	-1.81792
C	-0.11516	-0.43375	1.15264
C	-0.07923	-1.42898	1.82488
C	-0.03577	-2.6154	2.6287
C	0.05698	-5.00698	4.09191
C	0.0479	-3.8504	1.97172
C	-0.07296	-2.58755	4.03035
C	-0.02645	-3.78348	4.75821
C	0.09408	-5.04084	2.70004

H	0.07779	-3.89261	0.88475
H	-0.0543	-3.77786	5.84527
H	0.093	-5.93357	4.65986
I	-0.19811	-0.80048	5.12778
H	0.15904	-5.9935	2.17987
H	0.01453	-0.23682	-1.54442

Table C.14. Cartesian coordinates for **4d**.

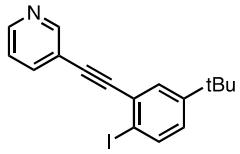

	X	Y	Z
H	-0.03841	3.62563	-1.89212
C	-0.03046	2.78586	-1.20288
C	-0.04513	0.60119	0.44255
C	0.31885	2.95765	0.12793
C	0.31043	1.84289	0.96365
C	-0.37971	0.53078	-0.90328
H	0.59119	3.93671	0.50593
H	0.57942	1.94808	2.01141
N	-0.3803	1.59676	-1.74051
C	-0.06423	-0.56177	1.27045
C	-0.07811	-1.53237	1.97848
C	-0.09364	-2.6899	2.82471
C	-0.13067	-5.03315	4.35472
C	-0.15686	-3.95149	2.21089
C	-0.0484	-2.6109	4.21911
C	-0.06724	-3.78194	4.97962
C	-0.17676	-5.1487	2.95721

H	-0.19087	-3.99424	1.12298
H	-0.033	-3.74219	6.06609
H	-0.1425	-5.90975	4.9973
I	0.04936	-0.78885	5.25586
C	-0.24619	-6.5068	2.23602
C	-1.534	-6.57894	1.38733
H	-1.5567	-5.8155	0.60201
H	-2.4252	-6.43685	2.0101
H	-1.62591	-7.55187	0.89045
C	0.98089	-6.66774	1.31281
H	1.01089	-5.90612	0.52599
H	0.97446	-7.64367	0.81337
H	1.91516	-6.59015	1.88152
C	-0.26077	-7.7213	3.19174
H	0.64495	-7.7607	3.80811
H	-0.3107	-8.66344	2.63263
H	-1.12885	-7.69792	3.86082
H	-0.66609	-0.41026	-1.36486

References

(1) Frisch, M. J.; Trucks, G. W.; Schlegel, H. B.; Scuseria, G. E.; Robb, M. A.; Cheeseman, R. J.; Scalmani, G.; Barone, V.; Mennucci, B.; Petersson, G. A.; et al. Gaussian 09, Revision E.01. Wallingford, CT 2013.

(2) Grimme, S.; Ehrlich, S.; Goerigk, L. Effect of the Damping Function in Dispersion Corrected Density Functional Theory. *J. Comput. Chem.* **2011**, *32*, 1456–1465.

(3) Weigend, F.; Ahlrichs, R. Balanced Basis Sets of Split Valence, Triple Zeta Valence and Quadruple Zeta Valence Quality for H to Rn: Design and Assessment of Accuracy. *Phys. Chem. Chem. Phys.* **2005**, *7*, 3297–3305.

(4) Lu, T.; Chen, F. Multiwfn: A Multifunctional Wavefunction Analyzer. *J. Comput. Chem.* **2012**, *33*, 580–592.

NMR Spectra

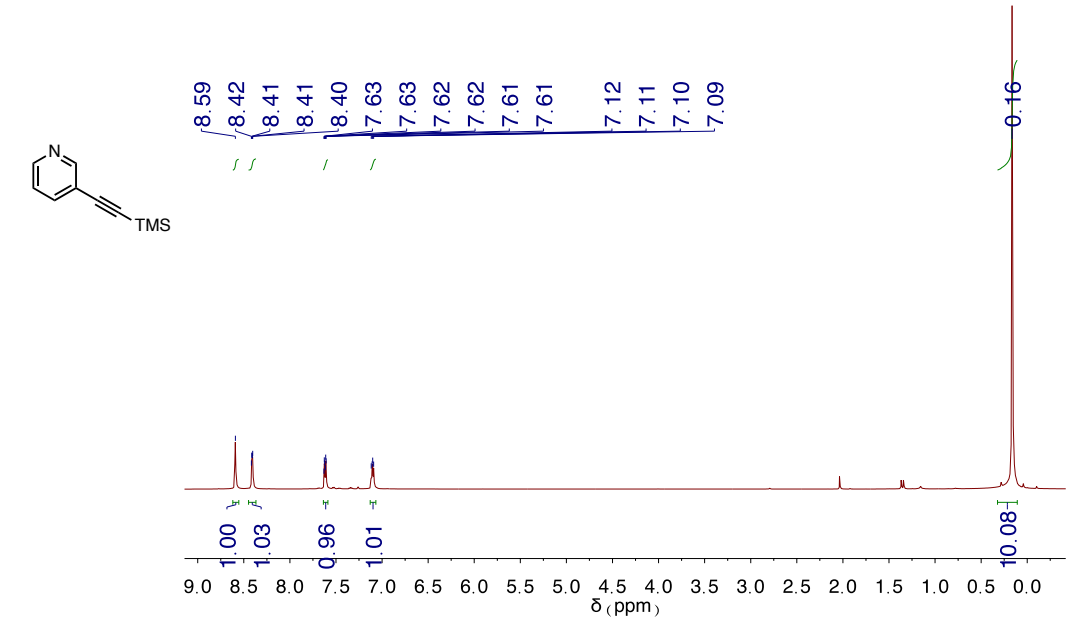

Figure C.9. [1]H NMR spectrum of TMS-protected 3-ethynylpyridine.

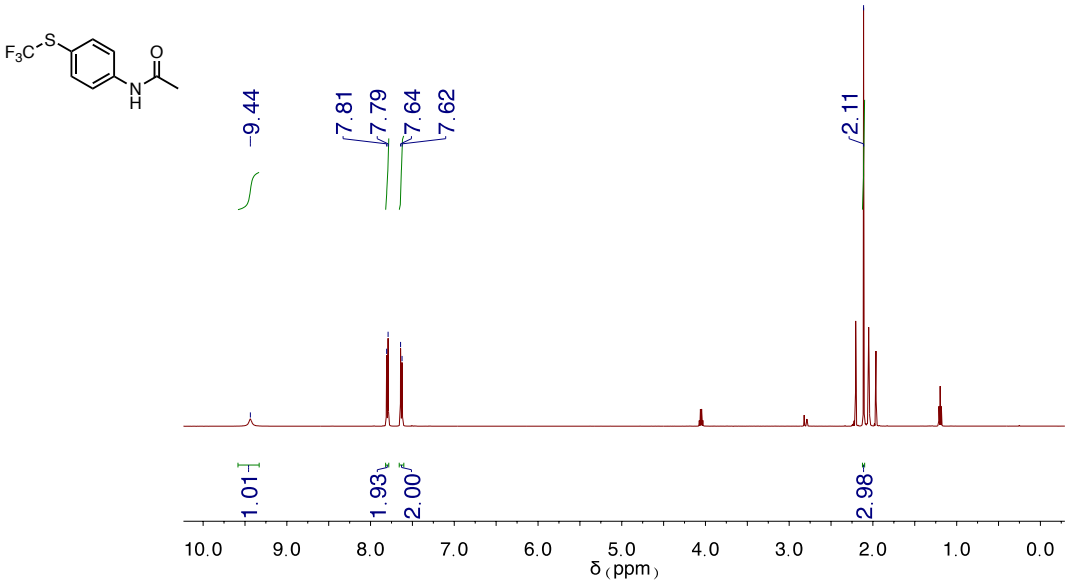

Figure C.10. [1]H NMR spectrum of 4-(trifluoromethylthio)acetamide. Wet with water and ethyl acetate.

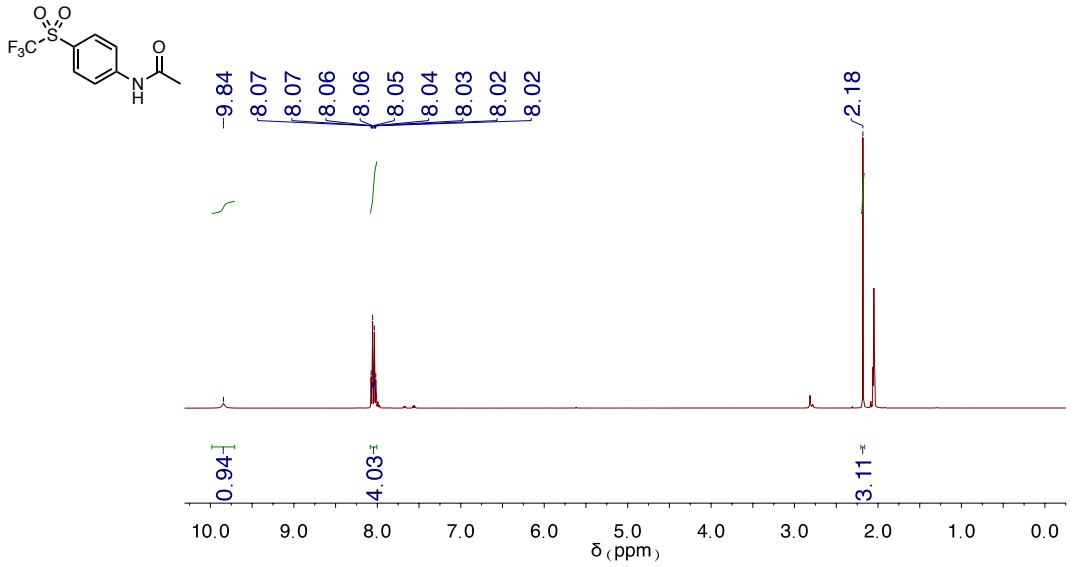

Figure C.11. [1]H NMR spectrum of N-[4-[(trifluoromethyl)sulfonyl]phenyl]acetamide.

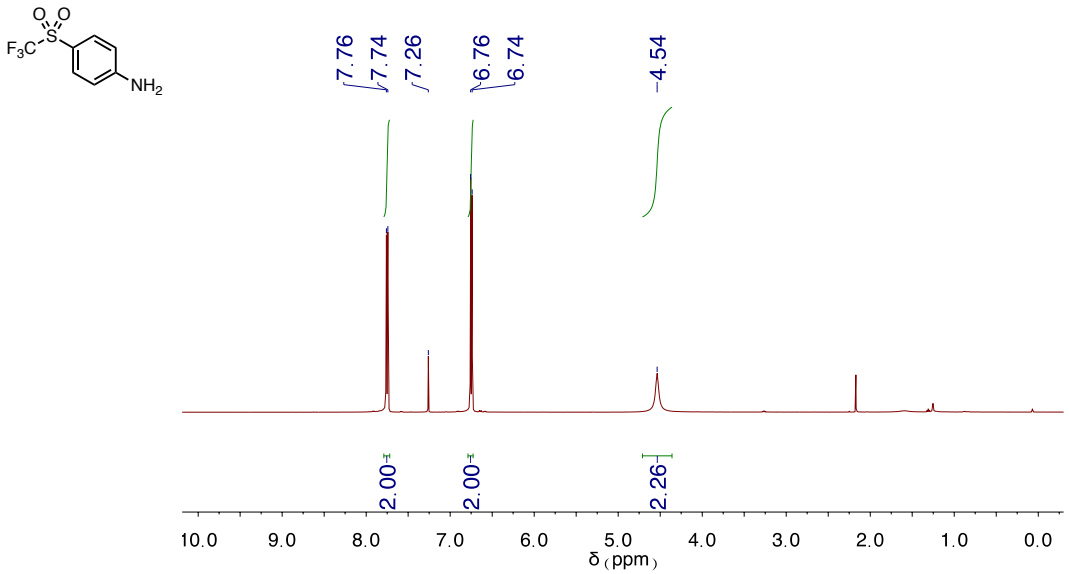

Figure C.12. [1]H NMR spectrum of N-[4-[(Trifluoromethyl)sulfonyl]phenyl]aniline.

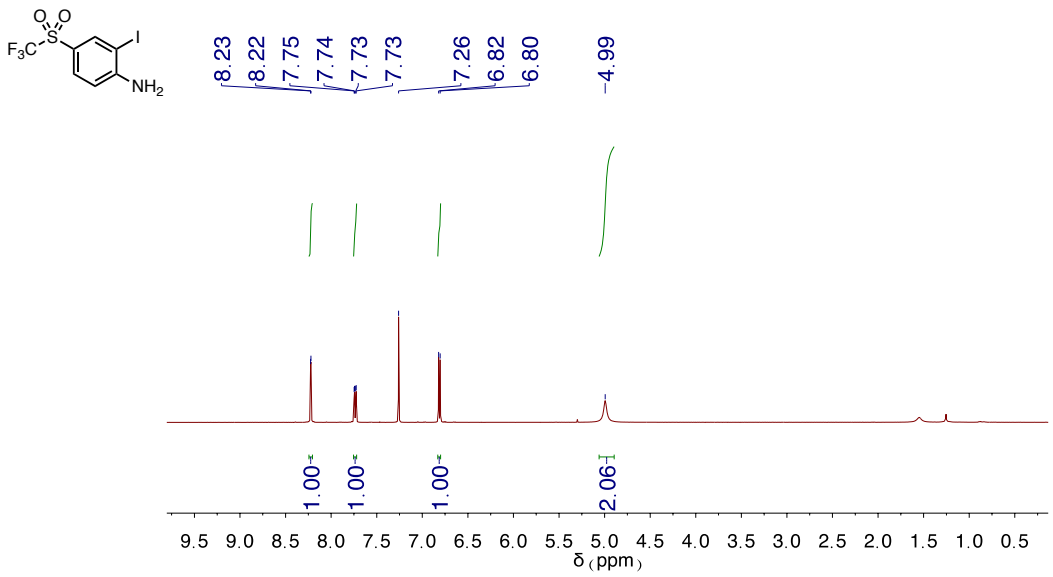

Figure C.13. ^{1}H NMR spectrum of **1a**.

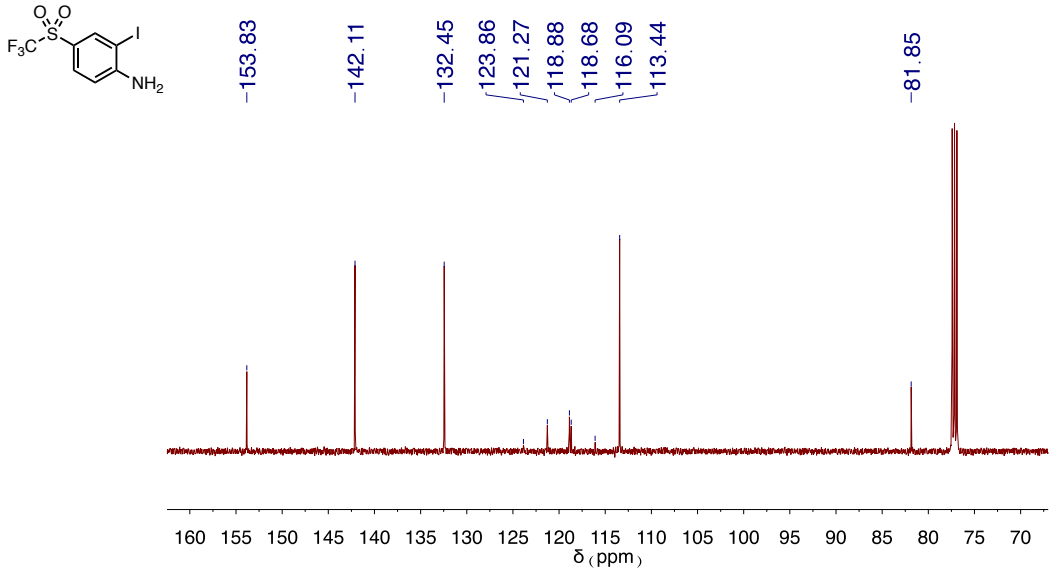

Figure C.14. ^{13}C NMR spectrum of **1a**.

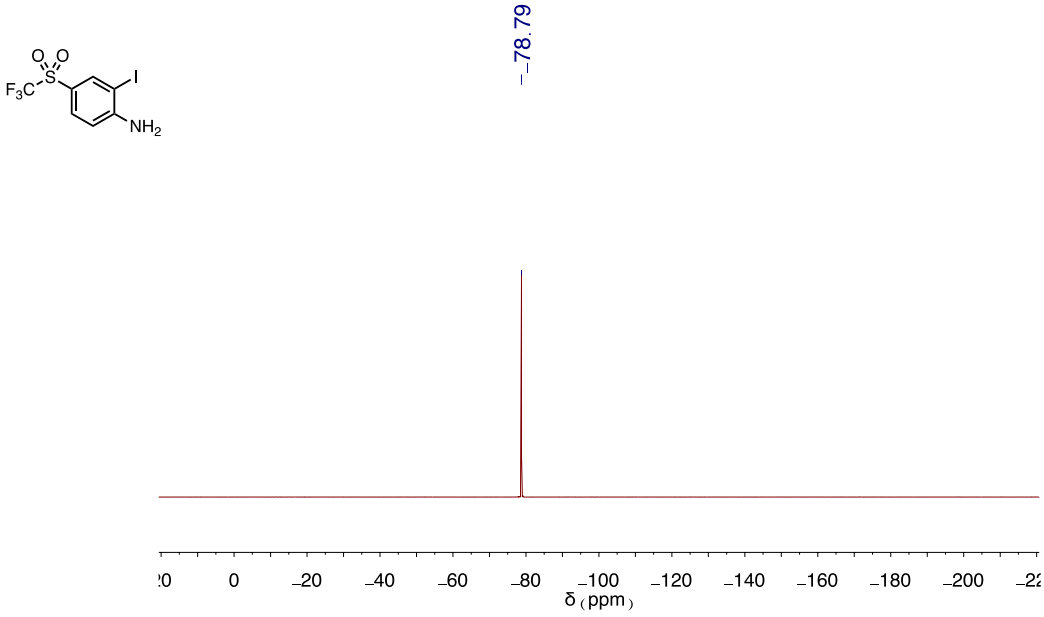

Figure C.15. ^{19}F NMR spectrum of **1a**.

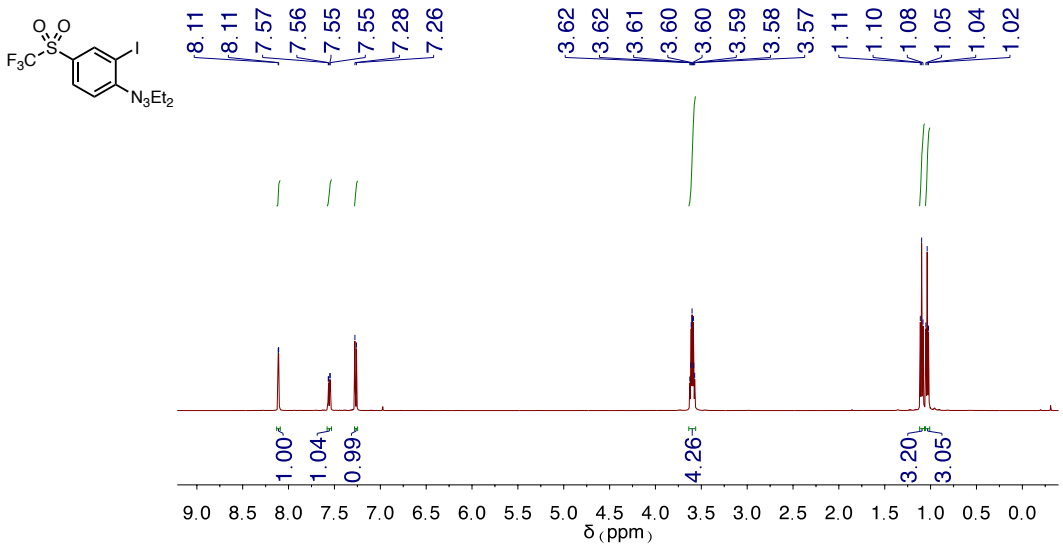

Figure C.16. ^{1}H NMR spectrum of **2a**.

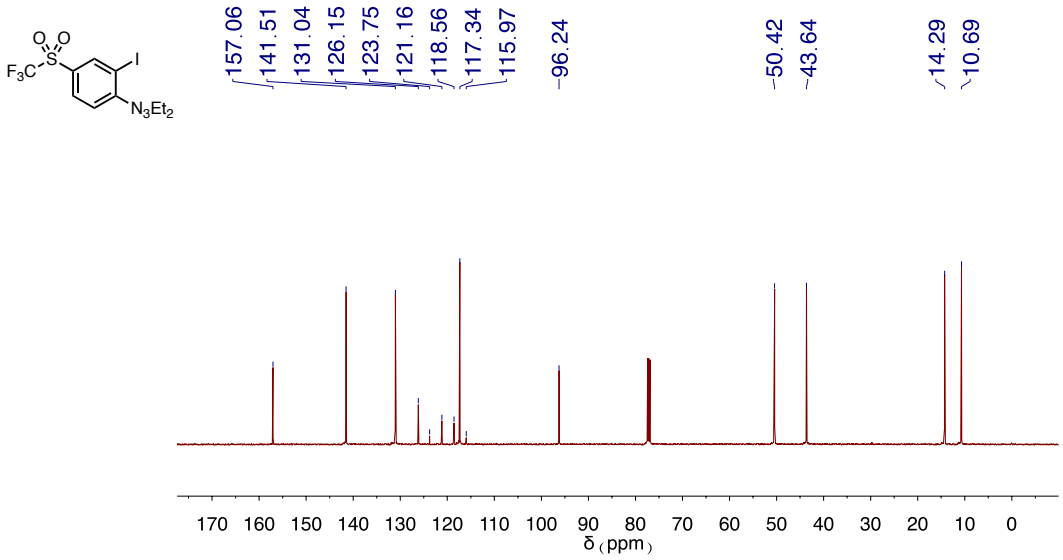

Figure C.17. ^{13}C NMR spectrum of **2a**.

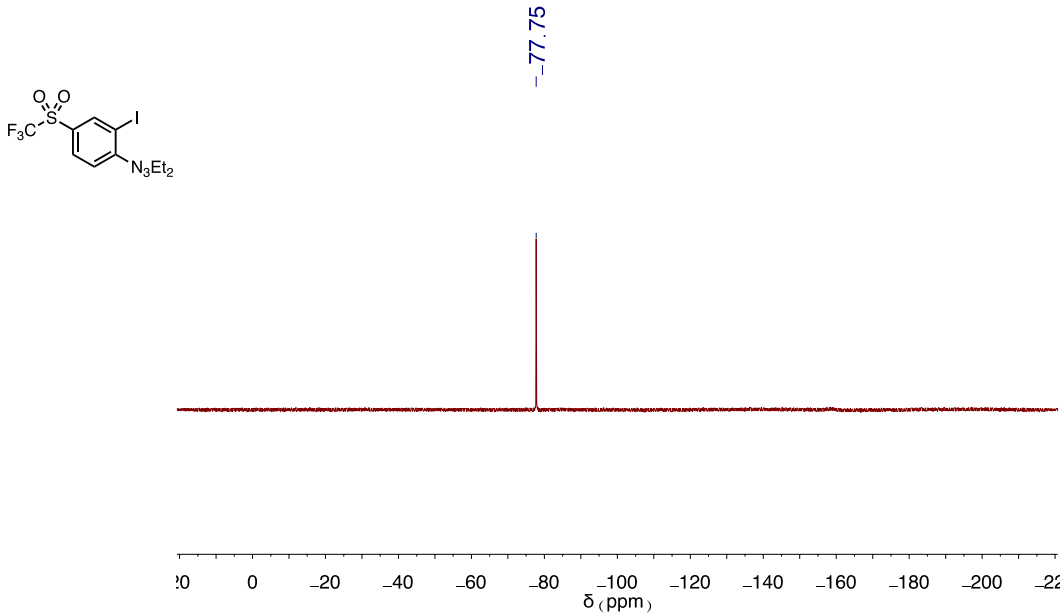

Figure C.18. ^{19}F NMR spectrum of **2a**.

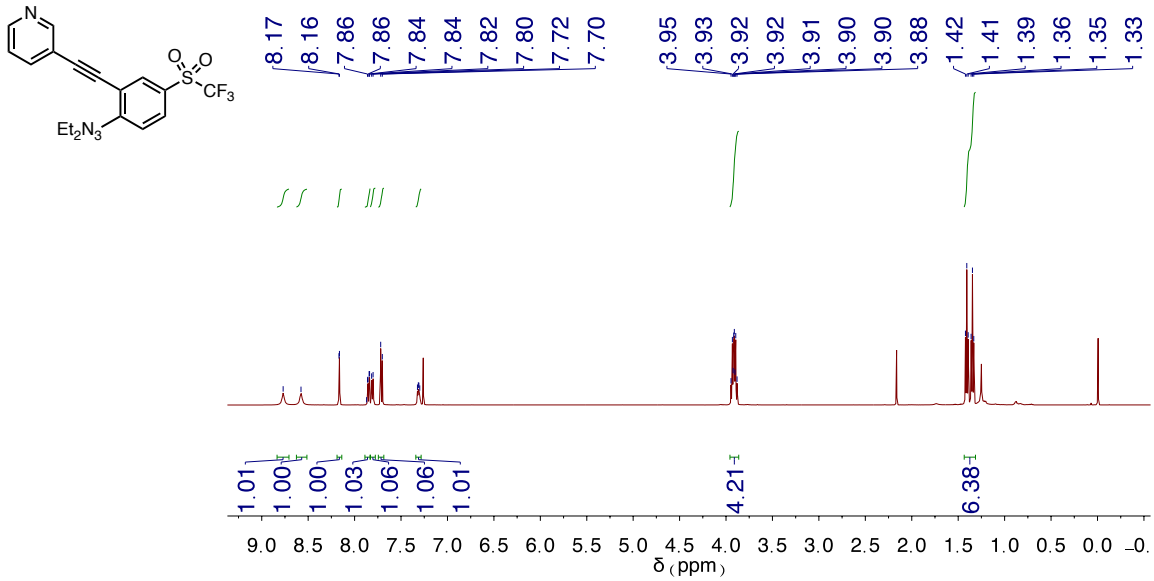

Figure C.19. ^{1}H NMR spectrum of **3a**. Wet with water and grease.

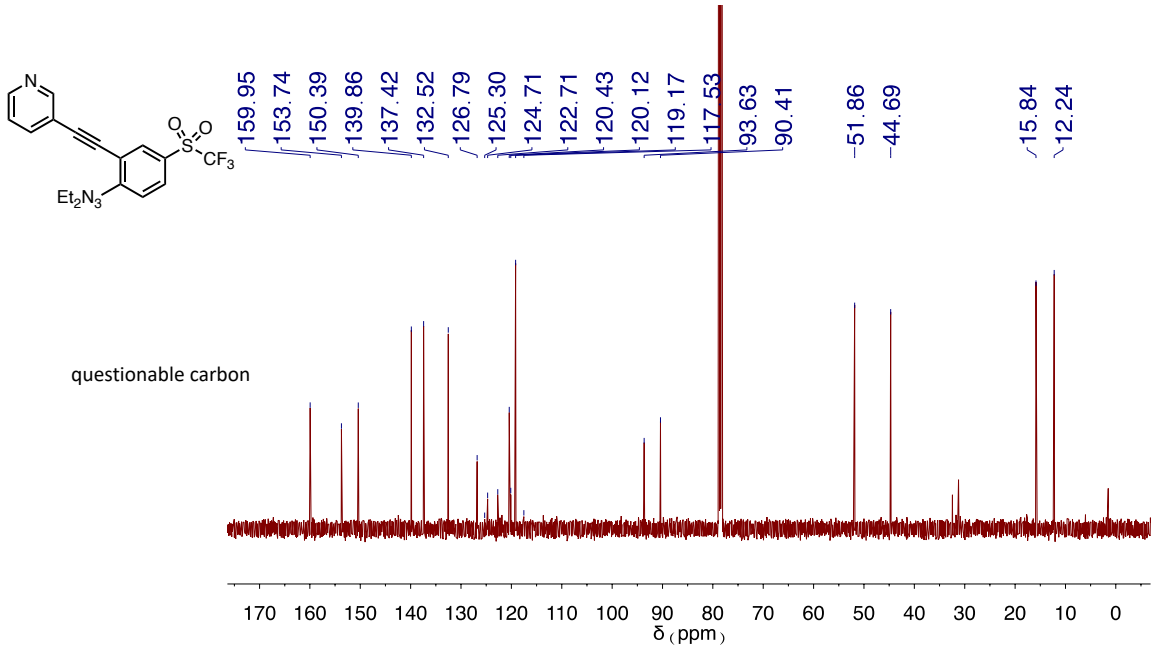

Figure C.20. ^{13}C NMR spectrum of **3a**. Contains grease.

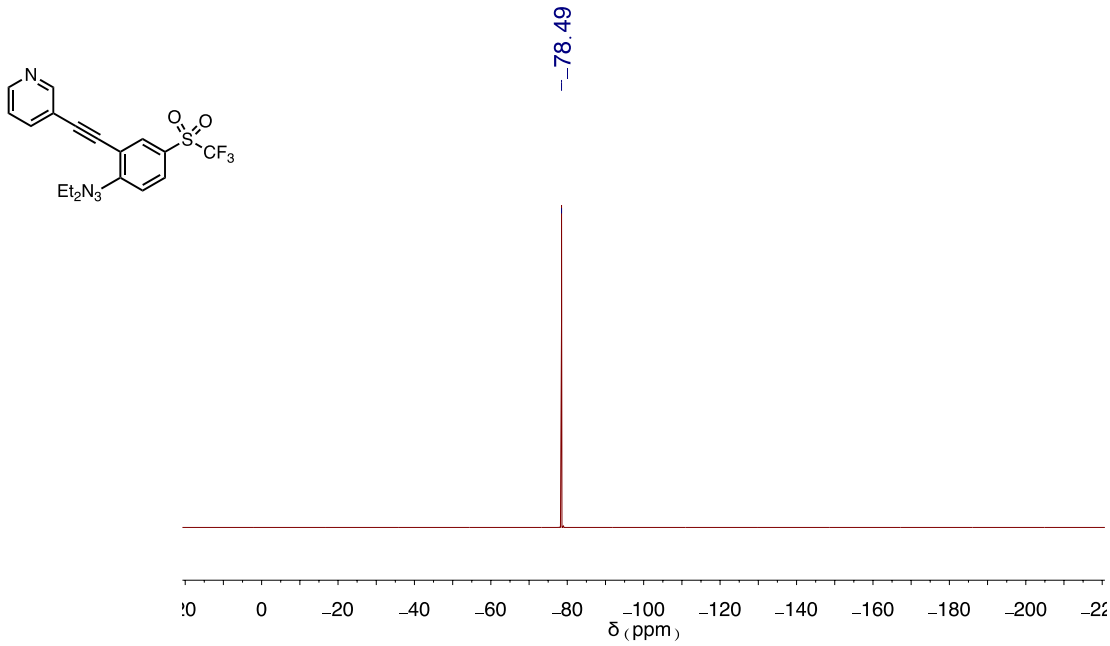

Figure C.21. ^{19}F NMR spectrum of **3a**.

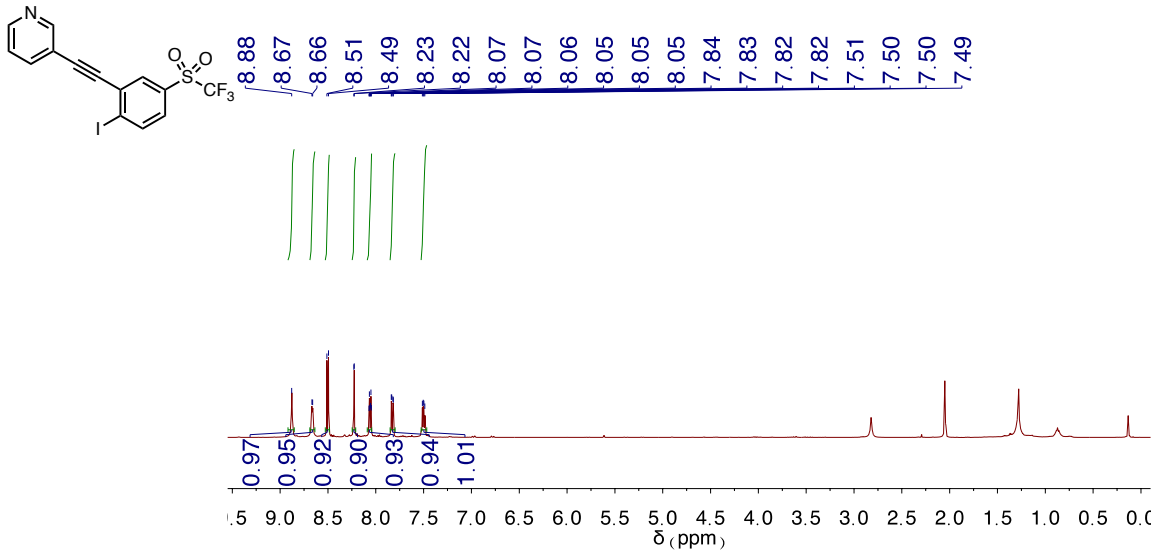

Figure C.22. ^{1}H NMR spectrum of **4a**. Wet with water and grease.

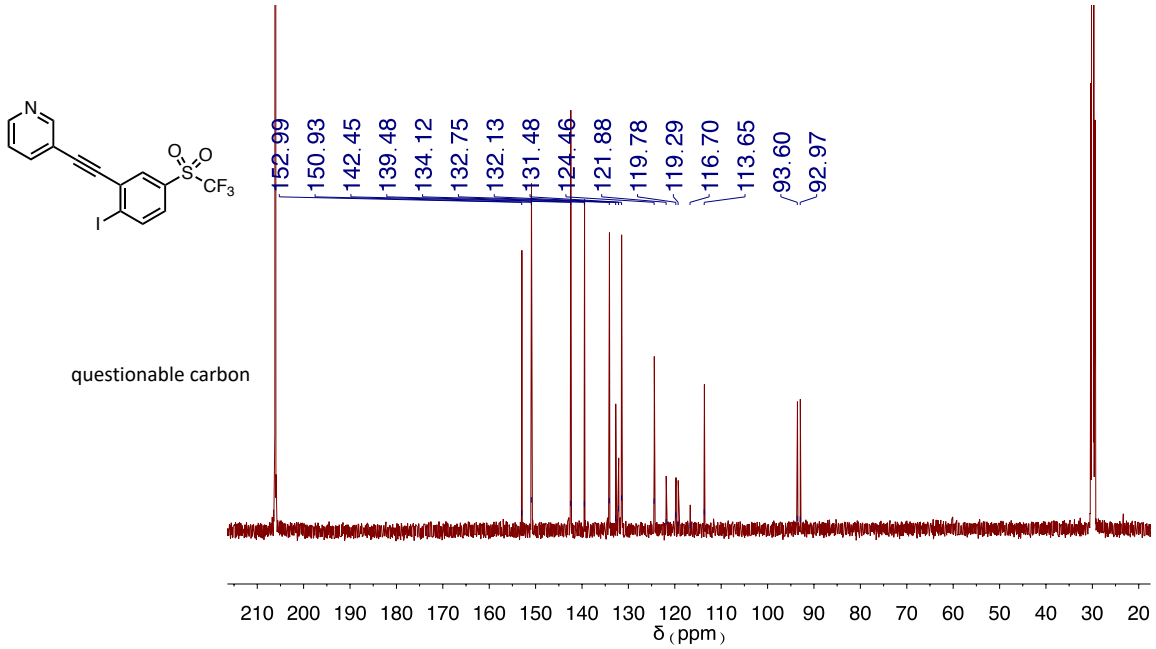

Figure C.23. ^{13}C NMR spectrum of **4a**.

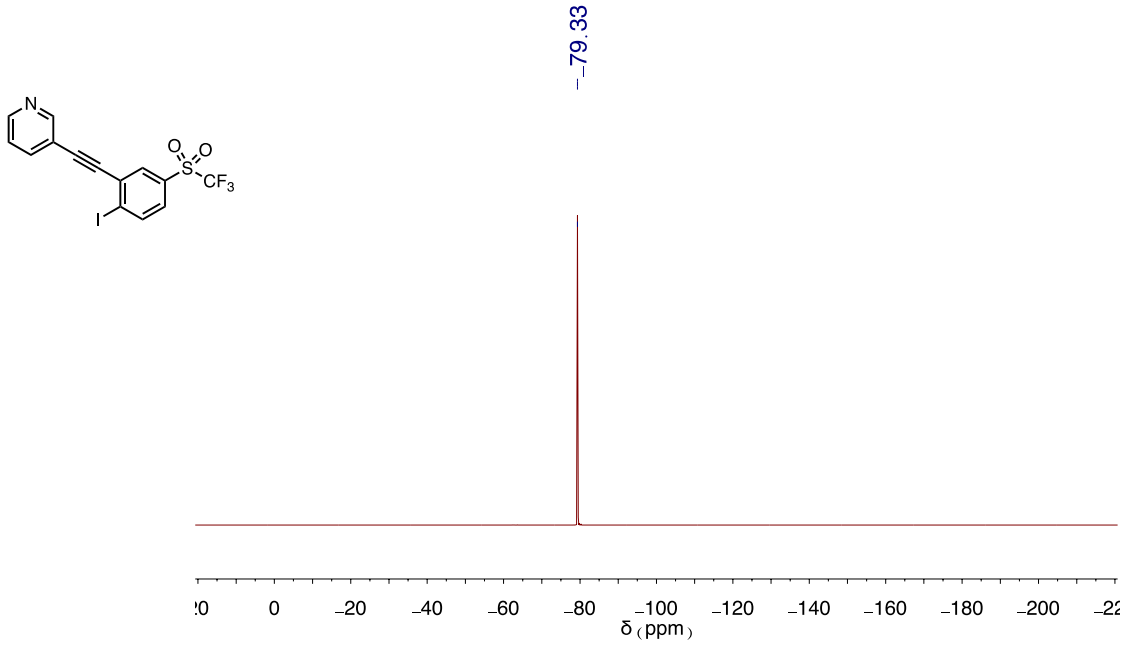

Figure C.24. ^{19}F NMR spectrum of **4a**.

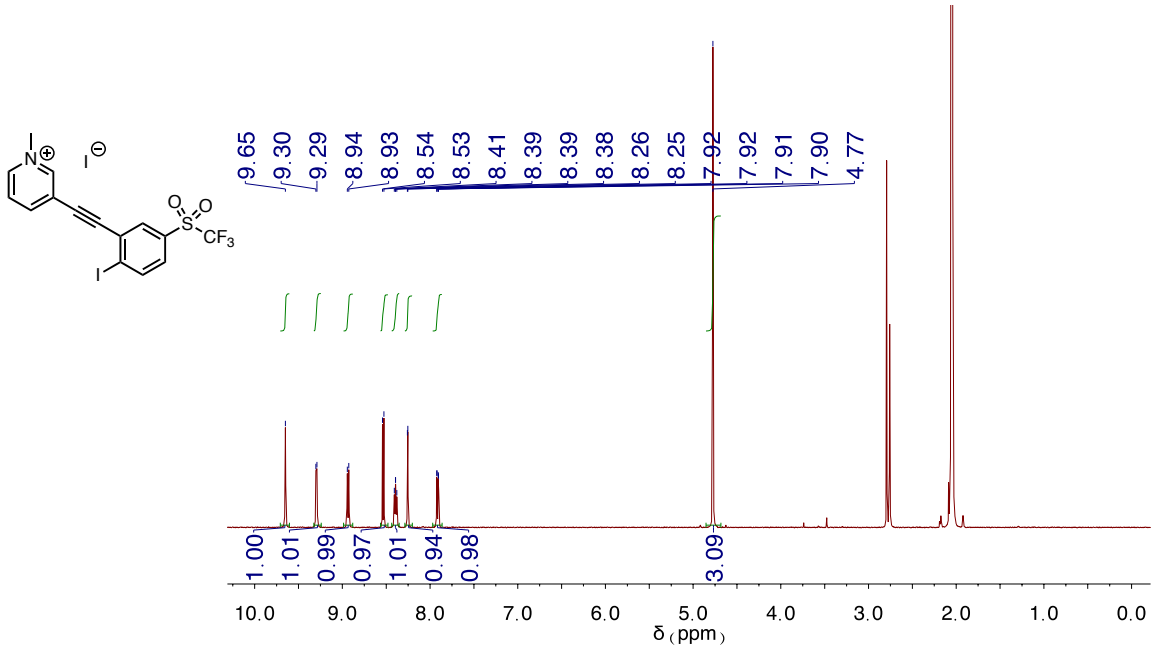

Figure C.25. ^{1}H NMR spectrum of **5a • I**$^{-}$. Wet with water.

need carbon in acetone

Figure C.26. ^{13}C NMR spectrum of **5a • I**$^{-}$.

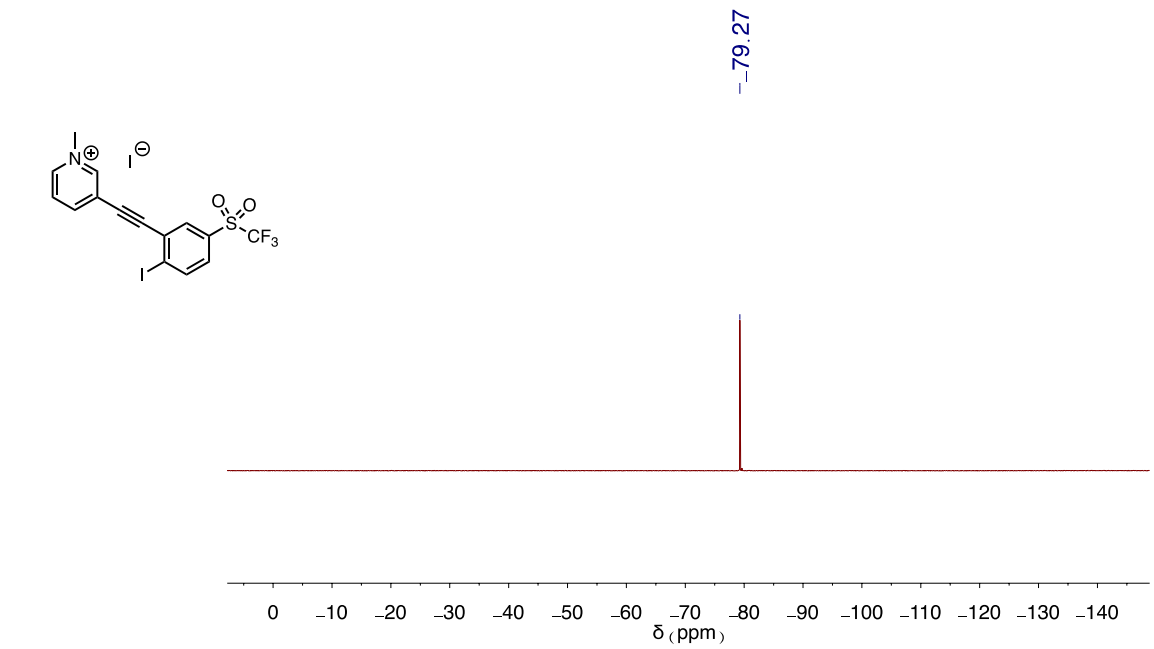

Figure C.27. ^{19}F NMR spectrum of **5a • I**$^{-}$.

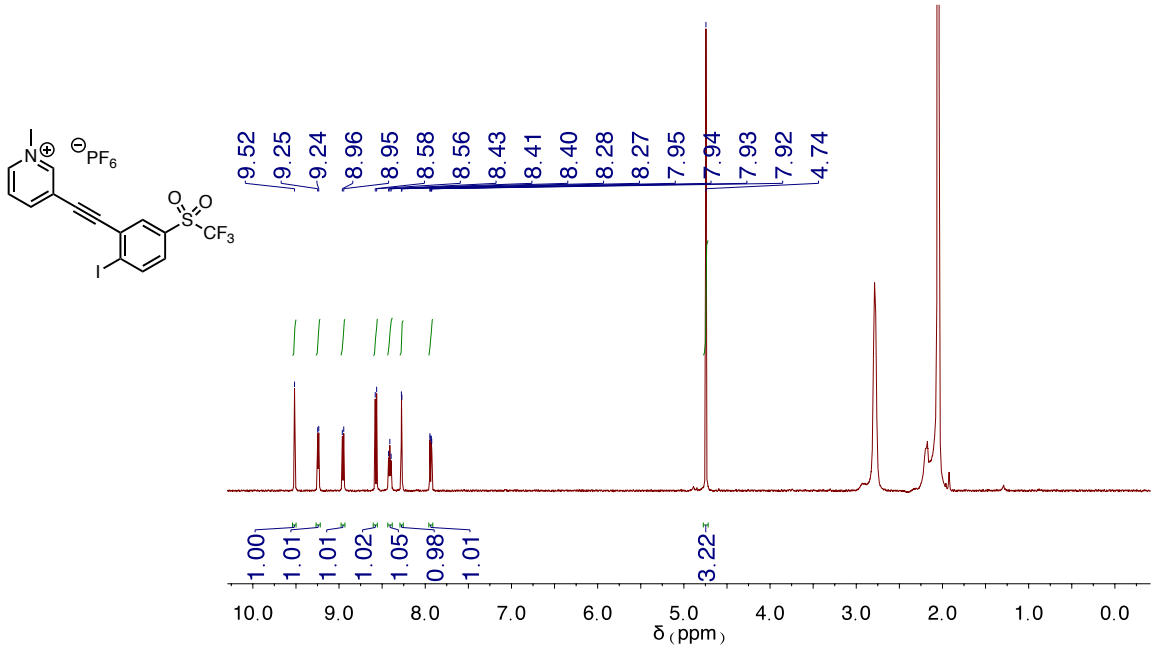

Figure C.28. ^{1}H NMR spectrum of **5a • PF$_6$**$^{-}$.

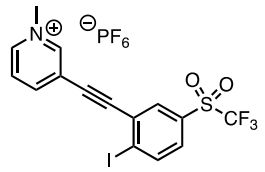

need carbon in acetone

Figure C29. ^{13}C NMR spectrum of **5a • PF_6^-**.

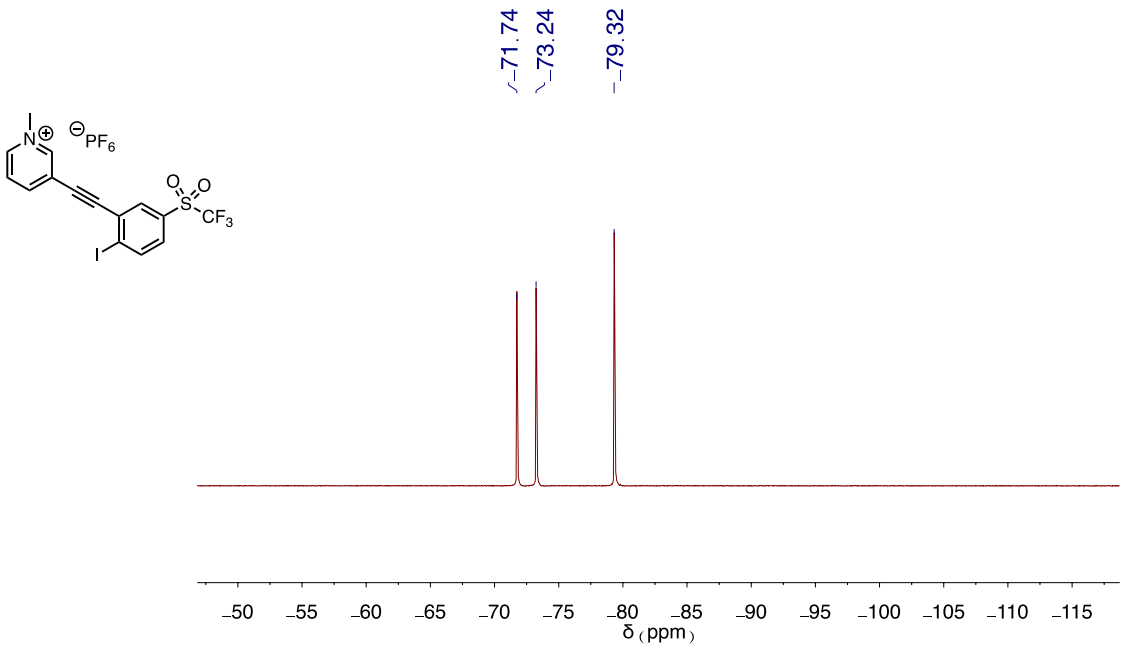

Figure C.30. ^{19}F NMR spectrum of **5a • PF_6^-**.

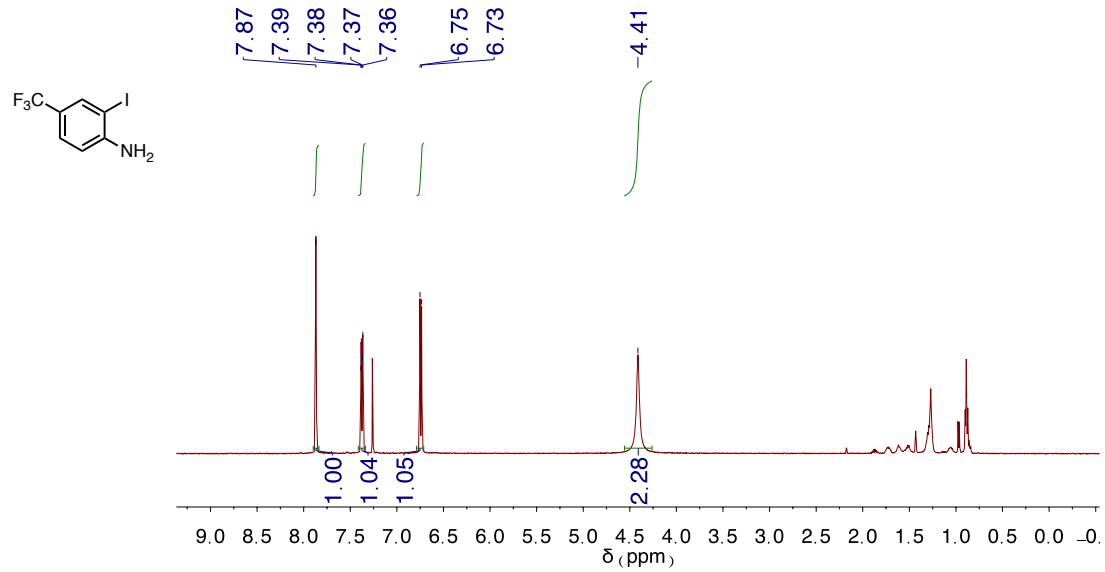

Figure C.31. [1]H NMR spectrum of **1b**.

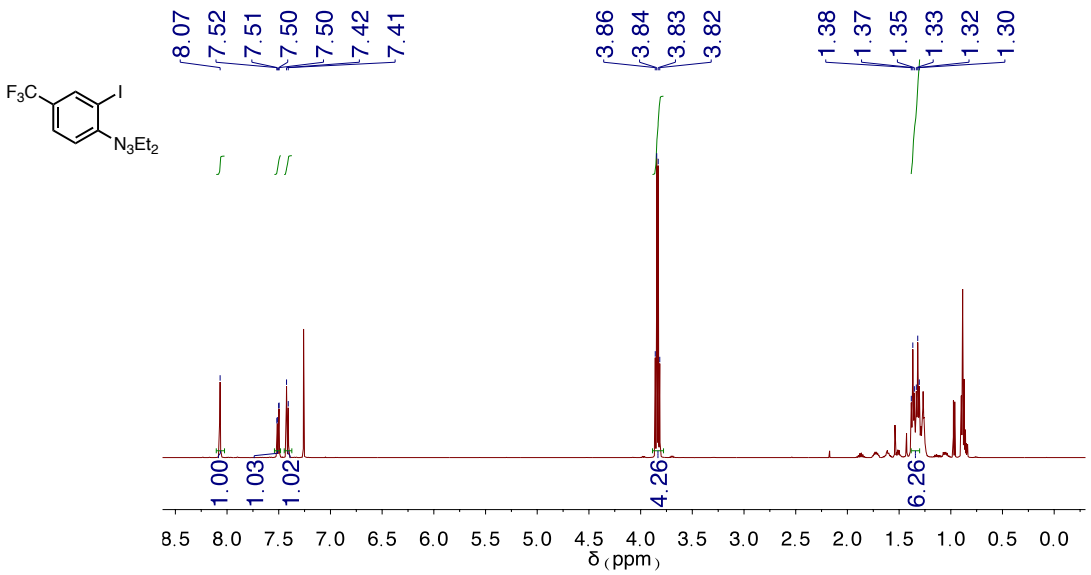

Figure C.32. [1]H NMR spectrum of **2b**.

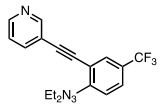

need more of

Figure C.33. ^{1}H NMR spectrum of **3b**.

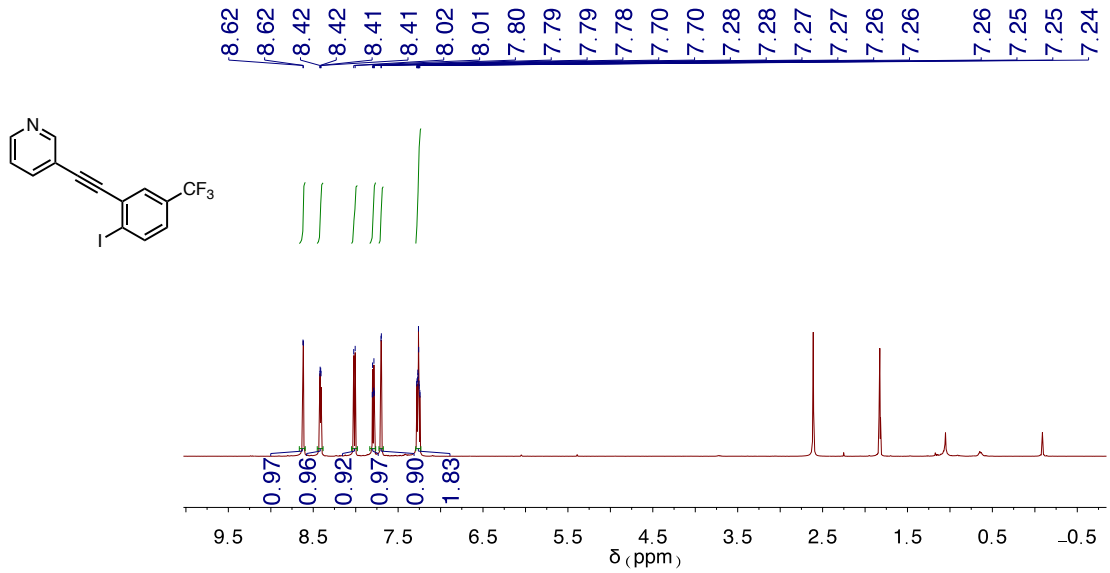

Figure C.34. ^{1}H NMR spectrum of **4b**.

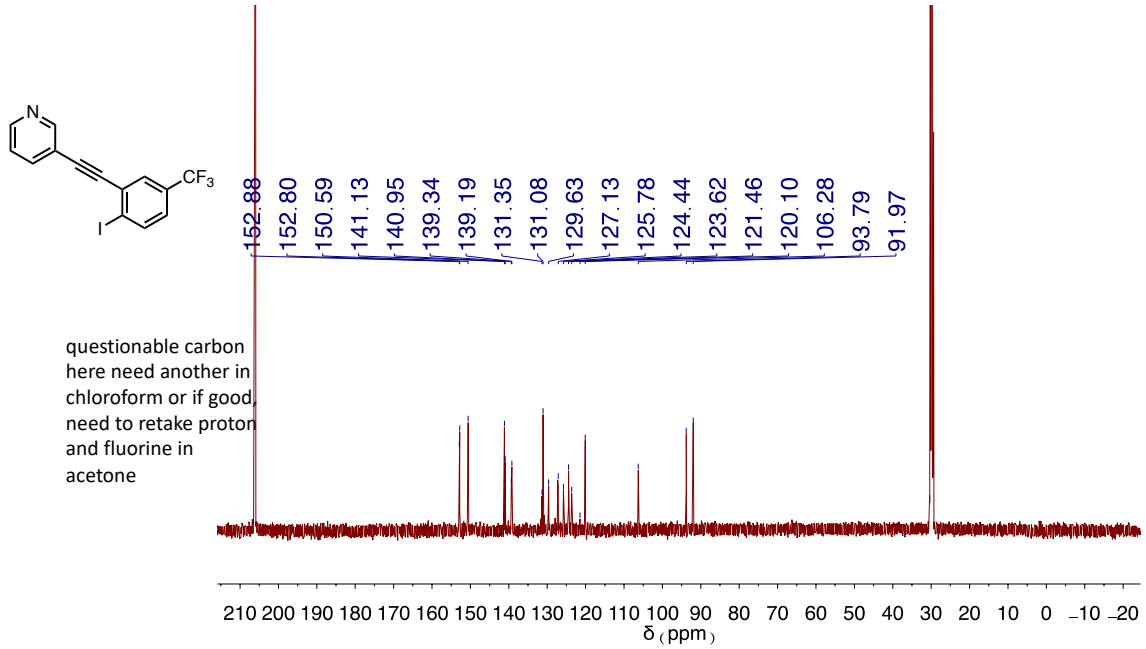

Figure C.35. ^{13}C NMR spectrum of **4b**.

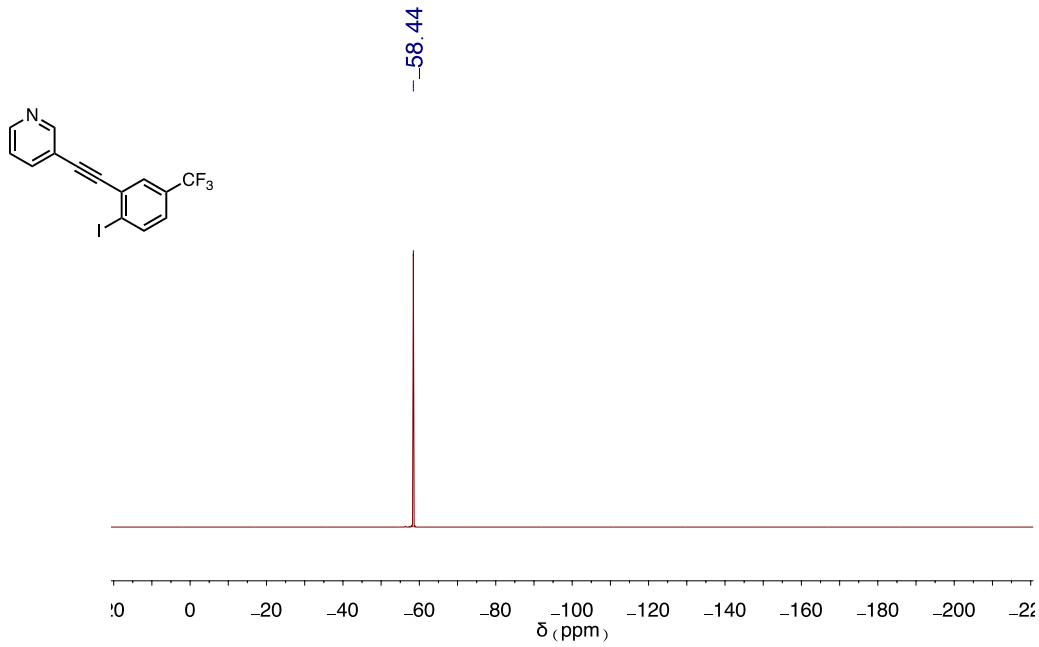

Figure C.36. ^{19}F NMR spectrum of **4b**.

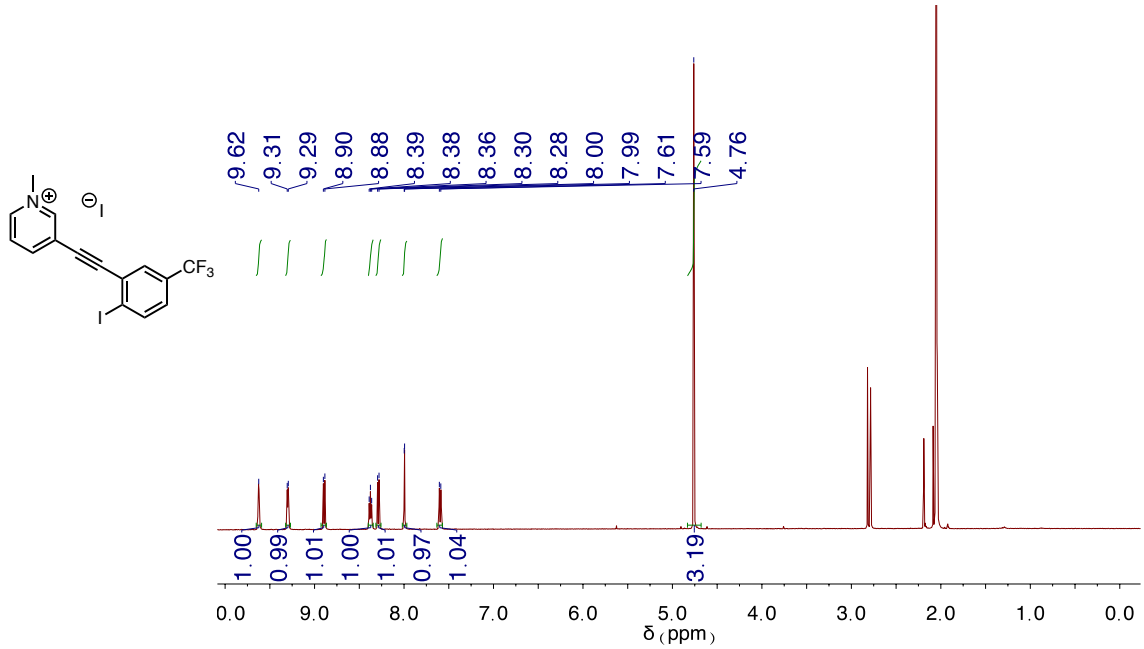

Figure C.37. ^{1}H NMR spectrum of **5b • I**$^{-}$.

Figure C.38. ^{13}C NMR spectrum of **5b • I**$^{-}$.

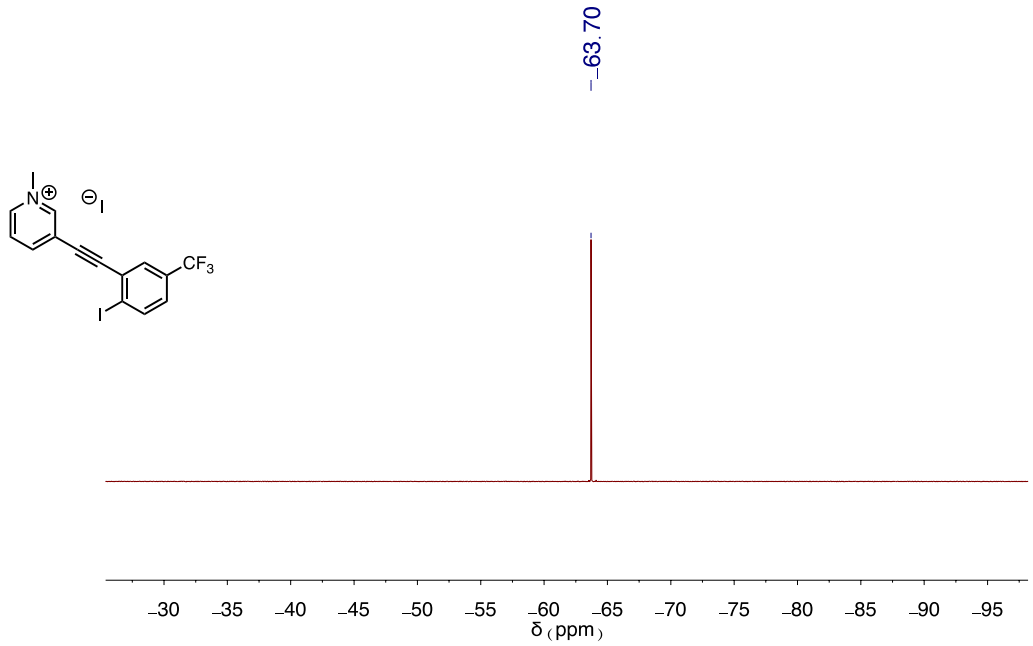

Figure C.39. ^{19}F NMR spectrum of **5b • I**$^{-}$.

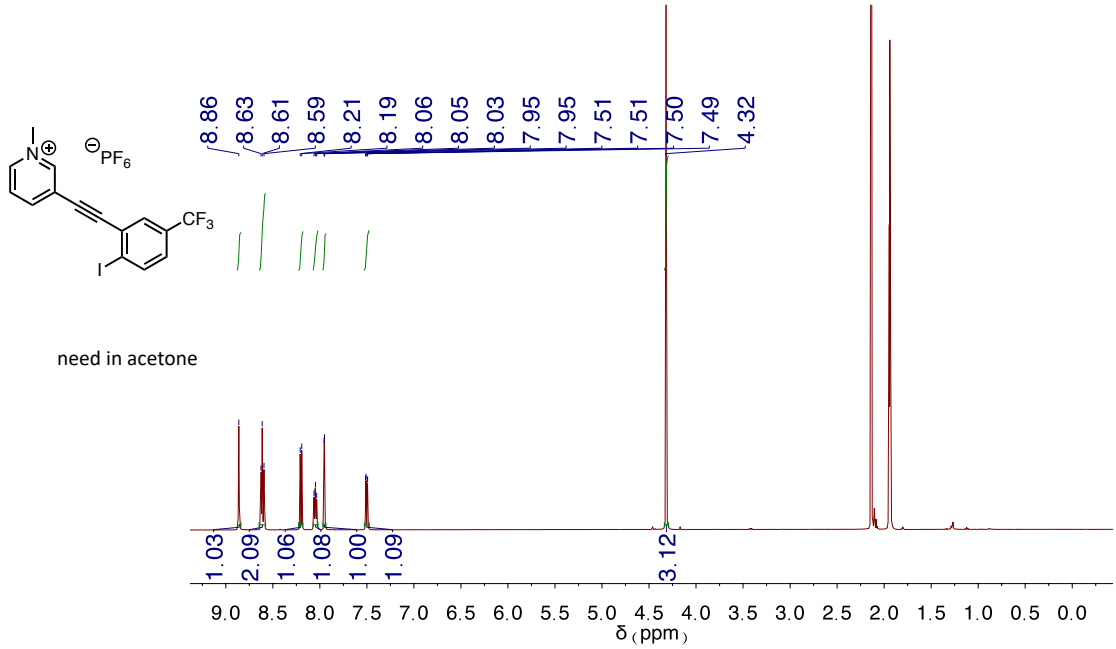

Figure C.40. ^{1}H NMR spectrum of **5b • PF_6^-**.

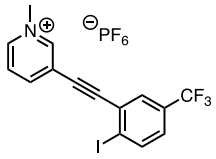

carbon needed in acetone

Figure C.41. ^{13}C NMR spectrum of **5b • PF_6^-**.

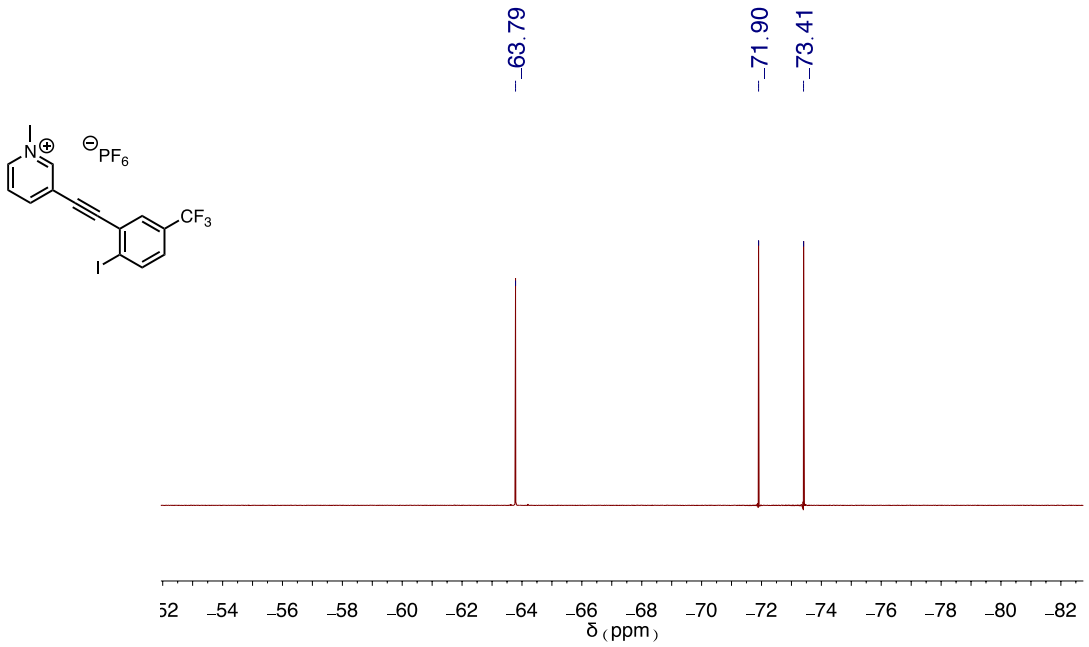

Figure C.42. ^{19}F NMR spectrum of **5b • PF_6^-**.

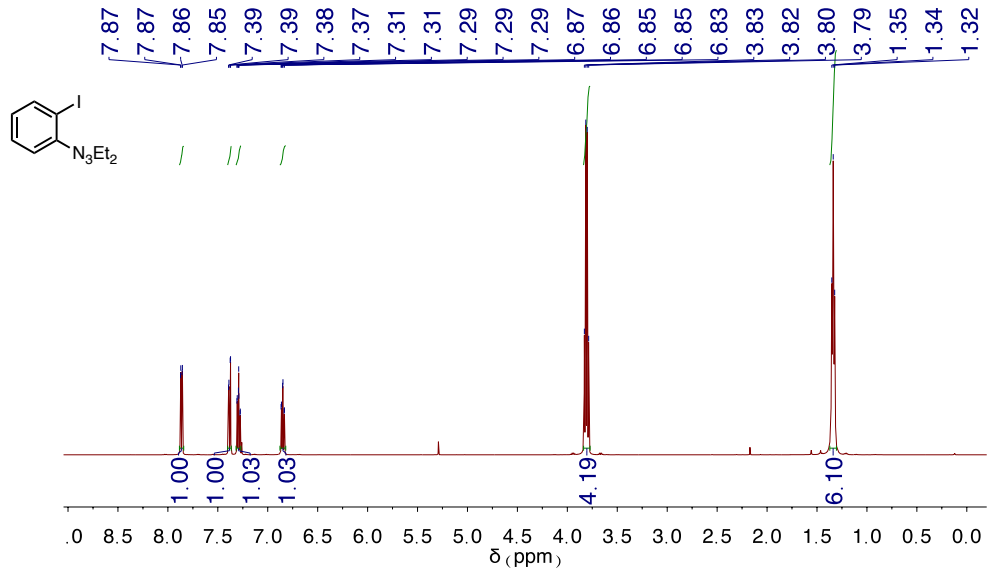

Figure C.43. [1]H NMR spectrum of **2c**.

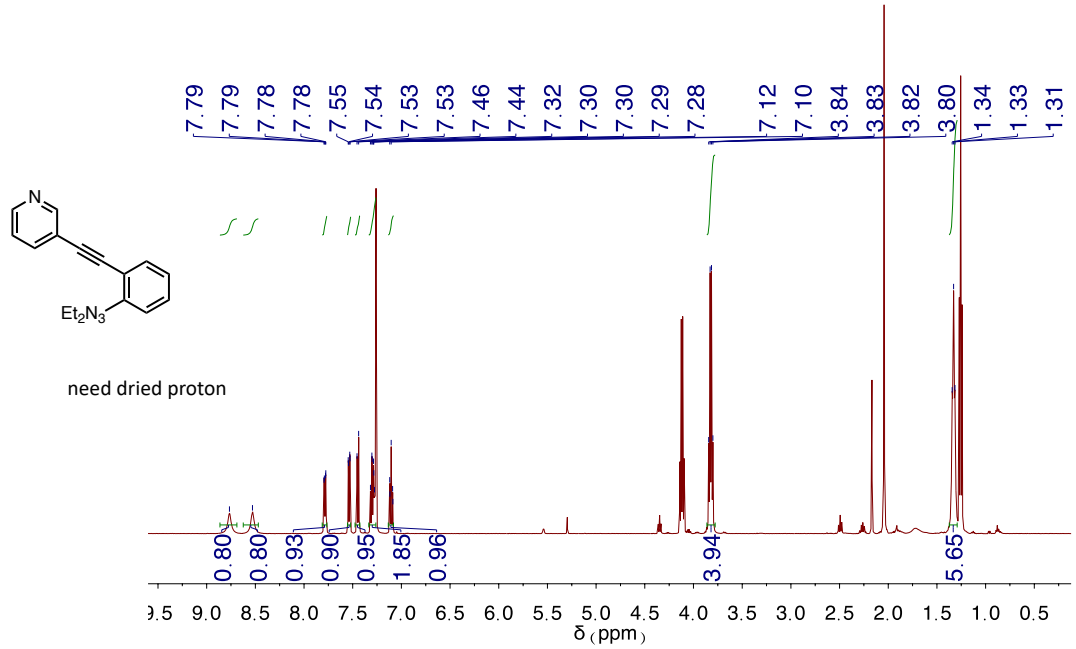

Figure C.44. [1]H NMR spectrum of **3c**.

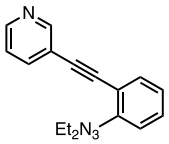

need carbon

Figure C.45. ^{13}C NMR spectrum of **3c**.

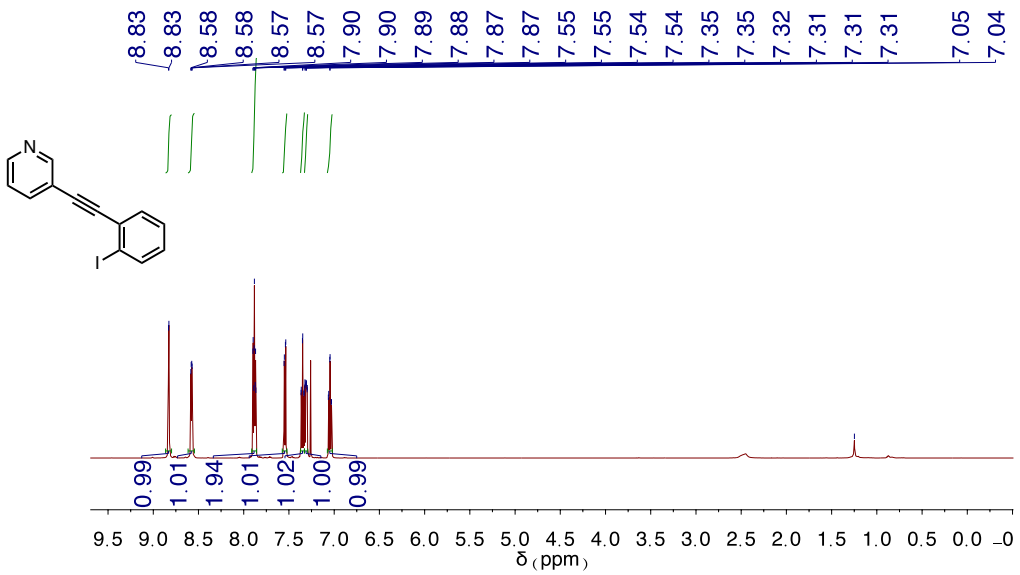

Figure C.46. ^{1}H NMR spectrum of **4c**.

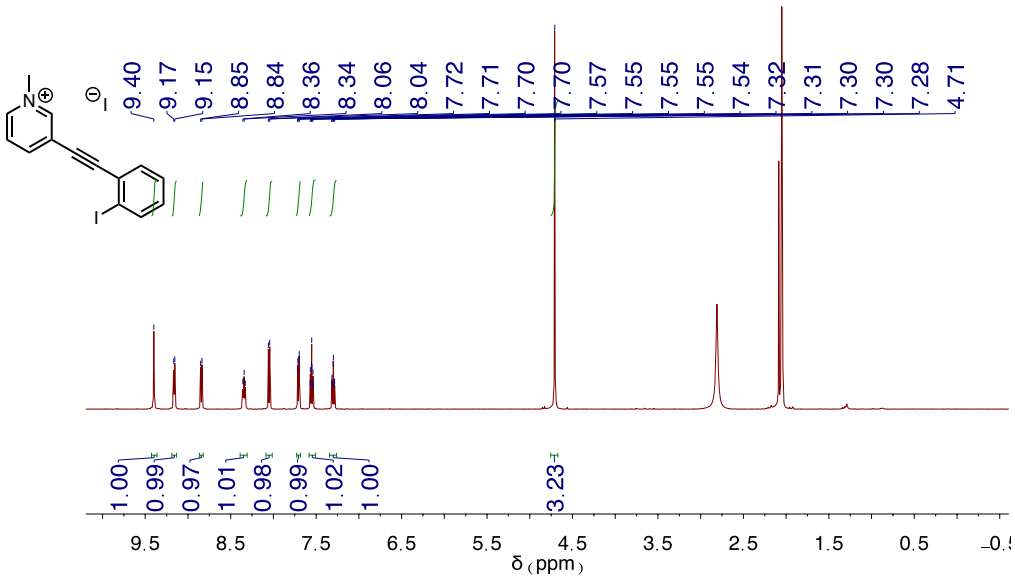

Figure C.47. ^{1}H NMR spectrum of **5c • I**$^{-}$.

need carbon AND FLUORINE

Figure C.48. ^{13}C NMR spectrum of **5c • I**$^{-}$.

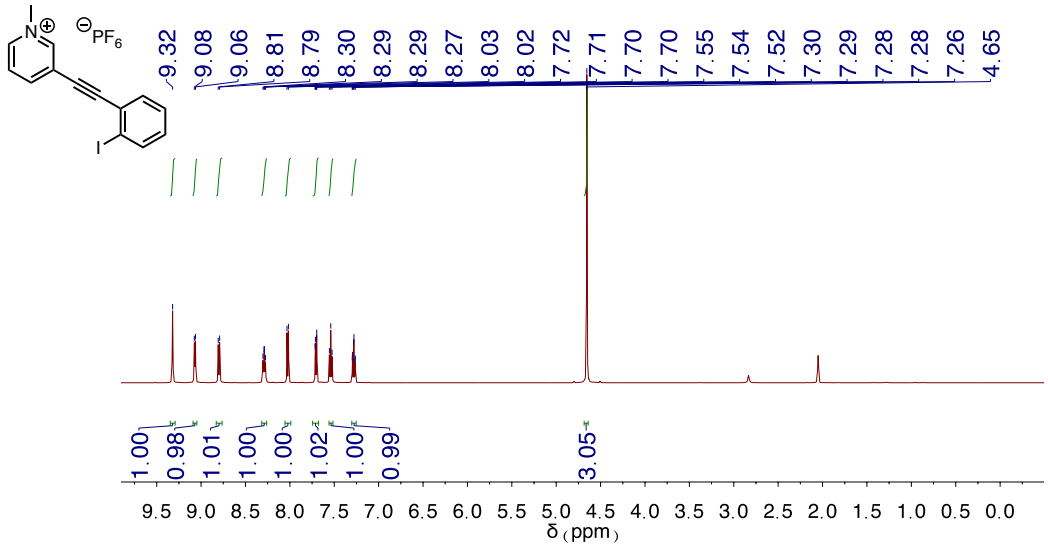

Figure C.49. ^{1}H NMR spectrum of **5c • PF_6^-**.

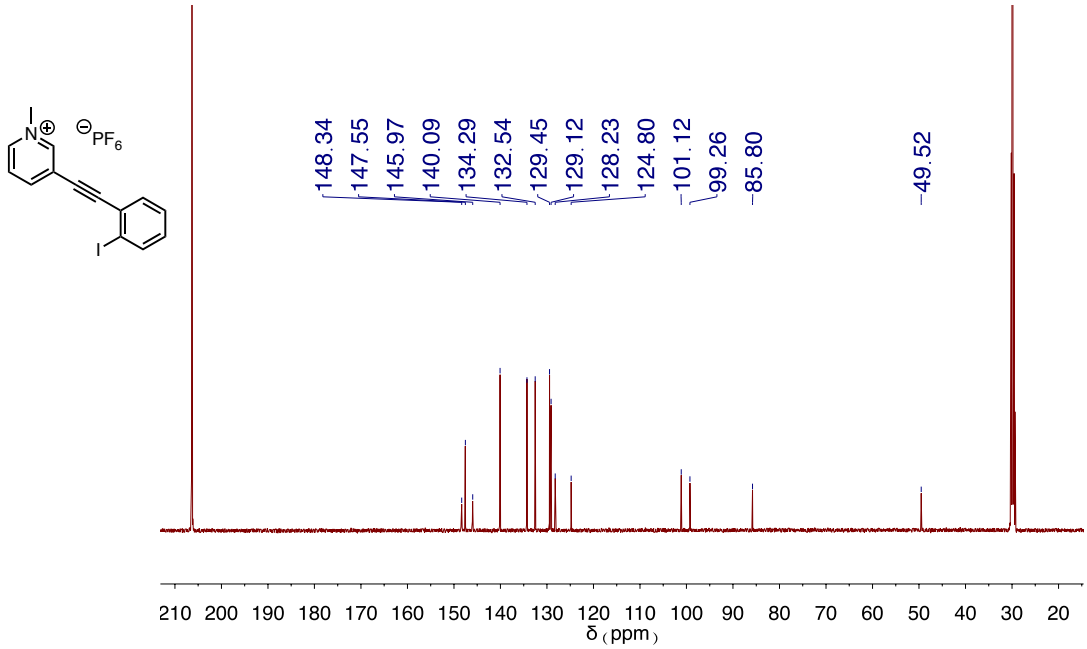

Figure C.50. ^{13}C NMR spectrum of **5c • PF_6^-**.

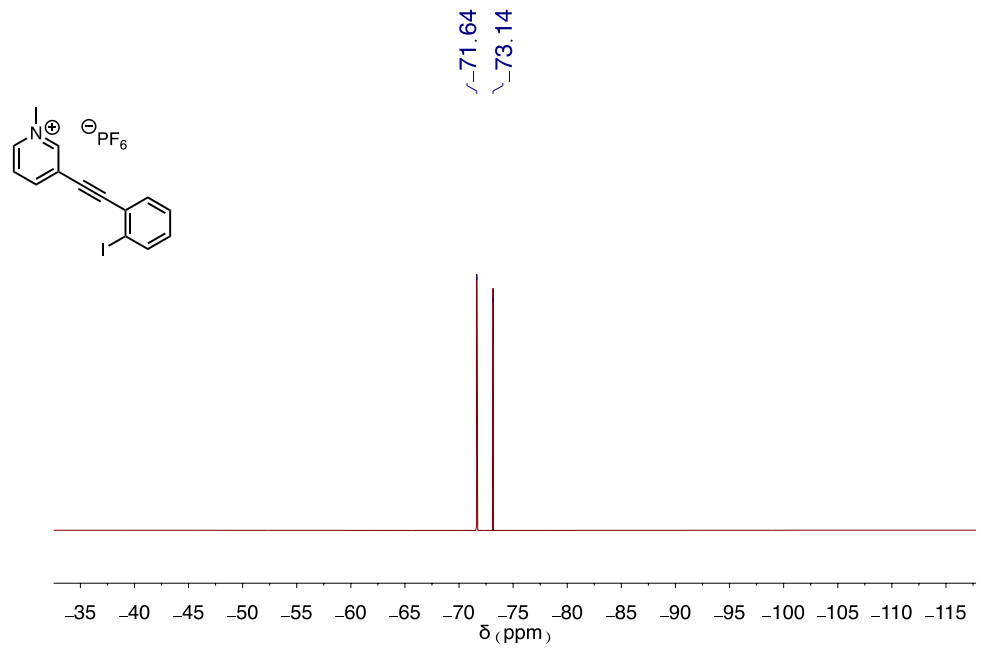

Figure C.51. ^{19}F NMR spectrum of **5c • PF_6^-**.

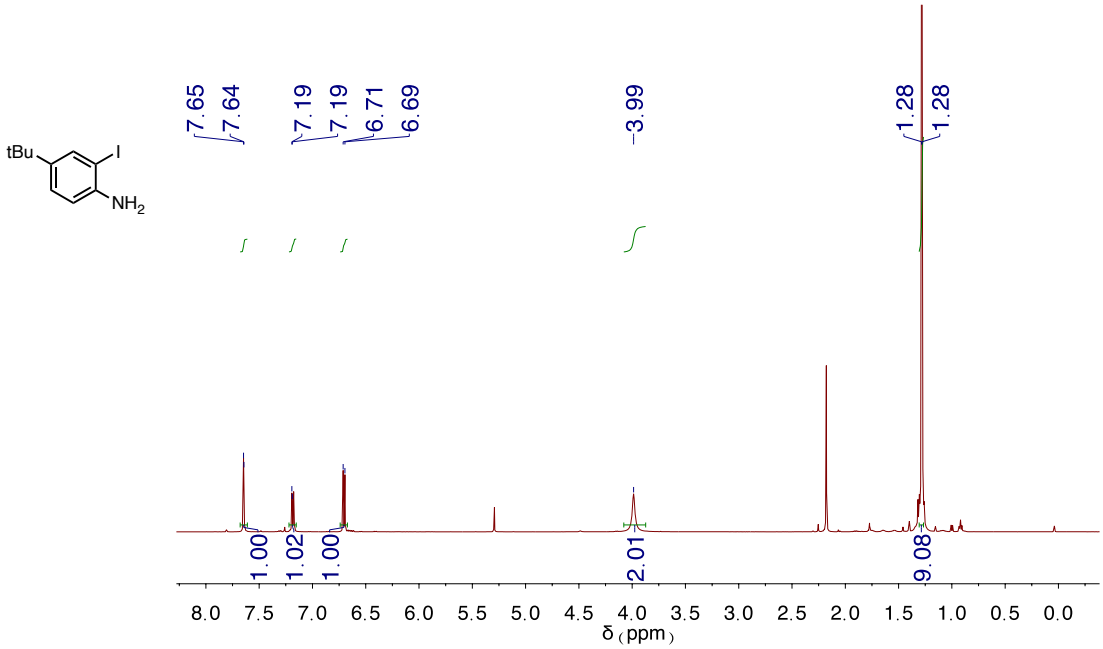

Figure C.52. ^{1}H NMR spectrum of **1d**. Wet with DCM and water.

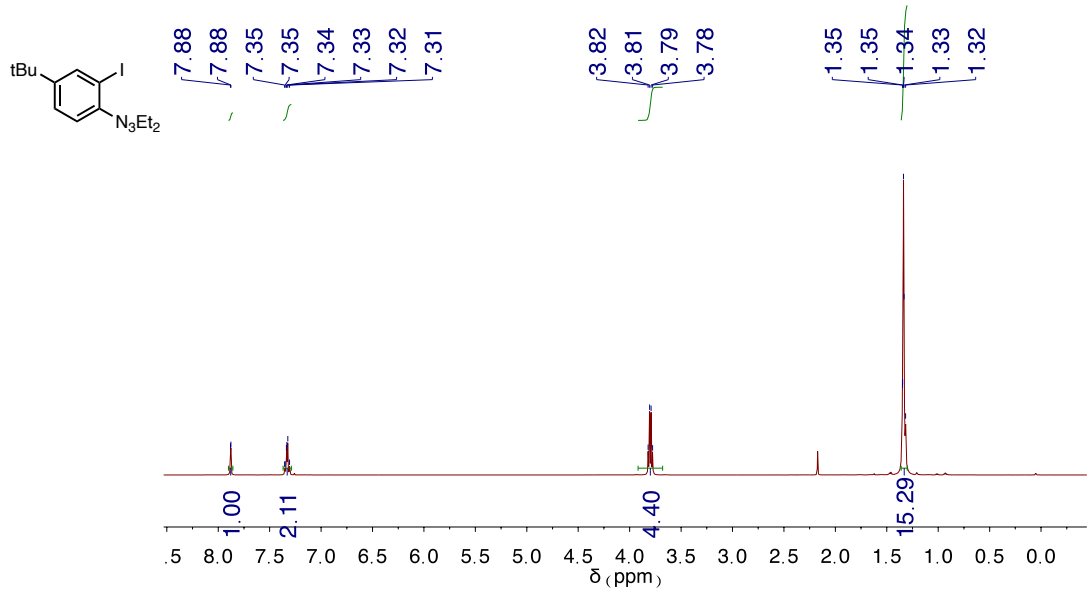

Figure C.53. [1]H NMR spectrum of **2d**.

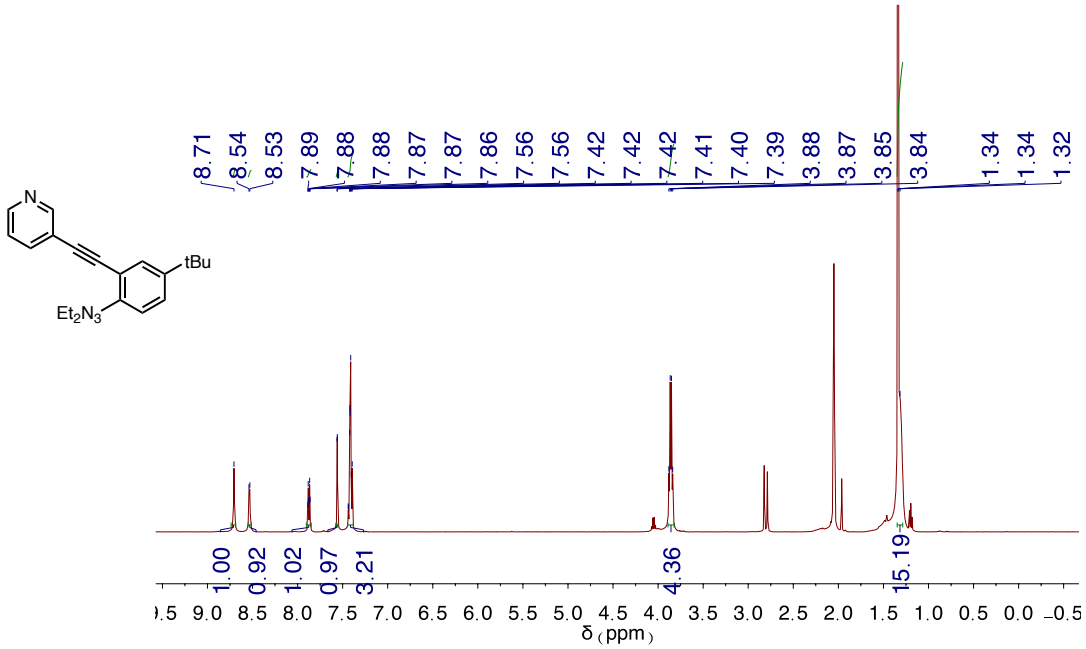

Figure C.54. [1]H NMR spectrum of **3d**. Wet with water and ethyl acetate.

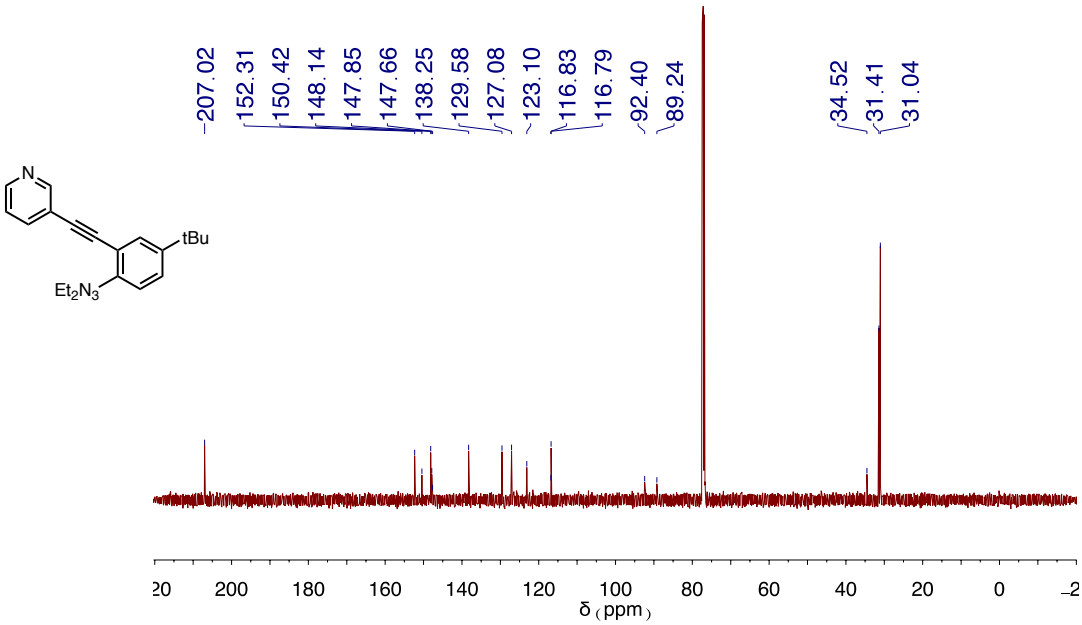

Figure C.55. ^{13}C NMR spectrum of **3d**.

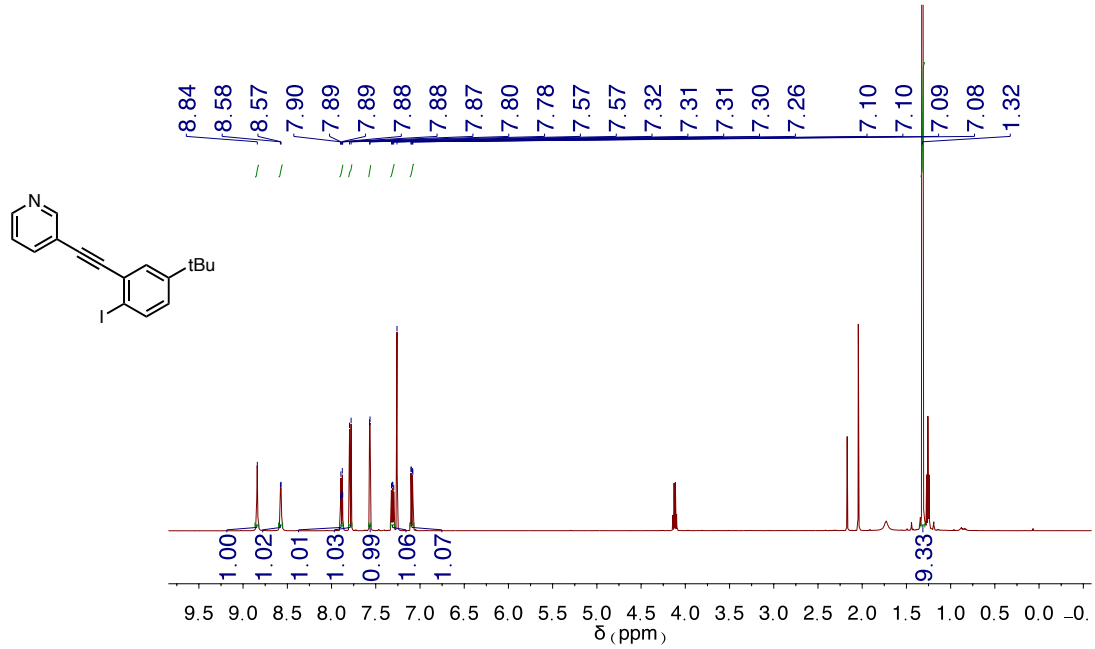

Figure C.56. ^{1}H NMR spectrum of **4d**. Wet with water and ethyl acetate.

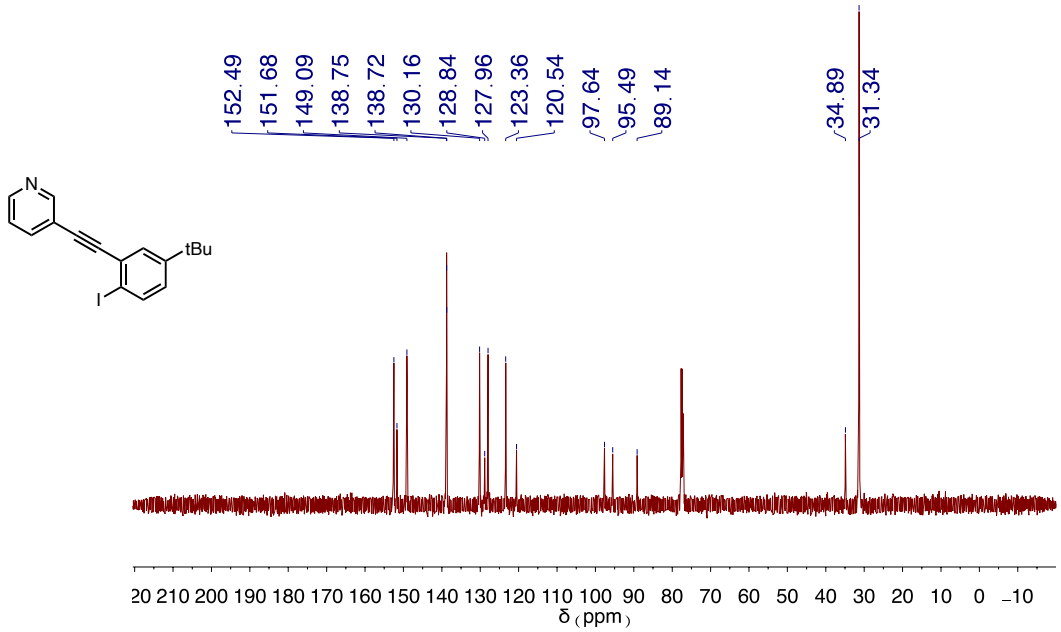

Figure C.57. ^{13}C NMR spectrum of **4d**.

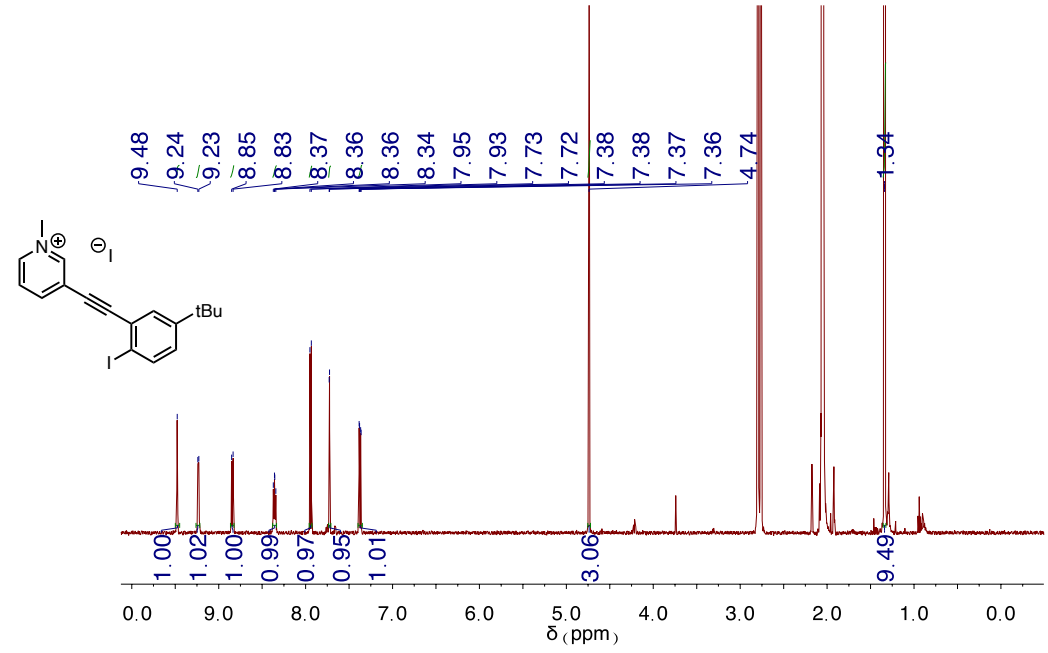

Figure C.58. ^{1}H NMR spectrum of **5d • I**$^{-}$. Wet with water.

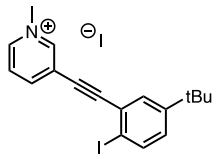

carbon in acetone needed

Figure C.59. ^{13}C NMR spectrum of **5d • I**$^{-}$.

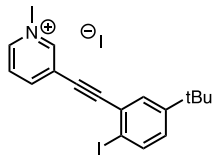

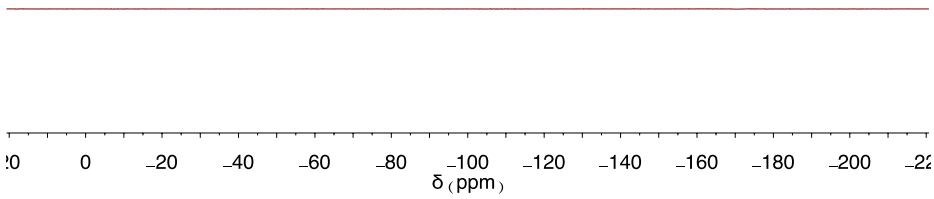

Figure C.60. ^{19}F NMR spectrum of **5d • I**$^{-}$.

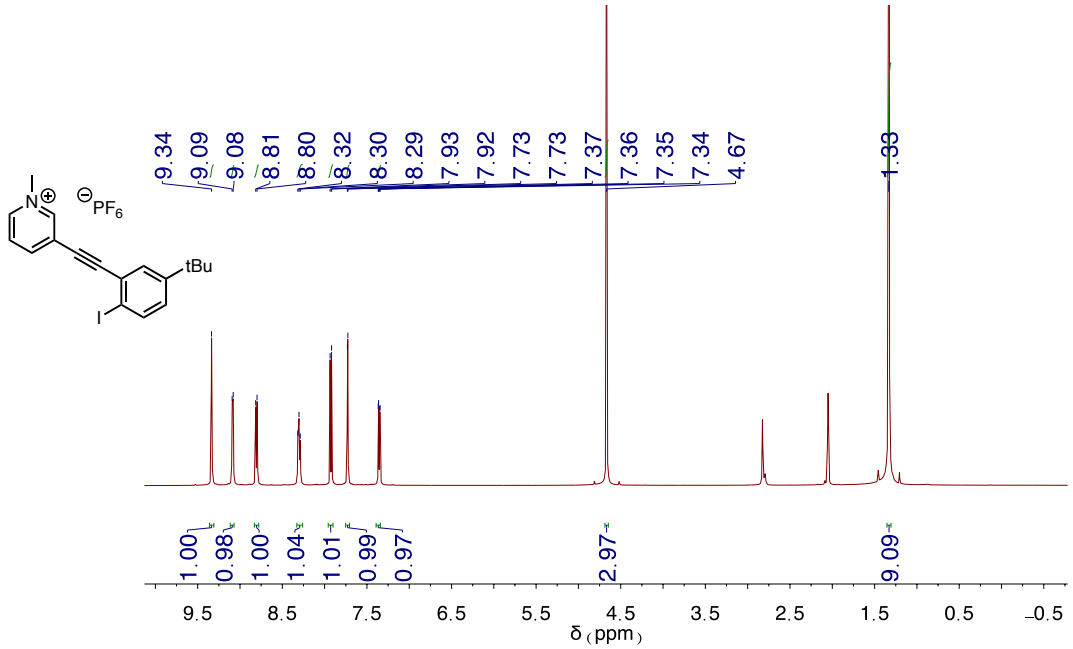

Figure C.61. ^{1}H NMR spectrum of **5d • PF_6^-**.

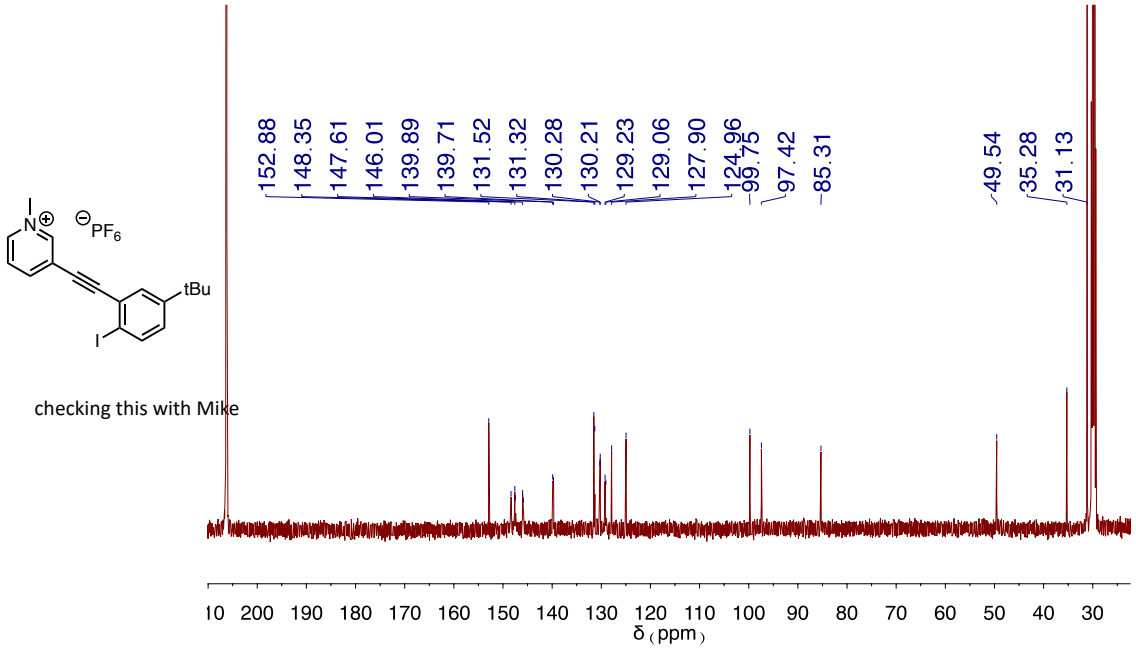

Figure C.62. ^{13}C NMR spectrum of **5d • PF_6^-**.

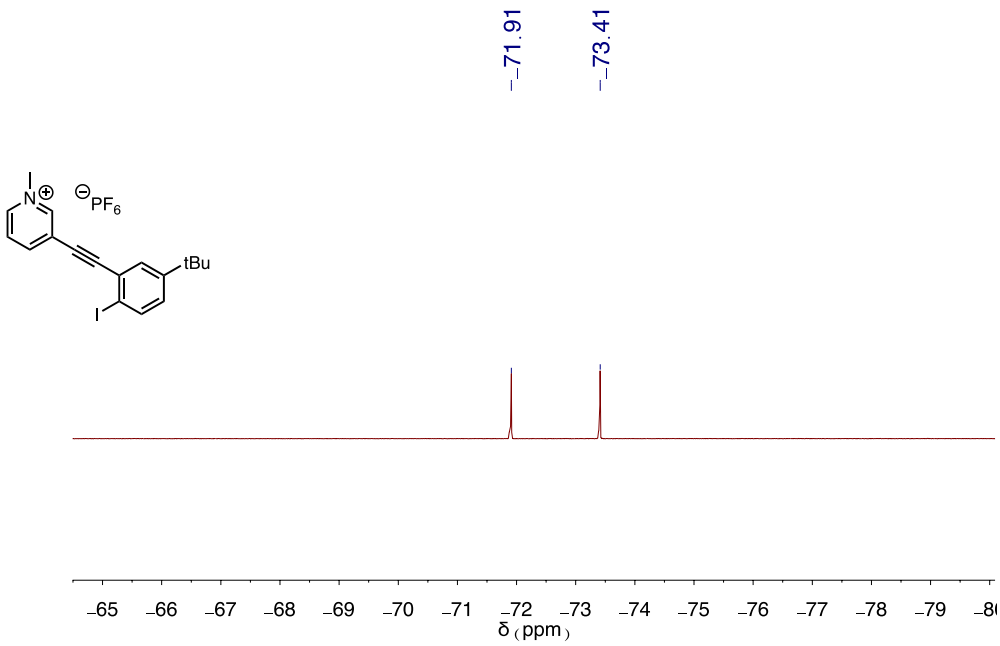

Figure C.63. ^{19}F NMR spectrum of **5d • PF_6^-**.

APPENDIX D

SUPPLEMENTARY CONTENT FOR CHAPTER FIVE

Synthesis

General Methods: All reagents were purchased from conventional commercial sources and used as received, unless otherwise noted. All NMR spectra were acquired at room temperature on a Bruker Avance-III-HD 600 MHz (^{1}H 600 MHz, ^{13}C 151 MHz, ^{19}F 565 MHz) spectrometer with a Prodigy multinuclear broadband BBO CryoProbe. ^{1}H and ^{13}C chemical shifts (δ) are reported in ppm relative to the residual $CHCl_3$ (^{1}H: 7.26 ppm, ^{13}C: 77.16 ppm) or CH_3CN (^{1}H: 1.94, ^{13}C: 118.26).

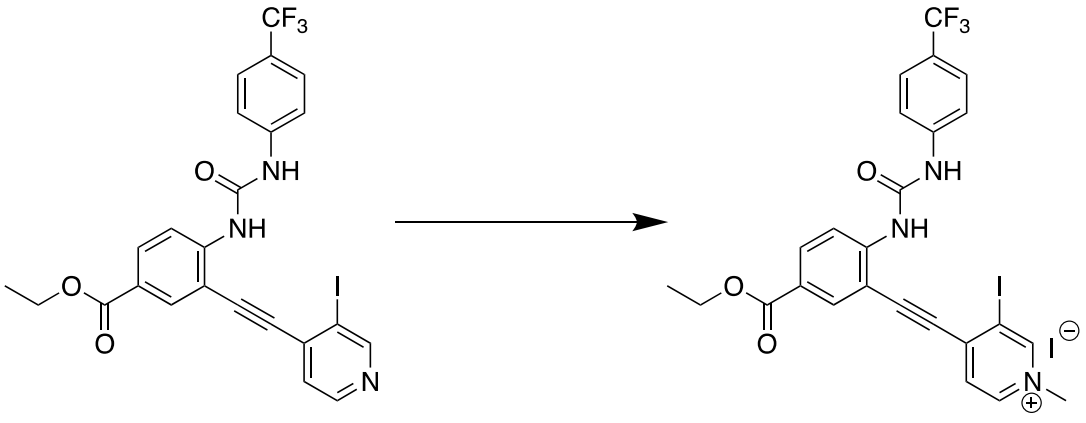

Methylated Urea and Iodo-Pyridine (1.6)

The receptor (0.030g, 0.0518 mmol) was weighed out into a narrow bomb flask and a small stir bar was added. Then ~1 to 2 mL of MeI was carefully pipetted over the scaffold until it was fully submerged. The bomb flask was then sealed and placed in a metal bead bath at room temperature. This bath was then set to heat to 110 °C and watched carefully. As soon as there was visible precipitation of the methylated receptor, as an orange-brown solid, the flask was removed from heat. This typically happened as soon as the flask had reached temperature, if not slightly before. The solution was let to cool down to room temperature and, upon chilling, was

carefully filtered. The precipitate was then washed with cold DCM before being scraped off of the filter paper into a massed scintillation vial to yield 0.026g of product (70%). ^{1}H NMR (500 MHz, Acetone-d_6) δ = 9.25 (s, 1H), 9.05 (s, 1H), 8.62 (d, *J*=4.9, 1H), 8.50 – 8.47 (m, 2H), 8.22 (d, *J*=2.1, 1H), 8.09 (dd, *J*=8.9, 2.1, 1H), 7.77 (d, *J*=8.5, 3H), 7.73 (d, *J*=4.9, 1H), 7.65 (d, *J*=8.5, 3H), 4.37 (q, *J*=7.1, 3H), 2.84 (s, 3H), 1.38 (t, *J*=7.1, 3H). ^{13}C NMR (126 MHz, Acetone-d_6) δ = 165.53, 157.96, 152.30, 149.66, 145.41, 143.81, 137.04, 134.49, 132.66, 127.59, 126.97 (q, *J*=3.9), 125.31, 124.49, 124.43, 119.55, 119.38, 111.02, 99.94, 96.49, 92.09, 61.62, 54.96, 14.58. ^{19}F NMR (471 MHz, Acetone-d_6) δ = -62.32.

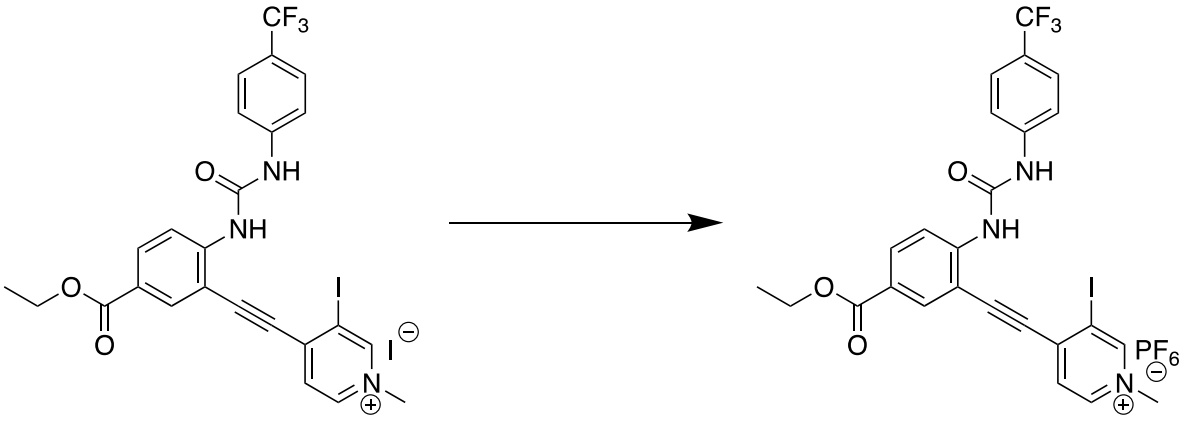

Tridentate Host Receptor (1)

The methylated scaffold (0.026g, 0.03605 mmol) was dissolved in ~6 mL of acetone (sonicating as needed to help solubilize it). Then ~3 mL of water was added to the scintillation vial which was set stirring. AgPF6 was then added and the reaction was left to stir for 1-2 hours. Upon visible precipitation the solution was filtered until translucent (ppt is not product) the filtrate is then subjected to reduced pressure to remove the acetone, at which point the receptor will crash out of the water. This aqueous solution was then filtered a second time to yield the receptor as a white solid (0.025g, 94%). ^{1}H NMR (500 MHz, Acetone-d_6) δ = 9.14 (s, 1H), 9.08 (s, 1H), 8.66

(d, *J*=4.9, 1H), 8.49 (d, *J*=8.9, 1H), 8.47 (s, 1H), 8.23 (d, *J*=2.1, 1H), 8.13 – 8.09 (m, 1H), 7.75 (t, *J*=7.5, 3H), 7.66 (d, *J*=8.5, 2H), 4.37 (q, *J*=7.1, 2H), 1.38 (t, *J*=7.1, 3H). ^{19}F NMR (471 MHz, Chloroform-*d*) δ = -57.14, -66.70, -68.20. ^{31}P NMR (202 MHz, Acetone-d_6) δ = -134.68 – -153.89 (m).

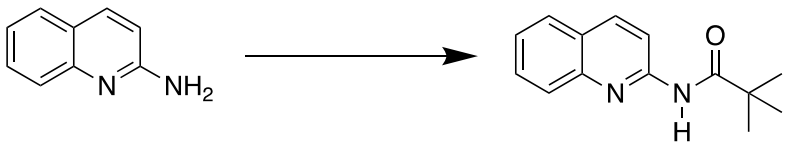

Protected Quinoline (2.1)

Aminoquinoline (1.00g, 6.9 mmols) was dissolved in DCM and set stirring in an ice bath. Once the reaction mixture reached 0 °C TEA (.91 mL, 7.6 mmols) was added to the flask followed by pivaloyl chloride (1.2 mL, 8.7mmols). After stirring for 15 minutes the ice bath was removed and the reaction was monitored by TLC. After completion the reaction mixture was washed with three times with $NaHCO_3$ and dried over Na_2SO_4. Finally, solvent was removed *in vacuo* to afford a pale-yellow oil (1.56 g, 6.83 mmols, 99% yield). If needed the product was purified by column chromatography over ethyl acetate and hexanes, though this could typically be avoided by running the reaction overnight. ^{1}H NMR (500 MHz, Chloroform-*d*) δ 8.46 (d, *J* = 9.0 Hz, 1H), 8.27 (s, 1H), 8.17 (d, *J* = 9.0 Hz, 1H), 7.82 (dq, *J* = 8.4, 0.9 Hz, 1H), 7.78 (dd, *J* = 8.0, 1.5 Hz, 1H), 7.66 (ddd, *J* = 8.4, 6.9, 1.5 Hz, 1H), 7.45 (ddd, *J* = 8.1, 6.9, 1.2 Hz, 1H), 1.38 (s, 7H). ^{13}C NMR (126 MHz, Chloroform-d) δ = 177.67, 151.38, 146.70, 138.69, 130.12, 127.72, 127.32, 126.50, 125.24, 114.42, 40.14, 27.65.

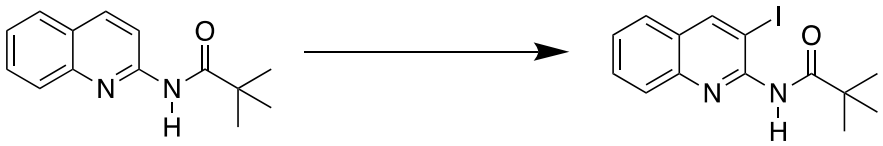

Protected Iodo-Quinoline (2.2)

Three round bottoms and two stir bars were left in a 150 °C oven to dry overnight. Dry Et_2O was procured from a solvent still, transferred into one of the dry round bottom flasks with a dry stir bar in it and set under N_2. Some of this Dry Et_2O was cannulated over to a second RBF, that has a stir bar and I_2 (1.24 equiv.) already in it. This second flask was set stirring, so the I_2 can fully dissolve before it is needed. The protected quinoline was then added to the first flask and set this stirring in a salted ice bath until it reached -20 °C. After that 2.2M nBuLi in hexanes was added dropwise via syringe at which point the pale yellow solution grew brighter before changing to a lime green color. After 3 hours of stirring at -20 °C the reaction mixture was a solid brown and is cooled to -80 °C in an acetone and dry ice bath. Once the desired temperature had been reached the solution of I_2 was cannulated in dropwise at which point the mixture changed back to a warmer yellow. The reaction mixture was left to stir overnight, slowly coming back up to room temperature. The next day the mixture was washed with saturated aqueous solution of $Na_2S_2O_3$, then dried and solvent removed. ^{1}H NMR (500 MHz, Chloroform-d) δ = 8.61 (s, 1H), 8.27 (s, 1H), 8.03 (d, J=8.5, 1.0, 1H), 7.69 (ddd, J=8.4, 6.9, 1.4, 1H), 7.65 (d, J=8.2, 1.4, 1H), 7.48 (ddd, J=8.1, 6.9, 1.2, 1H), 1.42 (s, 9H). ^{13}C NMR (126 MHz, Chloroform-d) δ = 176.29, 148.40, 148.01, 146.52, 130.66, 128.87, 127.62, 126.56, 126.32, 85.86, 40.52, 27.75.

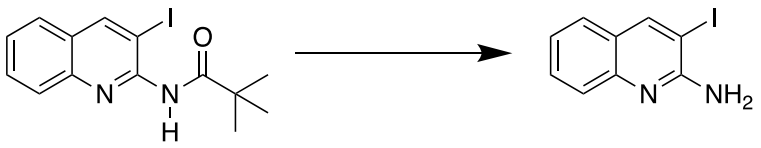

3-Iodo-2-Amino-Quinoline (2.3)

Iodoaminoquinoline (1.5 mmols, 0.55g, 1 equiv) was dissolved in a minimal amount of dioxane and set stirring in a round bottom flask. Then a solution of 4 N HCl (9.3 mmols, 2.39 mL, 6 equiv.) was added and let stir at room temperature for about an hour and a half. Then the solution was heated to reflux and left stirring overnight. The next day the reaction mixture has transitioned from a translucent pale yellow to a dark blue. The reaction mixture was then quenched with saturated aqueous solution of $NaHCO_3$ until a basic pH was reached and washed in ether with brine. Finally, the organic phase was dried with Na_2SO_4, filtered and the solvent was removed in vacuo to give a crude product. This was purified by an ethyl acetate/hexanes plug to give pure product in an 83% yield. ^1H NMR (500 MHz, Chloroform-d) δ = 8.40 (s, 1H), 7.63 (dd, J=8.5, 1.1, 1H), 7.57 (ddd, J=8.4, 6.8, 1.5, 1H), 7.52 (dd, J=8.0, 1.4, 1H), 7.25 (ddd, J=8.1, 6.8, 1.2, 1H), 5.40 (s, 2H). ^{13}C NMR (126 MHz, CDCl3) δ 155.01, 147.37, 147.25, 130.41, 126.42, 125.92, 125.21, 123.15, 80.51, 77.04, 0.03.

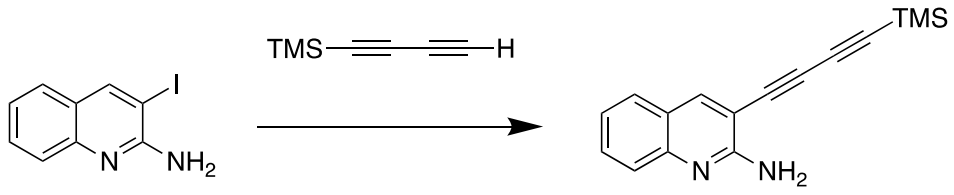

TMS Protected Diyne Quinoline (2.4)

TMS-protected buta-1,3-diyne was selectively deprotected according to known literature procedures with MeLiLiBr. Iodoaminoquinoline was dissolved in a 75 mL of a 50/50 mixture of THF and TEA and set stirring under N_2 sparging until completely outgassed. The CuI (0.02

equiv.) and $Pd(PPh_3)_2Cl_2$ (0.05 mol) were added and the solution stirred at room temperature overnight. The next day, after verifying that the reaction ran to completion by TLC, the solvent was removed *in vacuo* and the product purified by column chromatography on silica gel with EtOAc and hexanes. ^1H NMR (500 MHz, Chloroform-d) δ = 8.07 (s, 1H), 7.60 (dt, J=8.8, 1.0, 1H), 7.56 (dtd, J=8.8, 3.7, 3.2, 1.5, 2H), 7.26 – 7.22 (m, 1H), 5.39 (s, 2H), 0.26 (s, 10H). ^{13}C NMR (126 MHz, Chloroform-d) δ = 156.86, 147.40, 142.69, 1313C NMR (126 MHz, Chloroform-d) δ = 156.86, 147.40, 142.69, 131.35, 127.58, 126.05, 123.36, 122.97, 104.74, 93.49, 87.32, 80.30, 72.02, -0.33.1.35, 127.58, 126.05, 123.36, 122.97, 104.74, 93.49, 87.32, 80.30, 72.02, -0.33.

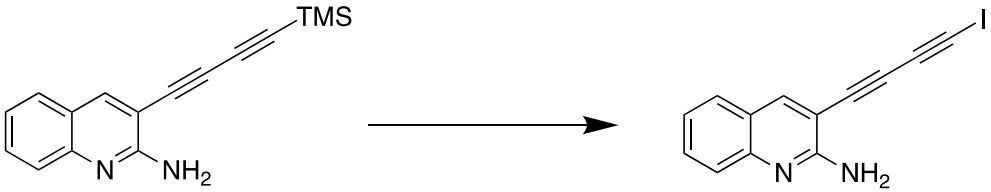

Iodo Diyne Quinoline (2.5)

The diyne quinoline (1.00 equiv) was dissolved in ACN and set stirring under N_2 to outgas. The round bottom flask was then wrapped in aluminum foil, to ensure dark conditions, and AgF (1.00 equiv.) was added and let stir for 20 minutes. After 20 minutes NIS (1.20 equiv.) was added, and the reaction was monitored by TLC until done. Upon the disappearance of all starting material the reaction was rotovapped down and then washed in water and EtOAc three times before drying over Na_2SO_4 and removing the solvent to yield the product as a brown solid. This product was collected and used as is for the next step without further purification.

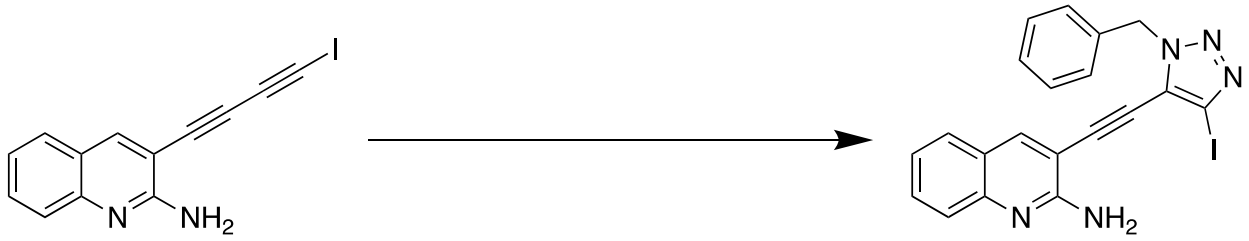

Cyclized Quinoline (2.6^{Bn})

The iodo-diyne (1 equiv.) was dissolved in a minimal amount of DMF and set stirring under N_2. Following outgassing lutidine (4 mol%), the azide (1 equiv.), and $CuI(PPh_3)_3$ (10 mol%) are added. These are left stirring at room temperature overnight. After completion the reaction mixture was diluted with EtOAc and washed with a saturated aqueous solution of NH_4Cl three times. The organic layer was then dried with Na_2SO_4 and concentrated under reduced pressure to yield the crude product as an oil. This was purified by column chromatography over silica gel using a EtOAc and Hexanes mixture (3:1) to yield the product.

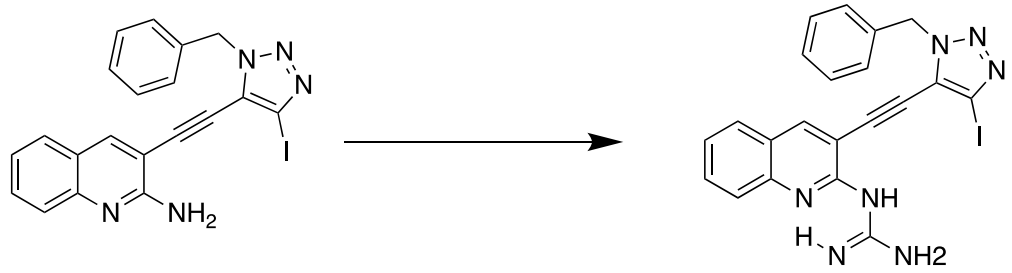

Quinoline Host Receptor (2^{Bn})

The newly cyclized compound (0.0429 g, 0.0951 mmol) was dissolved in a minimal amount of a 50/50 mixture of water and 1,4 dioxane and set stirring. Cyanamide (0.0048 g, 0.1141 mmol) and $Sc(OTf)_3$ catalyst (0.0047g, 0.0095 mmol) were added to the reaction. This was then heated to 100 °C and left stirring for 2 days. The crude mixture was then taken up in EtOAc and washed with a saturated solution of $NaCO_3H$, to crash the product out as its carbonate salt analog. While

the final product was never able to be isolated alone its existence in the crude reaction mixture was confirmed by mass spec. HRMS (TOF-MS-ES+) for $C_{21}H_{16}IN_7$ [M+H] +: calcd 493.05, found 493.0512.

NMRs

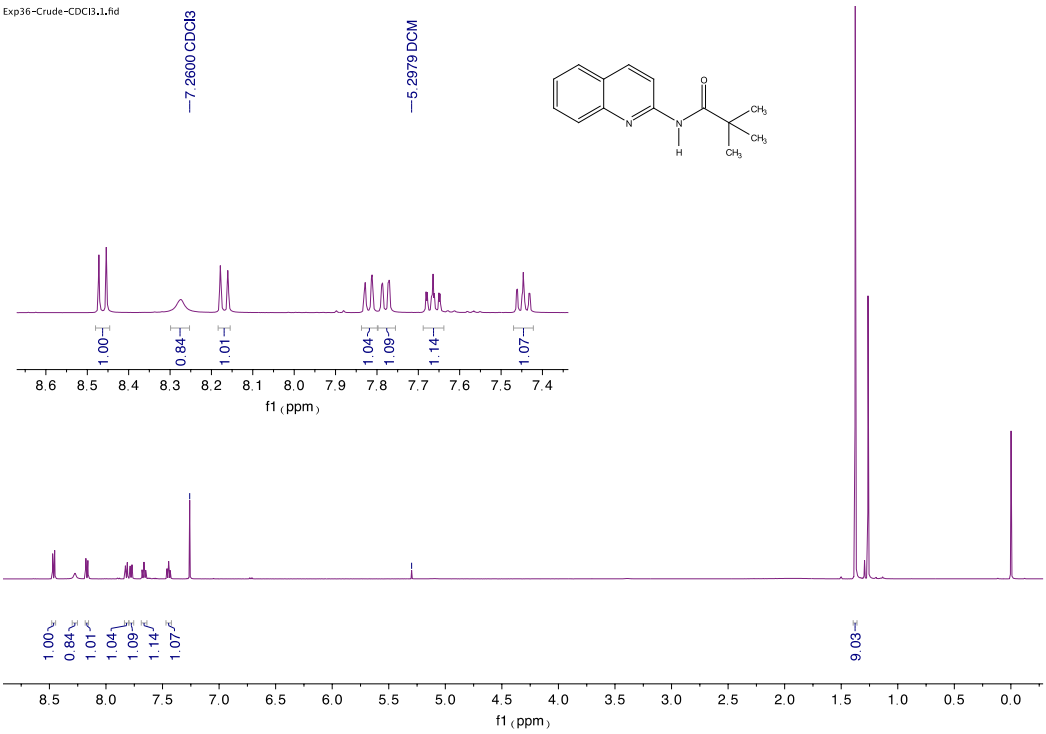

Figure D.1. ^{1}H NMR spectrum of **protected quinoline**

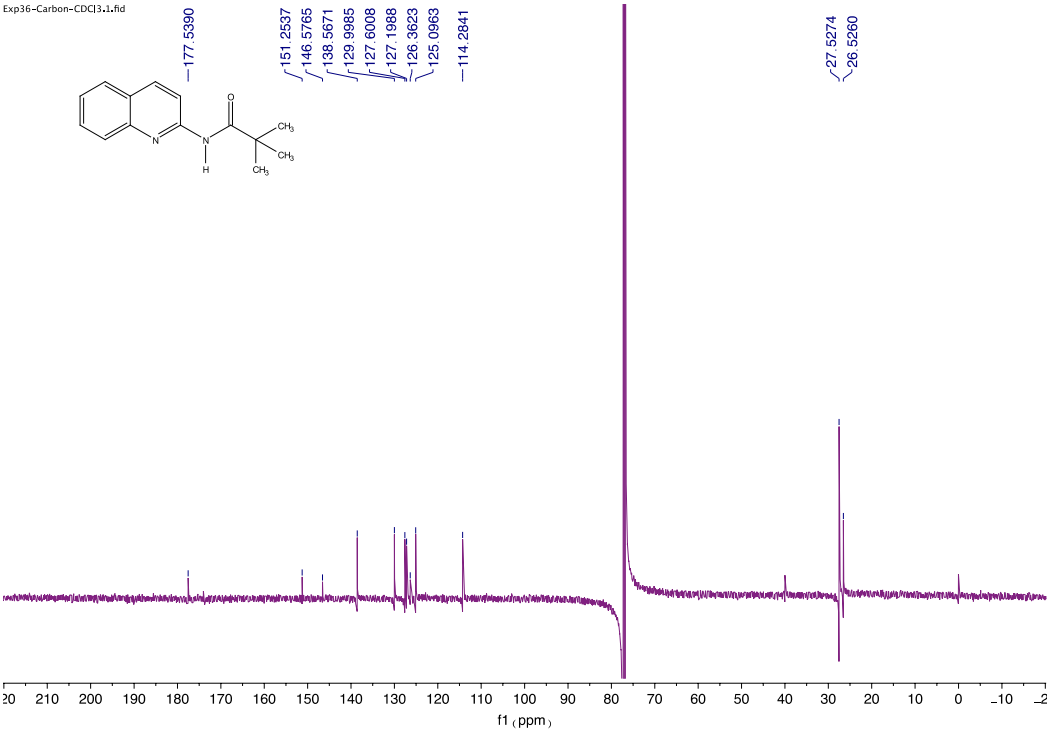

Figure D.2. ^{13}C NMR spectrum of **protected quinoline**

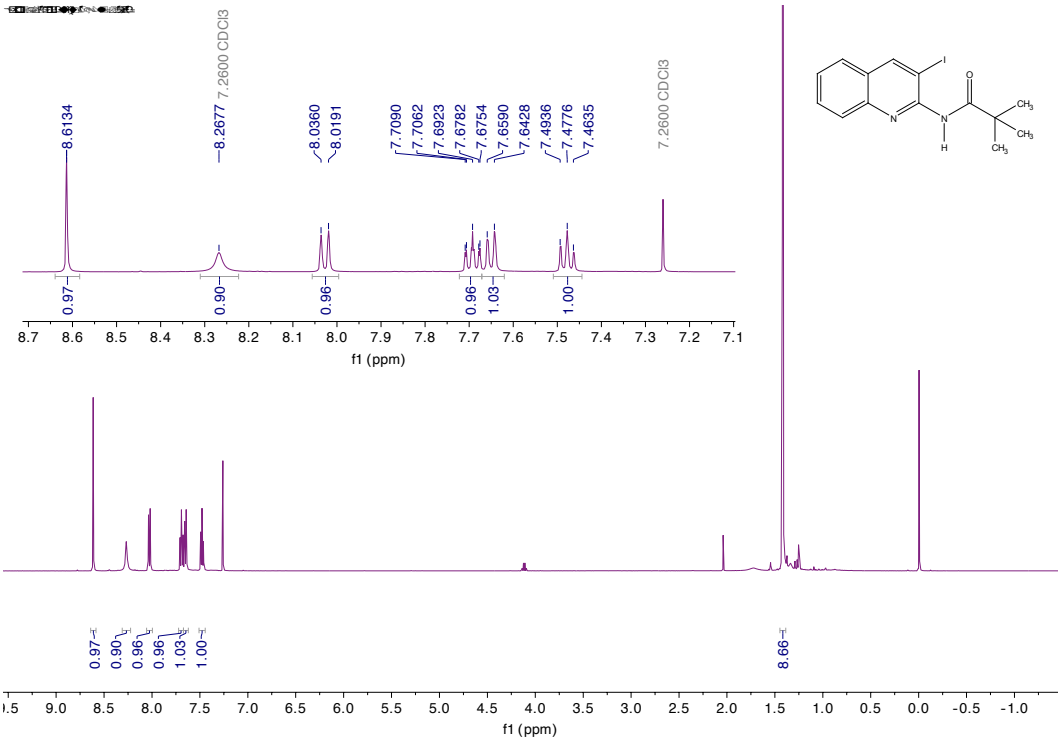

Figure D.3. ^{1}H NMR spectrum of **protected iodo-quinoline**

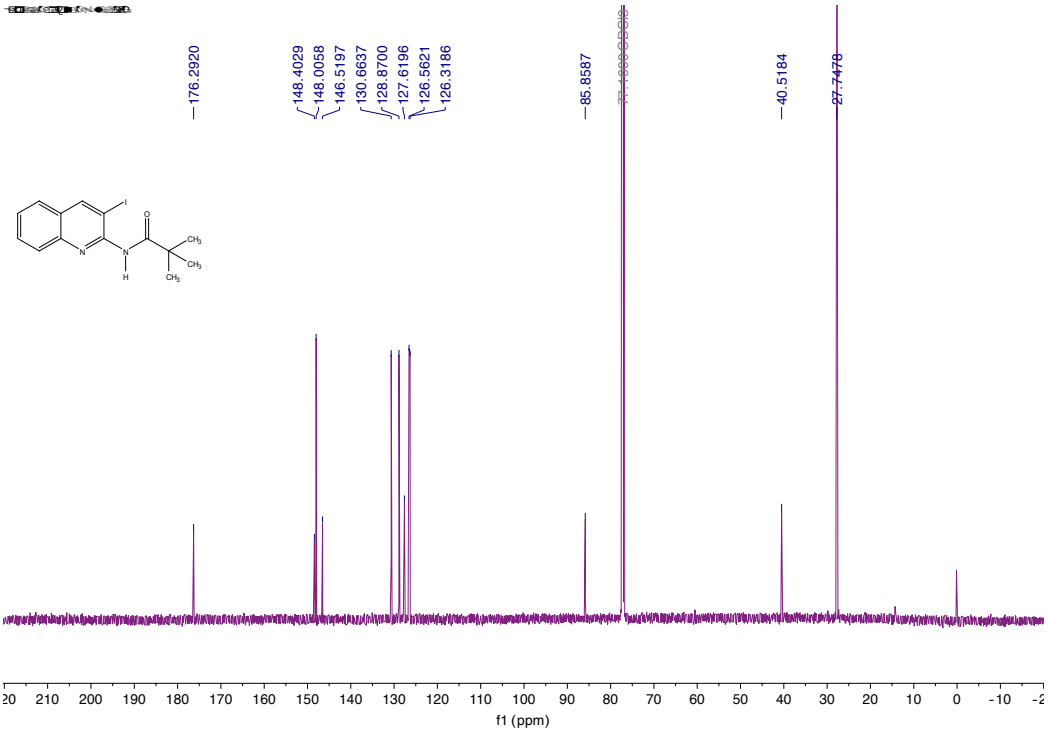

Figure D.4. ^{13}C NMR spectrum of **protected iodo-quinoline**

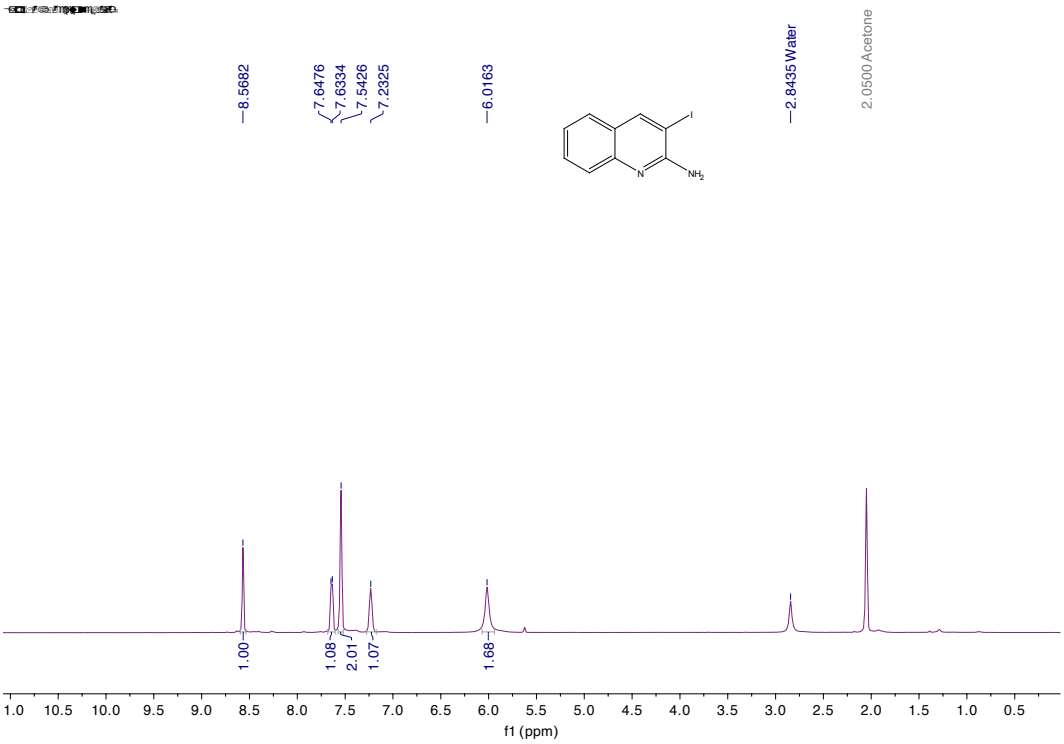

Figure D.5. ^{1}H NMR spectrum of **3-Iodo-2-Amino-Quinoline**

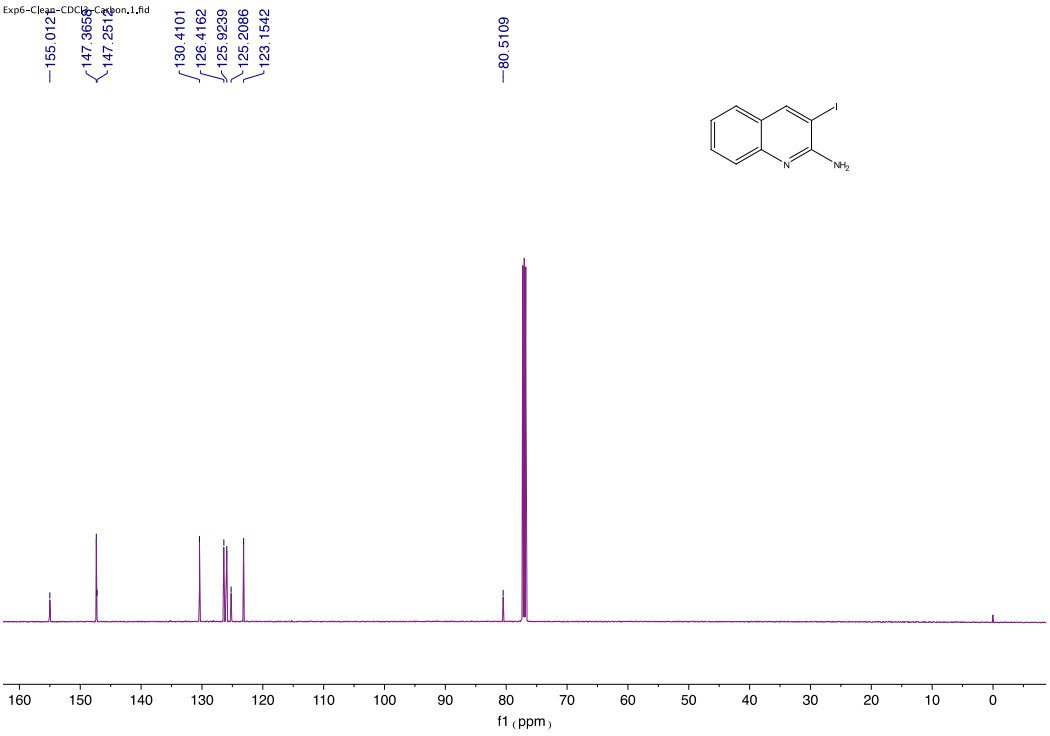

Figure D.6. ^{13}C NMR spectrum of **3-Iodo-2-Amino-Quinoline**

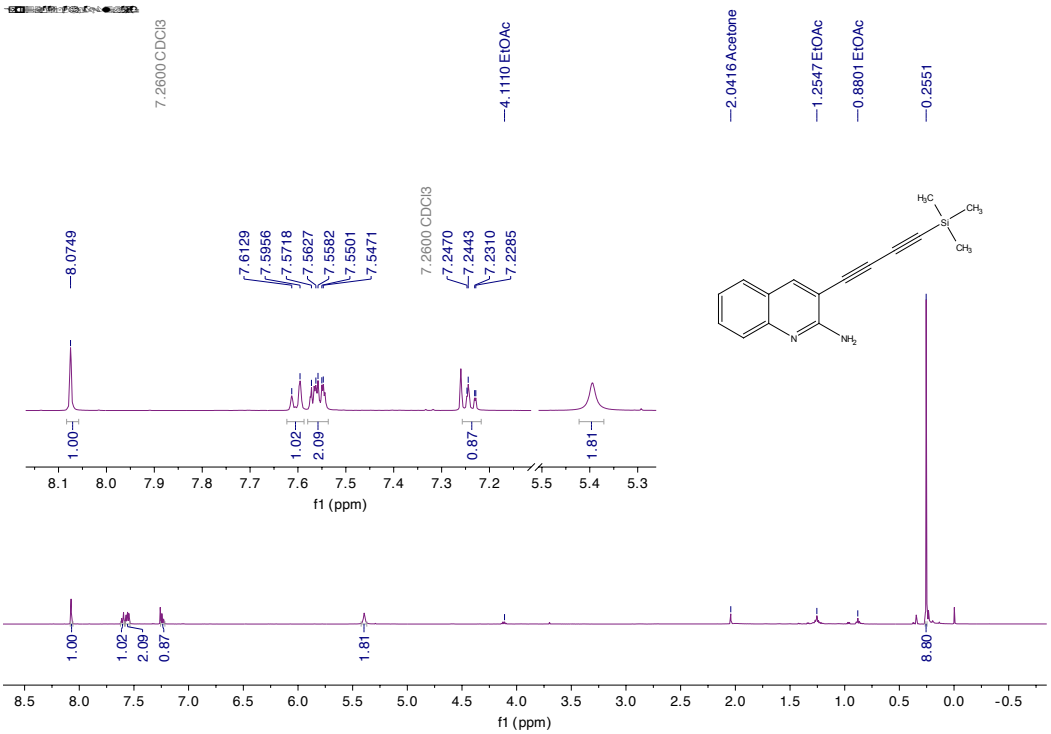

Figure D.7. ^{1}H NMR spectrum of **TMS protected diyne quinoline**

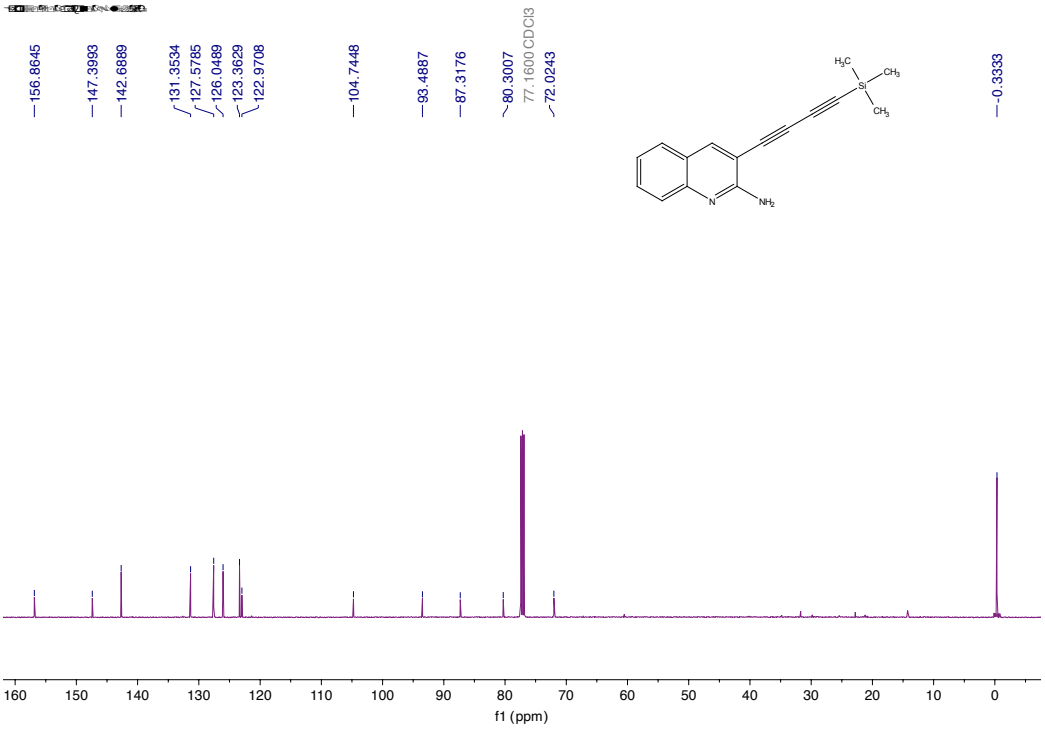

Figure D.8. ^{13}C NMR spectrum of **TMS protected diyne quinoline**

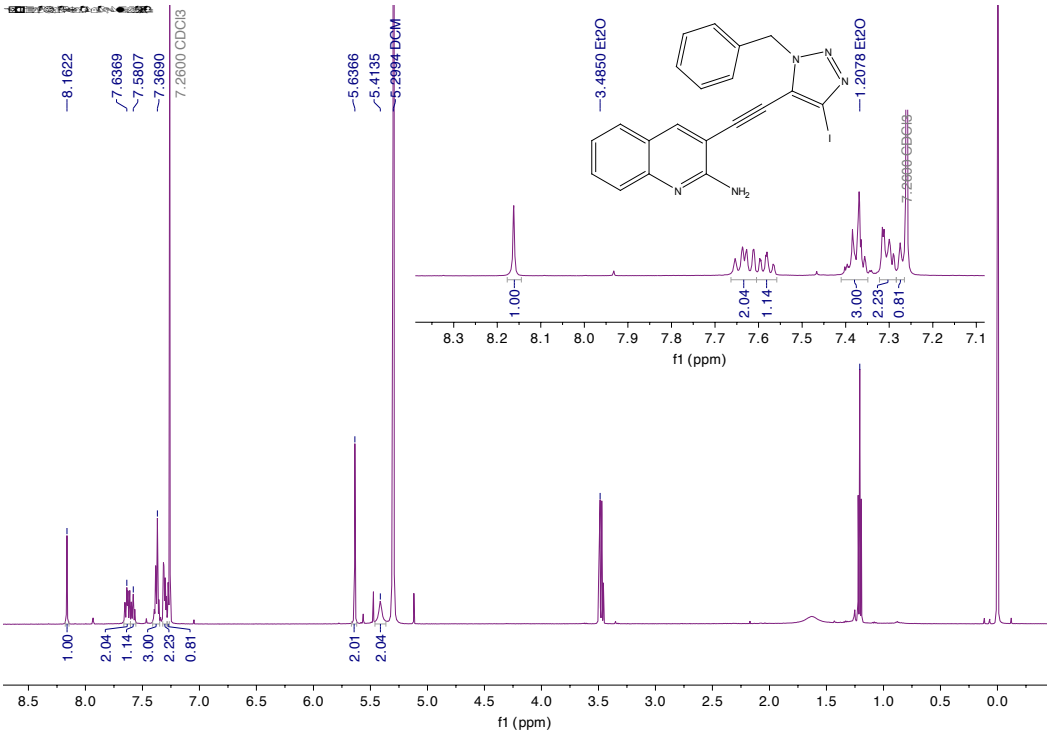

Figure D.9. [1]H NMR spectrum of **cyclized quinoline**

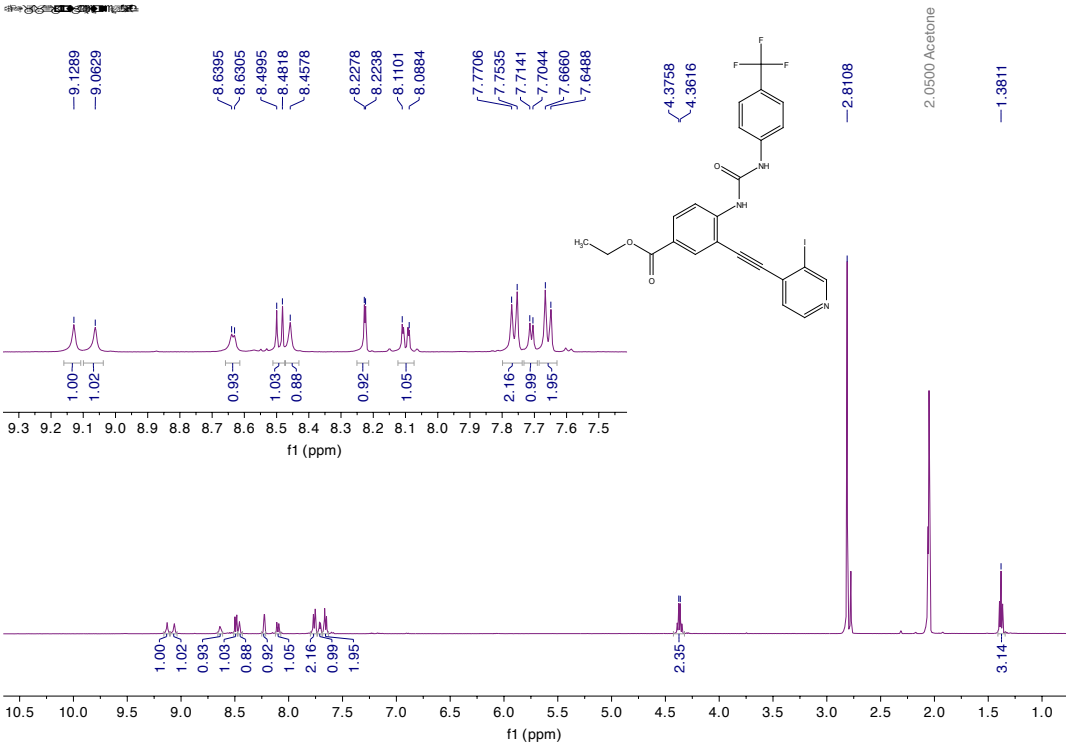

Figure D.10. [1]H NMR spectrum of **precursor 1.5**

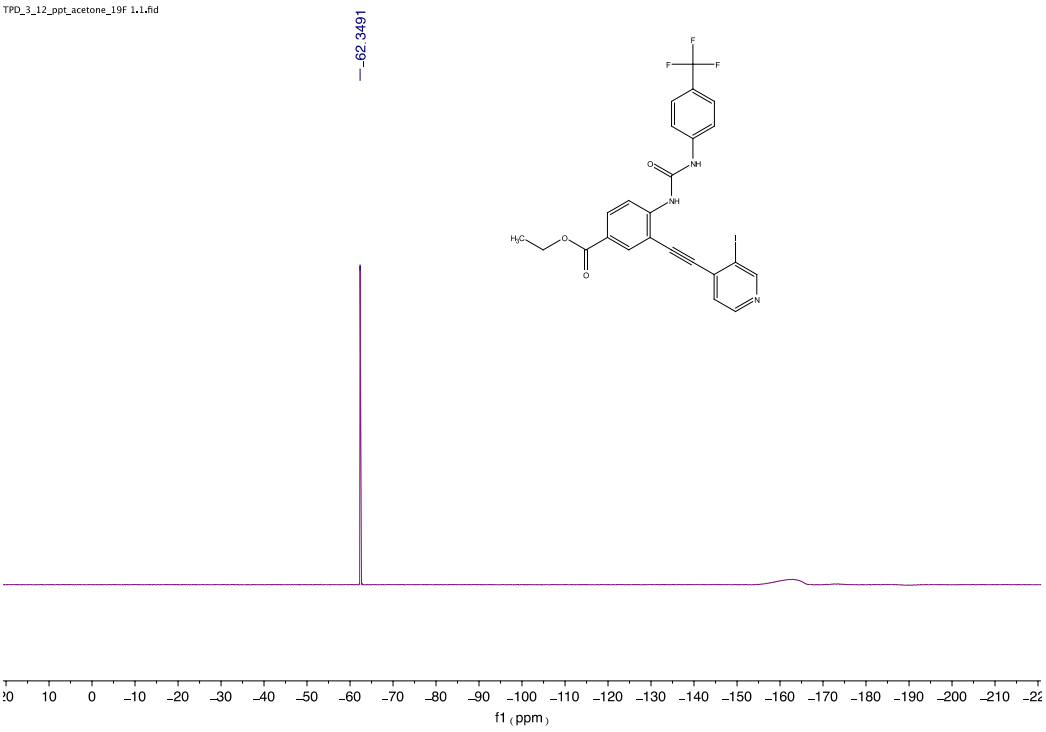

Figure D.11. ^{19}F NMR spectrum of **precursor 1.5**

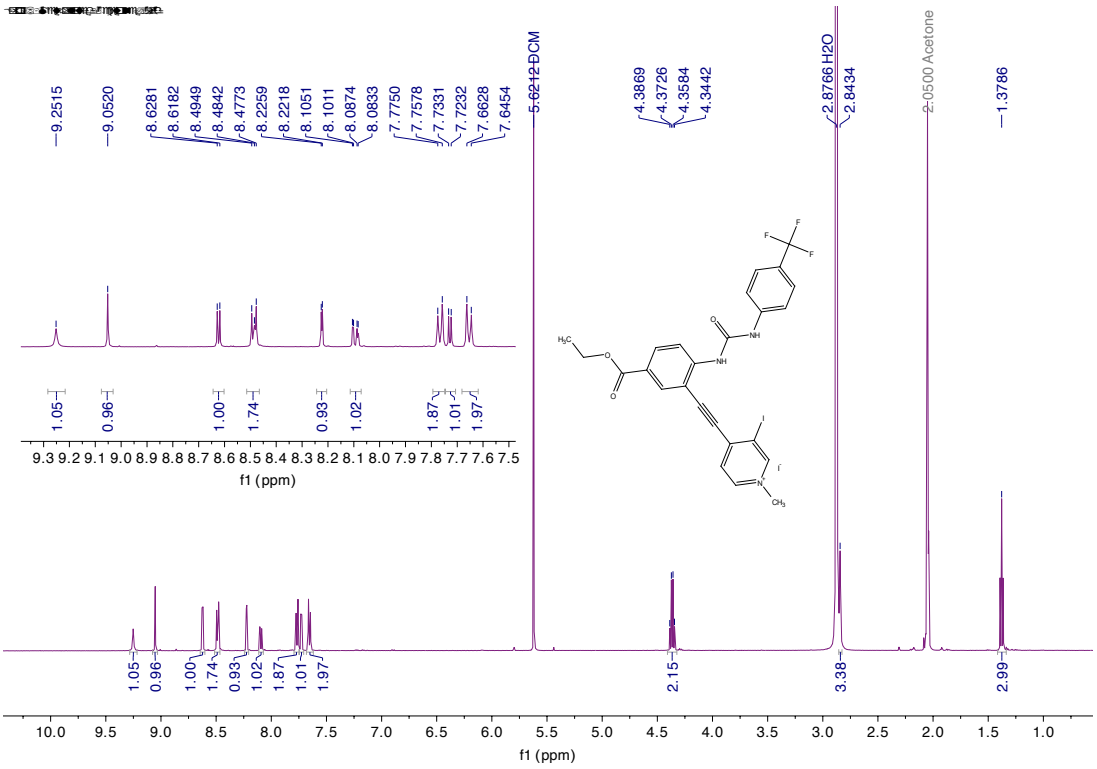

Figure D.12. ^{1}H NMR spectrum of **precursor 1.6**

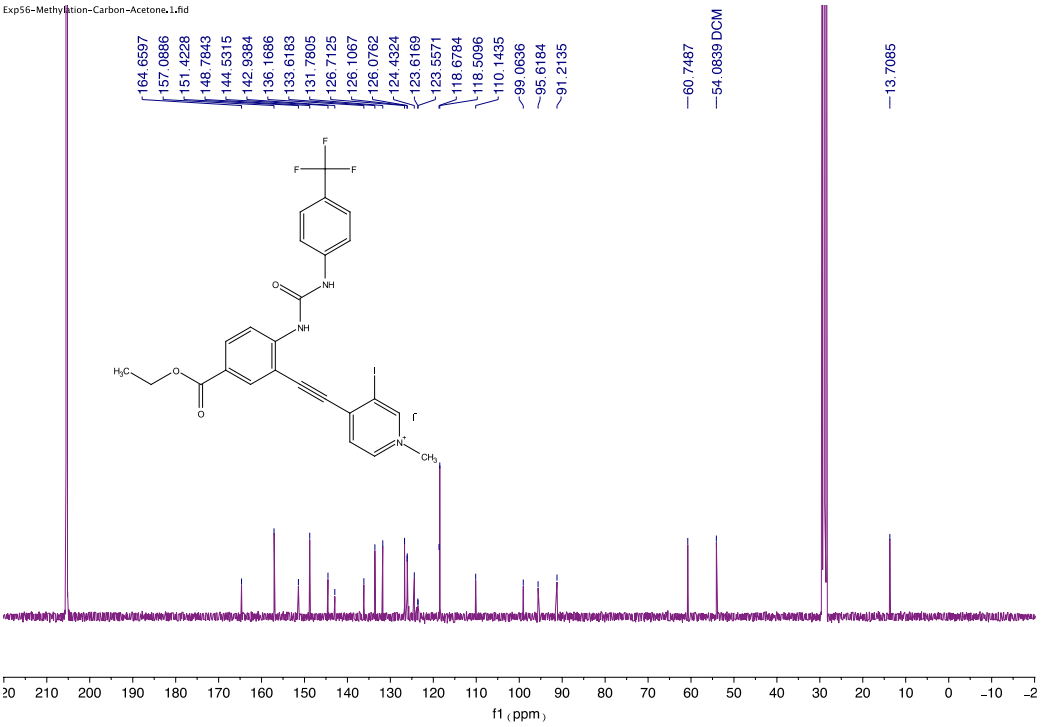

Figure D.13. ^{13}C NMR spectrum of **precursor 1.6**

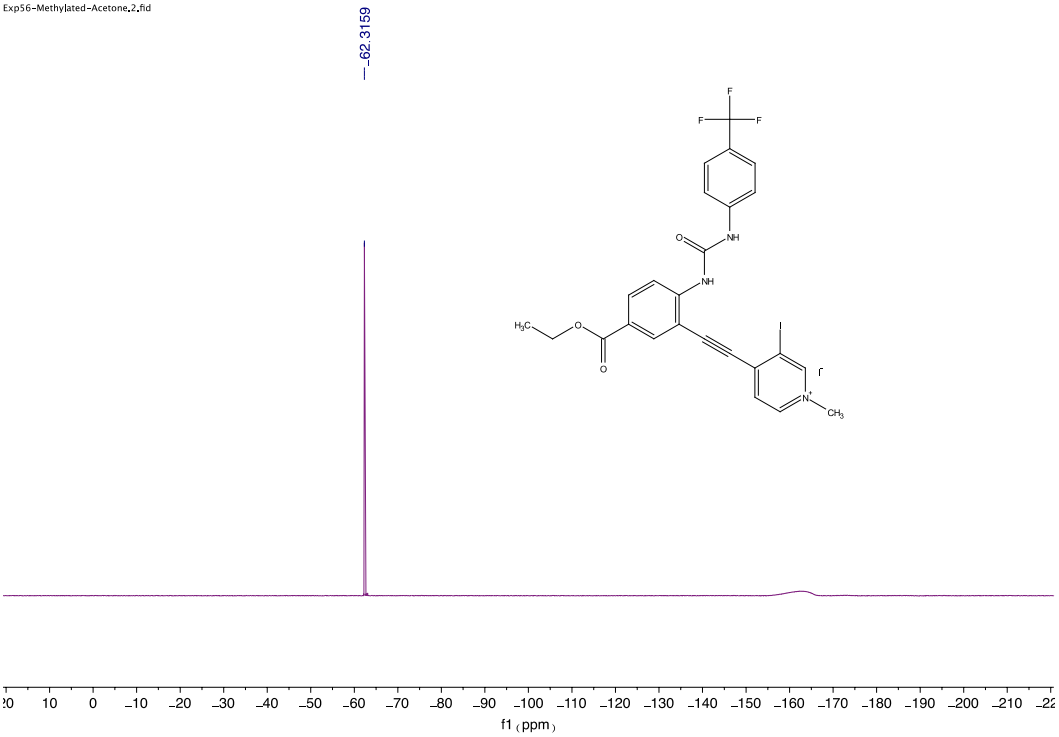

Figure D.14. ^{19}F NMR spectrum of **precursor 1.6**

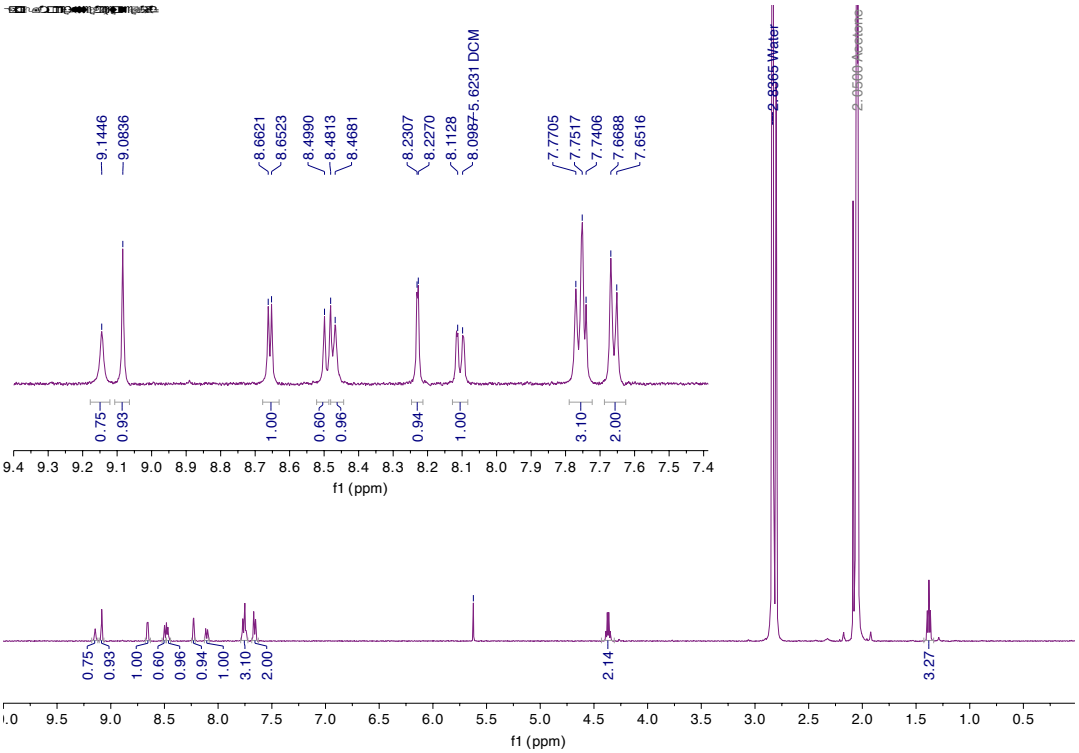

Figure D.15. ^{1}H NMR spectrum of **Host Receptor 1^{PF6}**

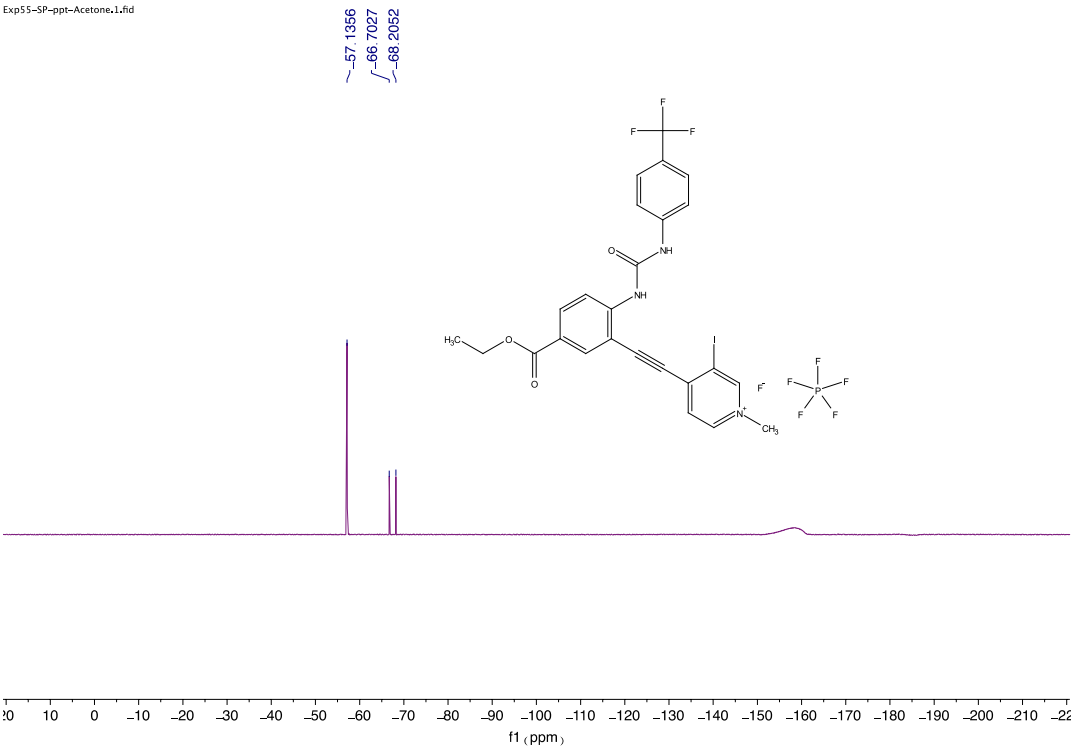

Figure D.16. ^{19}F NMR spectrum of **Host Receptor 1^{PF6}**

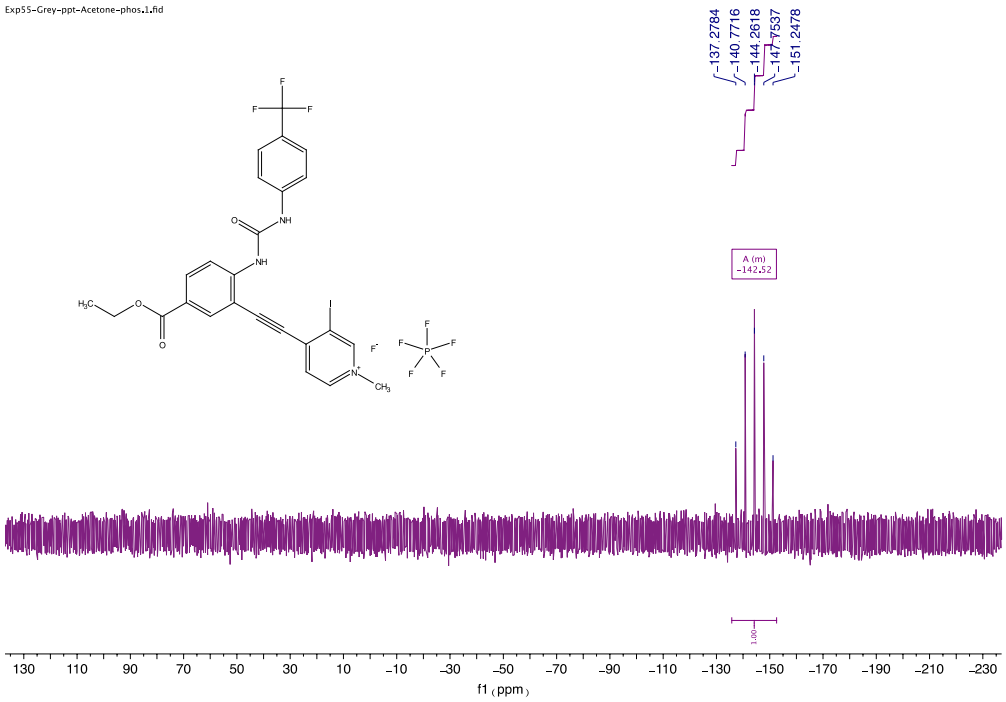

Figure D.17. ^{31}P NMR spectrum of **Host Receptor 1^{PF6}**

^{1}H NMR Titrations.

General Methods. ^{1}H NMR spectra were acquired at room temperature on a Varian Inova 500 MHz spectrometer (^{1}H: 500.11 MHz). ^{1}H chemical shifts (δ) are expressed in ppm relative to residual CH3CN (^{1}H: 1.94 ppm) shifts. A solution of host in 10% DMSO-*d6*/CD_3CN (0.73-1.9 mM) was prep in 3 or 4 mL volumetric flasks. 500 μL of this host solution was added to a septum-sealed NMR tube. The remaining host solution was used to prepare a host/guest (NBu_4Cl, NBu_4Br, or NBu_4I) stock solution in 2 or 3 mL volumetric flasks, respectively. Aliquots of the host/guest solution were incrementally added to the NMR tube using gas-tight Hamilton syringes, and ^{1}H NMR spectra were recorded, at 25 °C, after each addition of guest. The Δδ of the NH protons were tracked to follow the progress of the titration and association constants were determined using Thordarson's Bindfit software.

Table D.1. Representative titration of receptor **1** with Cl^- in 10% DMSO-*d6*/CD_3CN.

Entry	V_{Guest} (μL)	[Guest] (M)	[Host] (M)	Equiv. Anion	δ1 (ppm)	δ2 (ppm)
0	0	0	0.000946816	0.00	9.66250	8.515
1	5	0.000275384	0.000946816	0.29	9.70870	8.531
2	5	0.000545368	0.000946816	0.58	9.87850	8.5806
3	10	0.00106976	0.000946816	1.13	10.28150	8.8036
4	10	0.001574364	0.000946816	1.66	10.56070	8.933
5	10	0.002060278	0.000946816	2.18	10.77210	9.0358
6	15	0.002756318	0.000946816	2.91	10.99810	9.1398
7	15	0.003415725	0.000946816	3.61	11.15700	9.2183
8	15	0.004041315	0.000946816	4.27	11.27180	9.2709
9	20	0.004827181	0.000946816	5.10	11.38460	9.3212
10	20	0.005562752	0.000946816	5.88	11.47290	9.3645
11	20	0.006252706	0.000946816	6.60	11.53340	9.3942
12	30	0.007210975	0.000946816	7.62	11.60970	9.4305
13	50	0.008631856	0.000946816	9.12	11.68670	9.4651
14	100	0.010956936	0.000946816	11.57	11.78640	9.5129
15	200	0.014246072	0.000946816	15.05	11.87130	9.5539
16	500	0.018694494	0.000946816	19.74	11.92860	9.5814
17	500	0.020946164	0.000946816	22.12	11.9434	9.5876

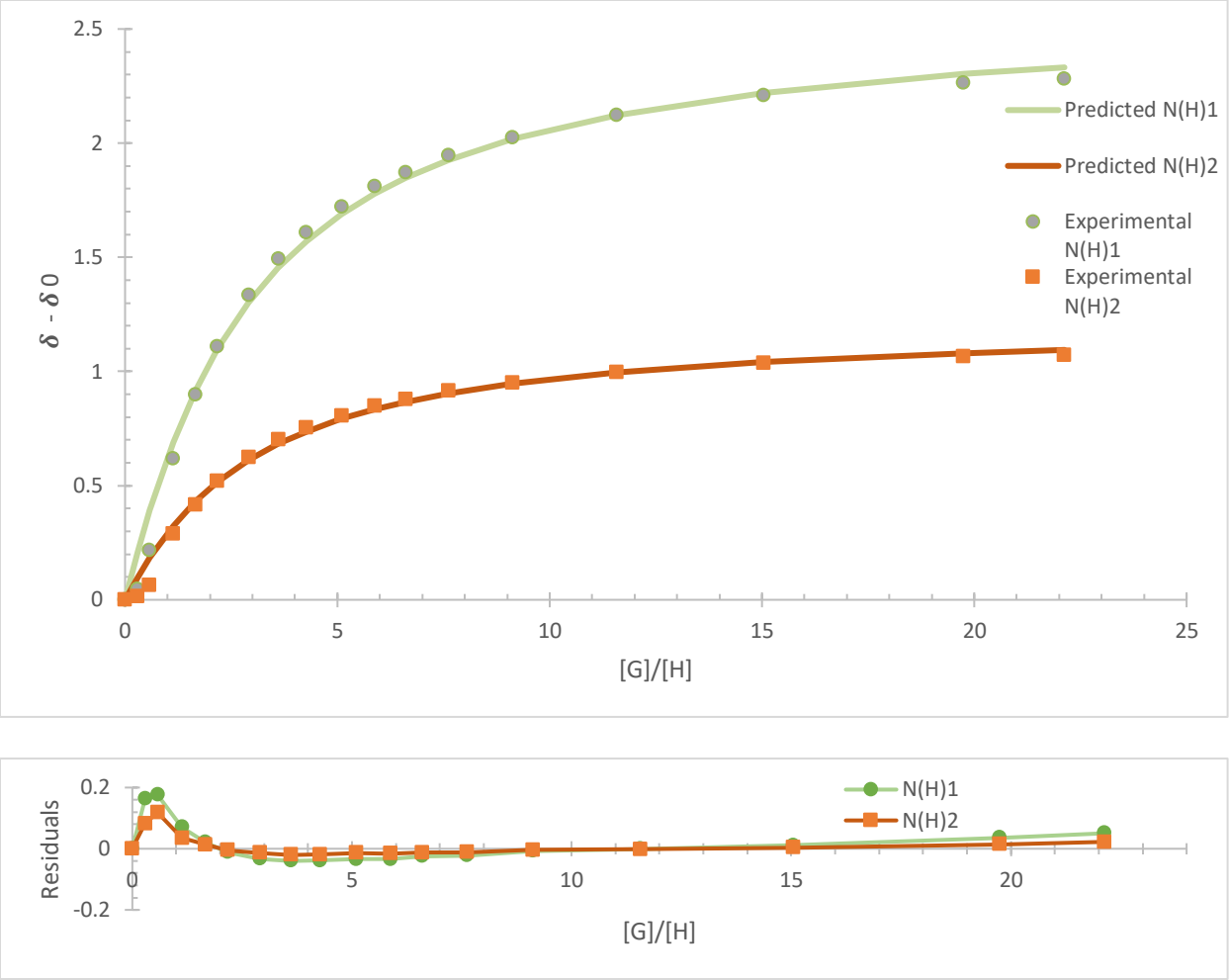

Figure D.19. Representative binding isotherm for Cl^- titration of receptor **1** in 10% DMSO-*d6*/CD_3CN as determined by ^1H NMR spectroscopy.

Table D.2. Representative titration of receptor **1** with Br^- in 10% DMSO-*d6*/CD_3CN.

Entry	Vguest (μL)	[Guest] (M)	[Host] (M)	Equiv. Anion	δ1 (ppm_	δ2 (ppm)
Host Alone	0	0	0.00132554	0	9.66550	8.51620
1	2.5	0.00024569	0.00132554	0.19	9.66700	8.51720
2	2.5	0.00048896	0.00132554	0.37	9.68070	8.52180
3	5	0.00096832	0.00132554	0.73	9.70790	8.53520
4	5	0.00143839	0.00132554	1.09	9.76420	8.56010
5	10	0.00235165	0.00132554	1.77	9.85890	8.60300
6	10	0.00323077	0.00132554	2.44	9.93740	8.63740

7	10	0.00407762	0.00132554	3.08	10.00420	8.66780
8	10	0.00489396	0.00132554	3.69	10.06420	8.69550
9	15	0.00606477	0.00132554	4.58	File Corrupted	
10	15	0.00717553	0.00132554	5.41	10.20370	8.75910
11	15	0.00823076	0.00132554	6.21	10.25520	8.78090
12	20	0.0095583	0.00132554	7.21	10.31050	8.80530
13	30	0.01139644	0.00132554	8.60	10.38580	8.83800
14	50	0.01410987	0.00132554	10.64	10.47160	8.87870
15	100	0.01851921	0.00132554	13.97	10.58820	8.92280
16	200	0.02469228	0.00132554	18.63	10.70940	8.98500
17	300	0.03039049	0.00132554	22.93	10.79140	9.02320
18	500	0.03566662	0.00132554	26.91	10.84980	9.04790
19	500	0.03864878	0.00132554	29.16	10.86270	9.05340

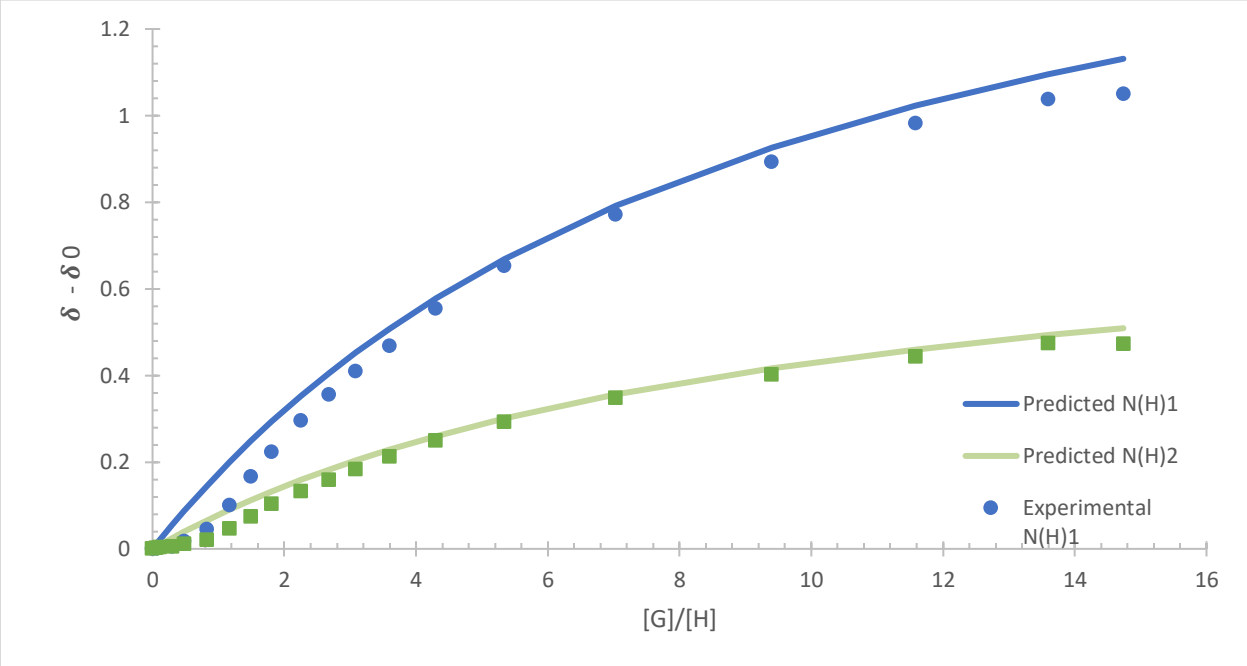

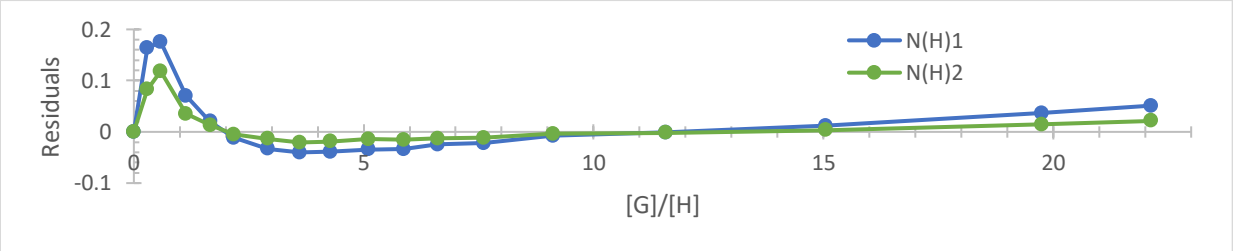

Figure D.20. Representative binding isotherm for Br^- titration of receptor **1** in 10% DMSO-*d6*/CD_3CN as determined by ^1H NMR spectroscopy.

Table D.3. Representative titration of receptor **1** with I^- in 10% DMSO-*d6*/CD_3CN.

Entry	Vguest (μL)	[Guest] (M)	[Host] (M)	Equiv. Anion	δ1 (ppm_	δ2 (ppm)
Host Alone	0	0	0.0010415	0	9.6622	8.5159
1	5	0.00025483	0.0010415	0.24467354	9.6641	8.517
2	5	0.00050466	0.0010415	0.48454956	9.6884	8.5273
3	10	0.0009899	0.0010415	0.95046259	9.6947	8.5326
4	10	0.00145684	0.0010415	1.398794	9.7042	8.5358
5	10	0.00190648	0.0010415	1.83052055	9.7095	8.5385
6	15	0.00255056	0.0010415	2.44893965	9.7131	8.5405
7	15	0.00316075	0.0010415	3.03481038	9.7168	8.5418
8	15	0.00373964	0.0010415	3.59063646	9.7211	8.544
9	20	0.00446684	0.0010415	4.28886426	9.7292	8.547
10	20	0.0051475	0.0010415	4.94240548	9.7317	8.5472
11	20	0.00578595	0.0010415	5.55541701	9.7327	8.5487
12	30	0.00667269	0.0010415	6.40682192	9.738	8.5506
13	50	0.00798751	0.0010415	7.66924988	9.7437	8.5537
14	100	0.01013902	0.0010415	9.73504109	9.755	8.5587
15	200	0.01318263	0.0010415	12.6573799	9.7683	8.5667
16	500	0.01729899	0.0010415	16.6097233	9.7885	8.5841
17	500	0.01938257	0.0010415	18.6102922	9.7969	8.5769
18	500	0.02064098	0.0010415	19.8185566	9.8006	8.5802

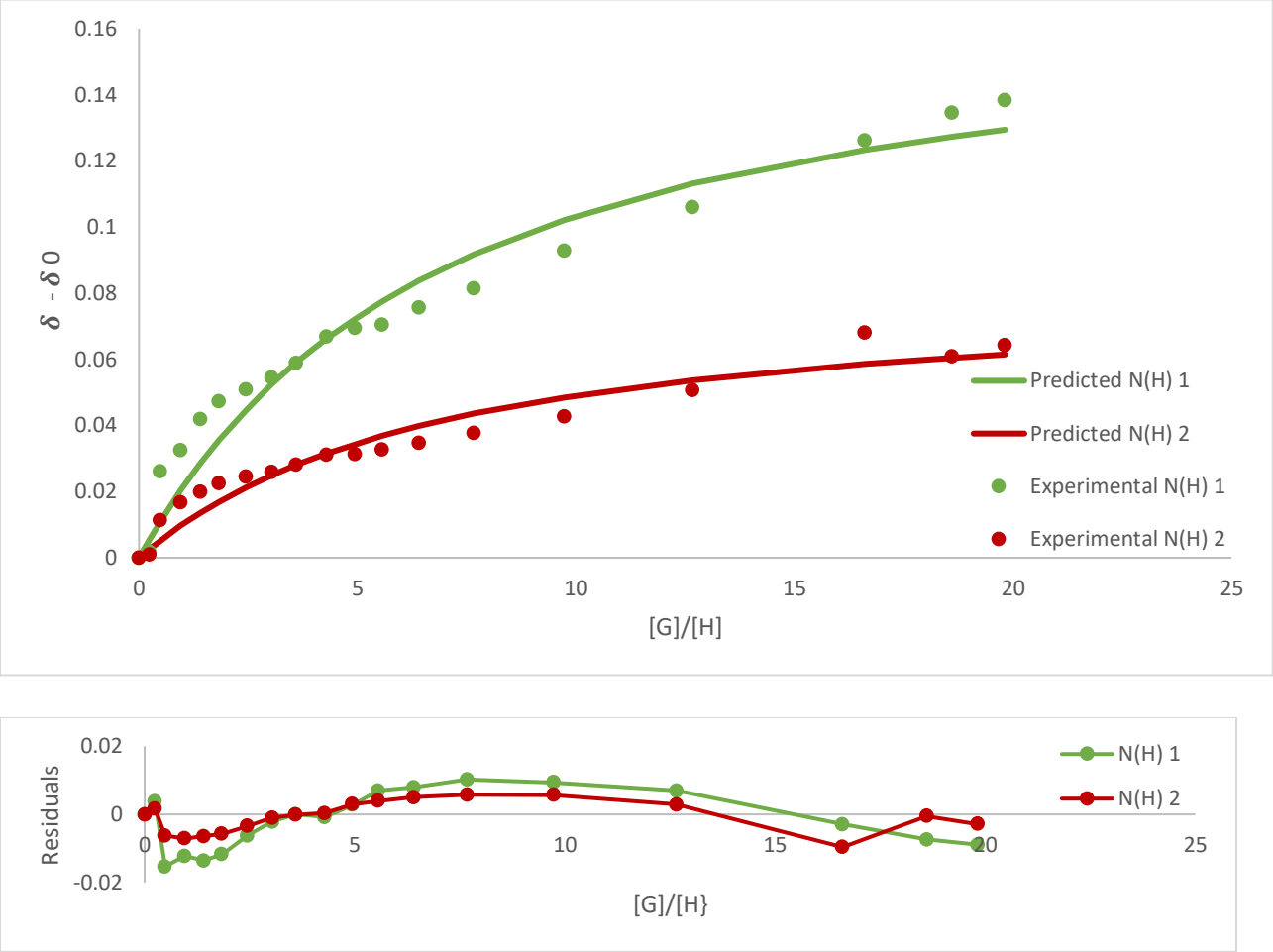

Figure D.21. Representative binding isotherm for I^- titration of receptor **1** in 10% DMSO-*d6*/CD_3CN as determined by ^1H NMR spectroscopy.

REFERENCES

Chapter 1:

(1) Sessler, J. L.; Gale, P. A.; Cho, W.-S. *Anion Receptor Chemistry*; Royal Society of Chemistry: Cambridge, 2006.

(2) Zyryanov, G. V; Palacios, M. A.; Anzenbacher Jr., P. Rational Design of a Fluorescence-Turn-On Sensor Array for Phosphates in Blood Serum Zuschriften. *Angew. Chemie* **2007**, *119*, 7995–7998.

(3) Hruska, K. A.; Mathew, S.; Lund, R.; Qiu, P.; Pratt, R. Hyperphosphatemia of Chronic Kidney Disease. *Kidney Int.* **2008**, *74* (2), 148–157.

(4) Schmidt, R. F.; Thews, G. *Human Physiology*, 2nd ed.; Springer: Berlin, 1989.

(5) Kanbay, M.; Goldsmith, D.; Akcay, A.; Covic, A. Phosphate - The Silent Stealthy Cardiorenal Culprit in All Stages of Chronic Kidney Disease: A Systematic Review. *Blood Purif.* **2009**, *27* (2), 220–230.

(6) Feng, H.; Wang, Y.; Jia, H.; Zhang, R.; Han, Q.; Meng, Q.; Zhiqiang, Z. Selective Detection of Inorganic Phosphates in Live Cells Based on a Responsive Fluorescence Probe. *New J. Chem.* **2017**, *41*, 9623–9630.

(7) Scott, C. C.; Gruenberg, J. Ion Flux and the Function of Endosomes and Lysosomes: PH Is Just the Start: The Flux of Ions across Endosomal Membranes Influences Endosome Function Not Only through Regulation of the Luminal PH. *BioEssays* **2011**, *33* (2), 103–110.

(8) Jentsch, T. J.; Stein, V.; Weinreich, F.; Zdebik, A. A. Molecular Structure and Physiological Function of Chloride Channels. *Physiol. Rev.* **2002**, *82* (2), 503–568.

(9) Berend, K.; Van Hulsteijn, L. H.; Gans, R. O. B. Chloride: The Queen of Electrolytes? *Eur. J. Intern. Med.* **2012**, *23* (3), 203–211.

(10) Beck, A.; Ernst, M. Kinetic Modeling and Selectivity of Anion Exchange in Donnan Dialysis. *J. Memb. Sci.* **2015**, *479*, 132–140.

(11) Matsuyama, K.; Sen, A. C.; Perrin, J. H. The Effects of PH, Calcium and Chloride Ions on the Binding of Tolmetin to Human Serum Albumin: Circular Dichroic, Dialysis and Fluorometric Measurements. *J. Pharm. Pharmacol.* **1987**, *39* (3), 190–195.

(12) Scanziani, M.; Häusser, M. Electrophysiology in the Age of Light. *Nature* **2009**, *461* (7266), 930–939.

(13) Saunders, J. H. Liquid and Solid-State Cl- -Sensitive Microelectrodes. Characteristics and Application to Intracellular Cl- Activity in Balanus Photoreceptor. *J. Gen. Physiol.* **1977**, *70* (4), 507–530.

(14) Nagai, T.; Ibata, K.; Park, E. S.; Kubota, M.; Mikoshiba, K.; Miyawaki, A. A Variant of Yellow Fluorescent Protein with Fast and Efficient Maturation for Cell-Biological Applications. *Nat. Biotechnol.* **2002**, *20*, 87–90.

(15) Tutol, J. N.; Peng, W.; Dodani, S. C. Discovery and Characterization of a Naturally Occurring, Turn-On Yellow Fluorescent Protein Sensor for Chloride. *Biochemistry* **2019**, *58* (1), 31–35.

(16) Yoon, D. W.; Gross, D. E.; Lynch, V. M.; Lee, C. H.; Bennett, P. C.; Sessler, J. L. Real-Time Determination of Chloride Anion Concentration in Aqueous-DMSO Using a Pyrrole-Strapped Calixpyrrole Anion Receptor. *Chem. Commun.* **2009**, No. 9, 1109–1111.

(17) Langton, M. J.; Serpell, C. J.; Beer, P. D. Anion Recognition in Water: Recent Advances from a Supramolecular and Macromolecular Perspective. *Angew. Chemie - Int. Ed.* **2016**, *55* (6), 1974–1987.

(18) Yu, X. H.; Hong, X. Q.; Mao, Q. C.; Chen, W. H. Biological Effects and Activity Optimization of Small-Molecule, Drug-like Synthetic Anion Transporters. *Eur. J. Med. Chem.* **2019**, *184*, 111782.

(19) Liu, Y.; Zhao, W.; Chen, C.-H.; Flood, A. H. Chloride Capture Using a C–H Hydrogen-Bonding Cage. *Science (80-.).* **2019**, *365*, 159–161.

(20) Tutol, J. N.; Lee, J.; Chi, H.; Faizuddin, F. N.; Abeyrathna, S. S.; Zhou, Q.; Morcos, F.; Meloni, G.; Dodani, S. C. A Single Point Mutation Converts a Proton-Pumping Rhodopsin into a Red-Shifted, Turn-on Fluorescent Sensor for Chloride. *Chem. Sci.* **2021**, *12*, 5655–5663.

(21) Watt, M. M.; Engle, J. M.; Fairley, K. C.; Robitshek, T. E.; Haley, M. M.; Johnson, D. W. "Off-on" Aggregation-Based Fluorescent Sensor for the Detection of Chloride in Water. *Org. Biomol. Chem.* **2015**, *13* (14), 4266–4270.

(22) Khatua, S.; Choi, S. H.; Lee, J.; Kim, K.; Do, Y.; Churchill, D. G. Aqueous Fluorometric and Colorimetric Sensing of Phosphate Ions by a Fluorescent Dinuclear Zinc Complex. *Inorg. Chem.* **2009**, *48* (7), 2993–2999.

(23) Zhang, Y. M.; Lin, Q.; Wei, T. B.; Wang, D. D.; Yao, H.; Wang, Y. L. Simple Colorimetric Sensors with High Selectivity for Acetate and Chloride in Aqueous Solution. *Sensors Actuators, B Chem.* **2009**, *137* (2), 447–455.

(24) Bazany-Rodríguez, I. J.; Martínez-Otero, D.; Barroso-Flores, J.; Yatsimirsky, A. K.; Dorazco-González, A. Sensitive Water-Soluble Fluorescent Chemosensor for Chloride Based on a Bisquinolinium Pyridine-Dicarboxamide Compound. *Sensors Actuators, B Chem.* **2015**, *221*, 1348–1355.

(25) Huang, X. H.; Lu, Y.; He, Y. B.; Chen, Z. H. A Metal-Macrocycle Complex as a Fluorescent Sensor for Biological Phosphate Ions in Aqueous Solution. *European J. Org. Chem.* **2010**, No. 10, 1921–1927.

(26) Martí, I.; Bolte, M.; Burguete, M. I.; Vicent, C.; Alfonso, I.; Luis, S. V. Tight and Selective Caging of Chloride Ions by a Pseudopeptidic Host. *Chem. - A Eur. J.* **2014**, *20* (24), 7458–7464.

(27) Kim, D. S.; Lynch, V. M.; Nielsen, K. A.; Johnsen, C.; Jeppesen, J. O.; Sessler, J. L. A Chloride-Anion Insensitive Colorimetric Chemosensor for Trinitrobenzene and Picric Acid. *Anal. Bioanal. Chem.* **2009**, *395* (2), 393–400.

(28) Buhlmann, P.; Nishizawa, S.; Xiao, K. P.; Umezawa, Y. Strong Hydrogen Bond-Mediated Complexation of H2PO4- by Neutral Bis-Thiourea Hosts. *Tetrahedron* **1997**, *53* (5), 1647–1654.

(29) Scherer, M.; Sessler, J. L.; Gebauer, A.; Lynch, V. A Bridged Pyrrolic Ansa-Ferrocene. A New Type of Anion Receptor. *Chem. Commun.* **1998**, 85–86.

(30) Snowden, T. S.; Anslyn, E. V. Anion Recognition: Synthetic Receptors for Anions and Their Application in Sensors. *Curr. Opin. Chem. Biol.* **1999**, *3* (6), 740–746.

(31) Sessler, J. L.; Cho, D. G.; Lynch, V. Diindolylquinoxalines: Effective Indole-Based Receptors for Phosphate Anion. *J. Am. Chem. Soc.* **2006**, *128* (51), 16518–16519.

(32) Prakash, V.; Saha, S.; Chakraborty, K.; Krishnan, Y. Rational Design of a Quantitative, PH-Insensitive, Nucleic Acid Based Fluorescent Chloride Reporter. *Chem. Sci.* **2016**, *7* (3), 1946–1953.

(33) Chakraborty, K.; Veetil, A. T.; Jaffrey, S. R.; Krishnan, Y. Nucleic Acid-Based Nanodevices in Biological Imaging. *Annu. Rev. Biochem.* **2016**, *85*, 349–373.

(34) Labuda, J.; Oliveira Brett, A. M.; Evtugyn, G.; Fojta, M.; Mascini, M.; Ozsoz, M.; Palchetti, I.; Paleček, E.; Wang, J. Electrochemical Nucleic Acid-Based Biosensors: Concepts, Terms, and Methodology (IUPAC Technical Report). *Pure Appl. Chem.* **2010**, *82* (5), 1161–1187.

(35) Jin, J.; Ouyang, X.; Li, J.; Jiang, J.; Wang, H.; Wang, Y.; Yang, R. Nucleic Acid-Modulated Silver Nanoparticles: A New Electrochemical Platform for Sensing Chloride Ion. *Analyst* **2011**, *136* (18), 3629–3634.

(36) Evans, N. H.; Beer, P. D. A Ferrocene Functionalized Rotaxane Host System Capable of the Electrochemical Recognition of Chloride. *Org. Biomol. Chem.* **2011**, *9* (1), 92–100.

(37) Parks, F. C.; Sheetz, E. G.; Stutsman, S. R.; Lutolli, A.; Debnath, S.; Raghavachari, K.; Flood, A. H. Revealing the Hidden Costs of Organization in Host-Guest Chemistry Using Chloride-Binding Foldamers and Their Solvent Dependence. *J. Am. Chem. Soc.* **2022**, *144* (3), 1274–1287.

(38) Liu, Y.; Parks, F. C.; Sheetz, E. G.; Chen, C. H.; Flood, A. H. Polarity-Tolerant Chloride Binding in Foldamer Capsules by Programmed Solvent-Exclusion. *J. Am. Chem. Soc.* **2021**, *143* (8), 3191–3204.

(39) Hua, Y.; Liu, Y.; Chen, C. H.; Flood, A. H. Hydrophobic Collapse of Foldamer Capsules Drives Picomolar-Level Chloride Binding in Aqueous Acetonitrile Solutions. *J. Am. Chem. Soc.* **2013**, *135* (38), 14401–14412.

(40) John, E. A.; Massena, C. J.; Berryman, O. B. Helical Anion Foldamers in Solution. *Chem. Rev.* **2020**, *120* (5), 2759–2782.

(41) Suk, J.; Jeong, K.-S. Indolocarbazole-Based Foldamers Capable of Binding Halides in Water. *J. Am. Chem. Soc. Commun.* **2008**, *130* (36), 11868–11869.

(42) Hua, Y.; Flood, A. H. Flipping the Switch on Chloride Concentrations with a Light-Active Foldamer. *J. Am. Chem. Soc.* **2010**, *132* (37), 12838–12840.

(43) Gale, P. A.; Caltagirone, C. Anion Sensing by Small Molecules and Molecular Ensembles. *Chem. Soc. Rev.* **2015**, *44* (13), 4212–4227.

(44) Tutol, J. N.; Kam, H. C.; Dodani, S. C. Identification of MNeonGreen as a PH-Dependent, Turn-On Fluorescent Protein Sensor for Chloride. *ChemBioChem* **2019**, *20* (14), 1759–1765.

(45) Zhang, P. F.; Yang, G. P.; Li, G. P.; Yang, F.; Liu, W. N.; Li, J. Y.; Wang, Y. Y. Series of Water-Stable Lanthanide Metal-Organic Frameworks Based on Carboxylic Acid Imidazolium Chloride: Tunable Luminescent Emission and Sensing. *Inorg. Chem.* **2019**, *58* (20), 13969–13978.

(46) Miyaji, H.; Sessler, J. L. Off-the-Shelf Colorimetric Anion Sensors. *Angew. Chemie - Int. Ed.* **2001**, *40* (1), 154–157.

(47) Carroll, C. N.; Berryman, O. B.; Johnson, C. A.; Zakharov, L. N.; Haley, M. M.; Johnson, D. W. Protonation Activates Anion Binding and Alters Binding Selectivity in New Inherently Fluorescent 2,6-Bis(2-Anilinoethynyl)Pyridine Bisureas. *Chem. Commun.* **2009**, No. 18, 2520–2522.

(48) Carroll, C. N.; Coombs, B. A.; McClintock, S. P.; Johnson, C. A.; Berryman, O. B.; Johnson, D. W.; Haley, M. M. Anion-Dependent Fluorescence in Bis(Anilinoethynyl)Pyridine Derivatives: Switchable ON-OFF and OFF-ON Responses. *Chem. Commun.* **2011**, *47* (19), 5539–5541.

(49) Tresca, B. W.; Zakharov, L. N.; Carroll, C. N.; Johnson, D. W.; Haley, M. M. Aryl C-H···Cl-Hydrogen Bonding in a Fluorescent Anion Sensor. *Chem. Commun.* **2013**, *49* (65), 7240–7242.

(50) Gavette, J. V.; Mills, N. S.; Zakharov, L. N.; Johnson, C. A.; Johnson, D. W.; Haley, M. M. An Anion-Modulated Three-Way Supramolecular Switch That Selectively Binds Dihydrogen Phosphate, H2PO4-. *Angew. Chemie - Int. Ed.* **2013**, *52* (39), 10270–10274.

(51) Hartle, M. D.; Hansen, R. J.; Tresca, B. W.; Prakel, S. S.; Zakharov, L. N.; Haley, M. M.; Pluth, M. D.; Johnson, D. W. A Synthetic Supramolecular Receptor for the Hydrosulfide Anion. *Angew. Chemie - Int. Ed.* **2016**, *55* (38), 11480–11484.

(52) Eytel, L. M.; Gilbert, A. K.; Görner, P.; Zakharov, L. N.; Johnson, D. W.; Haley, M. M. Do CH–Anion and Anion–π Interactions Alter the Mechanism of 2:1 Host–Guest Complexation in Arylethynyl Monourea Anion Receptors? *Chem. - A Eur. J.* **2017**, *23* (17), 4051–4054.

(53) Würthner, F.; Kaiser, T. E.; Saha-Möller, C. R. J-Aggregates: From Serendipitous Discovery to Supramolecular Engineering of Functional Dye Materials. *Angew. Chemie - Int. Ed.* **2011**, *50* (15), 3376–3410.

(54) Schmidtchen, F. P.; Berger, M. Artificial Organic Host Molecules for Anions. *Chem. Rev.* **1997**, *97* (5), 1609–1646.

(55) Palacios, M. A.; Nishiyabu, R.; Marquez, M.; Anzenbacher, P. Supramolecular Chemistry Approach to the Design of a High-Resolution Sensor Array for Multianion Detection in Water. *J. Am. Chem. Soc.* **2007**, *129* (24), 7538–7544.

(56) Robertson, C. C.; Perutz, R. N.; Brammer, L.; Hunter, C. A. A Solvent-Resistant Halogen Bond. *Chem. Sci.* **2014**, *5* (11), 4179–4183.

(57) Metrangolo, P.; Neukirch, H.; Pilati, T.; Resnati, G. Halogen Bonding Based Recognition Processes: A World Parallel to Hydrogen Bonding. *Acc. Chem. Res.* **2005**, *38* (5), 386–395.

(58) Desiraju, G. R.; Ho, P. S.; Kloo, L.; Legon, A. C.; Marquardt, R.; Metrangolo, P.; Politzer, P.; Resnati, G.; Rissanen, K. Definition of the Halogen Bond (IUPAC Recommendations 2013). *Pure Appl. Chem.* **2013**, *85* (8), 1711–1713.

(59) Clark, T.; Hennemann, M.; Murray, J. S.; Politzer, P. Halogen Bonding: The σ-Hole. *J. Mol. Model.* **2007**, *13* (2), 291–296.

(60) Cavallo, G.; Metrangolo, P.; Milani, R.; Pilati, T.; Priimagi, A.; Resnati, G.; Terraneo, G. The Halogen Bond. *Chem. Rev.* **2016**, *116*, 2478–2601.

(61) Beale, T. M.; Chudzinski, M. G.; Sarwar, M. G.; Taylor, M. S. Halogen Bonding in Solution: Thermodynamics and Applications. *Chem. Soc. Rev.* **2013**, *42* (4), 1667–1680.

(62) Lohrman, J. A.; Deng, C.-L.; Shear, T. A.; Zakharov, L. N.; Haley, M. M.; Johnson, D. W. Methanesulfonyl-Polarized Halogen Bonding Enables Strong Halide Recognition in an Arylethynyl Anion Receptor. *Chem. Commun.* **2019**, *55*, 1919–1922.

Chapter 2:

(1) L. Basabe-Desmonts, D. N. Reinhoudt and M. Crego-Calama, *Chem. Soc. Rev.*, 2007, **36**, 993.

(2) L. D. Lavis and R. T. Raines, *ACS Chem. Biol.*, 2008, **3**, 142–155.

(3) M. Vendrell, D. Zhai, J. C. Er and Y.-T. Chang, *Chem. Rev.*, 2012, **112**, 4391–4420.

(4) J. Du, M. Hu, J. Fan and X. Peng, *Chem. Soc. Rev.*, 2012, **41**, 4511.

(5) I. Tabakovic, K. Tabakovic, M. Trkovnik and Z. Stunic, *Organic Preparations and Procedures International*, 1985, **17**, 133–137.

(6) Y. Song, Z. Chen and H. Li, *COC*, 2012, **16**, 2690–2707.

(7) A. Stefanachi, F. Leonetti, L. Pisani, M. Catto and A. Carotti, *Molecules*, 2018, **23**, 250.

(8) R. S. Becker, S. Chakravorti, C. A. Gartner and M. de Graca Miguel, *Faraday Trans.*, 1993, **89**, 1007.

(9) S. M. Sethna and N. M. Shah, *Chem. Rev.*, 1945, **36**, 1–62.

(10) K. Tabaković and I. Tabaković, *Journal of Heterocyclic Chemistry*, 1992, **29**, 383–385.

(11) T. M. Pereira, D. P. Franco, F. Vitorio and A. E. Kummerle, *CTMC*, 2018, **18**, 124–148.

(12) M. Riveiro, N. De Kimpe, A. Moglioni, R. Vazquez, F. Monczor, C. Shayo and C. Davio, *CMC*, 2010, **17**, 1325–1338.

(13) D. Cao, Z. Liu, P. Verwilst, S. Koo, P. Jangjili, J. S. Kim and W. Lin, *Chem. Rev.*, 2019, **119**, 10403–10519.

(14) J. L. Abernethy, *J. Chem. Educ.*, 1969, **46**, 561.

(15) R. D. H. Murray, J. Méndez and S. A. Brown, *The natural coumarins: occurrence, chemistry, and biochemistry*, Wiley, Chichester ; New York, 1982.

(16) Anamika, D. Utreja, Ekta, N. Jain and S. Sharma, *COC*, 2019, **22**, 2509–2536.

(17) S. Govori, *Synthetic Communications*, 2016, **46**, 569–580.

(18) F. G. Medina, J. G. Marrero, M. Macías-Alonso, M. C. González, I. Córdova-Guerrero, A. G. Teissier García and S. Osegueda-Robles, *Nat. Prod. Rep.*, 2015, **32**, 1472–1507.

(19) M. Tasior, D. Kim, S. Singha, M. Krzeszewski, K. H. Ahn and D. T. Gryko, *J. Mater. Chem. C*, 2015, **3**, 1421–1446.

(20) X. Liu, Z. Xu and J. M. Cole, *J. Phys. Chem. C*, 2013, **117**, 16584–16595.

(21) S. Nad, M. Kumbhakar and H. Pal, *J. Phys. Chem. A*, 2003, **107**, 4808–4816.

(22) G. Jones and M. A. Rahman, *J. Phys. Chem.*, 1994, **98**, 13028–13037.

(23) L. Cisse, A. Djande, M. Capo-Chichi, F. Delatre, A. Saba, A. Tine and J.-J. Aaron, *Spectrochimica Acta Part A: Molecular and Biomolecular Spectroscopy*, 2011, **79**, 428–436.

(24) M. Cigáň, J. Donovalová, V. Szöcs, J. Gašpar, K. Jakusová and A. Gáplovský, *J. Phys. Chem. A*, 2013, **117**, 4870–4883.

(25) A. Gandioso, R. Bresolí-Obach, A. Nin-Hill, M. Bosch, M. Palau, A. Galindo, S. Contreras, A. Rovira, C. Rovira, S. Nonell and V. Marchán, *J. Org. Chem.*, 2018, **83**, 1185–1195.

(26) Z.-S. Wang, Y. Cui, K. Hara, Y. Dan-oh, C. Kasada and A. Shinpo, *Adv. Mater.*, 2007, **19**, 1138–1141.

(27) F. Bu, R. Duan, Y. Xie, Y. Yi, Q. Peng, R. Hu, A. Qin, Z. Zhao and B. Z. Tang, *Angew. Chem. Int. Ed.*, 2015, **54**, 14492–14497.

(28) J.-X. Chen, W. Liu, C.-J. Zheng, K. Wang, K. Liang, Y.-Z. Shi, X.-M. Ou and X.-H. Zhang, *ACS Appl. Mater. Interfaces*, 2017, **9**, 8848–8854.

(29) K. Hara, T. Sato, R. Katoh, A. Furube, Y. Ohga, A. Shinpo, S. Suga, K. Sayama, H. Sugihara and H. Arakawa, *J. Phys. Chem. B*, 2003, **107**, 597–606.

(30) S. A. Swanson, G. M. Wallraff, J. P. Chen, W. Zhang, L. D. Bozano, K. R. Carter, J. R. Salem, R. Villa and J. C. Scott, *Chem. Mater.*, 2003, **15**, 2305–2312.

(31) Y. Jung, J. Jung, Y. Huh and D. Kim, *Journal of Analytical Methods in Chemistry*, 2018, **2018**, 1–11.

(32) A. B. Ahvale, H. Prokopcová, J. Šefčovičová, W. Steinschifter, A. E. Täubl, G. Uray and W. Stadlbauer, *Eur. J. Org. Chem.*, 2008, **2008**, 563–571.

(33) M. B. de Macedo, R. Kimmel, D. Urankar, M. Gazvoda, A. Peixoto, F. Cools, E. Torfs, L. Verschaeve, E. S. Lima, A. Lyčka, D. Milićević, A. Klásek, P. Cos, S. Kafka, J. Košmrlj and D. Cappoen, *European Journal of Medicinal Chemistry*, 2017, **138**, 491–500.

(34) G. C. Enoua, G. Lahm, G. Uray and W. Stadlbauer, *J. Heterocyclic Chem.*, 2014, **51**, E263–E275.

(35) G. A. Strohmeier, W. M. F. Fabian and G. Uray, *HCA*, 2004, **87**, 215–226.

(36) G. Uray, K. S. Niederreiter, F. Belaj and W. M. F. Fabian, *HCA*, 1999, **82**, 1408–1417.

(37) W. M. F. Fabian, K. S. Niederreiter, G. Uray and W. Stadlbauer, *Journal of Molecular Structure*, 1999, **477**, 209–220.

(38) T. Tashima, *Bioorganic & Medicinal Chemistry Letters*, 2015, **25**, 3415–3419.

(39) J. R. Casley-Smith, R. G. Morgan and N. B. Piller, *N Engl J Med*, 1993, **329**, 1158–1163.

(40) J. P. Bard, C.-L. Deng, H. C. Richardson, J. M. Odulio, J. E. Barker, L. N. Zakharov, P. H.-Y. Cheong, D. W. Johnson and M. M. Haley, *Org. Chem. Front.*, 2019, **6**, 1257–1265.

(41) C. L. Vonnegut, A. M. Shonkwiler, M. M. Khalifa, L. N. Zakharov, D. W. Johnson and M. M. Haley, *Angew. Chem. Int. Ed.*, 2015, **54**, 13318–13322.

(42) M. J. S. Dewar and V. P. Kubba, *J. Am. Chem. Soc.*, 1960, **82**, 5685–5688.

(43) I. G. M. Campbell and J. K. Way, *J. Chem. Soc.*, 1961, 2133.

(44) Y. Sun and N. Cramer, *Angew. Chem. Int. Ed.*, 2017, **56**, 364–367.

(45) W. Tang and Y.-X. Ding, *J. Org. Chem.*, 2006, **71**, 8489–8492.

(46) J. Yan, Q. Li, J. A. Boutin, M. P. Renard, Y. Ding, X. Hao, W. Zhao and M. Wang, *Acta Pharmacologica Sinica*, 2008, **29**, 752–758.

(47) D. Zhao, C. Nimphius, M. Lindale and F. Glorius, *Org. Lett.*, 2013, **15**, 4504–4507.

(48) S. Park, B. Seo, S. Shin, J.-Y. Son and P. H. Lee, *Chem. Commun.*, 2013, **49**, 8671.

(49) L. Liu, A.-A. Zhang, Y. Wang, F. Zhang, Z. Zuo, W.-X. Zhao, C.-L. Feng and W. Ma, *Org. Lett.*, 2015, **17**, 2046–2049.

(50) Z.-Q. Lin, W.-Z. Wang, S.-B. Yan and W.-L. Duan, *Angew. Chem. Int. Ed.*, 2015, **54**, 6265–6269.

(51) Z. Wang, B. S. Gelfand and T. Baumgartner, *Angew. Chem. Int. Ed.*, 2016, **55**, 3481–3485.

(52) Y.-N. Ma, X. Zhang and S. Yang, *Chem. Eur. J.*, 2017, **23**, 3007–3011.

(53) N. A. Takaesu, E. Ohta, L. N. Zakharov, D. W. Johnson and M. M. Haley, *Organometallics*, 2017, **36**, 2491–2493.

(54) C. Deng, J. P. Bard, J. A. Lohrman, J. E. Barker, L. N. Zakharov, D. W. Johnson and M. M. Haley, *Angew. Chem. Int. Ed.*, 2019, **58**, 3934–3938.

(55) C.-L. Deng, J. P. Bard, L. N. Zakharov, D. W. Johnson and M. M. Haley, *J. Org. Chem.*, 2019, **84**, 8131–8139.

(56) C.-L. Deng, J. P. Bard, L. N. Zakharov, D. W. Johnson and M. M. Haley, *Org. Lett.*, 2019, **21**, 6427–6431.

(57) T. A. Schaub, S. M. Brülls, P. O. Dral, F. Hampel, H. Maid and M. Kivala, *Chem. Eur. J.*, 2017, **23**, 6988–6992.

(58) C. Romero-Nieto, A. López-Andarias, C. Egler-Lucas, F. Gebert, J. Neus and O. Pilgram, *Angew. Chem. Int. Ed.*, 2015, **54**, 15872–15875.

(59) A. Fukazawa, H. Osaki and S. Yamaguchi, *Asian Journal of Organic Chemistry*, 2014, **3**, 122–127.

(60) E. Regulska and C. Romero-Nieto, *Dalton Trans.*, 2018, **47**, 10344–10359.

(61) N. Grenon and T. Baumgartner, *Inorg. Chem.*, 2018, **57**, 1630–1644.

(62) P. Gong, K. Ye, J. Sun, P. Chen, P. Xue, H. Yang and R. Lu, *RSC Adv.*, 2015, **5**, 94990–94996.

(63) X.-D. Jiang, J. Zhao, D. Xi, H. Yu, J. Guan, S. Li, C.-L. Sun and L.-J. Xiao, *Chem. Eur. J.*, 2015, **21**, 6079–6082.

(64) F. Mathey, *Chem. Rev.*, 1988, **88**, 429–453.

(65) N. Avarvari, P. Le Floch and F. Mathey, *J. Am. Chem. Soc.*, 1996, **118**, 11978–11979.

(66) W.-C. Sun, K. R. Gee and R. P. Haugland, *Bioorganic & Medicinal Chemistry Letters*, 1998, **8**, 3107–3110.

(67) J. R. Quinn, S. C. Zimmerman, J. E. Del Bene and I. Shavitt, *J. Am. Chem. Soc.*, 2007, **129**, 934–941.

(68) A. M. Brouwer, *Pure and Applied Chemistry*, 2011, **83**, 2213–2228.

(69) K. Kuroda, Y. Maruyama, Y. Hayashi and T. Mukaiyama, *BCSJ*, 2009, **82**, 381–392.

Chapter 3:

(1) C. L. Vonnegut, B. W. Tresca, D. W. Johnson and M. M. Haley, *Chemistry - An Asian Journal*, 2015, **10**, 522–535.

(2) M. D. Hartle, R. J. Hansen, B. W. Tresca, S. S. Prakel, L. N. Zakharov, M. M. Haley, M. D. Pluth and D. W. Johnson, *Angew. Chem. Int. Ed.*, 2016, **55**, 11480–11484.

(3) J. A. Lohrman, C.-L. Deng, T. A. Shear, L. N. Zakharov, M. M. Haley and D. W. Johnson, *Chem. Commun.*, 2019, **55**, 1919–1922.

(4) H. A. Fargher, N. Lau, L. N. Zakharov, M. M. Haley, D. W. Johnson and M. D. Pluth, *Chemical Science*, 2019, **10**, 67–72.

(5) N. Lau, L. N. Zakharov and M. D. Pluth, *Chem. Commun.*, 2018, **54**, 2337–2340.

(6) L. M. Eytel, H. A. Fargher, M. M. Haley and D. W. Johnson, *Chem. Commun.*, 2019, **55**, 5195–5206.

(7) O. B. Berryman, C. A. Johnson, C. L. Vonnegut, K. A. Fajardo, L. N. Zakharov, D. W. Johnson and M. M. Haley, *Crystal Growth & Design*, 2015, **15**, 1502–1511.

(8) P. D. Beer and P. A. Gale, *Angew. Chem. Int. Ed.*, 2001, 31.

(9) M. J. Langton, C. J. Serpell and P. D. Beer, *Angew. Chem. Int. Ed.*, 2016, **55**, 1974–1987.

(10) S. Kubik, *Chem. Soc. Rev.*, 2010, **39**, 3648.

(11) L. M. Eytel, A. C. Brueckner, J. A. Lohrman, M. M. Haley, P. H.-Y. Cheong and D. W. Johnson, *Chem. Commun.*, 2018, **54**, 13208–13211.

(12) H. A. Fargher, N. Lau, H. C. Richardson, P. H.-Y. Cheong, M. M. Haley, M. D. Pluth and D. W. Johnson, *J. Am. Chem. Soc.*, 2020, **142**, 8243–8251.

(13) A. Borissov, I. Marques, J. Y. C. Lim, V. Félix, M. D. Smith and P. D. Beer, *J. Am. Chem. Soc.*, 2019, **141**, 4119–4129.

(14) K. Kavallieratos, C. M. Bertao and R. H. Crabtree, *J. Org. Chem.*, 1999, **64**, 1675–1683.

(15) Corwin. Hansch, A. Leo and R. W. Taft, *Chem. Rev.*, 1991, **91**, 165–195.

(16) L. Xu, Z. Liu, W. Dong, J. Song, M. Miao, J. Xu and H. Ren, *Org. Biomol. Chem.*, 2015, **13**, 6333–6337.

(17) Y. Wang, Y. Zhou, X. Ma and Q. Song, *Org. Lett.*, 2021, **23**, 5599–5604.

(18) M. Jash, B. Das and C. Chowdhury, *J. Org. Chem.*, 2016, **81**, 10987–10999.

(19) M. M. Watt, J. M. Engle, K. C. Fairley, T. E. Robitshek, M. M. Haley and D. W. Johnson, *Org. Biomol. Chem.*, 2015, **13**, 4266–4270.

(20) Y. Liu, A. Sengupta, K. Raghavachari and A. H. Flood, *Chem*, 2017, **3**, 411–427.

(21) P. Thordarson, *Chem. Soc. Rev.*, 2011, **40**, 1305–1323.

(22) D. Brynn Hibbert and P. Thordarson, *Chem. Commun.*, 2016, **52**, 12792–12805.

(23) A. M. S. Riel, D. A. Decato, J. Sun, C. J. Massena, M. J. Jessop and O. B. Berryman, *Chem. Sci.*, 2018, **9**, 5828–5836.

(24) C. A. Lipinski, *Drug Discovery Today: Technologies*, 2004, **1**, 337–341.

(25) I. J. Bazany-Rodríguez, D. Martínez-Otero, J. Barroso-Flores, A. K. Yatsimirsky and A. Dorazco-González, *Sensors and Actuators B: Chemical*, 2015, **221**, 1348–1355.

Chapter 4:

(1) K. Berend, L. H. van Hulsteijn and R. O. B. Gans, *Eur. J. Intern. Med.*, 2012, **23**, 203.

(2) C. D. Meletis, *J Evid. Based Complementary Altern. Med.*, 2011, **16**, 190.

(3) K. J. Bowman, *Science*, 2019, **365**, 124.

(4) J. Pancholi and P. D. Beer, *Coord. Chem. Rev.*, 2020, 213281.

(5) R. Hein and P. D. Beer, *Chem. Sci.*, 2022, **13**, 7098.

(6) W. Kunz, J. Henle and B. W. Ninham, *Curr. Opin. Colloid Interface Sci.*, 2004, **9**, 19.

(7) K. P. Gregory, G. R. Elliott, H. Robertson, A. Kumar, E. J. Wanless, G. B. Webber, V. S. J. Craig, G. G. Andersson and A. J. Page, *Phys. Chem. Chem. Phys.*, 2022, **24**, 12682.

(8) Y. Liu, W. Zhao, C. H. Chen and A. H. Flood, *Science*, 2019, **365**, 159.

(9) Craig. C. Robertson, J. S. Wright, E. J. Carrington, R. N. Perutz, C. A. Hunter and L. Brammer, *Chem. Sci.*, 2017, **8**, 5392.

(10) B. W. Tresca, L. N. Zakharov, C. N. Carroll, D. W. Johnson and M. M. Haley, *Chem. Commun.*, 2013, **49**, 7240.

(11) M. M. Watt, J. M. Engle, K. C. Fairley, T. E. Robitshek, M. M. Haley and D. W. Johnson, *Org. Biomol. Chem.*, 2015, **13**, 4266.

(12) C. N. Carroll, B. A. Coombs, S. P. McClintock, C. A. Johnson II, O. B. Berryman, D. W. Johnson and M. M. Haley, *Chem. Commun.*, 2011, **47**, 5539.

(13) C. A. Lipinski, F. Lombardo, B. W. Dominy and P. J. Feeney, *Adv. Drug Deliv. Rev.*, 1997, **23**, 3.

(14) C. A. Lipinski, *Drug Discov. Today Technol.,* 2004, **1**, 337.

(15) E. Corradi, S. V. Meille, M. T. Messina, P. Metrangolo and G. Resnati, *Angew. Chem. Int. Ed.*, 2000, **39**, 1782.

(16) H. A. Fargher, N. Lau, L. N. Zakharov, M. M. Haley, D. W. Johnson and M. D. Pluth, *Chem. Sci.*, 2019, **10**, 67.

(17) L. M. Lee, M. Tsemperouli, A. I. Poblador-Bahamonde, S. Benz, N. Sakai, K. Sugihara and S. Matile, *J. Am. Chem. Soc.*, 2019, **141**, 810.

(18) M. S. Taylor, *Coord. Chem. Rev.* 2020, **413**, 213270.

(19) A. Borissov, I. Marques, J. Y. C. Lim, V. Félix, M. D. Smith and P. D. Beer, *J. Am. Chem. Soc.*, 2019, **141**, 4119.

(20) C. C. Robertson, R. N. Perutz, L. Brammer and C. A. Hunter, *Chem. Sci.*, 2014, **5**, 4179.

(21) T. Bunchuay, A. Docker, A. J. Martinez-Martinez and P. D. Beer, *Angew. Chem. Int. Ed.*, 2019, **58**, 13823.

(22) J. A. Lohrman, C.-L. Deng, T. A. Shear, L. N. Zakharov, M. M. Haley and D. W. Johnson, *Chem. Commun.*, 2019, **55**, 1919.

(23) D. A. Decato, A. M. S. Riel and O. B. Berryman, *Crystals*, 2019, **9**, 522.

(24) A. M. S. Riel, D. A. Decato, J. Sun, C. J. Massena, M. J. Jessop and O. B. Berryman, *Chem. Sci.*, 2018, **9**, 5828.

(25) M. Giese, M. Albrecht, T. Krappitz, M. Peters, V. Gossen, G. Raabe, A. Valkonen and K. Rissanen, *Chem. Commun.*, 2012, **48**, 9983.

(26) M. Giese, M. Albrecht and K. Rissanen, *Chem. Commun.*, 2016, **52**, 1778.

(27) G. R. Desiraju, P. S. Ho, L. Kloo, A. C. Legon, R. Marquardt, P. Metrangolo, P. Politzer, G. Resnati and K. Rissanen, *Pure Appl. Chem.*, 2013, **85**, 1711.

(28) D. Brynn Hibbert and P. Thordarson, *Chem. Commun.*, 2016, **52**, 12792.

(29) P. Thordarson, *Chem. Soc. Rev.*, 2011, **40**, 1305.

(30) S. W. Robinson, C. L. Mustoe, N. G. White, A. Brown, A. L. Thompson, P. Kennepohl and P. D. Beer, *J. Am. Chem. Soc.*, 2015, **137**, 499.

(31) H. A. Fargher, N. Lau, H. C. Richardson, P. H.-Y. Cheong, M. M. Haley, M. D. Pluth and D. W. Johnson, *J. Am. Chem. Soc.*, 2020, **142**, 8243.

Chapter 5:

(1) A. M. S. Riel, R. K. Rowe, E. N. Ho, A.-C. C. Carlsson, A. K. Rappé, O. B. Berryman and P. S. Ho, *Acc. Chem. Res.*, 2019, **52**, 2870–2880.

(2) O. B. Berryman, C. A. Johnson, L. N. Zakharov, M. M. Haley and D. W. Johnson, *Angew. Chem. Int. Ed.*, 2008, **47**, 117–120.

(3) B. W. Tresca, L. N. Zakharov, C. N. Carroll, D. W. Johnson and M. M. Haley, *Chem. Commun.*, 2013, **49**, 7240.

(4) C. L. Vonnegut, B. W. Tresca, D. W. Johnson and M. M. Haley, *Chemistry - An Asian Journal*, 2015, **10**, 522–535.

(5) L. M. Eytel, A. C. Brueckner, J. A. Lohrman, M. M. Haley, P. H.-Y. Cheong and D. W. Johnson, *Chem. Commun.*, 2018, **54**, 13208–13211.

(6) J. A. Lohrman, C.-L. Deng, T. A. Shear, L. N. Zakharov, M. M. Haley and D. W. Johnson, *Chem. Commun.*, 2019, **55**, 1919–1922.

(7) H. A. Fargher, N. Lau, L. N. Zakharov, M. M. Haley, D. W. Johnson and M. D. Pluth, *Chemical Science*, 2019, **10**, 67–72.

(8) H. A. Fargher, N. Lau, H. C. Richardson, P. H.-Y. Cheong, M. M. Haley, M. D. Pluth and D. W. Johnson, *J. Am. Chem. Soc.*, 2020, **142**, 8243–8251.

(9) G. Turner, A. Docker and P. D. Beer, *Dalton Trans.*, 2021, **50**, 12800–12805.

(10) R. Tepper, B. Schulze, H. Görls, P. Bellstedt, M. Jäger and U. S. Schubert, *Org. Lett.*, 2015, **17**, 5740–5743.

(11) N. L. Kilah, M. D. Wise, C. J. Serpell, A. L. Thompson, N. G. White, K. E. Christensen and P. D. Beer, *J. Am. Chem. Soc.*, 2010, **132**, 11893–11895.

(12) L. Fotović, N. Bedeković and V. Stilinović, *Crystal Growth & Design*, 2021, **21**, 6889–6901.

(13) P. Thordarson, *Chem. Soc. Rev.*, 2011, **40**, 1305–1323.

(14) D. Brynn Hibbert and P. Thordarson, *Chem. Commun.*, 2016, **52**, 12792–12805.

(15) R. D. Shannon, *Acta Cryst A*, 1976, **32**, 751–767.

(16) Y. Jung, J. Jung, Y. Huh and D. Kim, *Journal of Analytical Methods in Chemistry*, 2018, **2018**, 1–11.

(17) J. Du, M. Hu, J. Fan and X. Peng, *Chem. Soc. Rev.*, 2012, **41**, 4511.

(18) F. Zapata, A. Caballero, N. G. White, T. D. W. Claridge, P. J. Costa, V. Félix and P. D. Beer, *J. Am. Chem. Soc.*, 2012, **134**, 11533–11541.

(19) D. Mungalpara, S. Stegmüller and S. Kubik, *Chem. Commun.*, 2017, **53**, 5095–5098.

(20) J. Shang, W. Si, W. Zhao, Y. Che, J.-L. Hou and H. Jiang, *Org. Lett.*, 2014, **16**, 4008–4011.

(21) A. Borissov, I. Marques, J. Y. C. Lim, V. Félix, M. D. Smith and P. D. Beer, *J. Am. Chem. Soc.*, 2019, **141**, 4119–4129.

(22) F. C. Parks, E. G. Sheetz, S. R. Stutsman, A. Lutolli, S. Debnath, K. Raghavachari and A. H. Flood, *J. Am. Chem. Soc.*, 2022, **144**, 1274–1287.

(23) J. M. Fourquez, A. Godard, F. Marsais and G. Quéguiner, *Journal of Heterocyclic Chemistry*, 1995, **32**, 1165–1170.